SOLAR THERMAL AND PHOTOVOLTAIC ELECTRICAL GENERATION IN LIBYA

YASSER A AMDAWI ALDALI

BSc. Mechanical Engineering

MSc. Mechanical Engineering

A thesis submitted in partial fulfilment of the requirements of Edinburgh Napier University for the degree of Doctor of Philosophy

February 2012

Declaration

I hereby declare that the contents of this thesis are original and have been submitted solely to Edinburgh Napier University in partial fulfilment of the requirements for the degree of Doctor of Philosophy (PhD).

Yasser A Amdawi Aldali

Signed

Dated

<u>Acknowledgements</u>

Solar Thermal and Photovoltaic Electrical Generation in Libya

Abstract

This thesis investigates the application of large scale concentrated solar (CSP) and photovoltaic power plants in Libya.

Direct Steam Generation (DSG) offers a cheaper and less risky method of generating electricity using concentrated solar energy than Heat Transfer Fluid (HTF) plant. However, it is argued that the location of a DSG plant can be critical in realising these benefits, and that the South-East part of Libya is ideal in this respect. The models and calculations presented here are the result of an implementation of the 2007 revision of the IAPWS equations in a general application based on Microsoft Excel and VBA. The hypothetical design for 50MW DSG power plant discussed in this thesis is shown to yield an 76% reduction in greenhouse gas emissions compared to an equivalent gas-only plant over the ten-hour daily period of operation. Land requirement is modest at $0.7km^2$.

A new method for improving the distribution of heat within the absorber tube wall was developed. Internal helical fins within the absorber tube have been proposed to provide a regularly pitched and orderly distribution of flow from the 'hot' to the 'cold' side of the absorber tube. Note that the irradiance profile on the absorber tube is highly asymmetric. A CFD simulation using FLUENT software was carried out for three types of pipes with different internal helical-fin pitch, and an aluminium pipe without fins. The results show that the thermal gradient between the upper and lower temperature for the pipe without a helical fin is considerably higher compared with the pipes with helical fins. Also, the thermal gradient between the two halves for the aluminium pipe (without a helical fin) is much lower when compared to the result for the traditional steel pipe (without a helical fin).

A 50MW PV-grid connected (stationary and tracking) power plant design in Al-Kufra, Libya has been carried out presently. A hetero-junction with intrinsic thin layer (HIT) type PV module has been selected and modelled. The effectiveness of the use of a cooling jacket on the modules has been evaluated. A Microsoft Excel-VBA program has been constructed to compute slope radiation, dew-point, sky temperature, and then cell temperature, maximum power output and module efficiency for this system, with and without water cooling for stationary system and for tracking system without water cooling. The results for energy production show that the total energy output is 114GWh/year without a water cooling system, 119GWh/year with a water cooling system for stationary system and 148GWh/year for tracking system. The average module efficiency with and without a cooling system for the stationary system is 17.2% and 16.6% respectively and 16.2% for the tracking system. The electricity generation capacity factor (CF) and solar capacity factor (SCF) for stationary system were found to be 26% and 62.5% respectively and 34% and 82% for tracking system. The payback time for the proposed LS-PV power plant was found to be 2.75 years for the stationary system and 3.58 years for the tracking system.

The modelling that was carried was based on the measurements conducted on the experimental system set in a city in the southern part of Turkey. Those measurements are recorded by a Turkish team at Iskanderun. As well as the current, voltage and cell temperature of the photovoltaic module, the environmental variables such as ambient temperature and solar irradiance were measured. These data were used for validation purposes. The correlation for the conversion of solar irradiation from horizontal to sloped surface indicated that the presently used model is highly successful reflected by the goodness of fit parameters: the coefficient of determination is 0.97, and the mean bias error -2.2W/m^2. Similarly, the cell temperature model used in the present thesis is validated by the following correlation parameters $R^2 = 0.97$ $^{\circ}$C, while MBE is 0.7 and RMSE = 2.1 $^{\circ}$C.

Glossary of Symbols & Abbreviations

ϕ = Latitude

β = Slope or tilt

γ = Surface Azimuth Angle

δ = Declination

ω = Hour angle

θ = Angle of incidence

θ_z = Zenith angle

γ_s = Solar azimuth angle

η_c = Efficiency of a solar cell

$(\tau\alpha)_e$ = Effective transmittance - absorptance product

α_G = Absorptivity of glass

ρ_{mirror} = Reflectivity of the mirror

ρ_f = Density of fluid, kg/m^3

υ_f = Kinematic viscosity of fluid, m^2/s

κ_f = Thermal conductivity of fluid, W/m K

κ_{eff} = Effective thermal conductivity, W/m K

ε_p = Emissivity of absorber tube

ε_g = Emissivity of glass covers tube

σ = Stefan-Boltzmann constant, $5.67*10\text{-}8 W/m^2\ K^4$

ρ_g = Density of vapour, kg/m^3

λ = Thermal conductivity, W/m K

μ_{voc} = Temperature coefficient of open circuit voltage, $V/^oC$

μ_{Isc} = Temperature coefficient of short circuit current, $A/^oC$

ρ_{albedo} = Average albedo of the ground

α_a = Solar altitude angle

α = Absorptance

τ = Transmittance/ Transmissivity

ε_{sky} = Sky emissivity

η_{mp} = Maximum power point efficiency of the PV module

A_p = Section area of the absorber tube, m^2

A_{mirror} = Area of mirror, m^2

AM = Air mass factor

b = Radial gap, m

C_b = Development cost,$

C_d = Design cost,$

C_i = Inverters cost,$

C_{in} = Installation cost,$

C_m = Module cost,$

C_w = Total cost,$

CR = Concentration ratio of the collector

D_{ci} = Inner diameter of glass cover, m

D_i = Absorber tube inner diameter, m

D_o = Outer diameter of absorber tube, m

f = Friction factor

F = Sky clarity index

FF = Filling factor, %

g = Gravitational acceleration, m/s^2

h = Enthalpy of water/steam substance, kJ/kg

h_b = Enthalpy for boundary, kJ/kg

h_f = Convective heat transfer coefficient, W/m^2 K

h_f = Specific enthalpy of saturated liquid, kJ/kg

h_g = Specific enthalpy of saturated vapour, kJ/kg

I_B = Horizontal beam irradiance, W/m^2

I_{bn} = Incident beam of flux, W/m^2

I_{BT} = Slope beam irradiance, W/m^2

I_d = Diode current, A

I_D = Horizontal diffuse irradiance, W/m^2

I_{DT} = Sky-diffuse irradiance, W/m^2

I_E = Horizontal extraterrestrial irradiance, W/m^2

I_G = Horizontal global irradiance, W/m^2

I_g = Ground-reflected radiation, W/m^2

I_{LG} = Light generated current, A

I_m = Current at maximum power of PV module, A

I_o = Reverse saturation current, A

I_S = Slope irradiation, W/m^2

I_{sc} = Short circuit current of PV module, A

I_{solar} = Beam irradiance, W/m^2

$I_{sun,c}$ = Sun constant, W/m^2

L = Characteristic dimension, m

m_f = Mass flow rate, kg/s

Mtoe = Million tonne oil equivalent

N_u = Nusselt number

P_{atm} = Atmospheric pressure, Pa

ΔP = Pressure drop, Pa

P_m = The maximum power of PV module, W

Pr = Prandtl number

P_w = partial pressure of water vapour

Q_{loss} = Energy loss, W

Ra* = Modified Rayleigh number

R_{eD} = Reynolds number

R_{Con} = Thermal resistance due to convection

R_{Rad} = Thermal resistance due to radaition

Rs = Series resistance of PV cell, Ω

Rsh = Shunt resistance of PV cell, Ω

S = Material strength, Pa

SF = Safety factor

s_f = Specific entropy of saturated liquid (kJ/kg K)

s_g = Specific entropy of saturated vapour (kJ/kg K)

T = Temperature, K

t = Wall thickness, m

T_a = Ambient temperature, ^{o}C

T_C = Cell temperature, ^{o}C

T_{dp} = Dew point temperature, ^{o}C

T_g = Glass covers temperature, ^{o}C

T_p =Absorber tube temperature,^{o}C

T_{sat} = Saturation temperature,K

T_{SKY} =Sky temperature, K

T_w =Water inlet temperature,^{o}C

U_L = Overall heat transfer coefficient, W/m^2 K

V_f =Average velocity, m/s

V_m =Voltage at maximum power of PV module, V

V_{oc} =Open circuit voltage of PV module, V

W_h = Humidity ratio

x   = Dryness fraction

υ   =Wind speed, m/s

Abbreviations

A	Ambient air
BOS	Balance of system
CFC	Capacity factor
CFD	Computational fluid dynamics
CSES	Centre of Solar Energy Studies
CSP	Concentrating solar power plants
DISS	Direct Solar Steam Generation System
DLR	German Aerospace Center
DNI	Direct normal irradiance
DOE	Department of Energy
DSG	Direct solar steam generation system
DSS	Dish Stirling System
EU-MENA	Europe the Middle East and North Africa
GCR	Ground cover ratio
G	Glass cover
GECOL	General Electric Company of Libya
GHG	Greenhouse gases
HIT	Hetero-junction with intrinsic thin layer
HTF	Heat transfer fluid
HVDC	High Voltage Direct Current
IAPWS	International Association for the Properties of Water and Steam
INDITEP	Integration of DSG Technology for Electricity Production
IEA	International Energy Agency
IF97	Industrial Formulation

IPCC	Intergovernmental Panel on Climate Change
LEPA	Low Energy Precision Application
LFS	Linear Fresnel system
LS-PV	Large scale photovoltaic power plants
MCRTM	Monte Carlo Ray-Trace method
NEA	National Energy Administration
NERC	National Energy Research Center of Jordan
NOCT	Nominal operation cell temperature
O&M	Operation and maintenance
OECD	Organisation for Economic Co-operation and Development
ORC	Organic Rankine Sycle
P	Steel absorber tube
PSA	Plataforma Solar de Almería
PTC	Parabolic Trough Collector
PTS	Parabolic Trough System
PV	Photovoltaic
REAOL	Renewable Energy Authority of Libya
SCF	Solar capacity factor
SEGS	Solar Energy Generating Systems
SSTB	Sarir-Sirt,Tazerbo Benghazi System
STC	Standard Test Conditions
STS	Solar Tower System
TREC	Trans-Mediterranean Renewable Energy Cooperation
UN	United Nation
VBA	Visual Basic Applications
W	Water/steam

WCJ	Water cooling jacket
WHO	World Health Organisation

Table of Contents

Chapter 3   70

Large-Scale DSG plant for Al-Kufra: Thermal analysis

Chapter 4

Solar absorber tube analysis: Thermal simulation using CFD

Chapter 5

Large-Scale PV plant for Al-Kufra: Energetic, economic and environmental impact analysis

Annexures

List of Publications   223

List of Figures and Tables

Figures

Chapter 3

Chapter 4

Chapter 5

Chapter 6

Tables

<u>Chapter 1</u>

<u>Chapter 2</u>

<u>Chapter 3</u>

CHAPTER 1

Introduction

"Within 6 hours deserts receive more energy from the sun than humankind consumes within a year".

Dr. Gerhard Knies

This thesis investigates the application of large scale concentrated solar (CSP) and photovoltaic power plants in Libya. The motivation behind this work is the increase in fossil energy prices and the desire by many to combat the causes of climate change.

1.0 Energy issues

Globally speaking, the present day energy scenario does not present an encouraging image. Fossil fuel depletion is very evident with the possibility of total exhaustion in a generation's time. A huge energy crisis is foreseeable until, or unless, radical steps are taken to change the present course of energy attainment.

According to Nakicenovic [1], primary energy consumption will continue to increase and reach 17,721 Mtoe in 2030 from about 9000 Mtoe in 1990. There are two reasons for this increase; namely rapid economic growth in developing countries, especially in Asia, and an explosion in the world's population [2]. Fossil fuel such as oil, natural gas and coal are finite energy sources. The International Energy Agency (IEA) [3] has estimated, as shown in Table 1.1, that the peak period of conventional oil production would be in the 2030's, even in optimistic scenarios (a high resource scenario). As a result the long term world energy problem, global warming, is another urgent issue because CO_2 emissions are caused by the combustion of fossil fuels. Fig1.1 shows the world primary energy supply and CO_2 emissions during the period from 1971-2030 [4].

Table 1.1 Oil resources and the peak period [3]

	Reference scenario	Low-resource scenario	High-resource scenario
Remaining ultimately recoverable resources base for conventional oil, as of January 1996 (billion barrels).	2626	1700	3200
Peak period of conventional oil production	2028-2032	2013-2017	2033-2037
Global demand at peak of conventional oil (million barrels/day).	121	96	142
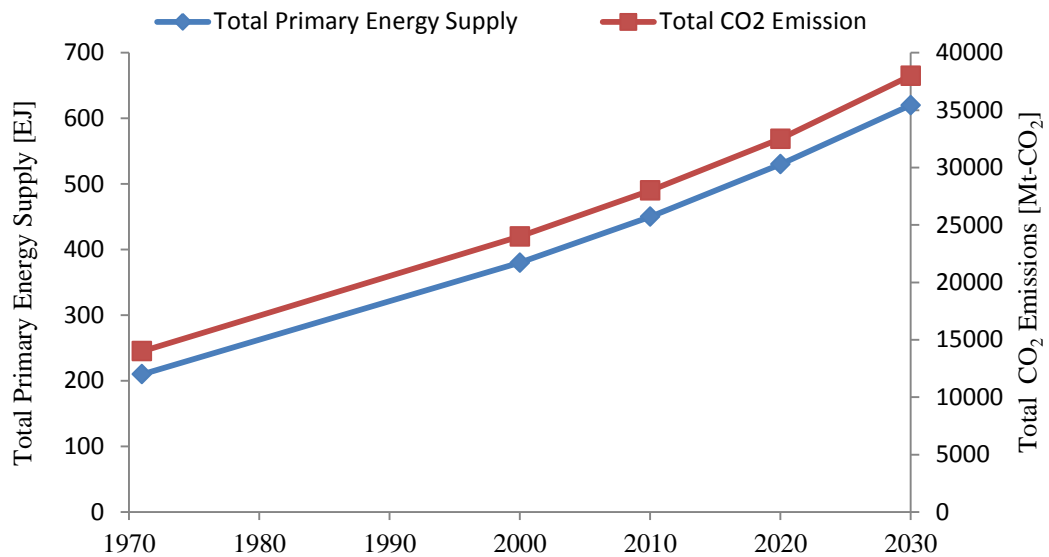
Figure 1.1 World primary energy supply and CO_2 emissions, 1971-2030 [4]

1.1 Climate change

According to the United Nations (UN) [5], climate change is a change in climate that is attributed directly or indirectly to human activity that alters the composition of the global atmosphere and which is in addition to the natural climate variability observed over a comparable time period.

According to the fourth assessment report of the Intergovernmental Panel on Climate Change IPCC [6] 'Most of the observed increase in global average temperature since the mid-20th century is very likely (greater than 90% probability) due to the observed increase in anthropogenic greenhouse gas concentrations'. The greenhouse gases (GHG) emissions trends show that the recent increase in GHG emissions is mainly due to an increase in CO_2 emission resulting from energy usage. Fig 1.2 shows the global anthropogenic GHG emissions in 2004.
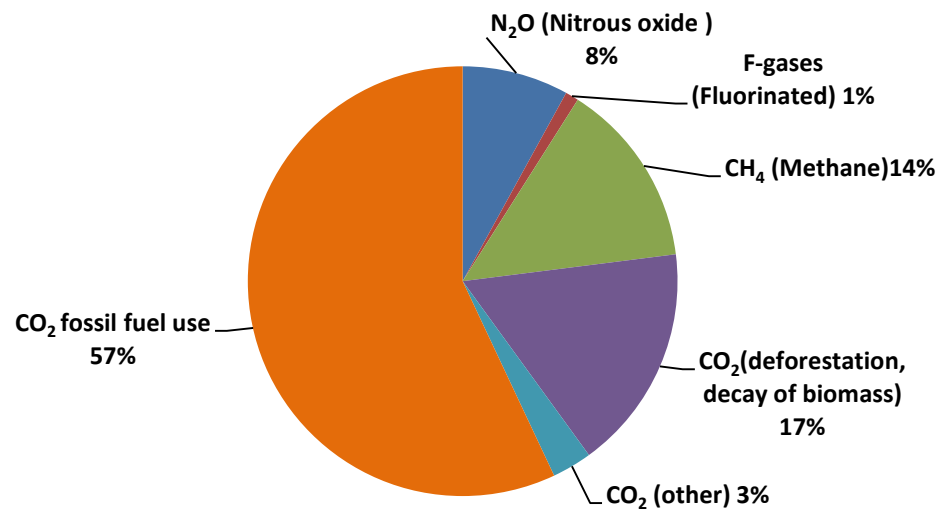
Figure 1.2 Global anthropogenic GHG emissions in 2004 [6]

In response, actions have been taken in order to reduce CO_2 emissions. An international agreement was reached at the climate change conference held at Kyoto, Japan, in 1994, legally binding most industrialised countries to reduce emissions of gases contributing to climate change. Energy consumption and environmental pollution can be reduced, without sacrificing wellbeing, by designing and employing energy saving equipment. Therefore renewable energies have the potential to meet these energy and environmental challenges.

Libya ratified the Kyoto Protocol in December 2006, and has since established policies for global warming prevention that aim at improving automotive fuel quality and reducing CO_2 emissions.

In Libya, GHG emissions from energy use are due to the combustion of oil and natural gas. The rapid growth of electricity consumption and the increasing use of domestic oil and natural gas have increased rapidly in recent years in Libya. Environment problems and limited fossil fuels [7] require new sustainable electricity generation options which utilise renewable energies.

1.1.1 Impacts of climate change

Climate change affects every aspect of human life. Economic losses are unavoidable due to climate change impacts such as extreme weather, including floods, droughts

4

and storms. According to the Stern Review [8] if action is not taken to curb carbon emissions, climate change could cost between 5 and 20 percent of annual global gross domestic product. This poses an increased threat to poorer nations where extra monetary funds are needed to address climate change impacts. Examples of extreme events in 2010 such as the monsoon-related floods in Pakistan, the summer heat wave in Russia and drought in the Amazon have affected millions of people, and huge amounts of money are needed for redevelopment of the affected areas.

Besides that, climate change directly impacts health. The World Health Organisation (WHO) [9] stated that people die every year from the side-effects of global warming with increased deaths in heat waves, and in natural disasters such as floods. This is compounded by changing patterns of life-threatening vector-borne diseases such as malaria and other existing and emerging infectious diseases. According to the IPCC [6], those people living in poverty would be worst affected by the effects of climate change.

Furthermore, the Organisation for Economic Co-operation and Development (OECD) [10] has shown potential water related tensions between nations that share common freshwater reserves - where 47% of the world's population will live in areas of high water stress in 2030. On top of that, to meet increasing demands for food and bio-fuels, world agricultural land use will need to expand by an estimated 10% by 2030. Hence this poses an increased pressure on agriculture and biodiversity development. ("A statistical analysis of the historical temperature-yield relationship indicates that on a global scale, warming from 1981-2002 very like offset some of the yield gains (for maize, wheat and barley) from technological advances, rising CO_2 and other non-climatic factors"). Yield for rice, soy and sorghum were less affected [11].

1.2 Increasing cost of energy

The issue of climate change and reducing CO_2 emissions is of greater importance because of the fact that the global energy demand is expected to increase by more than 53% by 2050 [12]. The crude oil price for July, 2011 was $97.19/barrel. This is $0.90 higher than June, 2011 with the average price of $96.29 being $20.82 higher

than July, 2010 price of $76.37 [13]. Fig 1.3 shows the crude oil price for the period from January, 2009 to June-2011.
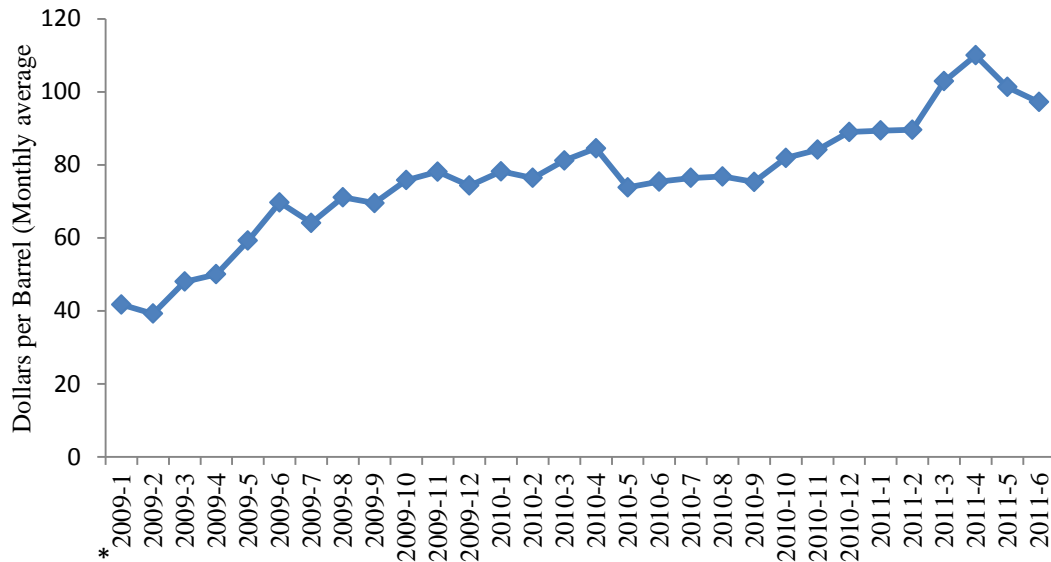
*Year & month

Figure 1.3 Crude oil price, 2009-2011

Electricity, as well as natural gas, LPG follows this oil price trend, with prices increasing every year.

At the same time, world energy demand is increasing, due to emerging market countries, China and India above all. The estimated global world growth of electricity consumption is 2.7% every year; in Middle East Arab Countries annual increases are expected to average about 3% until 2030 [14]. The Libyan energy supply and demand will be discussed in Chapter 2.

In this scenario, all world governments are involved in promoting rational use of energy, energy saving, renewable energy sources. They also pay much more attention than before to the energy market development, which could also deeply affect local life conditions such as industry growth, new employment, banking, commercial and service systems, etc.

A common idea (for all countries that do not belong to Middle East area) is they produce oil, they are floating on oil, so they couldn't be interested in energy saving, in renewable energy sources. Thus, one might wonder, whether or not this common idea is really true. Above all, is it convenient for all Middle East Countries (Libya being one of these countries)?

1.3 Aims and objectives

In this thesis the author has investigated how a large scale CSP and PV power plants could be utilised to produce electricity in Libya. The electricity generated from these methods would be used to meet the domestic demand in Libya and, if there was a surplus of electricity generation, it could be exported to Europe where energy demands are much higher [15].

The project aims are to;

1. Identify and assess the existing situation in Libya with respect to power generation, transmission and distribution along with the current forecast demand for energy.

2. Identify the solar energy potential in Libya and evaluate the suitable solar energy technologies to be used in Libya, i.e. solar – PV or solar thermal and critically appraise the options for electricity generation.

3. Critically explore the mechanism by which solar generation can be obtained to meet the domestic electricity demand.

To achieve these aims, the following tasks have been undertaken.

1. Collecting data for the whole power generation sector in Libya including thermal power plants, the current situation of Libyan electricity generation and economic as well as environmental impact of power plants in Libya.

2. Analysing the performance of a 50MW DSG (Direct steam generation) Plant Model for Al-Kufra region which is located in

Southern Libya based on the thermodynamic and thermophysical properties of water/steam substance.

3. Investigating the resulting effect on heat transfer as well as the uniformity of heat distribution within the 3D absorber tube wall geometry with different internal helical fins, and an aluminium pipe without fins using computational fluid dynamics (CFD) simulation.

4. Examining the design of a 50MW PV power plant (stationary and tracking) which has been modelled on the conditions pertaining to Al-Kufra. Furthermore, a comparison between stationary and tracking PV plant with respect to landscape impact and performance is made.

5. Examining the effect of the cell temperature on the efficiency of a PV module in an attempt to improve the efficiency by using the application of a water cooling jacket (WCJ). Laboratory-based experimental work has been carried out to achieve this objective.

1.4 The structure of the thesis

The structure of the thesis attempts to generate a framework within which the above objectives can be promoted and illustrated. The research outline is fulfilled in the following chapters as summarised below:

Chapter 2: Literature Review. This chapter aims to give information about the energy supply and demand in Libya; including hydrocarbon supply and export, electricity generation situation and environmental impact as well as the potential for solar energy in Libya. It then provides a general review of the commercially available concentrating solar power plants (CSP) and photovoltaic solar power plants (PV), as well as review of work by other researchers in this field.

Chapter 3: Thermal analysis for a large-scale Direct Steam Generation (DSG) plant. This chapter discusses modeling the performance of a 50MW DSG plant in a chosen location in the Southern East of Libya based on the thermodynamic and

thermophysical properties of water/steam substance. Furthermore, the chapter describes the development of a software tool based on Microsoft Excel and Visual Basic for Applications (VBA) which draws upon established physical relationships in the heat transfer literature to perform plant capacity calculations in a fast and convenient manner.

Chapter 4: Solar absorber tube analysis: Thermal simulation using CFD. This chapter deals with direct steam systems and proposes incorporation of internal helical fins within the absorber tube collector to improve performance. A CFD simulation using FLUENT software was carried out for three types of steel pipes with different internal helical fins, and an aluminium pipe without fins. This was done to investigate the resulting effect on heat transfer as well as the uniformity of heat distribution within the absorber tube walls.

Chapter 5: Large-Scale PV plant for Al-Kufra: Energetic, economic and environmental impact analysis. This chapter describes the design of a 50MW PV power plant model (stationary and tracking) which has been modelled on the climatic conditions pertaining to Al-Kufra.

Chapter 6: Influence of environmental factors on PV performance. This chapter focuses specifically on the effect of the cell temperature on the efficiency of a PV module in an attempt to improve the efficiency by the application of a water cooling jacket (WCJ). Furthermore, this chapter further concentrates on the verification of the mathematical modelling comparison with segmental results through.

Chapter 7: Conclusions and future work. This chapter draws important conclusions from each aspect of the presented work. The potential for future work is also discussed.

References

[1]. Nakicenovic., N. *World Energy Outlook 2007: CO2 Emissions Pathways Compared to Long-Term CO₂ Stabilization Scenarios in the Literature and IPCC AR4*. 2007; Available from: http://www.worldenergyoutlook.com/docs/weo2007/co2_scenarios.pdf.

[2]. IEA, *World Energy Outlook 2007*, 2007.

[3]. IEA, *World Energy Outlook 2004*, 2004.

[4]. Kurokawa, K., Keiichi K., *Energy from the Desert.*2003: Earthscan Publications Ltd

[5]. UNFCCC., *United Nations Framework Convention on Climate Change*, 1994.

[6]. IPCC, *Climate Change 2007-The Physical Science Basis, Contribution of Working Group I to Fourth Assessment Report of the IPCC*, 2007a.

[7]. Eljrushi, G., Veziroglu, T . *Solar hydrogen energy system for Libya. .* International Journal of Hydrogen Energy, 1990. **15**(12): p. 885-894.

[8]. *STERN REVIEW:The Economics of Climate Change*, 2006.

[9]. WHO. *10 facts on climate change and health*. 2009 [cited 2011 13 July]; Available from: http://who.int/features/factfiles/climate_change/en/index.html.

[10]. OECD, *OECD Environmental Outlook to 2030*, 2008.

[11]. Lobell, D., Field,C., *Global scale climate-crop yield relationship and the impacts of recent warming*, 2007, Environ Res Lett.

[12]. IER, *Is 80 Percent Renewable Energy by 2050 Possible?Depends on Who Is Making the Forecast*, 2011.

[13]. *U.S. Energy Information Administration,World Crude Oil Prices* 2011; Available from: http://www.eia.gov/dnav/pet/pet_pri_wco_k_w.htm.

[14]. Yaacoub, W., *Solar solution*, in *Arabian business* 2007.

[15]. TREC, *The Trans-Mediterranean Renewable Energy Cooperation*, 2007.

CHAPTER 2

Literature Review

Chapter Map

2
Literature Review

2.0
Overview

2.1
Libyan energy supply and demand

- **2.1.1** The country
- **2.1.2** Hydrocarbon supply and export
- **2.1.3** The Libyan electricity generation situation
- **2.1.4** Environmental impact

2.2
Potential for solar energy in Libya

- **2.2.1** Solar radiation fundamentals
- **2.2.2** The Libyan Climate
- **2.2.3** The Libyan desert
- **2.2.4** Technical know-how

2.3
Concentrating solar power plant (CSP)

- **2.3.1** Liner Fresnel System (LFS)
- **2.3.2** Dish Stirling System (DSS)
- **2.3.3** Solar Tower System (STS)
- **2.3.4** Parabolic Trough System (PTS)

2.4
Large scale photovoltaic power plants (LS-PV)

- **2.4.1** introduction
- **2.4.2** Factors affecting the performance of PV systems
- **2.4.3** The photovoltaic IV curve
- **2.4.4** Large scale (LS-PV) Photovoltaic system

2.5
Conclusion

2.0 Overview

"Solar thermal and photovoltaic electrical generation in Libya" is a broad theme encompassing several discrete topics. This chapter describes the specifics of large-scale generation of solar electricity. The chapter reviews the Libyan energy supply and demand including hydrocarbon supply and export, the Libyan electricity generation situation and environmental impact as well as the potential for solar energy in Libya. It then provides a general review of commercially available concentrating solar power plants (CSP) and photovoltaic solar power plants (PV), work by other researchers in this field. The chapter concludes by discussing problems which presently prevent the development of some technologies and presents potential solutions.

2.1 Libyan energy supply and demand

2.1.1 The country

Libya is an oil producing country located in the middle of north Africa, with a coast of around 2000km length on the Mediterranean sea. Libya has a land area of 1,750,000 sq km and 88% of this land is desert. The population of the country is 6 million, mostly located along a thin strip adjacent to the coastline [1]. According to the UN, the annual population growth rate for 2000-2005 was 1.93%, with a projected population of 6.9 million by the year 2015.

2.1.2 Hydrocarbon supply and export

The Libyan conventional sources of energy as of January 2011 may be summed up as follows.

According to the Oil and Gas Journal [2], Libya contained an estimated 78.8EWh of proven oil reserves. Libya accounts for 32% of the total oil reserves for Africa [2]; Fig 2.1 shows the top six African oil proven reserve holders. The principal oil reservoirs are located in the Sirte basin, which is responsible for 90% of the country's oil output. The crude oil produced is generally light and very low in sulphur.

E= 10^{18}
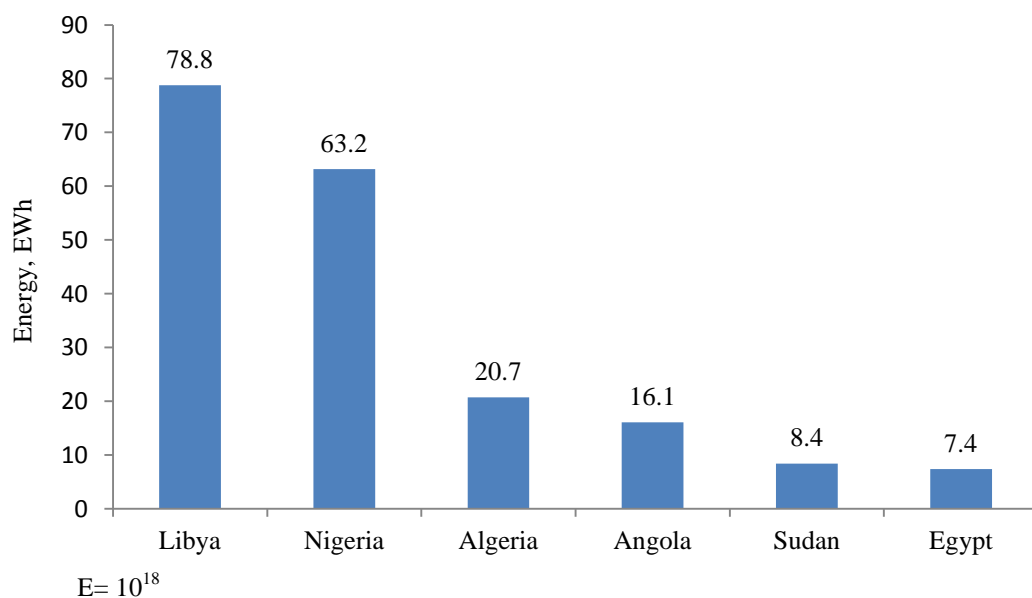
Figure 2.1 Top African proven oil reserve holders, 2011[2]

Libya had 16PWh of proven natural gas reserves as of January 2011. Some Libyan experts believe that with more exploration, reserves may possibly reach 20.4-29.3PWh. The main producing gas fields are located at Attahadi, Defa-Waha, Hatiba, Zelten, Sahl, and Assumud.

With such large natural gas reserves, Libya is looking to increase its gas exports, particularly to Europe. Libyan natural gas production and exports are increasing, with the opening of the "Greenstream" pipeline to Europe in late 2004[2]. Fig 2.2 shows the top five African Natural Gas proven reserve holders, 2011.

P= 10^{18}
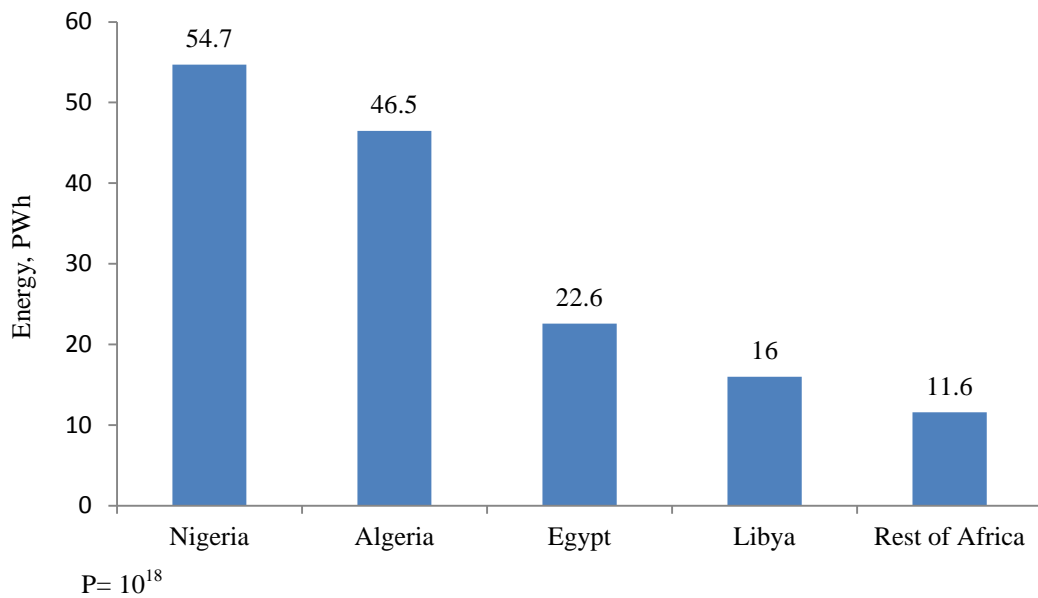
Figure 2.2 Top African natural gas proven reserve holders, 2011[2]

2.1.3 The Libyan electricity generation situation

The General Electric Company of Libya (GECOL) is totally government owned and is responsible for the operation of the entire power sector in the country. All power plants in Libya have been installed by GECOL since it was established in 1984. Fig 2.3 shows the location of the installed power plants in Libya.
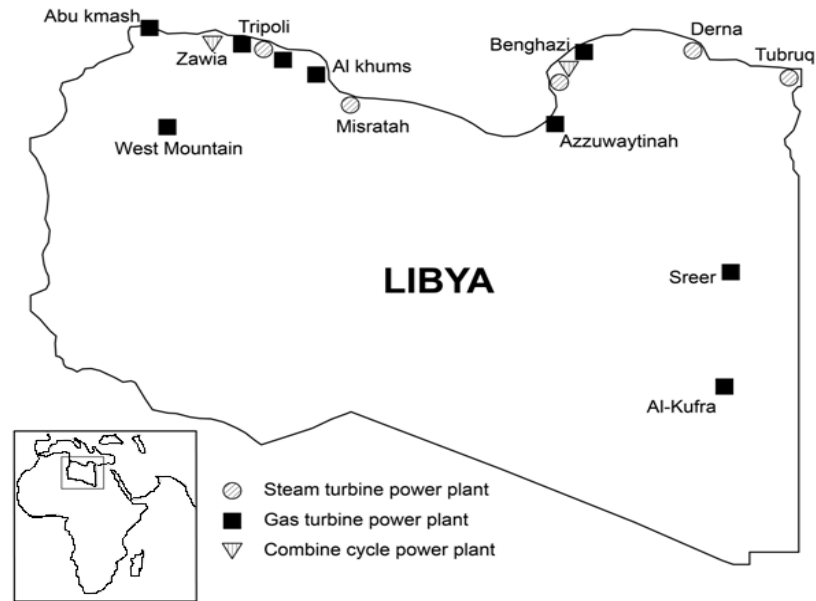
Figure 2.3 Installed power plants in Libya

Libya has a total installed power generation capacity of 6.3GW. The national electric grid consists of an ultra high voltage capacity of 400kV with a total circuit length of 442km, and a high voltage transmission level of 220kV with a total circuit length 13,677km. The sub transmission voltage level is 66kV, with a total circuit length of 13,973km. The distribution network's voltage level is 30kV with a total circuit length of 6,583km [3].

The electric energy production in Libya is provided by gas-turbine, steam-turbine and combined cycle power plants, which use heavy oil, light oil and natural gas respectively. Gas turbine and combined cycle power plants have a share of 30% and 20% respectively in total installed power capacity, the share of steam power plants is 50% in total. Furthermore, some small diesel power plants are also used to contribute to the energy supply, especially in remote areas [3, 4]. Table 2.1 list the electric power plants in Libya.

Table 2.1 Electric power plants in Libya [4]

Name of power plant	No of units	Provided by	Rated capacity, MW	Date of Commissioning	Type of fuel
Tripoli west power station/West Tripoli	5	Alsthom France	325	1976	HFO
Tripoli west power station/West Tripoli	2	Bharat Heavy Electric Ltd	240	1980	HFO&LFO
Khoms steam power plant/ Khoms	4	Deutsh Babcock	480	1982	*HFO,LFO &NG
Steel power plant/ Musrata	6	Hyundai	507	1990	HFO&NG
Derna steam power plant /Derna	2	BBC	130	1985	HFO
Tobruk steam power plant /Tobruk	2	ABB	130	1985	HFO
North Benghazi steam power plant/Benghazi	4	Babcock	160	1979	LFO
Tripoli south gas power station /Swani	5	ABB	500	1994	LFO
Khoms gas power plant/ Khoms	4	ABB	600	1995	LFO&NG
Benghazi north combined cycle power plant/Benghazi	5	DAEWOO& ABB	810	2005-06	LFO&NG
Zwitina gas power plant /Zwitina	4	ABB	200	1994	LFO&NG
Zawia combined cycle power plant Zawia	9	ALSTOM HYUNDAI &ABB	1386	2005-07	LFO&NG
Abokammash gas power plant/ Abokammash	3	WestingHouse	45	1982	LFO
Al-Kufra gas power plant/ Al-Kufra	2	Fiat Avio	50	1982	LFO
Sreer gas power plant	3	WestingHouse	45	1990	LFO&NG
Western mountain power plant	4	BHEL	624	2005-06	LFO&NG

*HFO = Heavy fuel oil, LFO = Light fuel oil and NG = Natural gas

The electrical energy consumption per capita has increased from 2276kWh in 2000 to 4000kWh in 2008. The electric energy consumption per capita in UK was 6055kWh in 2008. In contrast the world-average consumption for the year 2008 was 2876kWh [5].

The national electric network is accessible to 99% of the population. Most of the electric network is concentrated on the coast, where most of the inhabitants live [6].

Fossil fuel-fired thermal power plants are used to meet all of the electrical energy demand. In Libya all of the electrical energy demand comes from fossil-fuelled power plants. Libya's power demand is growing rapidly (around 6%-8% annually) and is therefore expected to reach 8GW by 2015 (see Fig 2.4).
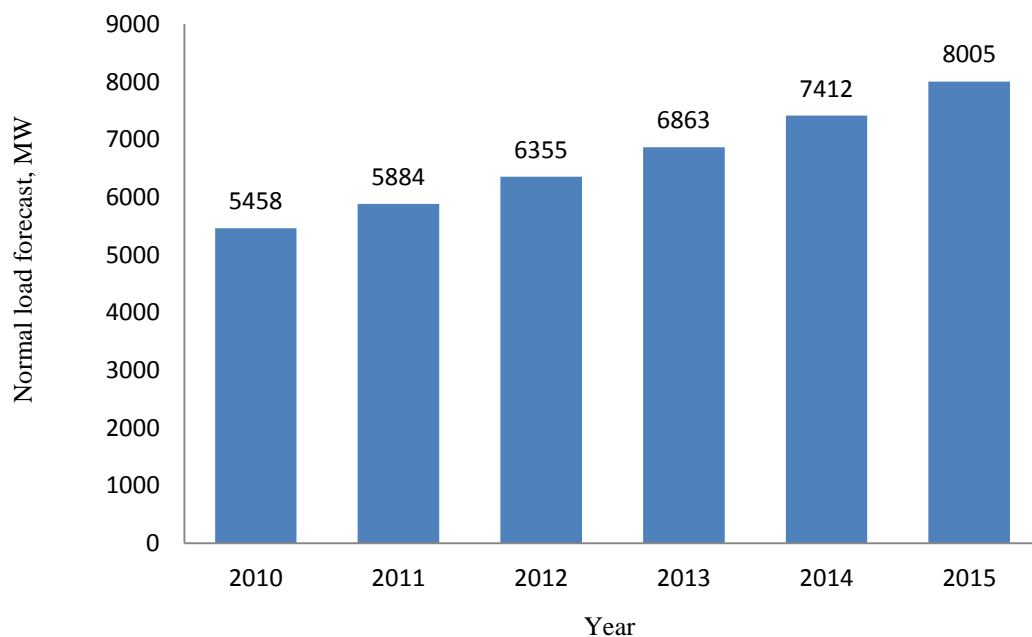
Figure 2.4 Future Libyan peak load growth to 2015 [7]

The growth in electricity power demand will out-strip production capacity and so GECOL plans to build new combined cycle and steam cycle power plants. As well as increasing generation capacity, GECOL also plans to upgrade and expand the country's power transmission grid. Table 2.2 shows the planned electricity generation infrastructure expansion [7].

Table 2.2 The future electricity- generation infrastructure expansion [7]

Under construction	Contract awarded	Planned
750MW Benghazi	750MW Sebha	750MW Tripoli East
750MW Misurata	1400MW Tripoli West	750MW Derna
312MW West Mountain	-	750MW Butraba
500MW Zwitina	-	500MW Tobruk
750MW Srir West	-	600MW Misurata
1400MW Sirte Gulf	-	-

2.1.4 Environmental impact

Libya is a signatory to the Kyoto Protocol, which is an international agreement linked to the United Nations Framework Convention on Climate Change. It sets binding targets for developed nations in reducing greenhouse gases. The main emitters of CO_2 in Libya are fuel combustion in the power generation sector, the transport sector and in industry. In total, energy-related emissions are responsible for almost all CO_2 emissions in the country. In 2003 petroleum accounted for more than 60% of carbon emissions in Libya and natural gas was responsible for around 40%. Fig 2.5 shows the CO_2 emission by sector [8].

Other sectors
34%

Electricity
generation
38%

Industry
8%

Transport
20%
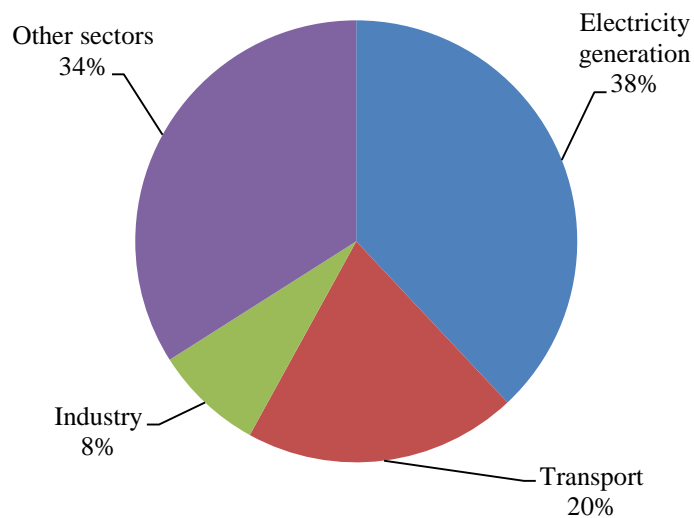
Figure 2.5 Libyan CO_2 emissions by sector for 2003 [9]

2.2 Potential for solar energy in Libya

In order to devise a system that uses solar radiation, it is important to study solar radiation in detail. A few facts on the sun, solar geometry and its radiation are given below:

- The temperature on the surface of the sun: 5780K (5510°C).
- Sun Diameter: $1.39*10^6$km.
- The mean distance between Sun and earth: 1.496×10^8km.
- The sun subtends an angle of 32 minutes 0.53° at the earth's surface.

An important point to note here is that because of the very large distance between the sun and the earth, the angle sun subtends on the earth's surface is small. Thus, the beam radiation received from the sun on the earth is almost parallel.

2.2.1 Solar radiation fundamentals
2.2.1.1 Solar constant

The sun constant $I_{sun,c}$ is the rate at which energy is received from the sun on a unit area, perpendicular to the rays of the sun, at the mean distance of the earth from the sun. It has a constant value outside the earth's atmosphere. After many experimental investigations into the value of the solar constant, a standard value of 1367W/m^2 has been established [11].

2.2.1.2 The earth and sun movement

The rotation of the earth about the sun and around its own axis is very involved and multifaceted. Over and above its rotation about its polar axis in one sidereal day and its orbital motion around the sun in a year, the tilt of the earth's axis varies from 22 to 25 degree over a period of around 41,000 years.

The greater the tilt, the more summer sunlight falls on the poles, partly contributing to glacial retreat. Furthermore, the earth wobbles like a spinning top in a cycle that lasts for 23,000 years, changing the fraction of sunlight that falls on each hemisphere.

Lastly, the earth's path around the sun alternates between a circular to elliptical orbit with a period of 100,000 years. A circular orbit results in less sunlight over the course of the year. A further point of interest is that owing to the earth's tidal drag, the day length has been slowly increasing at the rate of 21.6µs per year [10].

2.2.1.3   Solar day

A solar day is defined to be the interval of time from the moment the sun crosses the local meridian to next time it crosses the same meridian. As the earth rotates in a diurnal cycle, as well as moves forward in its orbit, the time required for one full rotation of the earth is less than a solar day by about 4 minutes.

2.2.1.4   Solar radiation at the earth's surface

Solar radiation received at the surface of the earth is subjected to the mechanisms of absorption and scattering as it passes through the earth's atmosphere and thus is not a constant value. The atmosphere at any location on the earth's surface is often broadly classified into two types an atmosphere without clouds and with clouds. In the former case, the sky is cloudless everywhere, while in the latter, the sky is partly or fully covered by clouds.

Less attenuation takes place in a cloudless sky, and as is obvious, maximum radiation is received on the earth's surface under the conditions of a cloudless sky [10].

2.2.1.5   Beam, diffuse and global radiation

Solar radiation received at earth's surface without change of direction, i.e. in line with the sun, is called beam or direct radiation. The radiation received at the earth's surface from all parts of the sky's hemisphere (after being subjected to scattering in the atmosphere) is called diffuse radiation. The sum of the beam and diffuse radiation is referred to as total or global radiation.

2.2.1.6   Solar radiation geometry

In order to find the beam energy falling on a surface having any orientation, it is necessary to convert the value of the beam flux coming from the direction of the sun

to an equivalent value corresponding to the normal direction to the surface. If θ is the angle between an incident beam of flux I_{bn} and normal to plane surface, then the equivalent flux falling normal to the surface is given by $I_{bn} \cos \theta$.

The latitude ϕ of a location is the angle made by the radial line joining the location to the centre of the earth with the projection of the line on the equatorial plane. By convention, the latitude is measured as positive for the northern hemisphere and varies from -90° to + 90°. The slope β is the angle made by the plane surface with the horizontal. It can vary from 0 to 180°.

The surface azimuth angle γ is the angle made in the horizontal plane between the horizontal line due south and the projection of the normal to the surface on the horizontal plane. It can vary from -180° to + 180°. Fig 2.6 shows the geometry of the sloped surface.
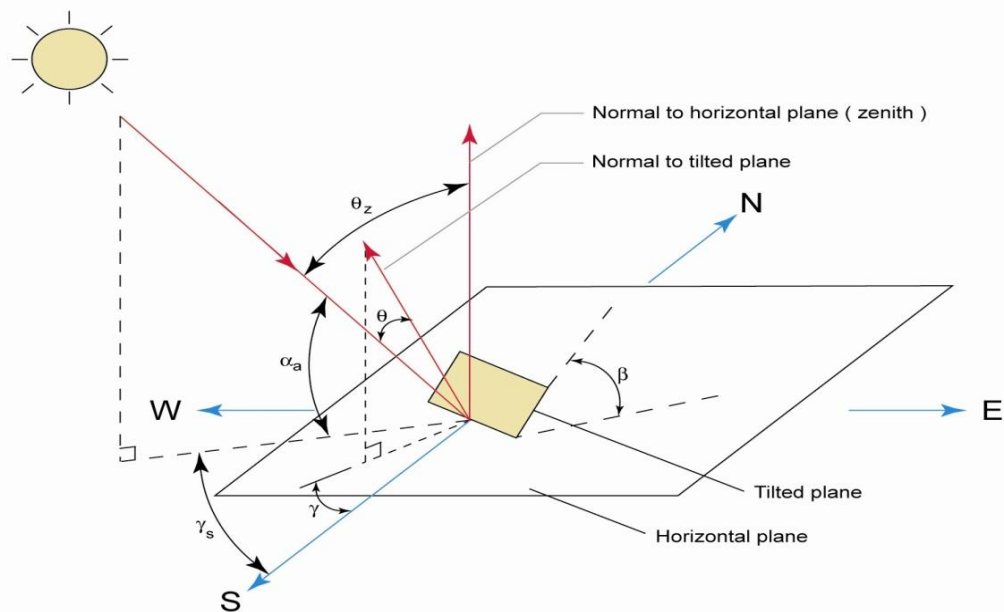
Figure 2.6 Solar geometry of a sloped surface [11]

2.2.2 The Libyan climate

At a macroscopic level, two regions of distinct Libyan weather can be identified,

1. Hot and arid Saharan desert climate
2. Relatively moderate coastal climate

2.2.2.1 Arid Sahara climate

The Sahara region of the desert makes it nearly uninhabitable and thus the bulk of the population lives near the coast. The world's highest temperature in shade (about 58°C) has been recorded in El Azizia (32.32N 13.35E) in the Sahara desert [12]. The annual precipitation moving inland from the coast declines and its variability increases. This can be quantified by the fact that the annual rainfall on the region is less than 25mm and that the world's most arid region, Sebha with only 10mm of precipitation, is in this region. In many areas, over 200 consecutive days without rainfall have been recorded and most rainfall occurs on a few days between November and January.

The Gibli, which is a major feature of Libyan climate, is the hot, arid wind that blows from the south over the entire country. This wind normally carries large quantities of sand dust, which immensely reduces visibility, turning the sky red. Gibli can occur several times a year. From a thermodynamic perspective, it's important to note that the heat of this wind can dramatically cause a drop in relative humidity within hours [12].

2.2.2.2 Coastal climate

Along the coast, the climate is cool and rainy during winter and becomes hot and dry during summer, with July and August being the warmest months. Average temperatures during the summer in Tripoli and Benghazi (that fall in the Mediterranean Zone) reach between the low 21°C and mid 27°C, and the low 16°C and mid 27°C respectively. The influence of the Saharan weather is evident in this zone and becomes stronger in the summer. Between October and March, prevailing westerly winds bring cyclonic storms and rain across northern Libya.

2.2.3 The Libyan desert

There are many good reasons for building solar power plants in the Libyan desert, firstly the prevalent solar energy income and secondly, the available area. The Libyan desert covers the entire range of Libyan longitude 11° 44' to 23° 58'E and a latitude range of 24° 17' through to 30° 3'N.

Around 88% of Libya's land area is desert, most of this area located in the heart of the sunbelt. The country is wealthy in solar radiation income with the daily average radiation on a horizontal plane being 7.5kWh/m^2/day in the southern region in Al-Kufra and 6kWh/m^2/day in the coastal region [13]. Fig 2.7 shows the distribution of average annual direct normal irradiance (DNI) across Libya and North Africa region.
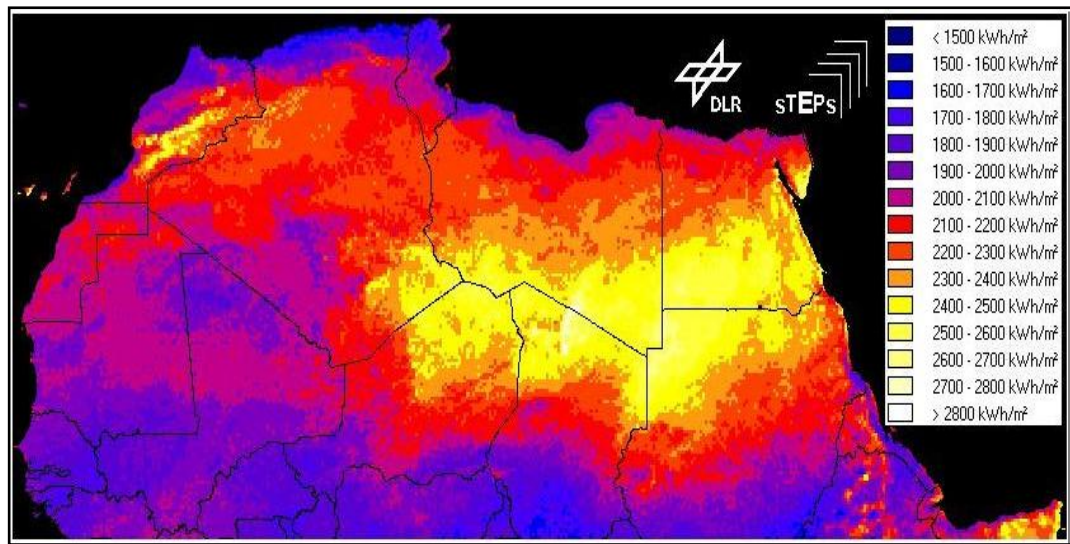
Figure 2.7 North Africa – Annual sum of Direct Normal Irradiation [14]

The number of sunshine hours amounts to more than 3500 hours per year [13]. Although the Libyan desert is truly arid and the average annual rainfall is less than 100mm over 93% of its surface area, there are however great reserves of groundwater, mostly located to the south.

There are four major underground basins, the Al-Kufra basin, Sirt basin, the Morzuk basin and the Hamada basin. The combined reserves of the first three of these basins are 35,000km^3 of water [15].

2.2.3.1　Climate in Al-Kufra

Al-Kufra is a small oasis town in the south of Libya and thus falls in the arid Saharan region. There are many technical and economic issues relating to using solar energy technologies in Al-Kufra. For example, high potential of solar energy, no cloud cover throughout the year, availability of large volumes of potable water from underground aquifers and a large flat area. With these factors it is important to study the climate of Al-Kufra.

The mean monthly values of temperature, wind speed and relative humidity are illustrated by Fig 2.8. The maximum average wind speed is about 5m/s in June and the minimum value is 3.8m/s in December. It is clear from Fig 2.8 that the wind speed is most active in summer and autumn season when conditions are appropriate for solar energy capture. The average maximum temperature in Al-Kufra is 34.9°C in August, while the minimum is 14.5°C in January. As shown in Fig 2.8 the humidity is low throughout the year, i.e. in January the relative humidity is 39.9% but in July it is 18.8%.
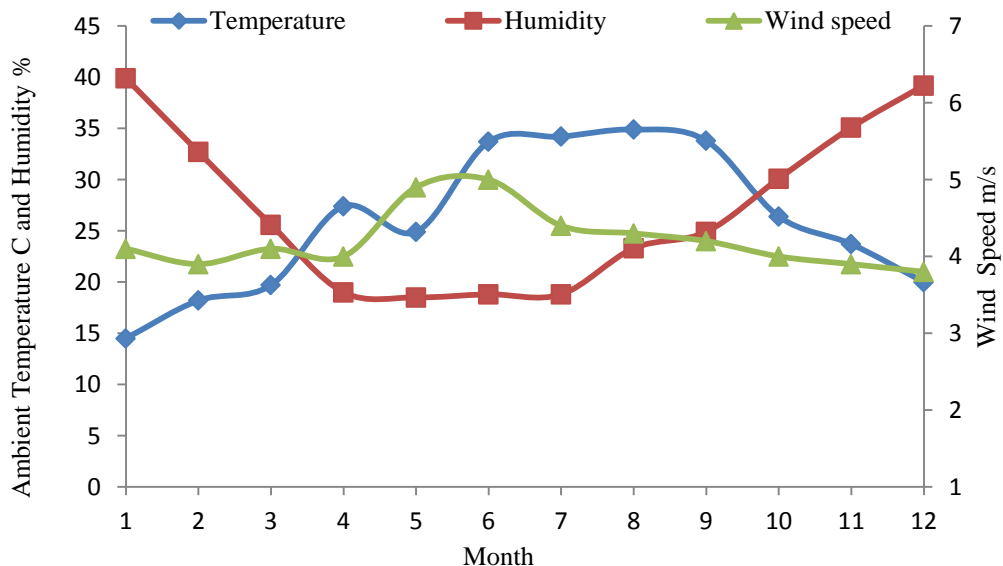
Figure 2.8 Monthly average ambient temperature, relative humidity and wind speed for Al-Kufra

2.2.4 Technical know-how

Libya has a well documented history of undertaking large scale engineering projects as demonstrated by the following:

2.2.4.1 Al-Kufra agriculture project

Libya launched, in the early 1970's, a cultivation project in Al-Kufra aimed at developing agriculture in the desert. Low Energy Precision Application (LEPA) type irrigation draws its water from beneath the ground surface. By 1972 the target area had been raised to 50,000 hectares. Rotating sprinklers provide the irrigation in circles of up to 1km diameter that are large enough to be seen from space [16].

2.2.4.2 Industrial river project

The Great Man-made River Water Supply Project is one of the world's largest civil engineering projects. Eventually over 6.0 million cubic meters of water will be conveyed every day from well fields deep in the Sahara desert to the population centers that are concentrated on the northern coastal strip. Concrete pipes of 4m diameter run for over 1500km to convey the water.

The Great Man-made River Project is totally dependent on the abstraction of groundwater basins to supply the water, and the majority of this water was collected arround 38,000 years ago, though some pockets are only 7,000 years old. The project has five Phases; Sarir-Sirt,Tazerbo Benghazi System, Jabal Hasaouna-Jefar System, Gadabiya/Sedada System, The Gedammes/Zwara System and Al-Kufra/Tazerbo System Jagboub/Tobruk System [17].

2.2.4.3 Photovoltaic (PV) application within the rural sector

PV systems were first used in Libya in 1976 and since then the number of application types and their role has grown considerably. The first system was one which supplied cathodic protection for an oil pipe line. Communication systems deployed PV systems from 1980, the first being used to supply energy to a microwave repeater station near Zella. Other applications include water pumping, rural electrification and illumination [9].

The first system was commissioned in 1976. The total number of PV systems in this field was around 320 by the end of 2006, with a total installed capacity of 650 kWp.

GECOL has installed 340 PV systems with total capacity 220kWp. Also the Sahara desert Center and the Centre of Solar Energy Studies (CSES) have installed 150 PV systems. Problems facing the electrification of all regions in any country are low population and remoteness from the electric networks. It is expensive to extend high voltage lines through the desert to provide electricity for a few hundred inhabitants.

Figure 2.9 Wade Marsite PV Central Plant [9]

Water pumping was considered one of the best PV applications in Libya at remote wells which are used to supply water for human and animals in rural places. The water pumping project consists of installing 40 PV systems with a total estimated peak power of 120kWp [9].

2.3 Concentrating solar power plant (CSP)

Concentrating Solar Power (CSP) as the name suggests, involves gathering solar radiation from a large area and focusing it on a narrow area high temperatures. Note that all such thermal applications are generically classified as CSP within the scientific literature.

CSP plants use the heat from solar radiation and represent solutions for generating electricity on a large scale that can supply several hundred thousand households.

There are different types of CSP technologies that use the heat contained in sunlight. The CSP techniques are: solar tower, parabolic dish and parabolic trough. Large scale use of solar energy for electricity production is currently in the demonstration phase. The plant area requires large unshaded fields and hence is feasible in sites with a plain terrain.

The technology has been existent for more than two decades, however in the late 1990's, it saw a decline in its popularity. Under the current economic climate, global warming scenario and with the Kyoto protocol treaty implemented, it has been picked up again and is seeing major investments at present as well as in the near future.

CSP plants vary in size and can be designed with capacities from 5MW to several hundred MW. The current world annual electricity consumption of 18000TWh could be met through CSP, which has a technical potential of 3,000,000TWh [18]. The potential areas for CSP in the Sahara desert have already been mapped out in the DESERTEC project. This project has seen an investment of 400bn Euros, and once completed, it will have the highest electricity production capacity through CSP plants in the world [19].

The Trans-Mediterranean Renewable Energy Cooperation (TREC) was founded in 2003 by The Club of Rome, the Hamburg Climate Protection Foundation and the National Energy Research Center of Jordan (NERC). TREC developed the concept of DESERTEC and has undertaken research in cooperation with the German

Aerospace Center (DLR). The DESERTEC, concept is to combine the large and technically accessible source of energy in the deserts with existing technology to improve global security of energy, water and the climate.
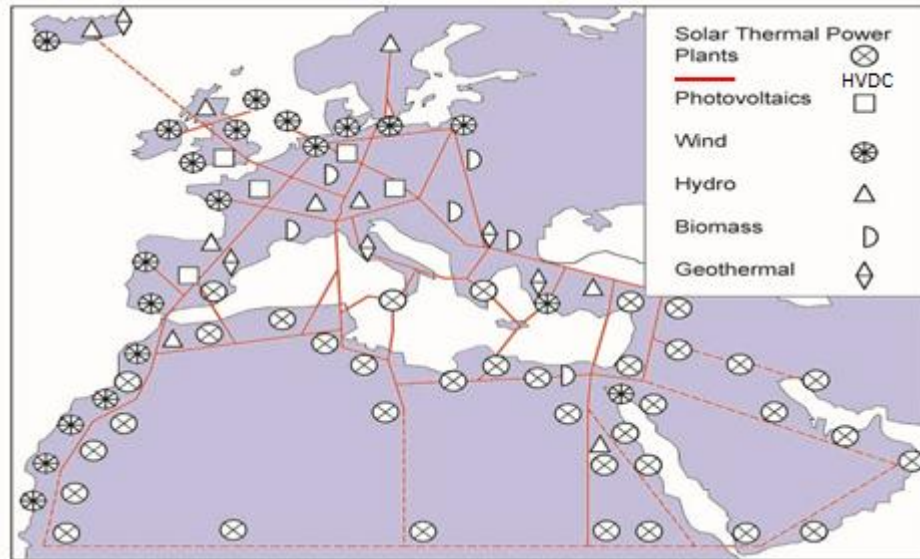
Figure 2.10 The DESERTEC Concept [20]

Europe, the Middle East and North Africa (EU-MENA) are being urged to cooperate in the production of electricity and desalinated water in the MENA deserts using the available resources and technology; CSP and wind turbines.

These technologies can not only meet the growing demand for electrical energy and fresh water in the MENA region itself, but also produce excess electrical power that can be transmitted via High Voltage Direct Current (HVDC) transmission lines to Europe, Fig 2.10 refers [20].

Lessons learnt from pilot projects will be of benefit for implementation of future power plants. Key examples of such pilot projects are now presented.

There are nine commercial parabolic trough plants with capacities from 30 to 80MW in the Mojave Desert in California, USA. These are collectively known as Solar Energy Generating Systems (SEGS) and were built from 1985 through to 1991. They have a combined capacity of 354MW, see Fig 2.11.

Figure 2.11 View of SEGS trough based solar thermal power plant in southern California [21]

A Commercial scale Dish Sterling power plant has been installed with a capacity of 5MW in Maricopa, USA in 2010 [18].

Spain has also been highly active in the development of solar thermal power plants. In 2004, Spanish legislation considerably improved the incentives for the first 200MW of CSP, fostering the development of this technology [18].

In 2008, the German Solar Power Group GmbH and the Spanish Laer S.L. embarked upon the joint installation of a solar thermal power plant in central Spain at Gotarrendura, a small renewable energy pioneering village, about 100km northwest of Madrid. This is based on the Fresnel collector technology of the Solar Power Group. The size of the power plant is 10MW and it combines a solar thermal collector with a fossil-fuelled co-firing unit as a backup system.

In 2010, 12 extra 50MW CSP plants have been either put into operation or will be shortly commissioned in Spain [18].

Another example is in the Andalucian desert of southern Spain, where a 20MW CSP plant has been installed. Over 1,200 heliostat mirrors, each with a collecting area of

$120m^2$, track the sun as it moves throughout the day and reflect the sunlight to the top of a 160m tower at the centre of the field. Steam is then generated which drives a steam turbine-generator set [22].

Egypt has completed its first utility-scale solar-thermal project in Al- Kuraymat. The plant has a capacity of about 140MW, 20MW from solar sources combining with a conventional fossil fuel portion of 120MW. The power plant consist of a parabolic trough collectors with total area about $130,800m^2$ capable of generating about $64MW_{th}$ of solar heat at a temperature of 393^oC [23].

In Algeria, a 150MW Hybrid solar natural gas power plant is being built in Hassi R'Mel. This power plant is designed to use 89% natural gas energy and 11% solar energy.

Morocco, has signed an agreement with Abengoa and ONE to build a 470MW CSP power plant at Beni Mathar. Table 2.3 shows the characteristics of the CSP plants built or under construction in Egypt, Algeria and Morocco [24].

Table 2.3 Main characteristics of CSP plants built or under construction in North Africa [24]

Location	Hassi R'Mel (Algeria)	Ain Beni Mathar (Morocco)	Kuraymat (Egypt)
Average solar resources (kWh/m^{2}year)	2500	2290	2431
Owner/Developer	SPP1[a]	ONE	NREA
Constructor	SPP1	Abengoa Solar	Iberdrol/Mitsui(CC) & Orascum/Flagsol
First year of construction	2007	2008	2008
Operator	SPP1	Abengoa Solar	[b]
Power utility	Sonatrach	ONE	EEA
First year of operation	2009	2009	2010
Overall output capacity (MW$_e$)	150	470	140
Net solar output capacity (MW$_{th}$/MW$_e$)	95/25	[b]/20	61/20
Solar field aperture area (km^2)	0.18	0.187	0.13
Solar field outlet temperature (^{o}C)	393	393	393
Steam turbine capacity (MW$_e$)	70	[b]	76
Gas turbine capacity (MW$_e$)	80	[b]	73

[a] Solar power plant 1, Abengoa(66%) and NEAL (34%) joint venture
[b] Unavailable data.

CSP plants can be used in many industrial applications, however at present CSP plants are used normally for electricity generation. One of the most important boundaries for choosing the most suitable technique for any proposed application is the operating temperature [25] as shown in Fig 2.12.
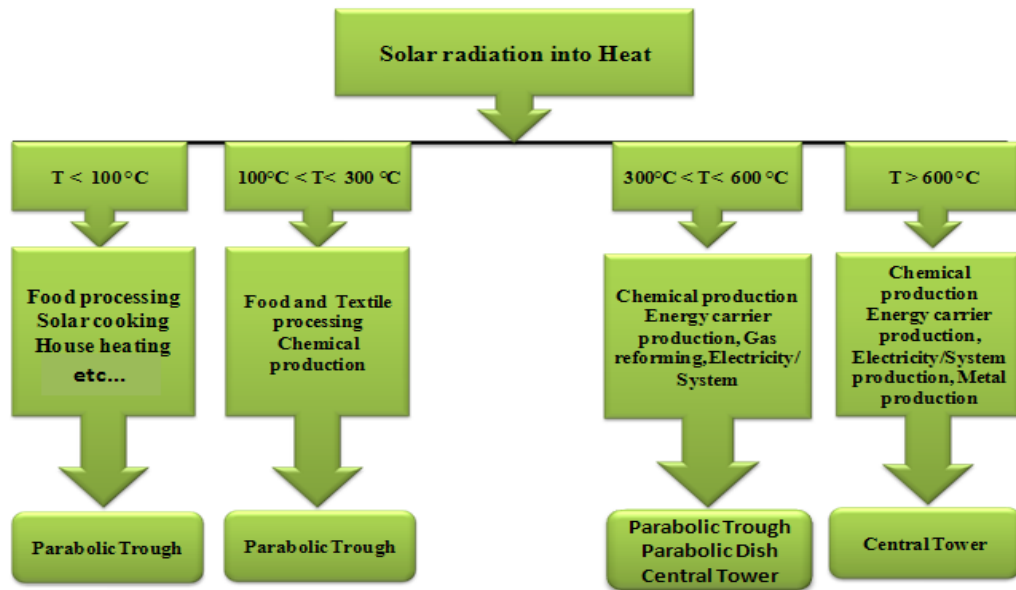
Figure 2.12 Applications of CSP [25]

2.3.1 Linear Fresnel System (LFS)

The Linear Fresnel-technology is a line-focusing type of CSP which is based on arrays of Fresnel reflectors which direct the sunlight to a several-meter high receiver. Usually, single-axis tracking of the flat mirrors is fixed on steel structure. Many frames are connected to each other to form modules along a row up to 450 meters long (see Figs 2.13 and 2.14). The receivers consist of either one metal tube or many tubes that are located above the mirrors at a predetermined height and coated by a heat-absorbent similar to that is used in parabolic trough technology to increase the heat absorption. Water, or occasionally a mixture of water and steam, flow inside the tubes, then the steam and water are separated at the exit of the tubes. Steam is then generated which drives a steam turbine-generator set. The Fresnel-technology has several technical advantages over the well-recognizable parabolic trough technology. Steam can be either generated directly without an intermediate Heat Transfer Fluid (HTF) or by a binary steam cycle. In addition, the Fresnel-technology more easily lends itself to factory production, which means less field construction is required [26].

Figure 2.13 The MAN linear Fresnel demo collector erected on the Plataforma Solar de Almería (PSA) [26]
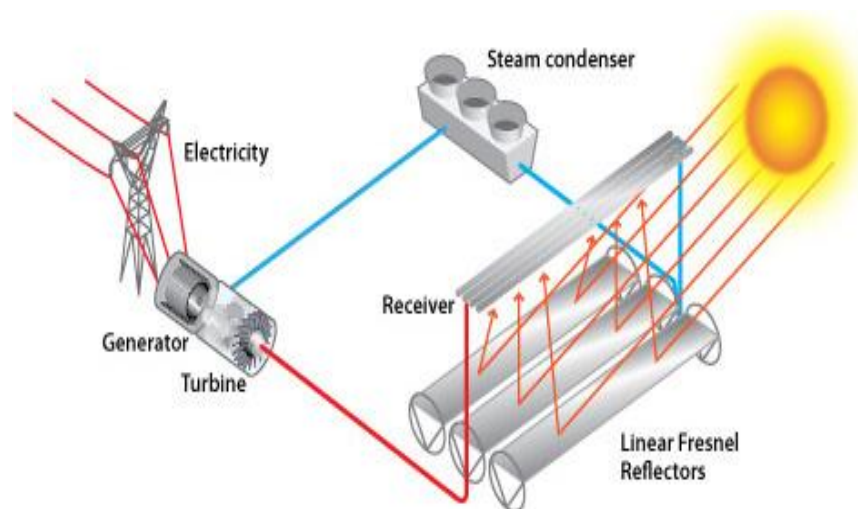
Figure 2.14 A linear Fresnel reflector power plant [26]

However, Fresnel-technology is much less grown-up and the lower steam temperature decreases the turbine efficiency. Furthermore, due to the absence of insulation around the recovery tubes, and the lower optical efficiency, heat losses are increased.

In Spain (Plataforma Solar de Almeria) a 800kW Linear Fresnel pilot system operating at 450 $^{\circ}$C has been tested with components developed by Solar Power Group and it is expected to be commercially viable by 2012. According to the

ATKEARNEY report 2010 [18], by 2015 Linear Fresnel can be expected to be operating with superheated steam at 500°C with an efficiency increase up to 18.1% relative to current operation with steam at 270°C.

2.3.2 Dish Stirling System (DSS)

Dish Stirling System (DSS) technology converts thermal energy to electricity by using a parabolic dish mirror to concentrate the solar radiation on an engine-generator set in the focal point of the reflector. The engine can be a gas turbine or a Stirling engine. The typical diameter of the parabolic dish varies from 5 to 15m with an output of 5 to 25kW [27]. This technology is suitable for decentralised power supply and remote locations. DSS technology presents the highest efficiency of CSP systems, the average annual engine efficiency reached 23% for a medium Direct Normal Irradiation (DNI) location Spain and 27% on high DNI locations like the USA. Fig 2.15 shows a parabolic dish solar collector.
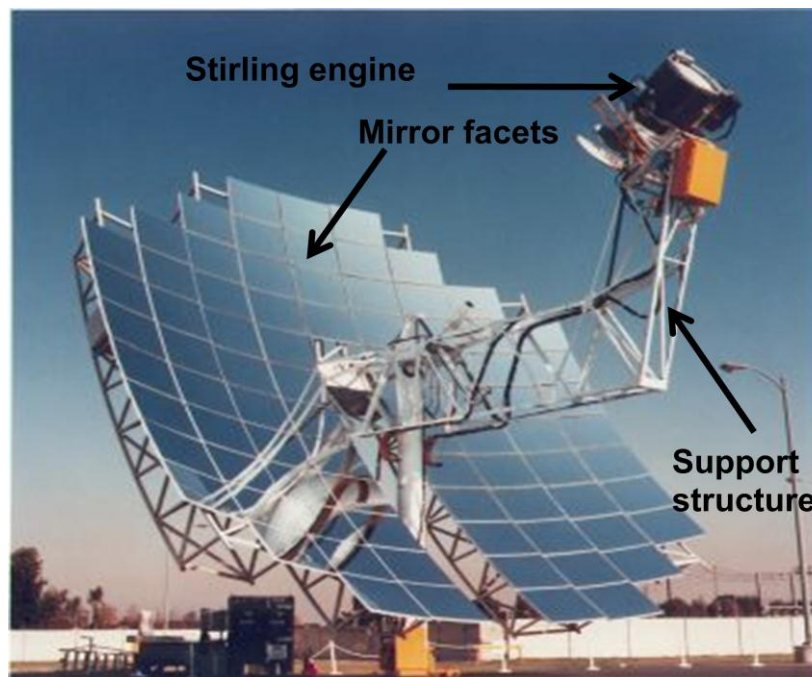
Figure 2.15 Dish Stirling System [28]

By 2015 and 2025, Stirling engine manufacturers improvements under development may contribute to an engine cost reduction of 20% and 35% respectively.

Furthermore it is expected that by 2015 improvement in the shaping mirror will reduce costs for DSS mirrors by 20% [18].

2.3.3 Solar Tower System (STS)

In the Solar Tower System (STS), solar radiation reflected from an array of large mirrors is concentrated on a receiver situated at the top of a supporting tower. After the initial commissioning of eight such plants in the 1980's, despite showing feasibility, they were not (deployed) commercially. These systems, also called the Power tower, in the current economic climate and depleting fossil fuel scenario have seen a resurgence in Europe recently. Fig 2.16 shows two types of solar thermal tower power plant, showing (a) an open volumetric receiver with steam turbine cycle and (b) a pressurized receiver with combined gas and steam turbine cycle.
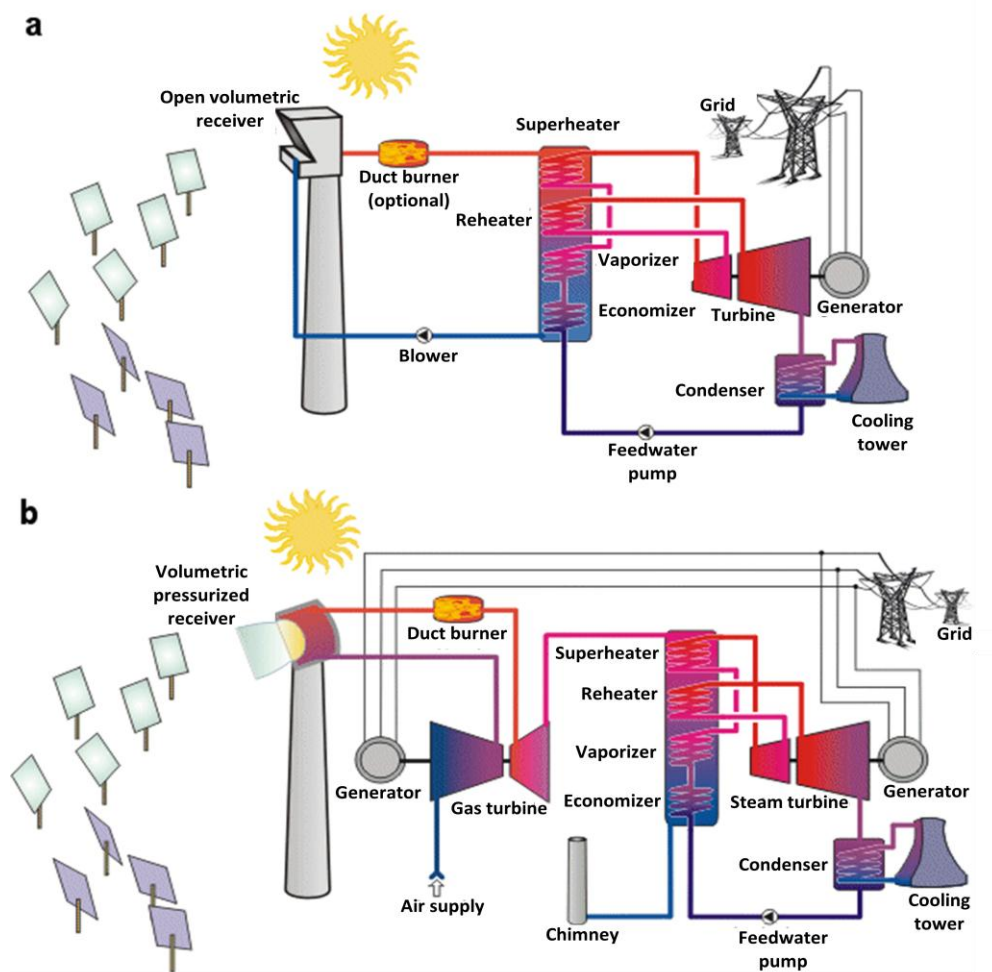
Figure 2.16 Schematic of two types of solar thermal tower power plant, showing (a) an open volumetric receiver with steam turbine cycle and (b) a pressurized receiver with combined gas and steam turbine cycle [29]

The large mirrors are called heliostats and their orientation can be controlled individually throughout the day thus reflecting beam radiation onto the receiver. A Large heliostat has an aperture area of 62 to $120m^2$. By 2012, sizes for large heliostats are expected to increase up to $150m^2$. Consequently, the total number of tracking system drives would decrease [18]. The most recent plant to be completed was PS10 in Spain which started commercial operation in March 2007. A few details of the plant are tabulated below in Table 2.4.

Table 2.4 PS10 details [30]

Output	$10MW_e$
Number of heliostats	624
Area of heliostat	$120m^2$
Receiver fluid	Water
Thermal storage medium	Water
Tower height	115m

A similar STS, PS20, was put into operation in Spain with a capacity of 20MW. Fig 2.17 shows solar tower technology, PS20.
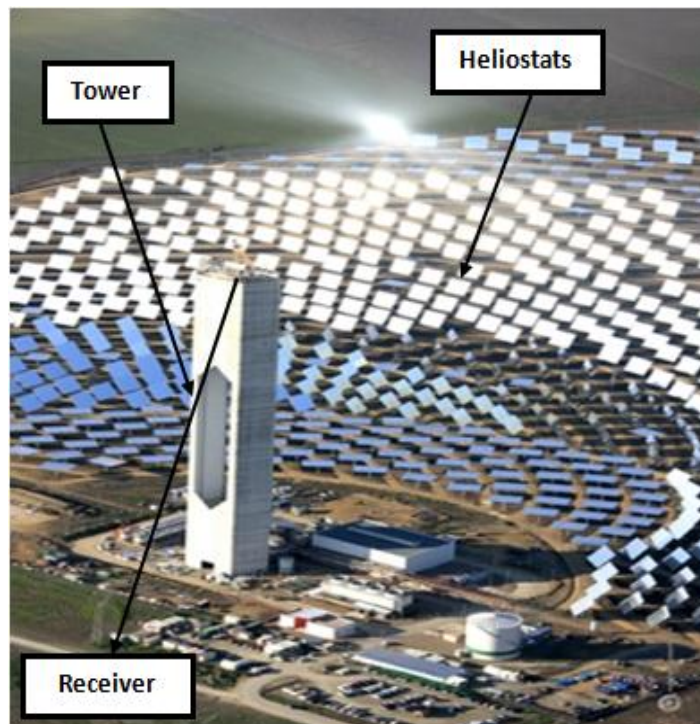
Figure 2.17 Solar tower technology, PS20 [30]

PS10 uses saturated steam that can reach temperatures in the order of 250°C. According to ATKEARNEY report 2010 [18], Abengoa Solar and Brightsource are currently developing receivers to be operating with superheated steam up to 540°C and boost efficiency by 28%.

2.3.4 Parabolic Trough System (PTS)

The following section presents a review of PTS through the projects which have been built during the past century, as well as the applications currently under development.

PTS uses a very large curved-shaped mirror similar to a parabolic reflector. The parabolic trough collector (PTC) is usually made of plastic films, glass silver mirrors and also polished metals. The absorber tube, (through which the liquid to be heated flows) is located at the focal axis. The glass envelope of a receiver tube has to be airtight-bonded to the steel pipe in order to maintain receiver's vacuum that prevents a loss of heat from the steel pipe and protects its special coating.

This absorber tube uses a special coating to maximize heat absorption and minimize heat losses. Two designs are currently in use, the older design in which oil is used as the primary heat collection medium along with a secondary water/steam circuit and a more modern direct steam generation system.
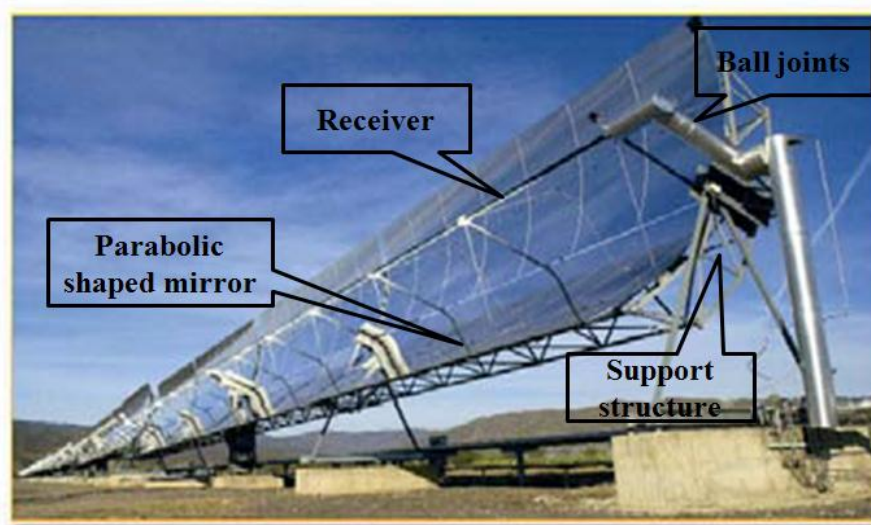
Figure 2.18 Parabolic trough system [22]

In the following section details of the Solar Electric Generation System (SEGS) using PTCs is presented.

2.3.4.1 Solar Electric Generation System (SEGS)

In our study of solar thermal power plants, it will be valuable to look at the Solar Electric Generation System (SEGS). These plants operate by aligning the parabolic trough collectors in the north-south axis. Collector tubes are made of stainless steel with selective coating applied. The pipe is encased inside a vacuum tube. Synthetic oil is heated up by these collectors to temperatures of 390°C and this oil is then used to run a Rankine cycle of 38% efficiency.

The plant produces electricity from sunlight for 8 hours a day and for continuous operation it is coupled with Natural gas. The last Large scale SEGS plant was erected in 1991 and because of its high capital cost at the time no new large size plant were erected [31].

2.3.4.2 Parabolic Trough Plant Configurations

Solar trough systems can be broadly classified into two categories in terms of operation, namely Solar only mode and Hybrid mode. In Solar only mode heat from the solar field is used to operate the thermal cycle and a thermal storage facility ensures operation stability after daytime. Hybrid systems commonly utilise boilers that run on fossil fuel for stability and night time operation. Details on both these operating modes are given below.

A. Solar only mode

In this configuration, the only energy resource running the thermal plant is the solar field, there is no fossil fuel boiler for backup or assistance. Thus to maintain stability, a thermal storage system is needed.

The average solar-operating hours are 10-12 hours during the summer and therefore, for the remaining time, the plant is operated by energy from thermal storage. Normally, the solar field starts running from sunrise to supply heat for the energy cycle. When the solar radiation is at its peak, the excess part of the energy supplied

by the solar field is fed to the thermal storage system. This excess energy can be harnessed for about 2-3 hours.

When solar energy is not sufficient to run the Rankine cycle, the storage system starts to supply some energy to the thermal cycle. After sunset the plant runs completely on the storage system.

Two power plants with a capacity of 50MW each are planned to be constructed in Spain with Solar only mode using molten salt in their planned thermal storage system. Fig 2.19 shows a solar thermal power plant with a thermal storage system.
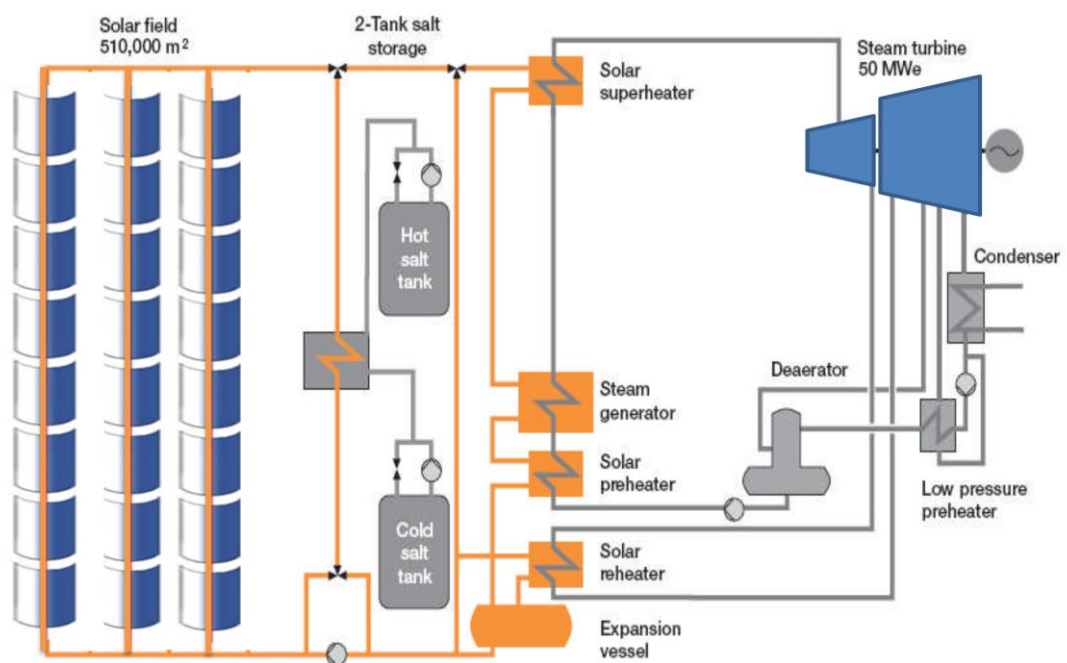
Figure 2.19 Solar thermal power plant with thermal storage system [31]

B. Hybrid systems

In hybrid systems backup fossil fuel boilers are used in parallel with the solar field to guarantee reliable operation at night-time or when no solar radiation is available. Figure 2.20 shows a hybrid solar trough power plant.
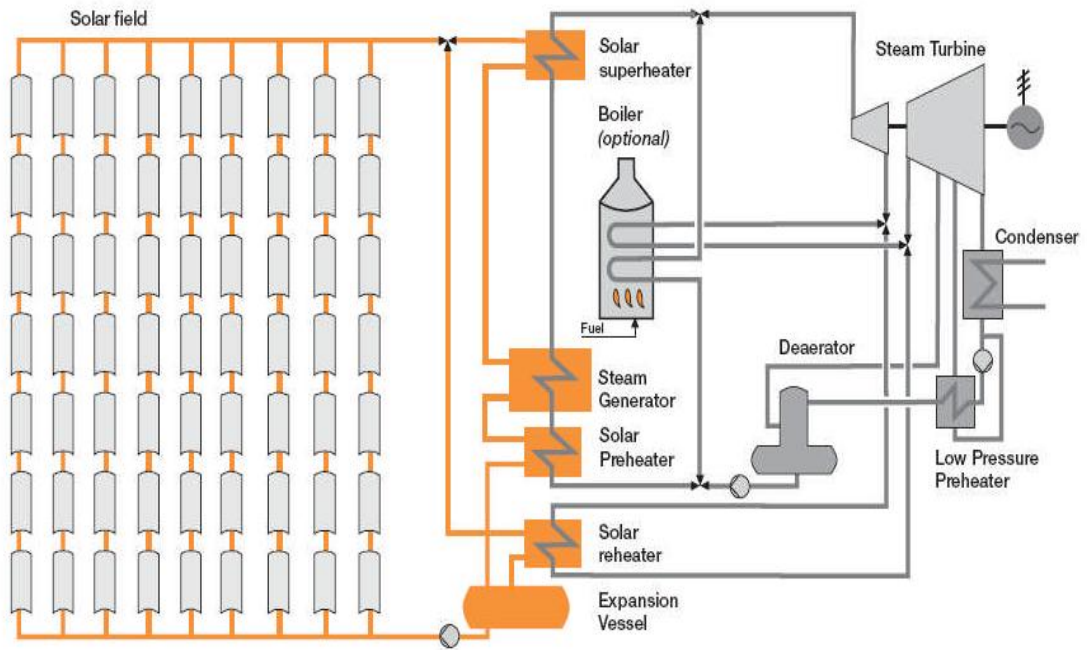
Figure 2.20 Solar trough system with fossil fuel backup [32]

These systems are comparatively flexible and stable. Many configurations have been introduced for hybrid systems and there can be more than one boiler. They can be used as or with an economiser, evaporator or superheated in the thermal cycle. Moreover in the hybrid systems one solar field or more is allocated in different positions either to heat the feed water or superheat the steam [33].

Currently, all the above mentioned commercial solar power plants use heat transfer fluid (HTF). With acceptable performance, temperatures of HTF cannot reach values as high as 400°C due to decomposition at higher temperature because the HTF is organic (benzene) based, according to ESTELA [18]. To avoid this obstacle, researchers and developers are focusing on the development of alternative fluid technology, for instance direct steam generation.

C. Organic Rankine Cycle

ORC power cycles are primarily used for lower temperature heat sources, such as geothermal orwaste-heat recovery. The low resource temperature results in low efficiency of the ORCs; however, ORCs can be designed to operate at substantially higher efficiencies for trough systems. Fig 2.21 shows the basic organic Rankine cycle [34].

Hundreds of megawatts of ORC power systems have been installed around the world. ORCs use organic (hydrocarbon) fluids that can be selected to best match the heat source and heat sink temperatures. They can use air-cooling instead of the evaporative wet cooling typically used at steam Rankine cycle plants. The hydrocarbon working fluids function like steam in the steam Rankine cycles. However, the ORC fluids are generally used at lower pressures. For safety reasons these fluids are condensed at above-atmospheric pressures. These factors greatly reduce the complexity and cost of ORC systems. In addition, smaller ORC systems can generally be run remotely, and they only periodically need on-site operator or maintenance intervention.
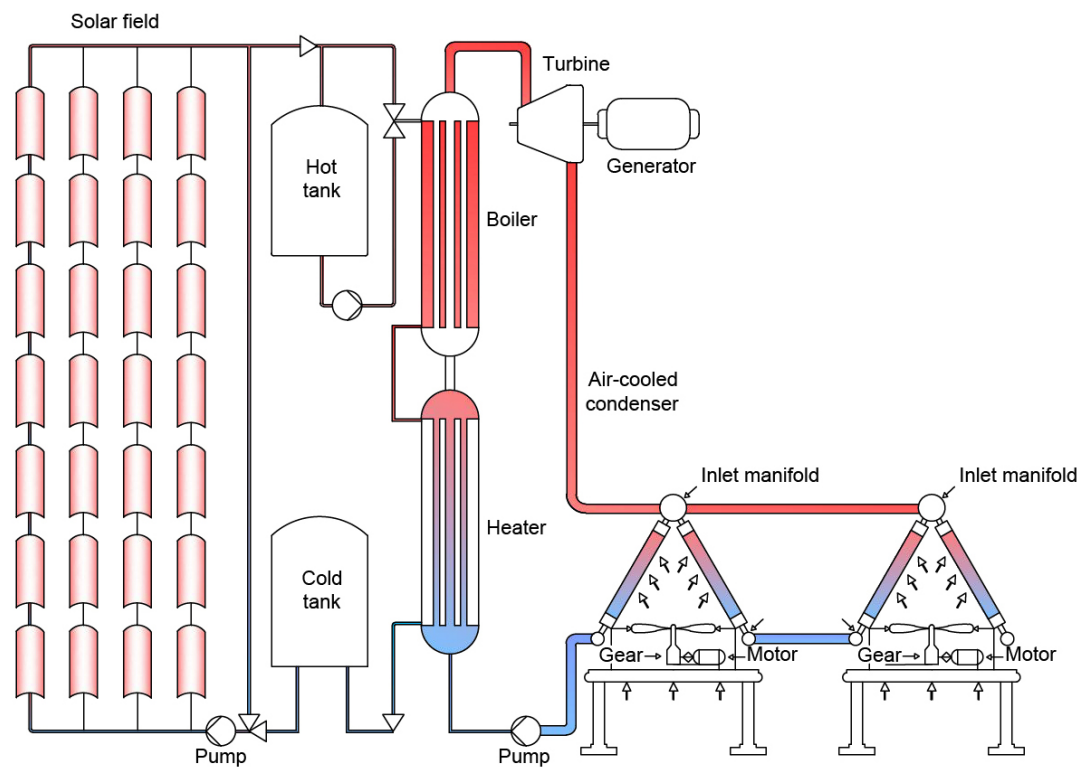
Figure 2.21 Basic Organic Rankine cycle [34]

The following are the primary advantages of an ORC power cycle for applications with troughs.

1. ORCs operate at lower temperatures; thus, the trough's operating temperatures can be reduced from 390°C to 304°C.

2. ORCs can be designed to use air-cooling for the power cycle. This, and the fact that the power cycle uses a hydrocarbon for a working fluid (instead of steam), means that the plant needs virtually no water to operate.

3. ORCs power cycle are simple and generally can be operated remotely.

It should be pointed out that ORC systems have a number of disadvantages as well. ORC systems generally have lower efficiencies than steam cycles that run at higher temperatures and pressures. However, the efficient steam cycles (approximately at 35% net) come at the price of more capital investment and the need for higher resource temperatures. The use of air-cooling means that ORC cycles are negatively impacted by high ambient temperatures [35].

D. Direct Steam Generation (DSG)

In a direct steam generation system (DSG), as the name suggests, steam is generated directly inside the absorber tube in the parabolic trough as opposed to indirect heating by HTF such as a synthetic aromatic fluid. The feasibility of DSG technology was demonstrated within the Direct Solar Steam Generation System (DISS) project funded by the European Union [36]. A collector loop with a length of 500m was erected at Plataforma Solar de Almerıa (Spain) which has now operated for more than 6000 hours.

For DISS, three different operating concepts have been studied namely the once-through mode, the recirculation mode and the injection mode of operation. It has been reported by Eck et al [36] ,that the recirculation concept proved to be the most stable and reliable mode of operation. This concept divides the collector loop into two parts, a combined pre-heating/evaporation section and a superheating section. The former is run with a water surplus in order to guarantee sufficient cooling of the absorber tube walls. The excessive water is removed from the steam by means of a phase separator and pumped back to the inlet of the loop through the recirculation line.

Based on the recirculation mode, design of a first pre-commercial power plant has been developed as a part of Integration of DSG Technology for Electricity Production (INDITEP) project [37] . The field, operated in recirculation mode,

consists of seven parallel rows with 1000m length each. For the phase separation at the end of the evaporation section each row is equipped with a compact field separator from which the water is drained to the buffer tank [37]. Compared to a central separation vessel used by all rows together, a reduction of thermal inertia, materials consumption and pressure loss over the whole loop is expected as long as the size of the field separators can be kept small.
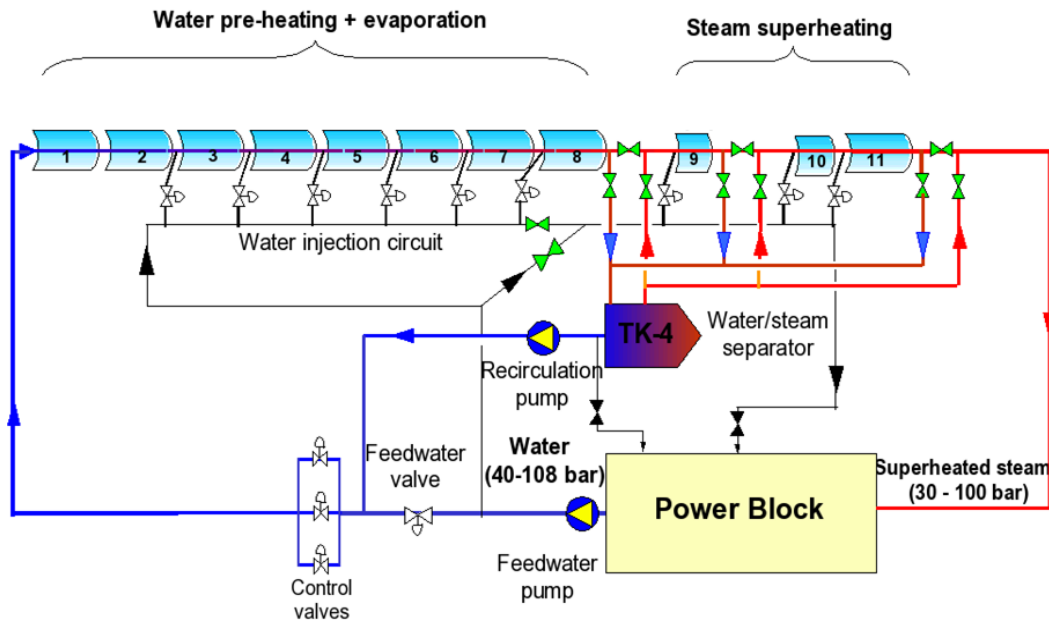
Figure 2.22 Schematic Diagram of a DISS facility at PSA [38]

Figure 2.23 DISS test loop at the PSA [24]

In addition to the PTCs, a DISS facility is composed of the following components:

- A Water-steam separator, only used in recirculation operational mode.

- Pumps for Feedwater and recirculation. The former pumps subcooled water into the row and the latter drains saturated liquid water from water-steam generator.

- Injectors are actuators to control temperature by injection of subcooled water from the injection line.

- Valves to let the system be configured in any of the three main operational modes and for control purposes.

- A Power Block a component representing any possible load process consuming the regulated outlet of thermal power from the plant. In this case, for water conservation during the experiments, the current implementation returns the thermodynamically state of the outlet superheated steam to subcooled liquid to be pumped by feedwater pump.

The main purpose of DISS Phase II (1998–2001) was experimental research on the three basic DSG processes (once-through, injection and recirculation) to find out which was the best for a commercial DSG plant. Experimental results showed that recirculation is the most feasible option for commercial application, regarding financial, technical and O&M related parameters [38].

- ***Once-Through.*** Lowest investment costs, least complexity and best performance, although great controllability problems and instabilities during operation. The system works as a distributed once-through boiler fed with subcooled water and superheated steam at outlet, at nominal operating conditions.

- ***Injection***. Better controllability and less instability, although highest investment costs. The system works as a once-through evaporator in which, at certain points in space, an injector arrangement help to control spatial temperature distribution along the whole row.

- ***Recirculation***. Better flow stability and better controllability, although second highest investment costs. In this mode, the water-steam separator placed in the row decouples two effective once-through evaporators: the first one is a flooded evaporator and the second is a dry-expansion one.
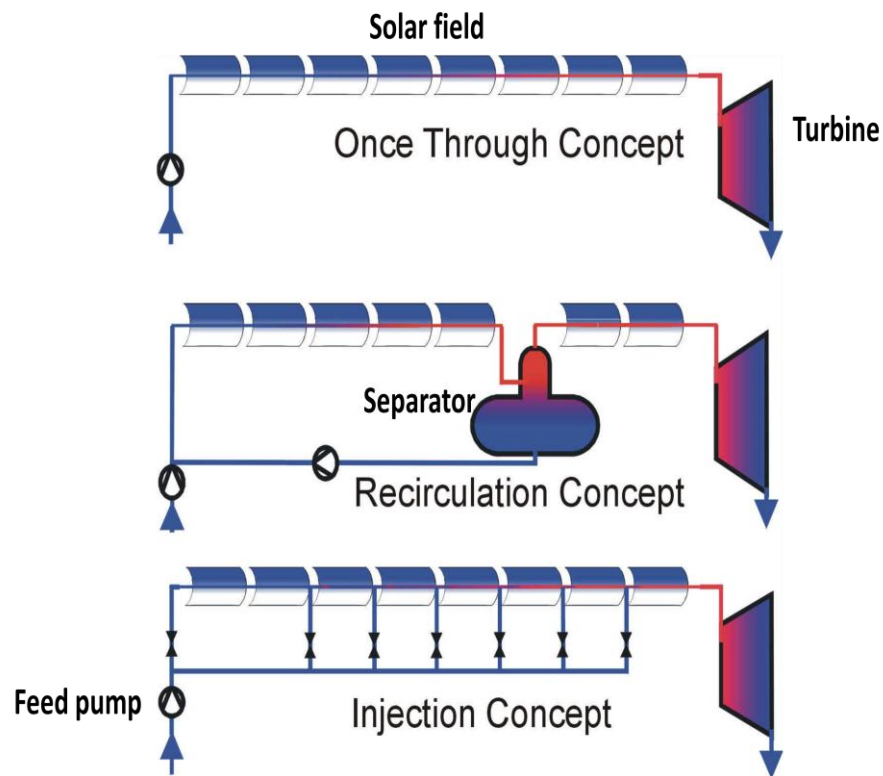
Figure 2.24 Direct steam generation in parabolic trough technology [38]

After operating the test facility for more than 5500 hours, the most important conclusion was the certainty that DSG is technically feasible in PTS with horizontal absorber tubes. Although several studies have been done for the commercial use of the DSG technology, the DSG has advantages and disadvantages when considered for operation, the advantages are examined as the following:

- Elimination of the environmental risks of the heat transfer fluid.
- DSG would enable higher operating temperatures over the current limit of around 400°C imposed by HTF which degrades at temperatures higher than 400°C.
- Increasing plant efficiency because the HTF/steam heat exchanger is unnecessary.
- DSG design is simplified and also maintenance and operation costs are reduced by eliminating the heat exchanger and auxiliary HTF systems.

These advantages combine to decrease the cost of the power produced by about 15% [32].

In the last three decades commercial projects have not opted for DSG due to the following disadvantages:

- DSG has a high operating pressure, this requires equipment which increases costs.
- Control systems are complex and expensive due to the two- phase flow inside the absorber tubes and the different thermophysical (transport) and thermodynamic properties.
- The instability in the steel absorber tubes due to thermal stresses.

In a common heat exchanger, where energy is being exchanged between two fluids, the temperature profile at any given cross section is quite uniform, barring the small temperature gradient across the thermal boundary layer. When one considers heat exchangers such as a water-tube boiler of a large power plant, there may be slight asymmetries of heat flux on the circular tubes due to the presence of radiant fields, such as heated walls of the boiler as well as radiation exchange from neighbouring water-tubes. A good discussion of such asymmetric radiation fields has been provided by Muneer et al [39].

In contrast, a parabolic solar flux concentrator that is presently the subject of discussion poses an interesting challenge for the receiver tube.

References are made herein to the work of Cheng [40] and Flores [41]. In the work of Cheng, with an aperture of 5m for the parabolic trough collector and the receiver tube length of 7.8m, the three-dimensional numerical simulation of coupled heat transfer characteristics in the receiver tube was performed by combining the Monte Carlo Ray-Trace method (MCRT) and FLUENT software. At best, the solar flux field is incident on only one-half of circumference resulting in highly asymmetric thermal boundary layer profile and temperature.

It has also been reported that the thermal stresses may cause a bending of the absorber tube, causing a rupture of the glass cover. This bending has been associated with the thermal gradient produced by the boiling of water, and the effects are related to the thermal conductivity of the absorber tube, the flow pattern and asymmetry of the temperature distribution on the absorber tube [41].

In DSG concepts, the position of the border between the two-phase region and the superheating section might vibrate along the absorber's length. The resulting thermal stress limits the durability of the absorber pipes and has to be considered when evaluating the DSG concept [42].

Helical fins have been suggested in the absorber tube to reduce the thermal stresses. This hypothesis was investigated further and is the subject of Chapter 4.

2.3.4.3 Orientation and tracking modes for parabolic trough system

To harness the maximum amount of solar radiation, the orientation and tracking of a parabolic trough system (PTS) is of paramount importance. A PTS is oriented with its focal axis pointed either in the east-west (E-W) or north-south (N-S) direction. In the east-west orientation, the focal axis is horizontal, while in the north-south orientation, the focal axis may be horizontal or inclined. Five different modes of tracking are discussed herein.

A. Mode I

In this mode, the collector is rotated about a horizontal E-W axis with a daily adjustment required to ensure that noon beam irradiation is normal to the collector aperture. See Fig 2.26a. In this mode, the aperture plane is an imaginary surface with either $\gamma = 0^o$ or $\gamma = 180^o$. The case of $\gamma = 0^o$ occurs when $(\phi-\delta) > 0$, while the case of $\gamma = 180^o$ occurs when $(\phi-\delta) < 0$. To calculate the slope β of the aperture plane, the condition at solar noon is substituted, viz. $\omega = 0^o$, $\theta = 0^o$ in

$$\cos\theta = \sin\phi \ (\sin\delta \ \cos\beta + \cos\delta \ \cos\gamma \ \cos\omega \ \sin\beta) + \cos\phi \ (\cos\delta \ \cos\omega \ \cos\beta - \sin\delta$$
$$\cos\gamma \ \sin\beta) \tag{2.1}$$

This result in

$$\beta = (\phi - \delta) \text{ for } \gamma = 0^o \tag{2.2a}$$

And $\beta = (\delta - \phi) \text{ for } \gamma = 180^o$ (2.2b)

The angle of incidence of the beam radiation on the plane throughout the day is obtained by putting Eq (2.2a) and (2.2b) in Eq (2.1). For both cases, $\gamma=0^o$ and $\gamma=180^o$, the same relation results, [11].

$$\cos\theta = \sin^2\delta + \cos^2\delta \, \cos\omega \tag{2.3}$$

B. Mode II

Mode II is similar to mode I, but with a continuous adjustment of the collector such that the beam irradiation is incident on the collector aperture with a minimum angle throughout the day. See Fig 2.26a. In this mode also, the aperture plane is an imaginary surface with $\gamma = 0^o$ or $\gamma = 180^o$. Eq (2.1) is applicable with $\gamma = 0^o$ or $\gamma = 180^o$. In order to find the condition to be satisfied for θ to be a minimum, the right hand side of the resulting equation is differentiated with respect to β and equate to zero. Thus,

$$\tan(\phi - \beta) = [\tan\delta/\cos\omega] \text{ for } \gamma = 0^o \tag{2.4a}$$

$$\tan(\phi + \beta) = [\tan\delta/\cos\omega] \text{ for } \gamma = 180^o \tag{2.4b}$$

Eq (2.4a) and (2.4b) can be used for finding the slope of the aperture plane. Eq (2.4a), corresponding to $\gamma = 0^o$, is used if the magnitude of the solar azimuth angle γ_s is less than 90°, while Eq (2.4b) corresponding to $\gamma = 180^o$ is used if the magnitude of the solar azimuth angle is greater than 90°.

The expression for the corresponding minimum angle of incidence is obtained by substituting Eq (2.4a)   and (2.4b) in the appropriate version of Eq (2.1)
For both cases,

$$\cos\theta = (1 - \cos^2\delta \, \sin^2\omega)^{1/2} \tag{2.5}$$

C. Mode III

In this mode the focal axis is N-S and horizontal. The collector is rotated about a horizontal N-S axis and adjusted continuously so that the solar beam makes the minimum angle of incidence with the aperture plane at all times. See Fig 2.26b.

In this mode, the surface azimuth angle $\gamma = +90^o$ before noon, and $\gamma = -90^o$ after noon. Thus, before noon, Eq (2.1) becomes

$$\cos\theta = (\sin\phi \sin\delta + \cos\phi \cos\delta \cos\omega) \cos\beta + \cos\delta \sin\omega \sin\beta \qquad (2.6)$$

In order to find the condition to be satisfied for θ to be a minimum, we differentiate the right hand side of Eq (2.6) with respect to β and equate to zero.

Thus, we get:

$$\beta = \tan^{-1}\left[\frac{\cos\delta \sin\omega}{\sin\phi \sin\delta + \cos\phi \cos\delta \cos\omega}\right] \qquad (2.7)$$

Eq (2.7) is used for finding the slope of the aperture plane at any time before noon. The expression for the corresponding minimum angle of incidence is obtained by substituting Eq (2.7) in (2.6), giving

$$\cos\theta = [(\sin\phi \sin\delta + \cos\phi \cos\delta \cos\omega)^2 + \cos^2\delta \sin^2\omega]^{1/2} \qquad (2.8)$$

After noon, i.e. with $\gamma = -90^o$,

$$\beta = \tan^{-1}\left[\frac{-\cos\delta \sin\omega}{\sin\phi \sin\delta + \cos\phi \cos\delta \cos\omega}\right] \qquad (2.9)$$

The expression for $\cos\theta$ remains the same.

D. Mode IV

The focal axis is N-S and inclined at a fixed angle equal to the latitude in this mode. Thus, it is parallel to the earth's axis. This orientation is sometimes referred to as a polar mount. The collector is rotated about an axis parallel to earth's axis at an angular velocity that is equal and opposite to the earth's rotational rate, it is adjusted such that at solar noon the aperture plane is an inclined surface facing due south. See Fig 2.26c. Thus, putting $\beta = \phi$ and $\omega = 0$ in Eq (2.10)

$$\cos\theta = \sin\phi (\sin\delta \cos\beta + \cos\delta \cos\omega \sin\beta) + \cos\phi (\cos\delta \cos\omega \cos\beta - \sin\delta$$
$$\cos\beta) = \sin\delta \sin(\phi-\beta) + \cos\delta \cos\omega \cos(\phi-\beta) \qquad (2.10)$$

we get,

$$\theta = \delta \qquad\qquad (2.11)$$

This also seen from Fig 2.25 in which the circle represents the longitude through the location of the collector. At all other times, since the collector is rotated at a speed equal to the earth's rate of rotation and about an axis parallel to the earth's axis, it follows that Eq (2.11) is still valid [11].
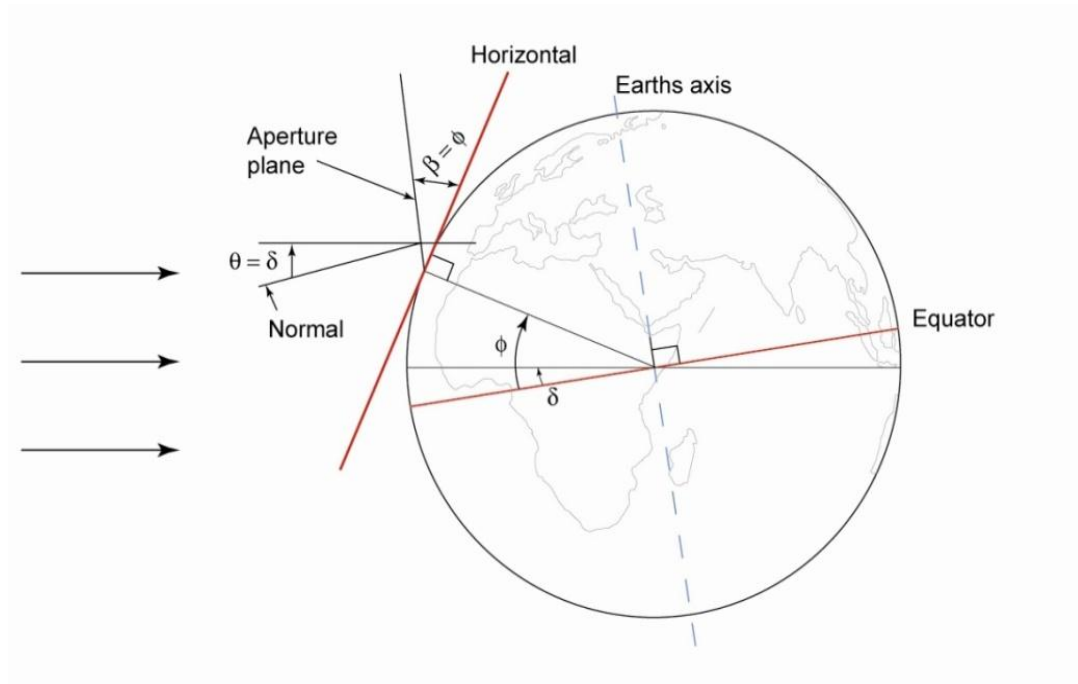
Figure 2.25 Tracking mode IV for parabolic trough collector [11]

E. Mode V

Mode V is similar to mode IV, but with the collector now subjected to a two-dimensional motion, i.e. the collector is rotated about the focal axis as well as about a horizontal axis perpendicular to this axis. See Fig 2.26c. The beam irradiation is thus always normal to the collector aperture. In this situation, obviously cos θ=1. It is easy to show that at solar noon,

$$\beta = |\phi - \delta| \qquad\qquad (2.12)$$

It is of interest to compare the amount of beam radiation which would be incident on a collector's aperture plane over a day if one adopted the various tracking modes. Monthly-average daily irradiation for five modes of tracking will be calculated using the same input data in Section 3.2.
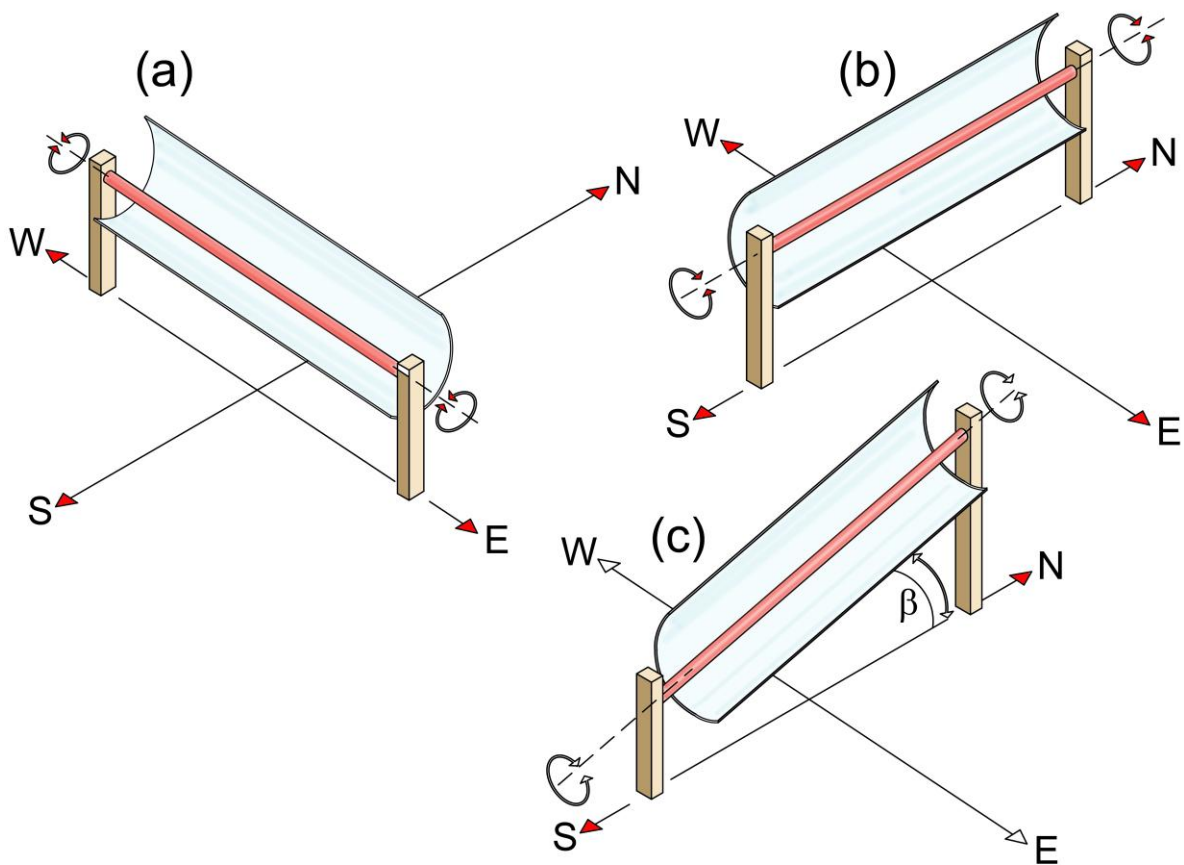
Figure 2.26 Asthmatic diagrams for tracking modes

2.4 Large scale photovoltaic power plants (LS-PV)

2.4.1 Introduction

Solar photovoltaic technology is employed for directly converting the solar energy into electrical energy by using the solar silicon cell. A solar or photovoltaic (PV) cell consists of a p-n junction, in which electrons and holes are created by assumption of solar radiation. The PV cells are typically combined into modules that typically hold 36 cells connected in a series and parallel combination. Silicon PV cells are either monocrystalline, polycrystalline or amorphous. According to Markvart[43], most commercially available PV modules are manufactured from polycrystalline silicon wafers. While their efficiency is lower than their monocrystalline counterparts, their reduced cost makes them more common.

The electricity generated can be utilised for different applications directly or through a battery storage system. Solar PV has been widely used for applications in space, remote areas and households, corresponding to various important activities including home lighting; it can specifically be of use in rural areas and connecting with local grid.

Solar cells convert solar radiation into electrical energy with a peak efficiency in the range of 9-19.2%, depending on the solar-cell type. In 1990, laboratory produced cells were reported as having efficiencies of over 30%. In addition, the cells produced in the world in that year had an aggregate peak generating capacity of 50MW [44].

2.4.2 Factors affecting the performance of PV systems

This section gives a summary of the literature related to the effect of the following environmental factors; irradiance, ambient temperature and wind speed.
A brief account of these effects is given below.

2.4.2.1 Irradiance (I, W/m^2)

Irradiance has a direct effect on the PV module output. An increase in irradiance, increase the PV output. Irradiance also affects the PV cell temperature, which is directly proportional to the irradiance and which effects the operational PV module voltage, thus effecting the PV output. This is discussed in detail in Chapter 5.

2.4.2.2 Ambient temperature (Ta., ^{o}C)

PV cell temperature is also directly proportional to ambient temperature. As discussed in (*A*), the cell temperature effects the PV module output. This will be discussed in detail in Chapter 5.

2.4.2.3 Wind speed (υ, m/s)

Wind speed also affects the cell temperature. In cold weather, as wind speed increases, the PV cell temperature decreases. Moreover, high wind speed may effect the performance of the system.

2.4.2.4 Solar altitude and solar spectrum

The solar irradiance intensity depends, among other things, upon the solar elevation angle γ_s.

This is measured from the horizontal. As the sun moves through the sky, the elevation angle changes during the day and also over the course of the year. When the solar altitude is perpendicular to the Earth, the sunlight takes the shortest path through the Earth's atmosphere. But if the sun is at a shallower angle, the path through the atmosphere is longer. This results in greater absorption and scattering of solar radiation and, hence, lower radiation intensity. The air mass factor (AM) specifies how many times the perpendicular thickness of the atmosphere the sunlight has to travel through the Earth's atmosphere. The relationship between solar altitude (height) γ_s and air mass is defined as follows:

$$AM = \frac{1}{\sin \gamma_s} \tag{2.14}$$

When the solar altitude is perpendicular ($\gamma_s = 90°$), AM = 1. This corresponds to the solar altitude at the equator at noon during the spring or autumn equinox.

The photoelectric conversion efficiency depends on matching of the incident spectrum with the cell's spectral response and the actual operating cell temperature. The change in power output as a function of the spectrum (AM) for PV modules based on crystalline and amorphous silicon is shown in Fig 2.27.
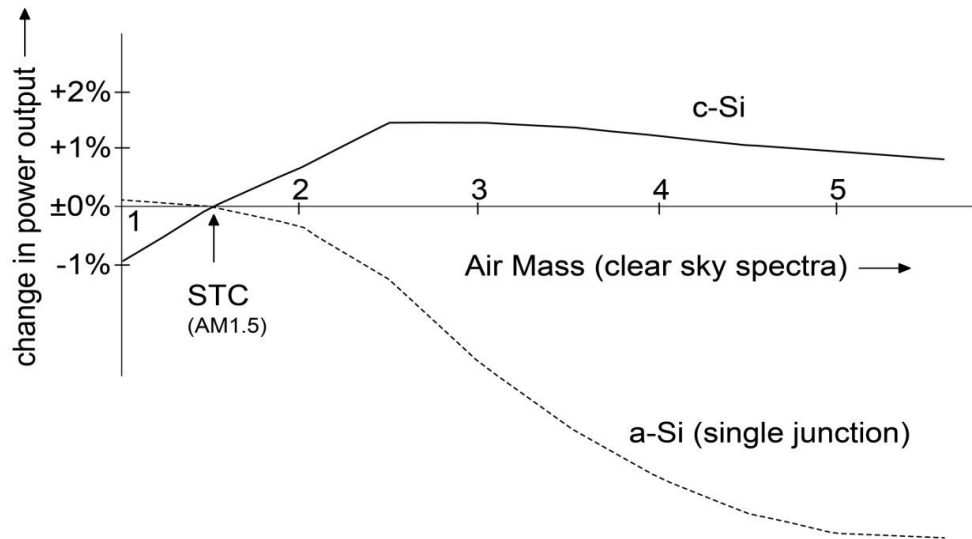
Figure 2.27 Change in power output as a function of the spectrum (AM) for PV modules [45]

Some of the characteristics of solar cells are as follows:

- **Short circuit current (I_{sc})**

  A short circuit current is an abnormal low-resistance connection between two nodes of an electrical circuit that are meant to be at different voltage. In circuit analysis, the term short circuit is used by analogy to designate a zero impedance connection between two nodes. This forces the two nodes to be at the same voltage. In an ideal short circuit, this means there is no resistance and no voltage drop across the short. In simple circuit analysis, wires are considered to be short. In real circuits, the result is a connection of nearly zero impedance, and almost no resistance. In such a case, the current drawn is limited by the rest of the circuit. This is achieved by connecting the positive and negative terminals by copper wire. I_{sc} does not vary much with temperature and this effect is normally ignored[43].

- **Open circuit voltage (V_{oc})**

  The term of open circuit voltage refers to the conditions when the difference of electrical potential between two terminals a device is infinity large i.e. when there is very high external load connected to the circuit with respect to

the internal resistance of the circuit. It may also be understood as the voltage for maximum load in circuit.

- **The maximum power (P_m) , maximum current(I_m) and maximum voltage(V_m)**

  The maximum power, (P_m) is the power produced when the product (*I*V*) is maximum (i.e. *P_m=I_m * V_m*) where I_m and V_m are respectively the current and voltage at maximum power. The maximum power can only be evaluated after the IV curve has been determined (see Fig 2.26).

- **Fill factor (FF)**

  Another defining term in the overall behaviour of solar cell is the fill factor (FF). This is the ratio of the maximum power point divided by the open circuit voltage (V_{oc}) and the short circuit current (I_{sc}):

  $$FF = \frac{P_m}{V_{oc} * I_{sc}} \tag{2.15}$$

  The fill factor is directly affected by the which values of the cells series and shut resistance. Increasing the shunt resistance (R_{sh}) and decreasing the series resistance (R_s) will lead to higher fill factor, thus resulting in greater efficiency, and pushing the cells output power closer towards its theoretical maximum.

- **Efficiency of a solar cell (η_c)**

  The efficiency of a solar cell is mathematically defined as

  $$\eta_c = \frac{I_m * V_m}{A_c * I} \tag{2.16}$$

  Where I_m and V_m are the current and voltage for maximum power, corresponding to solar intensity I.

2.4.3. The photovoltaic IV curve

The main features of a PV IV curve are the short circuit current (I_{sc}), the open circuit voltage (V_{oc}), the maximum power (P_m), the current at maximum power (I_m) and the voltage at maximum power (V_m). These parameters were defined in section 2.4.2.

The IV characteristic shown in Fig 2.28 is a function of both irradiance and cell temperature as represented in Fig 2.29. As the irradiance increases, I_{sc} increases

linearly while V_{oc} increases logarithmically. An increase in PV cell's temperature, on the other hand, results in a slight linear increase in I_{sc} coupled with a significant linear decrease in V_{oc} [46, 47].
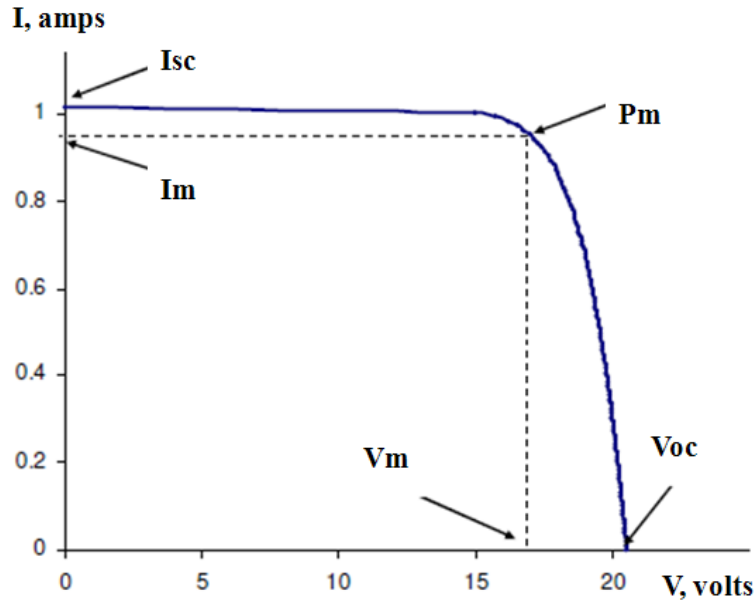
Figure 2.28 Typical IV characteristic of a PV module
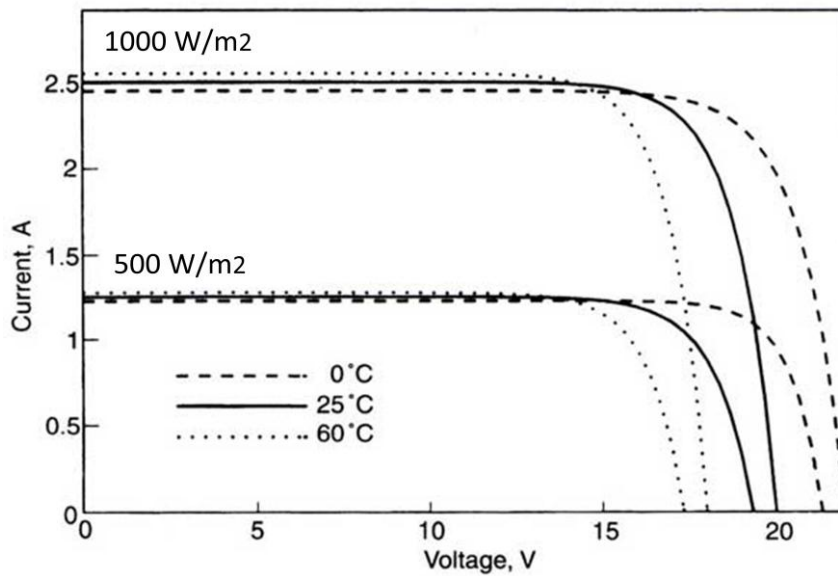
Figure 2.29 The effect of irradiance and cell temperature on the IV characteristic [42]

Although there is an increase in current with temperature, the overall effects of increased cell temperature is decrease in power due to the large decrease in voltage.

Dyk et al [48] reported that the abovementioned cell temperature effect on module performance. Furthermore, Parretta et al [49] reported that 7% of all energetic losses are due to the cell temperature effect. They reported that at ambient temperatures of 25°C, PV modules will be operating at temperatures above ambient temperatures and can lose up to 14% of their potential energy production. According to Nishioka et al [50], the annual output energy of their PV system increased by about 1% for an improvement of 0.1% / ^{o}C in the temperature coefficient. In conclusion, they stated that the cell temperature has an important effect on the power output from the cell. This will be discussed in detail in Chapter 5.

2.4.4. Large scale (LS-PV) Photovoltaic systems

PV technology is one of the most attractive options of the renewable energy technologies. As a result, the small-scale dispersed stand-alone as PV power systems, moreover the small and medium-sized building-integrated grid-connected PV power systems have proven great potentials, consequently Large Scale Photovoltaic systems (LS-PV) may represent a future option for the world energy supply.

LS-PV systems consist of one plant or an aggregation of multiple units operating in harmony and distributing in the same district with outputs which range between 10MW to several gigawatts.
The following are the advantages of LS-PV systems [51]:

- Desert and semi-arid lands are available and normally have high potential irradiance.
- The estimated potential of such areas can easily supply the estimated world energy needs by the middle of the 21st century.
- In accordance with the world energy demand, LS-PV capacity can be increased step by step.
- LS-PV systems have near zero carbon emission and do not pollute the environment.

Nowadays, more than 900MW-scale PV systems are operational, and the capacity of such MW-scale PV systems is expanding year by year, Fig 2.30 shows the trends in MW-scale PV systems installation [52].
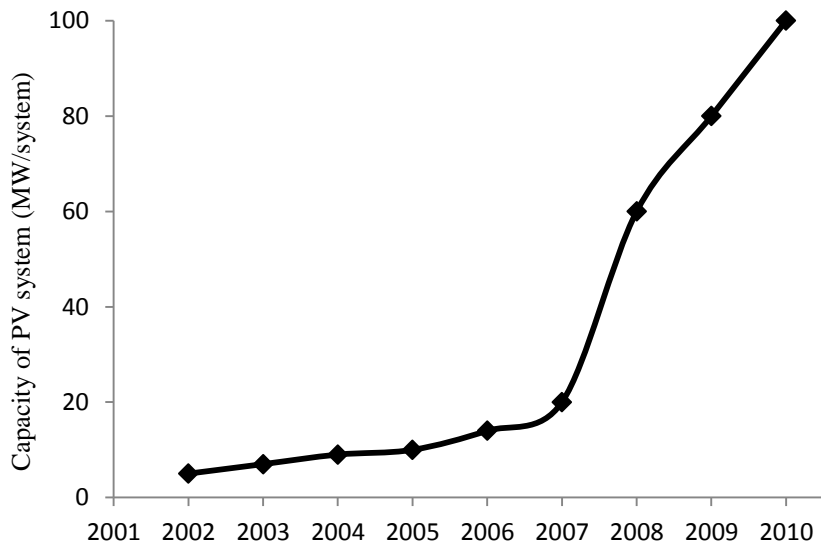
Figure 2.30 Trends in MW-scale PV systems installation[52]

2.4.4.1 Stationary and two-axis tracking system

Most photovoltaic modules are installed at stationary tilt and oriented towards the equator. The optimum tilt angle is usually determined by the nature of the application. According to Duffie and Beckman [53], Photovoltaic modules which are to provide maximum generation over the year should be inclined at an angle equal to the latitude of the site.

According to Markvart [54], the amount of total energy output can be increased if the PV modules track the sun. For instance, Full two-axis tracking will increase the energy available by almost 40% over a stationary PV module, at the angle of latitude at the expense, however, of increased complexity and cost. Also, according to Kurokawa et al [51], the maximum output of tracking PV modules, at all times of the year, is higher and spread over more daylight hours than in the case of stationary modules. Furthermore, the highest capacity factors are generated with trackers which

follow the sun throughout the day to keep the panel optimally oriented towards the sun.

Figure 2.31 1MW MECASOLAR trackers for a photovoltaic solar project in California [55]

However, it has two disadvantages. The first is that considerably more land area is required in order for the PV modules not to shade one another. This means that the total energy output per land usage for LS-PV of PV power plant based on two-axis trackers would therefore be considerably lower than for stationary system. The second drawback is that, each tracker requires two motors in order to keep it locked on the sun's changing position.

2.4.4.2 LS-PV installations around the world

The global PV market in 2010 witnessed a massive growth with 15GW of new capacity being added to the existing 25GW that was already installed. PV technology has the potential to contribute to at least 20% of world's electricity supply by the year 2050.

Over $20 billion of investments were made in this technology in the year 2010 alone with a total of two million PV installations now reported as up and running. Strong growth has been reported by European countries which now account for 70% of the global market, though there have been strong growths reported within the North

American, Japanese, Chinese and Australian markets. In addition, activity is also picking up in the Sunbelt countries of Africa, the Middle East and India. A one-third reduction in the PV module cost within the past five years alone is indeed impressive. Fig 2.32 shows the historical downward trend of PV module and system costs. Note that the drop in cost is pegged to the year 1985. Thus, the cost in year 2010 has dropped by 80%.
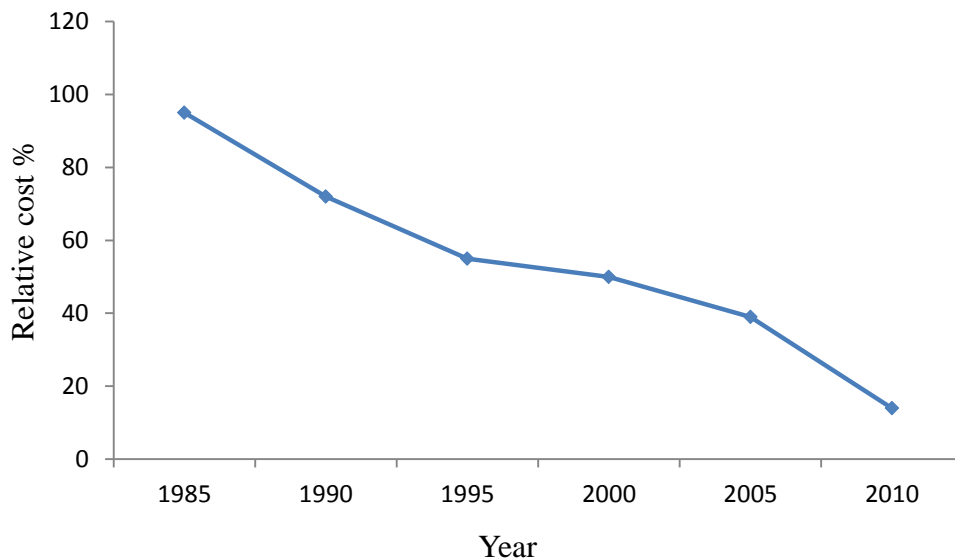
Figure 2.32 Chronology of PV module and system costs

Europe in particular is playing a leading role in the development and deployment of solar PV technology, though of late China is also showing strong growth in this area of activity. Germany is the world leader in terms of installed solar PV technology with 15GW of installed peak capacity. The corresponding figures for Italy, Belgium and France are 1,500, 292 and 285MW. After the EU, Japan and USA were respectively the second and third largest markets with total installed capacities of 484 and 475MW. A point worth mentioning is that since the earthquake and tsunami related damage to the Fukushima plant in 2011, the Japanese energy policy is shifting away from nuclear-power generation and this may indeed help deployment of PV on a much faster scale.

A. Europe

Presently around 81% of the world's large-scale power generating photovoltaic plants are installed in Europe. Spain is the most dynamic of the European PV markets at present, and a huge increase in installed power capacity in the year 2007 was observed [56].

More than 70% of all European large-scale photovoltaic plants are located in Spain with a combined capacity of $2.3GW_p$, followed by Germany, $698MW_p$, and Italy with $70MW_p$ [57].

ACCIONA has put photovoltaic plants into service that total $115MW_p$ at the end of the year 2009. Of these, $69MW_p$ are in Spain, particularly the so-called 'solar gardens', and $46MW_p$ in Portugal in the plant at Amareleja (Moura), one of the biggest in the world in terms of grid-connected capacity.

Recently, E.ON opened its first photovoltaic solar farm, near the southern French town of Le Lauzet. The size of the power plant is 1MW, and could be extended to 5MW subject to the availability of a suitably-sized grid connection [58].

Currently, the Rovigo project in Italy is the largest PV power plant in Europe being bigger than the 60MW solar farm in Olmedilla, Spain, and the 50MW project in Strasskirchen, Germany. In the first full year of operation, the system is expected to generate sufficient energy to power more than 17,000 homes and avoid the emission of 41,000 tons of CO_2 This is equivalent to taking 8,000 cars off the road [59].

The power plant covers an area of more than $850,000m^2$. The 280,000 modules were installed by Isolux Corsan, using 840km of cables and more than 6,000 tons of steel for the metal substructures.

Figure 2.33 Rovigo solar PV plant, Italy [59]

B. Asia

In 2011, two photovoltaic power plants have been installed in Sakai by Sharp and the Kansai Electric Power Company. The combined size of these plants would be 28MW. Furthermore, according to the National Energy Administration (NEA) in Beijing, China wants to increase installed solar power plant capacity from the current 180MW to 2GW by 2011 and 20GW by 2020 [60].

Conergy AG has installed a 3MW solar photovoltaic (PV) power plant in Karnataka, India. The power plant consists of 13,000 modules and covers $0.07km^2$ to produce 4 GWh for the local grid. India's National Solar Mission aims for 20GW of solar power in India by 2020 [61].

C. Middle East

Masdar City, Abu Dhabi, is the most ambitious sustainable developments in the world today - it will be the world's first zero carbon, zero waste city that will be powered entirely by renewable energy sources.

Masdar City linked its first 10MW solar array to the United Arab Emirates electricity grid. Around 87,777 photovoltaic panels were designed and built by Abu Dhabi-

based Enviromena Power Systems, with construction on the array being started in August 2008 [62].

From these examples, it is obvious that MW-scale PV systems are not a rarity. As the capacity of the MW-scale PV systems expands, year by year, the capacity will reach 100MW in a few years time [50]. A GW- scale PV plant consisting of several 100MW-scale PV systems is expected to be realized by the mid-21st century. In future, LS-PV systems would be able to become an option for many large remote and desert regions in the world.

The examine and evaluate the potential of LS-PV of PV power generation systems in the southern region of Libya at Al-Kufra. This will be discussed in Chapter 5.

2.5 Conclusion

The purpose of this chapter has been to review the literature available on the Libyan energy supply and demand, potential for solar energy in Libya and large scale concentrated solar (CSP) and photovoltaic power plants in Libya. All of the literature discussed in this chapter related to the potential for solar energy in Libya and the electrical power generation technologies of solar energy.

Overall, Libya consumed 22.17 billion kWh of electricity in 2010. Libya's electricity demand is growing at a rapid rate (around 6%-8% annually) and the country will require significant additional capacity in coming years. An opportunity exists to utilise the high solar radiation levels incident on the south of the country to meet this demand.

Due to its near tropical location, Libya is blessed with plenty of daily sunshine hours and no cloud cover all year round. The measured noon clearness-index, often exceeding 0.84, is an ideal candidate for large-scale generation of solar electricity.
Al-Kufra, which is a region located in Southern-East Libya has an excellent solar energy potential ranging from 2,200 to 2,600 kWh/m^2/year of direct normal irradiation. This region is also well known with its large aquifers of high-quality ground water.

The discussion in this chapter clarified that large scale concentrated solar (CSP) and photovoltaic power plants are treated separately. In the case of CSP, the parabolic trough power plant is the most proven technology of all the CSP technologies and the study has been focussed on direct steam generation in a parabolic trough system. It was noted that several studies have been carried out and showed that there is instability in the steel absorber tube, due to the highly concentrated solar flux on only one-half of the circumference of the absorber tube, this problem and proposed solutions will be discussed in detail in Chapter 4.

About 88% of the area of Libya is occupied by the Sahara desert, this area can be used for production of clean energy implementing LS-PV power systems by using a stationary and a two-axis solar tracking LS-PV power plant, this will discussed in detail in Chapter 5.

References

[1]   Saleh Ibrahim IM. Prospects of renewable energy in libya. Renewable Energy. 1998;14,135.

[2]   Energy in formation administration. 2011 [cited; Available from: http://eia.doe.gov/cabs/Libya/Oil.html

[3]   Statistics figures 2008. 2008 [cited; Available from: http://www.gecol.ly/aspx/Statistics.aspx

[4]   AUPTDE 2006 [cited; Available from: http://www.auptde.org/NewSite/user/User_Def1.aspx?PID=201

[5]   Bank GTW. Electric power consumption (kWh per capita) 2010 [cited; Available from: http://ddp-ext.worldbank.org/ext/ddpreports/ViewSharedReport?REPORT_ID=9147&REQUEST_TYPE=VIEWADVANCED

[6]   El-Arroudi K, Moktar,M. Demand Side Management in Libya Tripoli: General Electric Company of Libya (GECOL), Transmission System Operation and Control Department; 2009.

[7]   El-Sheikh S. The Libyan electricity network-Present and future infrastructure:Towards an international electricity market. 2008 [cited; Available from: www.auptde.org/newsite/UploadFiles/Activitypaperfile/329.ppt

[8]   Energy Efficiency and Renewable Energy Libya - National study; 2007.

[9]   Ekhlat M, Salah,I.,Kreama,N. Energy Efficiency and Renewable Energy Libya - National study; 2007.

[10]   T.Muneer. Solar radaition and daylight models 2004

[11]   Sukhatme S, Nayak,K. Solar energy, Principles of thermal collection and storage. Third edition ed. New Delhi: McGraw-Hill Publishing Company Limited 2008.

[12]   AlFenadi Y. Hottest temperature record in the world, El Azizia, Libya.

[13]   Saleh Ibrahim IM. Photovoltaic in libya applications, and evaluations. *in Interna- tional Conference on renewable energy for developing countries*. Washington 2006.

[14]   Broesamle H, Mannstein, H.,Schillings, C.,Trieb, F. Assessment of solar electricity potentials in North Africa based on satellite data and a geographic information system. Solar Energy. 2001;70(1):1-12.

[15]   Pallas P. Water Resources of the Socialist people's Libyan Arab Jamahiriya; 1980.

[16]   FAO's Information System on Water and Agriculture. 2006 [cited;
         Available from:
         http://www.fao.org/nr/water/aquastat/countries/libya/libya_cp.pdf

[17]   Abdelrhem I, Khalim,R.,Amiruddin,I. Integrated Groundwater Management
         for Great Man-Made River Project in Libya. European Journal of Scientific
         2008;22:562-9.

[18]   Kearney AT. Solar Thermal Electricity 2025. Duesseldorf,Germany: GmbH;
         2010.

[19]   Electrical cooperation between euorpe and north africa. 2011 [cited 2011
         26-07-2011]; Available from: http://www.desertec.org/en/news/

[20]   TREC. The Trans-Mediterranean Renewable Energy Cooperation; 2007.

[21]   Concentrating Solar Power Systems. 2008 [cited; Available from:
         http://solar-thermal.anu.edu.au/high_temp/concentrators/basics.php

[22]   Lafuent JQ, V. P20:Solar tower technology. European Sustainable Energy
         Review. 2008 2008(2):27-9.

[23]   The first solar thermal power plant in Egypt. Egypt: New and Renewable
         Energy Authority; 2007.

[24]   Ferna´ndez-Garcı´a A, Zarza,E.,Valenzuela, L.,Pe´ rez, M. . Parabolic-
         trough solar collectors and their applications. Renewable and Sustainable
         Energy 2010;14(7):1695-721

[25]   European Research on Concentrated Solar Thermal Energy. Brussels 2004.

[26]   Linear Concentrator Systems. 2008 [cited; Available from:
         http://www.eere.energy.gov/basics/renewable_energy/linear_concentrator.ml

[27]   Concentrating Solar Power Now. Berlin, Germany: DLR,The Federal
         Ministry for the Environment,Nature Conservation and Nuclear Safety
         (BMU); 2002.

[28]   Sterling Energy Systems Featured in Design News. 2006 [cited; Available
         from:
         http://thefraserdomain.typepad.com/energy/2006/03/sterling_energy.html

[29]   Solar thermal power plants. 2003 [cited; Available from:
         http://www.volker-quaschning.de/articles/fundamentals2/index_e.html

[30]   Abengoa Solar begins operation of the world's largest solar power tower
         plant. 2009 [cited; Available from:
         http://www.abengoasolar.com/sites/solar/en/about_us/general/news/archive/2
         009/20090427_noticias.html

[31]   Herrmann U, Kelly, Bruce.,Price, Henry. Two-tank molten salt storage for
         parabolic trough solar power plants. Energy. 2003;29(5-6):883-93.

[32]   Solar Thermal Power 2020 - Exploiting the Heat from the Sun to Combat
         Climate Change,: Greenpeace and the European Solar Thermal Industry
         Association; 2003. Report No.: ISBN:90- 73361-82-6.

[33]   Hosseini R, Soltani,M. ,Valizadeh,G. Technical and economic assessment of
         the integrated solar combined cycle power plants in Iran. 2005;30(10):1541-
         55

[34]   Barber-Nichols. NREL n-Pentane Solar Rankine Cycle Analysis and
         Review,Final Report to NREL; 2000. Report No.: NREL/TP-550-31240.

[35]   Hank Price. VH. Modular Trough Power Plant Cycle and Systems Analysis;
         2002. Report No.: NREL/TP-550-31240.

[36]   Eck MZ, E.Eickhoff,, M.Rheinländer, J.Valenzuela L. Applied research
         concerning the direct steam generation in parabolic troughs. Solar Energy.
         2003;74(4):341-51.

[37]   Valenzuela L, Zarza, Eduardo.,Berenguel, Manuel.,Camacho, Eduardo F.
         Control concepts for direct steam generation in parabolic troughs. Solar
         Energy. 2005;78(2):301-11.

[38]   Yebra LJ, Berenguel, M., Zarza,E., Dormido,S. Object Oriented Modelling of
         DISS Solar Thermal Power Plant. The Modelica Association. 2006
         September 4th – 5th.

[39]   Muneer T, Kubie J, Grassie T. Heat Transfer – A problem solving based
         approach. London: Taylor and Francis 2003.

[40]   Cheng ZD, He,Y.L. ,Xiao ,J. , Tao,Y.B. , Xu,R.J. . Numerical Study of Heat
         Transfer Characteristics in the Solar Receiver Tube Combined With MCRT
         Method. *Proceedings of the International Solar Energy Conference* ASME
          2009.

[41]   Flores V, Almanza,R. Behavior of the compound wall copper–steel receiver
         with stratified two-phase flow regimen in transient states when solar
         irradiance is arriving on one side of receiver. Solar Energy. 2004;76:195–8.

[42]   Hirsch T, Eck, Markus. Dynamics and control of parabolic trough collector
         loops with direct steam generation. Solar Energy. 2007;81(2):268 - 79.

[43]   Markvart T. Solar Electricity. 2nd ed: John Wiley & Sons 2000.

[44]   Green M, A. Solar Cells, Operating Principles, Technology and System
         Applications. New Jersey: Prentice Hall 1982.

[45]   Society GE. Planning and installing photovoltaic systems: A guide for
         installations, architects and engineers. : London, Earthscan. 2008.

[46]   Buresch M. Photovoltaic Energy Systems,Design and Installation. New
         York: McGraw-Hill Book Company 1983.

[47]   Mallick TK, Eames,P.C.,Hyde,T.J.,Norton,B. The design and experimental characterisation of an asymmetric compound parabolic photovoltaic concentrator for building facade integration in the UK, . Solar Energy. 2004;77:319-27.

[48]   Dyk EE, Meyer, E. L.,Vorster, F. J.,Leitch, A. W. R. . Long-term monitoring of photovoltaic devices Renewable Energy. 2002;25(2):183-97.

[49]   Parretta A, Sarno,A .,Vicari,L. Effects of solar irradiation conditions on the outdoor performance of photovoltaic modules. Optics Communications 1998;153 153-63.

[50]   Nishioka K, Hatayama,T.,Uraoka, Y.,Fuyuki,T.,Hagihara, R.,Watanabe,M. . Field-test analysis of PV system output characteristics focusing on module temperature. Solar Energy Materials & Solar Cells   2003;75:665–71.

[51]   Kurokawa K, Keiichi,K,. . Energy from the Desert: Earthscan in UK and USA 2007.

[52]   Kurokawa K, Keiichi,K,. . Energy from the Desert: Earthscan in UK and USA 2009.

[53]   Duffie JA, and Beckman, W.A.,. Solar Engineering of Thermal Processes. 2nd ed. New York: Wiley Interscience 1991.

[54]   Markvart T. Photovoltaic solar energy conversion: School of Engineering Sciences,University of Southampton; 2002.

[55]   PROINSO supplies 1 MW of MECASOLAR trackers for photovoltaic solar project in California; 2010.

[56]   Lenardic D. Large-Scale Photovoltaic Power Plants; Annual Report 2007.

[57]   Denis L, Rolf, H. Pvresources annual review displays development of utility-scale PV power plants: all-time records in capacity and growth in 2008. 2009 [cited; Available from: http://www.solarserver.com/solarmagazin/solar-report_0509_e_3.html

[58]   Alnaser WE, Alnaser NW. Solar and wind energy potential in GCC countries and some related projects. Journal of Renewable and Sustainable Energy. 2009;1(2):022301.

[59]   SunEdison Activates Really Big Solar PV Plant in Italy. 2010 [cited; Available from: http://www.getsolar.com/blog/sunedison-activates-really-big-solar-pv-plant-in-italy/14457/

[60]   Dennis W. China raises solar target Engineering and Technology 2009:8.

[61]   Conergy deploys 3 MW solar PV power plant in India. 2010.

[62]   Stromsta K-E. Masdar connects 10MW solar farm to UAE's power grid. RECHARGE. 2009.

CHAPTER 3

Large-Scale DSG plant for Al-Kufra: Thermal analysis

Chapter Map
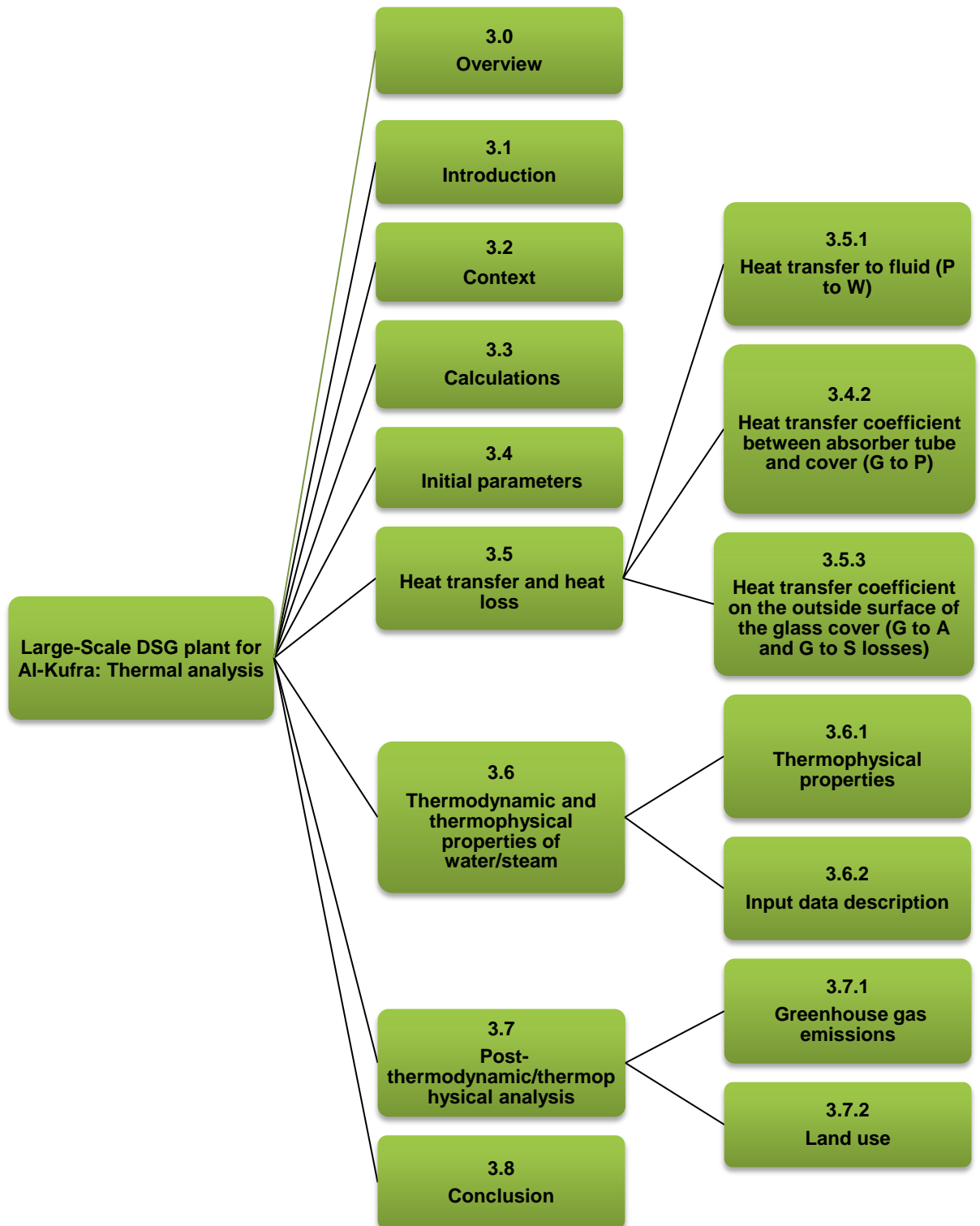
3.0 Overview

This chapter presents the analysis performance of a 50MW DSG (Direct steam generation) plant for southern Libya based on the thermodynamic and thermophysical properties of water/steam substance.

As mentioned in section 2.3.4.2 C, a DSG plant has advantages and disadvantages compared to other methods for generating electricity from solar radiation. Whatever the method of generation, reliable models for the design of plant and for the estimation of energy yield, greenhouse gas emissions and land use are required in order to justify the investment in plant construction.

This chapter presents arguments for the use of DSG in preference to other forms of generation in particular locations according to the prevailing environmental and economic conditions. In addition, the chapter describes the development of a software tool based on Microsoft Excel and Visual Basic for Applications (VBA) which draws upon established physical relationships in the heat transfer literature to perform plant capacity calculations in a fast and convenient manner.

The results of the VBA program determine the solar fraction of the plant, and on the basis of the results further calculations are performed to estimate greenhouse gas emissions and land use. Construction costs are also estimated based on formulae from previous work.

3.1 Introduction

Direct Steam Generation (DSG) in the absorber pipe, without a heat exchanger, eliminates the need for the synthetic oils typically used as the HTF and offers several advantages over the indirect design [1]:

- Environmental risks associated with synthetic HTF such as fires and leaks are eliminated.
- A higher maximum temperature can be sustained compared to the current limit of around 400 °C above which synthetic HTF tends to degrade.
- Overall plant efficiency is higher because the oil/steam heat exchanger is unnecessary. This makes the solar field requirement and investment lower.
- Plant design is simplified with the elimination of the heat exchanger and auxiliary thermal oil systems.
- The simplified design has lower operation and maintenance costs since an auxiliary heating system for HTF is unnecessary, and there is no requirement to replace a proportion of the HTF each year.

One of the major barriers to the commercialisation of DSG technology, however, is a complete understanding of the two-phase water/steam flow within the system [2].

This chapter reports on the development of a software model of the thermodynamic and thermophysical properties of water and steam in a hypothetical 50MWe DSG plant which takes into account the environmental conditions in the chosen geographical location. In addition, the model includes land requirement calculations for the plant, and the specification of a secondary natural gas-fuelled boiler required to maintain the design output of the overall facility. For simplicity, this chapter does not consider the engineering implications of the balance of plant required for maintaining a steady flow rate around the closed loop circulation system, or for condensing the exhaust steam from the turbine ready for re-circulation. This constitutes the main limitation on the work presented.

3.2 Context

Following on from an earlier feasibility study for a DSG plant generating less than 1MW by Aldali et al [3], the design context for the current study is a 50MW plant located at 24° 17′N, 23° 15′E at Al-Kufra in the South-Eastern part of Libya, an area which forms part of the Sahara desert. This location benefits from a high average clearness-index of 0.64[4] and in addition there is ample supply of water from subterranean aquifers and local production of natural gas.

The aim of the model is to describe the thermodynamic and thermophysical properties of the water and steam which act as the heat transfer vector. Using the results from the model, other practical calculations can be performed, such as establishing the length of absorber tube capable of delivering the design capacity of 50MW through solar energy alone during periods of peak insolation, and calculating the natural gas requirement for a supplementary boiler to maintain the design capacity at other times. The geographical advantages of the chosen location minimise the logistical issues related to the supply of water and natural gas; however, other resources including capital finance are scarce. A priority is therefore to minimise construction and operation costs, and this has implications for the plant's design.

The hypothetical plant is assumed to be a closed cycle, once-through design. Eck and Steinmann [5] note several disadvantages with once-through systems compared to injection or recirculation systems based on their experience on the European Direct Solar Steam (DISS) project; however, the simplicity of the once-through design eliminates the need for additional components such as water/steam separators and injectors, and so is preferred on cost grounds (see section 2.3.4.2 C). In addition, the majority of the disadvantages identified are related to the transient effects of variable cloud cover. Because cloud cover is negligible at the location selected for the hypothetical plant, such issues are therefore also negligible. Some predictable increase in turbidity related to dust storms has been identified during April and May [3]; however, this is of a relatively persistent nature and does not give rise to the same rapid variations discussed by Eck and Steinmann [5].

The plant itself is based on the DISS design [6] and consists of two sub-systems, the solar field and the power block. The solar field is assumed to consist of a series of standard loops, each of which comprises many solar collectors connected in series.

Following on from the study detailed in Chapter 2 section 2.3.4.3, five modes of operation can be identified for parabolic trough collectors according to their orientation and sun tracking capabilities:

- Mode 1 offers a horizontal focal axis along the E-W plane. The collector is rotated about a horizontal E-W axis with a daily adjustment required to ensure that noon beam irradiation is normal to the collector aperture.
- Mode 2 is similar to mode 1, but with a continuous adjustment of the collector such that the beam irradiation is incident on the collector aperture with a minimum angle throughout the day.
- Mode 3 is similar to mode 2, but with a horizontal focal axis along the N-S plane.
- Mode 4 is similar to mode 3, but with the focal axis being at a fixed inclination that is equal to the latitude of the location. The collector is rotated about an axis parallel to earth's axis at an angular velocity that is equal and opposite to the earth's rotational rate.
- Mode 5 is similar to mode 4, but with the collector now subjected to a two-dimensional motion, i.e. the collector is rotated about the focal axis as well as about a horizontal axis perpendicular to this axis. The beam irradiation is thus always normal to the collector aperture.

Trigonometric relations for the above modes of operation and the quantities of solar energy collection routines are available in standard texts, and can be used to compile the data in Table 3.1 for Al-Kufra. The final row in table is the annual-averaged daily irradiation calculated as the average of the monthly figures. The values in Table 3.1 were calculated using the same input data and method as described in section 2.3.4.3. From a practical and energy collection standpoint, modes 2, 3 and 4 are the most common.

Furthermore, modes 2 and 3 offer a further advantage of the ability to connect collectors in series. Note that there is a substantial energy gain from mode 3 of operation as opposed to mode 2 and hence the former was selected for the present design study.

Table 3.1 Monthly-averaged daily irradiation for five modes of tracking, kWh/m^2

	Mode 1	Mode 2	Mode 3	Mode 4	Mode 5	Global Horizontal
Jan	6.2	6.3	6.3	7.5	8.0	4.3
Feb	6.1	6.2	6.7	7.7	7.9	5
Mar	5.8	5.8	7.1	7.6	7.6	5.7
Apr	5.5	5.6	7.1	7.1	7.2	6.1
May	5.7	5.7	7.2	6.8	7.2	6.4
Jun	6.2	6.3	7.8	7.2	7.8	7
Jul	6.5	6.6	8.2	7.7	8.3	7.3
Aug	6.5	6.5	8.3	8.1	8.4	7
Sep	6.0	6.0	7.5	7.8	7.8	6.1
Oct	5.9	5.9	6.8	7.6	7.7	5
Nov	6.4	6.5	6.5	7.7	8.1	4.6
Dec	6.0	6.1	5.6	6.8	7.5	3.9
***ADI**	6.1	6.1	7.1	7.5	7.8	5.7

*ADI: the annual-averaged daily irradiation calculated as the average of the monthly figures

Collector loops are connected in parallel as described by Al-Soud and Hrayshat [7] so that calculations can be performed for one loop and the results multiplied by an appropriate factor. The balance of plant, including boiler, turbine, condenser and feed pump, is contained in the power block. The present chapter makes no attempt to specify these components, focussing instead on the calculations related to the energy yield from the solar field.

3.3 Calculations

The model is divided into three main elements as shown in Fig 3.1 where the second element is the critical one for this study. It is implemented in Microsoft Visual Basic for Applications (VBA) using Microsoft Excel as the user interface and main application platform. Because the calculations are iterative and use a series of data values as input, the standard tabular arrangement of data in a spreadsheet is ideal. VBA provides a fully functional structured programming environment in which to implement the required algorithms without having to develop an original user interface.

1: Determine the initial parameters for the main calculations

↓

2: Determine the exit conditions of the steam from the solar field

↓

3: Perform post-thermodynamic / thermophysical analysis
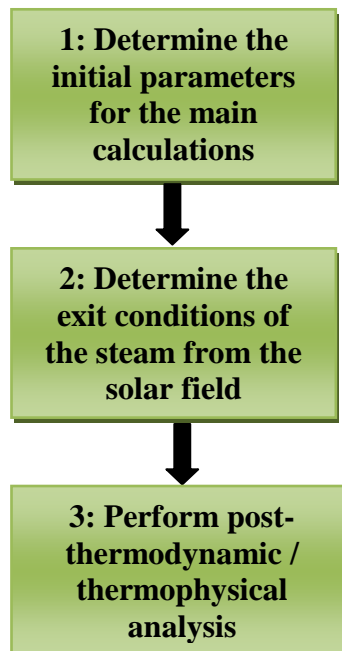
Figure 3.1 Process overview

3.4 Initial parameters

The conditions which determine the behaviour of the water/steam circulating through the absorber tubes can be grouped into 4 sets. Of these, some are the result of calculations performed on the basis of observational data, some are taken from the results of earlier work, and others are assumptions. Table 3.2 sets out the details.

Table 3.2 Initial parameters

Physical dimensions of collector construction			Reference
1.	Inner diameter of absorber tube	50mm	[6]
2.	Outer diameter of absorber tube	70mm	[6]
3.	Inner diameter of glass cover	85mm	[6]
4.	Outer diameter of glass cover	90mm	[6]
5.	Aperture presented by one collector	5.76m	[6]
Physical characteristics of the materials used in the construction of the collectors			
6.	Transmissivity of glass cover	0.85	[8]
7.	Emissivity of absorber tube	0.05	[8]
8.	Emissivity of glass cover	0.88	[8]
9.	Absorptivity of absorber tube	0.95	[8]
Prevailing environmental/thermodynamic conditions			
10.	Ambient temperature	28°C	
11.	Wind speed	$3ms^{-1}$	
12.	Pressure	10MPa	
13.	Enthalpy of input water	$104.4kJkg^{-1}$	
Plant design parameters			
14.	Mass flow rate of water/steam for one loop	$0.8kgs^{-1}$	[6]
15.	Mass flow rate of water/steam for DSG power plant (56 loops)	$44.8 \ kgs^{-1}$	
16.	Length of one solar collector absorber tube	79.5m	
17.	Concentration ration PT collector	25.87	
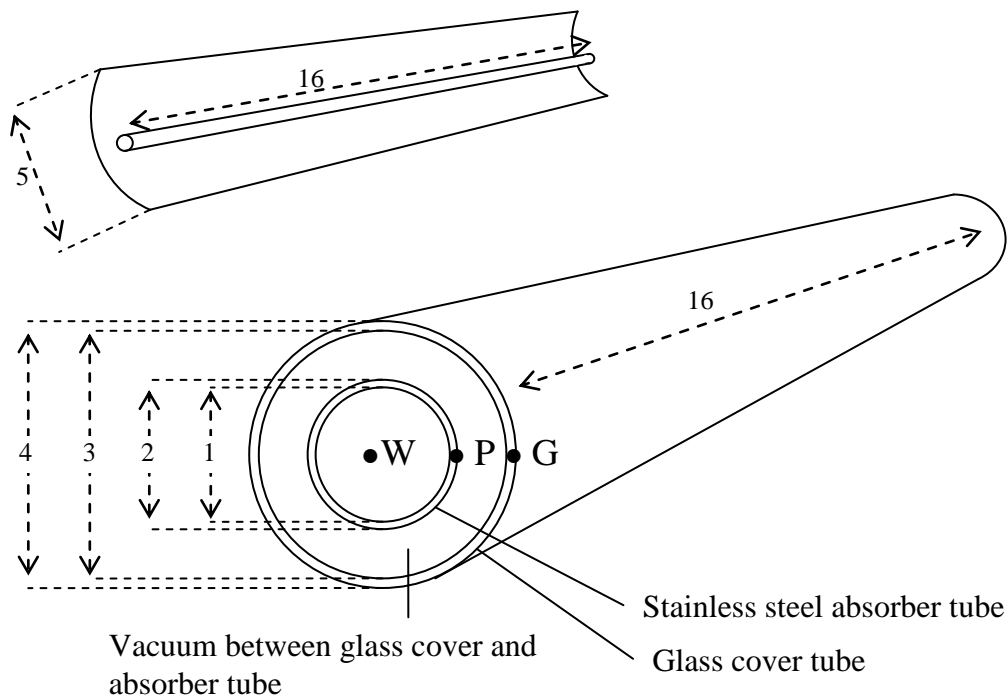
Figure 3.2 Physical construction of solar collectors

3.5 Heat transfer and heat loss

A thermal network is used to model the performance of the solar collectors, the schematic of which is shown in Fig 3.3.

A = Ambient air
S = Sky
G = Glass tube
P = Steel absorber tube
W = Water/steam
A_{mirror} = area of mirror
I_{solar} = Beam irradiance
R_{Con} = Thermal resistance due to convection
R_{Rad} = Thermal resistance due to radaition
$(\tau\alpha)_e$ = Effective transmittance - absorptance product
α_G = Absorptivity of glass
ρ_{mirror} = Reflectivity of the mirror
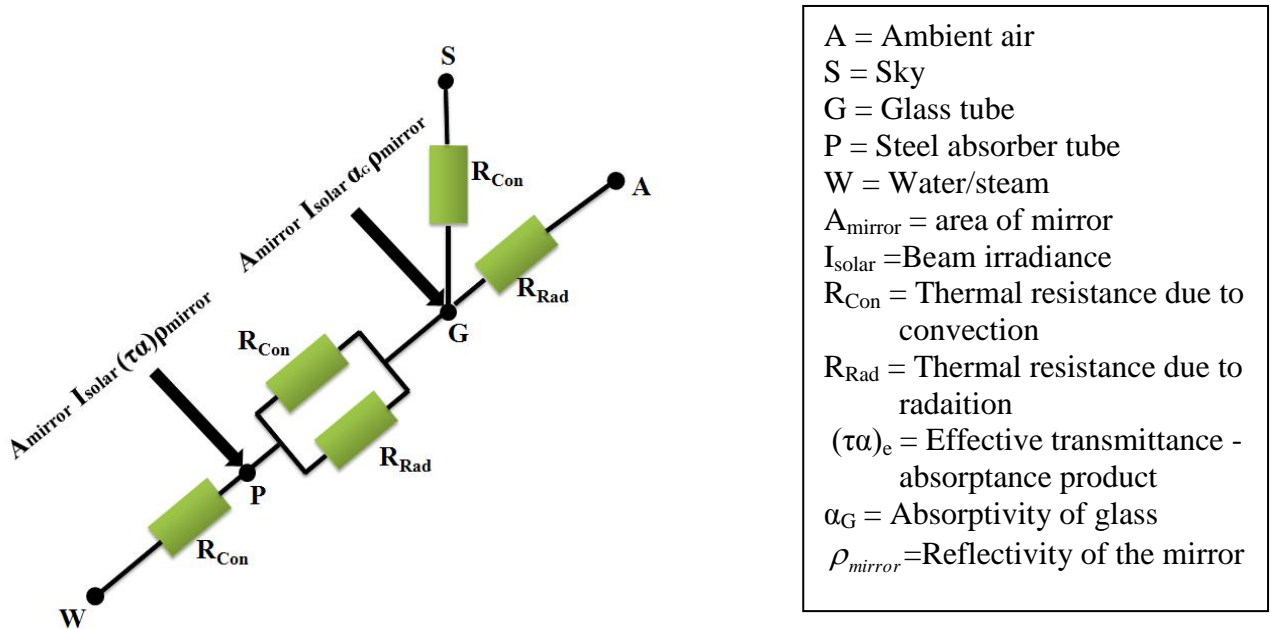
Figure 3.3 Thermal network

The glass cover absorbs a fraction of the irradiation which helps to reduce the thermal losses from the absorber tube. Due care is therefore taken for all such energy absorption and convective/radiative exchanges between the nodes in the diagram. Note that nodes W, P and G correspond to the points in Fig 3.2 with the same labels. The calculations set out below are implemented by the VBA program.

3.5.1 Heat transfer to fluid (P to W)

The fluid flow area inside the absorber tube is given by:

$$A_p = \frac{\pi D_i^2}{4}$$

(3.1)

where:

A_p: Section area of the absorber tube (m^2)

Di: Absorber tube inner diameter (m)

The average velocity of the flow inside the absorber tube is given by:

$$V_f = \frac{m_f}{\rho_f A_p}$$

(3.2)

where:

V_f: Average velocity (m/s)

m_f : mass flow rate (kg/s)

ρ_f: density of fluid (kg/m^3)

To evaluate whether the flow is laminar or turbulent, the Reynolds number is given by:

$$\text{Re} = \frac{V_f D_i}{\upsilon_f}$$

(3.3)

where:

υ_f: Kinematic viscosity of fluid (m^2/s)

For a Reynolds number less than 2000, the flow is laminar and the Nusselt number is given by Kays et al [9] .

$$N_u = 3.66$$

(3.4)

On the other hand, for a Reynolds number greater than 2000, the flow is turbulent and the Nusselt number requires a more complex calculation. Several methods have been proposed [10]; however, errors as large as 25% may result from their use. Such errors may be reduced to less than 10% through the use of more recent, but generally more complex, correlations [11] . The following correlation, widely used and attributed to Petukhov [12] is used in the VBA.

$$N_u = \frac{(f/8)\,\text{Re}\ \ \text{Pr}_f}{1.07 + 12.7(f/8)^{1/2}(\text{Pr}^{2/3} - 1)}$$

(3.5)

where:

f : Friction factor

The friction factor may be obtained from the Moody diagram or, for smooth tubes, from the following equation:

$$f = (0.79 \ln \text{Re} - 1.64)^{-2} \tag{3.6}$$

This correlation is valid for $0.5 < \text{Pr} < 2000$ and $10^4 < \text{Re} < 5*10^6$

$$h_f = \frac{N_u \kappa_f}{D_i} \tag{3.7}$$

where:

h_f: Convective heat transfer coefficient (W/m^{2}K)

κ_f : Thermal conductivity of fluid W/m-K

3.5.2 Heat transfer coefficient between absorber tube and cover (G to P)

The natural convection heat transfer coefficient h_{pgc} for the enclosed annular gap between absorber tube and glass tube is calculated by correlation due to Raithby and Hollands [13].

$$\frac{\kappa_{eff}}{\kappa} = 0.317(Ra^*)^{1/4} \tag{3.8}$$

where:

κ_{eff}: Effective thermal conductivity (W/mK)

Ra^* : Modified Rayleigh number given by:

$$(Ra^*)^{1/4} = \frac{\ln\left(\dfrac{D_{ci}}{D_o}\right)}{b^{3/4}\left(\dfrac{1}{D_o^{3/5}} + \dfrac{1}{D_{ci}^{3/5}}\right)^{5/4}} Ra^{1/4} \tag{3.9}$$

D_o : Outer diameter of absorber tube (m)

D_{ci} : Inner diameter of glass cover (m)

b : Radial gap

$$b = \frac{(D_{ci} - D_o)}{2} \tag{3.10}$$

Rayleigh number R_a may be calculated by the following equation:

$$Ra = \left(\frac{(g\beta\Delta TL^3)}{\upsilon_{air}^2}\right)\text{Pr}_{air} \tag{3.11}$$

where

g : Gravitational acceleration (m/s^2)

L : Characteristic dimension

β : Volumetric thermal expansion coefficient (K^{-1}) (see Eq 3.12)

$$\beta = \left(\frac{T_p + T_g}{2} \right)^{-1}$$ (3.12)

where:

T_p: Absorber tube temperature ($^{\circ}$C)

T_g: Glass covers temperature ($^{\circ}$C)

The natural convection heat transfer coefficient h$_{pgc}$ is calculated by:

$$h_{pgc} = \frac{2\kappa_{eff}}{D_o \ln(D_{ci} - D_o)}$$ (3.13)

The radiative heat transfer coefficient, h$_{pgr}$ between absorber tube and glass cover:

$$h_{pgr} = \frac{\sigma(T_p + T_g)(T_p^{\ 2} + T_g^{\ 2})}{\left(\dfrac{1}{\varepsilon_p} \right) + \left(\dfrac{1 - \varepsilon_g}{\varepsilon_g} \right)\left(\dfrac{D_o}{D_{co}} \right)}$$ (3.14)

where:

ε_p: Emissivity of absorber tube

ε_g: Emissivity of glass covers tube

σ : Stefan-Boltzmann constant, $5.67*10^{-8}$ W/m^{2}K^4

The total heat transfer coefficient between absorber tube and glass cover is

$$h_{pg} = h_{pgc} + h_{pgr}$$ (3.15)

3.5.3 Heat transfer coefficient on the outside surface of the glass cover (G to A and G to S losses)

Depending on the ambient air velocity the Reynolds number is calculated and then the flow boundary layer evaluated. Air properties are evaluated as functions of the ambient air temperature T$_a$.

$$\upsilon_{air} = f(T_f)$$

$$\kappa_{air} = f(T_f)$$

$$\mathrm{Pr}_{air} = f(T_f)$$

Note that T_f is the film temperature $= \left(\dfrac{T_a + T_g}{2} \right)$ (3.16)

$$\text{Re} = \frac{V_{air} D_{co}}{\upsilon_{air}} \tag{3.17}$$

To evaluate convective heat transfer coefficient h_{ga} on the outside surface of the glass cover, Churchill and Bernstein [14] have proposed a single comprehensive equation that covers the entire range of R_e for which data are available, as well as wide range of Pr. The equation is recommended for all $\text{R}_e \text{Pr} > 0.2$ and has a form

$$N_u = 0.3 + \frac{0.62 \text{Re}_{air}^{1/2} \text{Pr}_{air}^{1/3}}{\left[1 + \left(\dfrac{0.4}{\text{Pr}_{air}}\right)^{2/3}\right]^{1/4}} \left[1 + \left(\frac{\text{Re}_{air}}{282000}\right)^{5/8}\right]^{4/5} \tag{3.18}$$

The heat transfer coefficient by convection from glass cover to ambient is:

$$h_{ga} = \frac{N_u \kappa_{air}}{D_{co}} \tag{3.19}$$

The radiative heat transfer coefficient, h_{gs} from glass cover to sky is:

$$h_{gs} = \frac{\sigma \varepsilon_c \left(T_{ga}^{\,4} - T_s^{\,4}\right)}{\left(T_{ga} - T_s\right)} \tag{3.20}$$

The energy balance performed for each of the three nodes G, P, W results in Eqs 3.21-3.23, and can be expressed as:

$$T_g = \frac{CR\rho_{mirror} I_b \alpha + h_{gs} T_S + h_{ga} T_a + \left(\dfrac{D_o}{D_{ci}}\right) h_{pg} T_p}{h_{gs} + h_{gs} + h_{pg}\left(\dfrac{D_o}{D_{ci}}\right)} \tag{3.21}$$

The absorber tube temperature is:

$$T_p = \frac{CR\rho_{mirror} I_b (\tau\alpha)_e + \left(h_{pf} T_{fi}\right) + \left(h_{pg} T_g\right)}{h_{pf} + h_{pg}} \tag{3.22}$$

The energy loss from absorber tube to glass cover is:

$$Q_{loss-pg} = \pi D_o L h_{pg}\left(T_p - T_g\right) \tag{3.23}$$

$$Q_{in} = A_{mirror}\rho_{mirror} I_b (\tau\alpha)_e \tag{3.24}$$

$$\mathbf{h}_o = \mathbf{h}_i + \frac{\left(Q_{in} - Q_{loss-pg}\right)}{\overset{\bullet}{m}_f}$$

(3.25)

CR, the concentration ratio of the collector is given by;

$$CR = \frac{W - D_o}{\pi D_o}$$

(3.26)

where W is the aperture.

The Darcy equation is used to evaluate the pressure drop;

$$\Delta P = \frac{4 f \rho L V^2}{2 D_i}$$

(3.27)

$$P_o = p_i - \Delta p$$

(3.28)

The thermodynamic code returns the temperature of the water/steam substance using the above two properties, $\mathbf{h}_o$ and P_o.

3.6 Thermodynamic and thermophysical properties of water/steam

The VBA code is based primarily on the Revised Release on the IAPWS Industrial Formulation 1997 for the Thermodynamic Properties of Water and Steam (IF97) provided by the International Association for the Properties of Water and Steam (IAPWS). This document defines the thermodynamic properties of the fluid phases of water and steam over a wide range of temperature and pressure [15]. IF97 identifies four main regions in the T-S diagram for the fluid phases of water and steam which correspond to the major states of the substance. Table 3.3 identifies the regions, the corresponding states of the substance, and the fundamental equations that can be used to model substance behaviour in each case.

Table 3.3 Four major regions in the state diagram for fluid water substance

Region	Phase	Abbreviation	Equation
1	Compressed liquid	CL	Gibbs free energy: $g(p, T)$
2	Superheated vapour	SUPV	Gibbs free energy: $g(p, T)$
3	Supercritical liquid	SCR	Helmholtz free energy: $f(\rho, T)$
4	Saturated mixture	SATM	Saturation pressure equation: $P_s(T)$

In order to reduce computing effort, IF97 also provides a series of 'backward equations' of the form T(P, h) for regions 2 and 3 for the calculation of thermodynamic properties as functions of pressure and enthalpy. These equations are numerically consistent with the basic ones, and allow calculation of properties without the need for iteration [15]. The backward equations effectively fragment the regions as shown in Fig 3.4. The substance also exhibits specific behaviour at the boundary between regions 2 and 3 (shaded area in Figure 3.4), and IF97 provides an auxiliary equation for the calculation of properties in that area known as the B23-equation. The backwards equations and the B23-equation are all implemented in the VBA code which takes starting pressure and enthalpy as its initial parameters. The VBA program code can be found in print in Appendix-A.
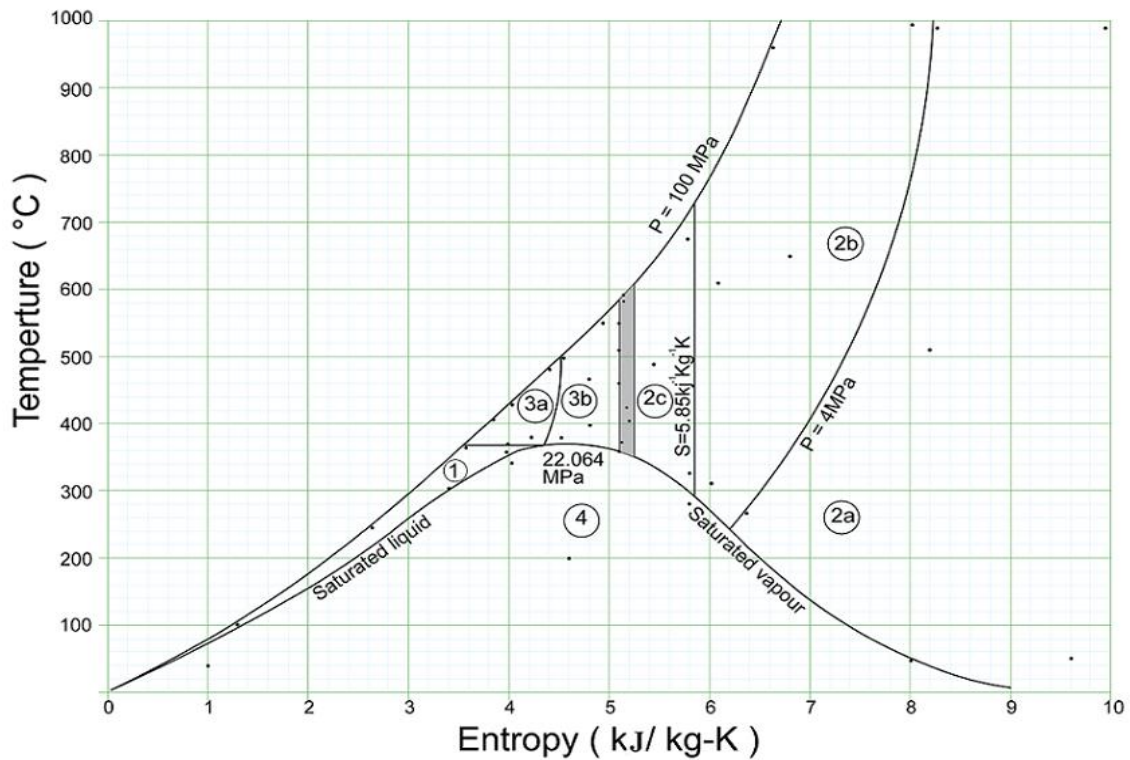
Figure 3.4 State diagram for fluid phases of water substance

The VBA code consists primarily of two nested program loops. The first iterates over a series of input values which represent the monthly-averaged hourly irradiation for a period of one year at the selected location. The data used in this study was provided by the Libyan Meteorological Office. The inner program loop iterates over the length of the absorber tube calculating the thermodynamic and thermophysical properties at 1-metre intervals. The output from the program is the series of values

shown in Table 3.4 which represent the final output characteristics of the substance for one standard loop in the solar field for each hour of operation.

Table 3.4 VBA program output variables

Symbol	Description
p	Pressure (bar)
h	Enthalpy of water/steam substance (kJ/kg)
T	Temperature (K)
T_{sat}	Saturation temperature (K)
h_f	Specific enthalpy of saturated liquid (kJ/kg)
s_f	Specific entropy of saturated liquid (kJ/kg K)
ρ_f	Density of liquid (kg/m^3)
h_g	Specific enthalpy of saturated vapour (kJ/kg)
s_g	Specific entropy of saturated vapour (kJ/kg K)
ρ_g	Density of vapour (kg/m^3)
state	State of the substance
x	Dryness fraction
h_b	Enthalpy for boundary (kJ/kg)
Region	Sub-region of the state chart corresponding to the particular combination of characteristics
Pr	Prandtl number
λ	Thermal conductivity (W/m K)
μ	Kinematic viscosity (m^2/s)
s	Specific entropy (kJ/kg K)
ρ	Density (kg/m^3)

The flowchart in Figure 3.6 shows how the inner program loop uses the quantities in Table 3.4 to determine which region of the phase chart is relevant, and therefore which fundamental equation is required to calculate the energy content of the substance. Of particular interest is the use of the B23-equation in step 3 to determine the appropriate state of the substance at the boundary between regions 2c and 3b.

The calculations take into account the amount of energy transferred to the water/steam per unit length of the absorber tube given the input irradiation. Essentially, this means repeating the calculations related to the thermal network in section 3.5.

3.6.1 Thermophysical properties

Transport properties are required when modelling the energy transfer between nodes in the thermal network shown in Fig 3.3. Among nodes P, G and A where convection and radiation are the dominant heat transfer modes, transport properties for air and water substance at the film temperature are required, while for transfer between nodes P and W transport properties for water are required at the water bulk temperature. In the former case, a digital computer property database for air, presented by Muneer et al [16] has been used. Data from Haar, Gallagher and Kell [17] has been used to provide a similar reference for the transport properties for water.

The reference data for transport properties were incorporated into the VBA as lookup tables. While Excel provides a convenient LOOKUP facility as a standard function, it only provides for one-dimensional search and cannot provide automatic interpolation between reference points. The VBA therefore contains two specific features for handling this aspect of the calculations:

1. An extension to the standard LOOKUP facility to provide one-dimensional interpolation for air properties
2. An independent VBA routine to provide one- or two-dimensional interpolation for water transport properties as appropriate.

The interpolation requirements for water transport properties are dependent on the state of the substance. In the saturated mixture state, properties are only dependent on temperature, and a one-dimensional search is required; as a compressed liquid or superheated vapour, properties depend on both temperature and pressure, and therefore a two-dimensional search must be used.

3.6.2 Input data description

The Key factor that affects the CSP plant size, performance and thus land occupation is the direct irradiation (beam irradiation).

For this power plant the monthly averaged global radiation on the horizontal plane was made available for Al-Kufra by the Libyan Meteorological Office. The Liu and

Jordan [18] model which describes the relationship between beam radiation emanating directly from the sun, and diffuse radiation that results from multiple reflections and scattering by atmospheric particles provides a reliable method for estimating the radiation incident on any given surface on an hourly basis given the monthly-averaged figures for the global combination of these two components [19]. Fig 3.5 describes the calculation scheme used.
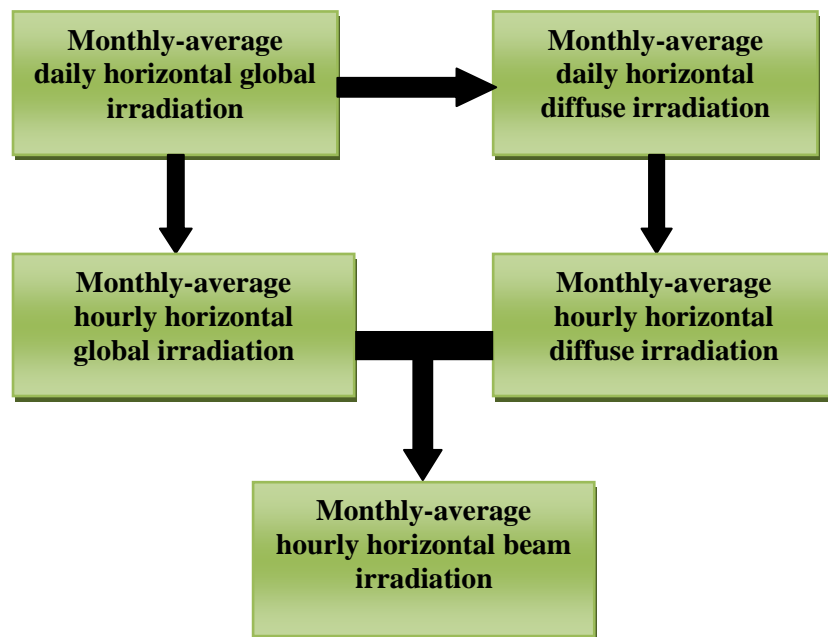
Figure 3.5 Calculation scheme for monthly-average hourly beam irradiation

The validation procedure for the VBA code involved the calculation of thermodynamic and thermophysical properties for the 35 known state points shown as solid dots in Fig 3.4.

Start
Given: P*, h*

Step 1

Find T_{sat} [$= f$(P*)]
Region 4

Step 2

Find h_f [$= f$(P*, T_{sat})]
Region 1

Find h_g [$= f$(P*, T_{sat})]
Region 2

Step 3

If h* < h_f, then state = Compressed Liquid. Find T [$= f$(P*, h*)]
Region 1

If $h_f \leq$ h* $\leq h_g$, then state = Saturated Mixture. T = T_{sat}

If h* > h_g, then state = Superheated Vapour. Find T [$= f$(P*, h*)]
Region 2a, 2b or 2c

If P* > 22.065 and h* < h_{b23n} and h > h_{cr}, then state = SCR

Given P*, h* / State = Saturated Vapour

If P* $\leq$ 4 MPa, find T [$= f$(P*, h*)]
Region 2a

If 4 MPa < P* $\leq$ 6.5467 MPa
or
If P* > 6.5467 MPa and h* $\geq h_{boundary}$, find T [$= f$(P*, h*)]
Region 2b

If P* > 6.5467 MPa and h* < $h_{boundary}$, find T [$= f$(P*, h*)]
Region 2c

Given P*, h* / State = SCR

$h_{boundary\ 3a3b}$ = 2019.64 + 3.7 P* - 0.0219 P*^{2} + (0.87511 * 10) P*^{3}

If $h_{boundary}$ > h*, find T [$= f$(P*, h*)]
Region 3a

If $h_{boundary} \leq$ h*, find T [$= f$(P*, h*)]
Region 3b

Figure 3.6 VBA program operation

89

3.7 Post-thermodynamic/thermophysical analysis

The results from the VBA program show that the total length of absorber tube required to satisfy the design parameters is 35,616m. This can conveniently be laid out in 56 standard loops with 8 collectors in each loop, each of which measures 79.5m. The results from the iterative calculations performed by the VBA program form the basis of further useful calculations that relate to the feasibility and cost of the plant.

3.7.1 Solar fraction

The design capacity of the plant is 50MWe, and the generator therefore requires a constant flow of superheated steam at the optimum pressure and enthalpy to deliver the target output. Assuming a generator efficiency of 85%, the required characteristics of the superheated steam would be P= 100 bar and h = 3419 kJ/kg.

Using trial-and-error, an optimum length for the absorber tube in this example case can be identified which delivers steam with the required characteristics from the solar field at times of peak insolation. In the input data, this occurs at 1130 during the month of August at which time the plant is operating on 100% solar energy. At other times, the enthalpy of the superheated steam needs to be raised to the required level by a supplementary natural gas boiler, thus yielding a solar fraction of less than 100%.

The amount of gas required at any given moment can be derived from the difference between the output of the solar field and the required energy level, a calculation which is performed by the VBA program. Assuming that the plant is in operation for 10 hours per day (0730 – 1730), the solar fraction is shown to be 76% and the power plant is able to produce superheated steam with only a small temperature lift required from the gas boiler to take the steam to its design operating condition of 516°C. Appendix- B shows the results of the complete simulation.

3.7.2 Greenhouse gas emissions

On the basis of the output from the main VBA program, the consequent greenhouse gas emissions from the plant can be estimated. In order to maintain the target output

of 50MW over the ten daily hours of operation, an annual contribution of 44GWh is required from the natural gas boiler. Applying the emissions factor of 0.56 used by the UK government [20], this would yield 24.6 thousand tonnes CO_2. Table 3.5 illustrates the emissions savings of the example plant over a plant of equivalent capacity completely dependent on natural gas as a fuel source. The results show that the DSG plant achieves a 76% reduction in emissions.

Table 3.5 Comparison of use of DSG and natural gas plant over a year's operation

Plant type	Fuel gas energy requirement (GWh)	Emissions ([*]ktCO$_2$)
50MW solar DSG with supplementary natural gas	44	24.6
50MW natural gas only	183	102.4
Difference	139	77.8

[*]kt: kiloton

3.7.3 Land use

The land area required for the plant is largely determined by the length of absorber tube, and therefore by the number of standard loops in the configuration. Fig 3.7 shows a possible layout based on the design presented by Al-Soud and Hrayshat [7] in which the total area is $0.7km^2$.
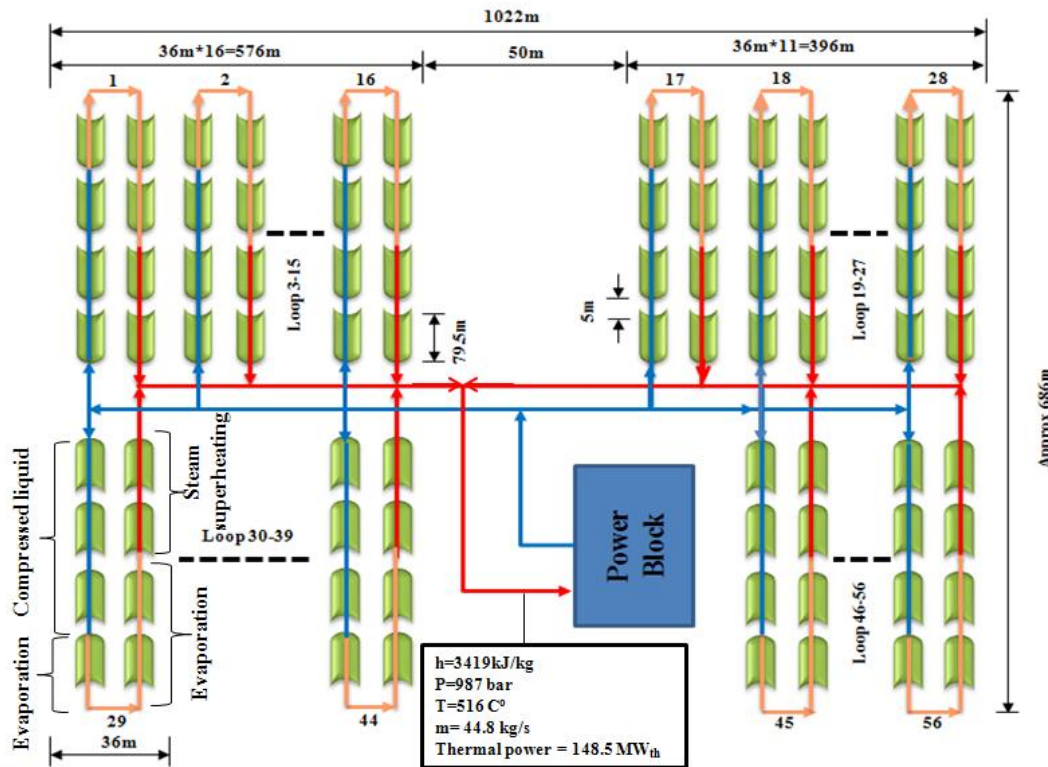
Figure 3.7 Layout plan of the proposed 50MW concentrating solar power plant

3.7.4 Cost

The main focus of this study has been to develop a straightforward method for calculating the energy delivered by the DSG solar field. The balance of plant which comprises the power block has not been considered. In addition, a generic solar collector has been used for calculation purposes. For these reasons a rigorous analysis of construction and operation costs are not possible at this point. However, the indicative costs for the type of plant described here can be suggested on the basis of work by Pitz-Paal et al [21] who also take the development of a 50MW DSG plant as their focus.

Table 3.6 Specific construction cost assumptions

Item	Pitz-Paal	Adjusted
Specific investment cost for solar field	190 €/m^2	214 €/m^2
Specific investment cost for power block	700 €/kW$_e$	788 €/kW$_e$
Specific land cost	2 €/m^2	2 €/m^2
Surcharge for construction, engineering and contingencies	20%	20%
Operation and maintenance	0.034 €/kW$_e$	0.038 €/kW$_e$

Table 3.6 lists the main categories of specific construction cost as given by Pitz-Paal et al [21]. Assuming an annual inflation rate of 3% from 2007 to 2011, these figures can be adjusted to 2011 using the method explained by Kumaranayake [22] and the results are shown in the right-hand column. These figures can then be used to calculate indicative costs for the proposed design as shown in Table 3. Although the specific costs have been increased to take account of inflation, the calculated total is slightly less than that presented by Pitz-Paal et al in 2007[21]. The primary reason for this is the smaller solar field required in the Libyan location.

Table 3.7 Constructions costs for the proposed Libyan plant

Item	Cost (€)
Solar field	43,901,706
Power block	39,400,000
Land	1,402,184
Construction surcharge	16,940,778
Total	101,644,668

Assuming an exchange rate of approximately 1.44499 Euro to the dollar, the total construction cost in dollars is $146,875,528. Further assuming an interest rate of 2% per annum, a feed-in tariff revenue of $0.45 per kWh and an increase in operation and maintenance costs of 3% per annum, the payback period for the plant can be calculated as two year and five months as illustrated in Fig 3.8.
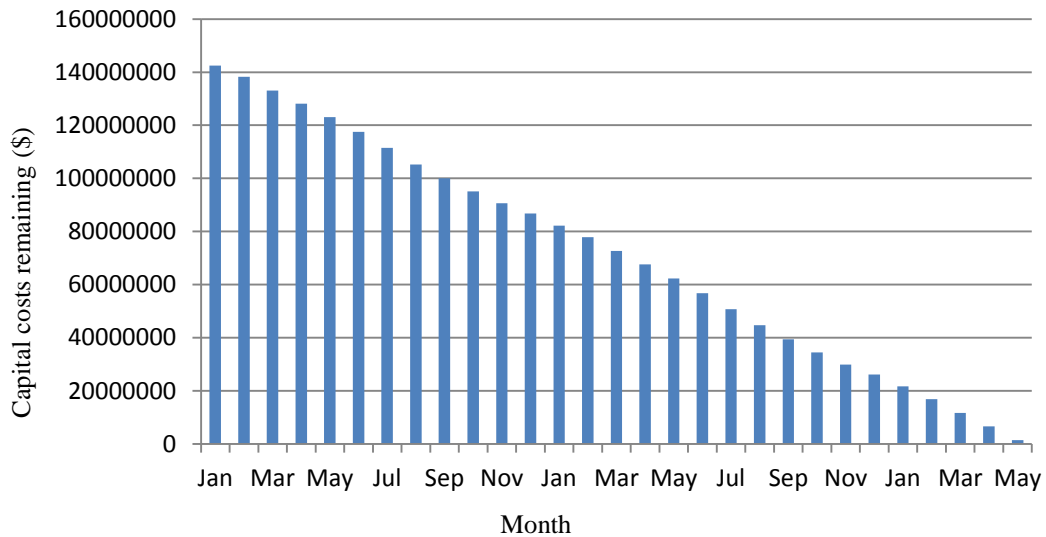
Figure 3.8 System construction payback

3.8 Conclusion

A DSG plant offers a cheaper and less risky method of generating electricity using concentrated solar energy than an HTF plant. However, it is argued above that the location of a DSG plant can be critical in realising these benefits, and that the south east part of Libya is ideal in this respect. The models and calculations presented here are the result of an implementation of the 2007 revision of the IAPWS equations in a general application based on Microsoft Excel and VBA.

The hypothetical design discussed in this chapter is shown to yield a 76% reduction in greenhouse gas emissions compared to an equivalent gas-only plant over the ten-hour daily period of operation. Land requirement is modest at 0.7km^2, especially in a desert region where there is little competition on land. However, the design only takes into account the thermodynamic and thermophysical behaviour of the water substance circulating in the system. Indicative construction costs are provided based on formulae developed by other authors; however, further work is required to fully

specify and cost the balance of plant which includes the circulatory and condensing equipment.

References

[1].   Zarza, E., *Generación directa de vapor con colectores solares cilindro parabólicos.Proyecto Direct Solar Steam (DISS).* , 2003, University of Seville.

[2].   Fernandez-Garcia, A., Zarza,E., Valenzuela,L., Perez,M.   , *Parabolic-trough solar collectors and their applications.* Renewable and Sustainable Energy Reviews, 2010. **14**(7): p. 1695-1721.

[3].   Aldali, Y., Henderson, D., Muneer, T. . *Prospects for large-scale solar thermal electricity generation from the Libyan desert: technical feasibility.* in *Proceedings of ES2009 ASME 3rd International Conference on Energy Sustainability* 2009. San Francisco, California, USA.

[4].   Bannani, F.K., Sharif, T.A.Ben-Khalifa, A.O.R. , *Estimation of monthly average solar radiation in Libya.* Theoretical and Applied Climatology, 2005. **83**: p. 211-215.

[5].   Eck, M., Steinmann, W.D. , *Direct steam generation in parabolic troughs: first results of the DISS project. .* Journal of Solar Energy Engineering 2002. **124**: p. 134–136.

[6].   Zarza, E., Valenzuela, L., Leon, J., Hennecke, K., Eck, M., Weyers, D., Eickhoff, M. , *Direct steam generation in parabolic troughs: Final results and conclusions of the DISS project.* Energy, 2004. **29**(5-6): p. 635-644.

[7].   Al-Soud, M.S., Hrayshat, E.S., *A 50 MW concentrating solar power plant for Jordan.* Journal of Cleaner Production 2009. **17**: p. 625–635.

[8].   Sukhatme, S.P., *Principles of thermal collection and storage*2008, New Delhi, India: Tata McGraw Hill Pub. Co. Ltd.

[9].   Kays, W.M., and Crawford,M.E. , *Convective heat and mass transfer.* 1980, New York.: McGraw-Hill.

[10].   Dittus, F.W., L.M.K. Boelter., *Publications on Engineering.University of California.* 1930. **2**: p. 443.

[11].   Bhatti, M.S., Shah, R.K . *Turbulent and Transition Flow Convective Heat Transfer in Ducts*, in *Handbook of single-phase convective heat transfer*, S. Kakaç, Shah, RK, Aung, W Editor 1987, Wiley-Inter-Science: New York.

[12].   Petukhov, B.S., *Heat Transfer and Friction in Turbulent Pipe Flow with Variable Physical Properties. .* Advances in Heat Transfer, 1970. **6**: p. 504–564.

[13].   Raithby, G.D., Hollands, K.G.T., *A general method of obtaining approximate solutions to laminar and turbulent free convective problems. .* Advances in Heat Transfer 1975. **11** p. 266-315.

[14]. Churchill, S.W., Bernstein, M. , *A correlating equation for forced convection from gases and liquids to a circular cylinder in cross flow.* Journal of Heat Transfer 1997. **99**: p. 300–306.

[15]. *The International Association for the Properties of Water and Steam (IAPWS) (2007) Revised Release on the IAPWS Industrial Formulation 1997 for the Thermodynamic Properties of Water and Steam.*

[16]. Muneer, T., Kubie, J., Grassie, T, *Heat Transfer – A problem solving based approach.* 2003, London: Taylor and Francis.

[17]. Haar, L., Gallagher, J.S., Kell, G.S. , *NBS/NRC steam Tables*1984, New York: Hemisphere Pub. Co.

[18]. Liu, H., Jordon, R. , *The interrelationship and characteristic distribution of direct, diffuse and total solar radiation.* Solar energy, 1960. **4**(1).

[19]. Tham, Y.W., Muneer, T., Davison, B., *Estimation of hourly averaged solar irradiation: evaluation of models. .* Building services research and technology, 2010. **31**(1).

[20]. Berg, B., *The ecology of building materials.*2001: Architectural Press,Butterworth-Heinemann,Oxford.

[21]. Pitz-Paal, R., Dersch, J., Milow, B., Téllez, F., Fernere, A., Langnickel, U., Steinfeld, A., Karni, J., Zarza, E., Popel, O., *Development steps for parabolic trough solar power technologies with maximum impact on cost reduction.* Journal of Solar Energy Engineering, 2007. **129**(4): p. 371–377.

[22]. Kumaranayake, L., *The real and the nominal? Making inflationary adjustments to cost and other economic data. .* Health Policy Plan, 2000. **15**: p. 230-4.

CHAPTER 4

Solar absorber tube analysis: Thermal simulation using CFD

Chapter Map

```
                        ┌─────────────────┐
                        │      4.0        │
                        │    Overview     │
                        └─────────────────┘

                        ┌─────────────────┐
                        │      4.1        │
                        │  Introduction   │
                        └─────────────────┘
                                                        ┌─────────────────────┐
                        ┌─────────────────┐             │       4.2.1         │
                        │      4.2        │             │  Geometry details   │
                        │ Computational   │             └─────────────────────┘
                        │ fluid dynamics  │
                        │ (CFD)           │             ┌─────────────────────┐
                        │ simulation      │             │       4.2.2         │
                        └─────────────────┘             │   Mesh details      │
                                                        └─────────────────────┘
┌─────────────────┐     ┌─────────────────┐
│       4         │     │      4.3        │             ┌─────────────────────┐
│ Solar absorber  │     │   Radiation     │             │       4.2.3         │
│ tube analysis:  │     │   profiles      │             │ Boundary conditions │
│ Thermal         │     └─────────────────┘             │ and materials       │
│ simulation      │                                     │ properties          │
│ using CFD       │     ┌─────────────────┐             └─────────────────────┘
└─────────────────┘     │      4.4        │
                        │ Bursting        │
                        │ pressure        │
                        └─────────────────┘

                        ┌─────────────────┐
                        │      4.5        │
                        │ Results and     │
                        │ discussion      │
                        └─────────────────┘

                        ┌─────────────────┐
                        │      4.6        │
                        │ Conclusion      │
                        └─────────────────┘
```
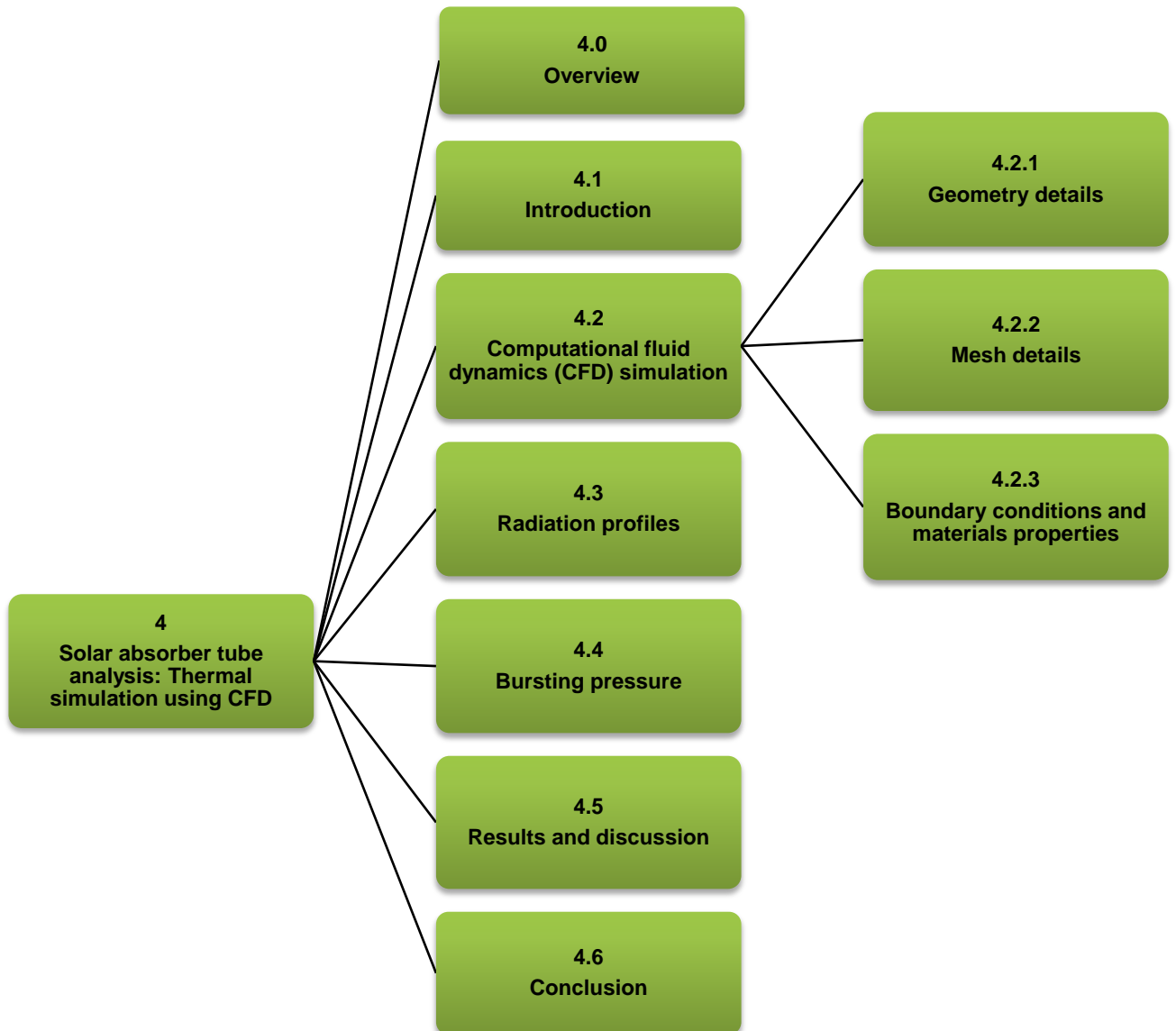
4.0 Overview

As mentioned earlier in Chapter 2, solar thermal power plants using parabolic trough collectors have been in use commercially for several decades in the deserts of California and a number of years in southern Spain. A number of plants are also approaching completion in North Africa countries, i.e. Egypt and Algeria.

Solar thermal power plants using parabolic trough collectors have traditionally used steel pipes, coated with selective coating (higher absorption and low emissivity) and encased within evacuated glass tube to suppress heat loss.

To date, two types of fluids have been used in such ventures, i.e. synthetic aromatic fluid which serves as the heat exchange medium or direct steam generation via circulation of water within the tubes. Fluid flow in parabolic trough systems leads to instability in the steel absorber tube, due to the highly concentrated solar flux on only one-half of the circumference of the absorber tube, which results in an asymmetrical distribution of temperature. This instability is manifest by thermal stresses which cause deflection and bending of the absorber tube [1].

This chapter deals with direct steam systems and proposes incorporation of internal helical fins within the absorber tube.

The purpose of the helical fin is to provide a regularly pitched and orderly distribution of flow from the 'hot' to the 'cold' side of the absorber tube. A CFD simulation using FLUENT software was carried out for three types of steel pipes with different internal helical fins, and an aluminium pipe without fins. This was done to investigate the resulting effect on heat transfer as well as the uniformity of the distribution of heat within the absorber tube walls.

4.1 Introduction

The absorber tube is located at the focal axis, through which the liquid to be heated passes. The tube is surrounded by a transparent cover, allowing a vacuum between the absorber tube and the glass-cover tube, the main function being to reduce heat loss. Two designs are currently in use, the traditional design in which oil is used as the primary heat collection medium, along with a secondary water/steam circuit, and a more modern direct steam generation system.

In a DSG system, steam is generated directly inside the trough collector as opposed to indirect heating by a heat transfer fluid (HTF). The feasibility of the direct steam generation technology was demonstrated within the DSG project funded by the European Union [2]. For DSG, three different operating concepts have been studied; the once-through mode, the recirculation mode and the injection mode.

In a common heat exchanger, where energy is being exchanged between two fluids, the temperature profile at any given cross section is quite uniform, barring the small temperature gradient across the thermal boundary layer. When one considers heat exchangers such as a water-tube boiler of a large power plant, there may be slight asymmetries of heat flux on the circular tubes due to the presence of radiant fields, such as heated walls of the boiler as well as radiation exchange from neighbouring water-tubes. A good discussion of such asymmetric radiation fields has been provided by Muneer et al [3].

In contrast, a parabolic solar flux concentrator that is presently the subject of discussion poses an interesting challenge for the receiver tube. References are made herein to work of Cheng et al [4] and Flores et al [1]. In the work of Cheng, (with a parabolic trough collector of 5m and a receiver tube aperture length of the 7.8m) the three-dimensional numerical simulation of coupled heat transfer characteristics in the receiver tube was performed by combining the MCRT Method and FLUENT software. At best the solar flux field is incident on only one-half of the circumference resulting in a highly asymmetric thermal boundary layer profile and temperature.

For the sake of development of the present argument the semi-circular side of the receiver directly opposed to the solar flux is named 'hot' and the other semi-circular side is named 'cold'. Note that the 'cold' side is the recipient of only the ambient solar flux, i.e. sky-diffuse and un-concentrated solar beam radiation.

When water flows through the above receiver tube at a significant velocity, it is inevitable that the bulk of the water will alternately contact the 'hot' and the 'cold' side, albeit in an irregular fashion, due to the turbulent nature of the flow. Such a flow of water produces large thermal stresses and thermal shocks.

It has also been reported that the thermal stresses may cause a bending of the absorber tube, causing a rupture of the glass cover. This bending has been associated with the thermal gradient produced by the boiling of water, and the effects are related to the thermal conductivity of the absorber tube, the flow pattern and asymmetry of the temperature distribution on the absorber tube [1].

In DSG concepts, the position of the border between the two-phase region and the superheating section might vibrate along the absorber's length; the resulting thermal stress limits the durability of the absorber pipes and has to be considered when evaluating the DSG concept [5].

This chapter suggests the use of internal helical fins in the absorber tube to reduce the thermal stresses and thus the uniformity of the distribution of heat within the absorber tube walls is suggested.

The purpose of the helical fin is to provide a regularly pitched and orderly distribution of heat flow from the 'hot' to the 'cold' side of the absorber tube. Fluent 6.2 was used for CFD analysis. A CFD simulation was carried out for three types of steel pipes with different internal helical fins, and an aluminium pipe without any fins.

4.2 Computational fluid dynamics (CFD) simulation

In the last two decades, CFD has emerged as an effective tool for solving complex flow problems. It provides an insight to flow details that in the past was unachievable through experimental means. The technology has been well received by the industry. CFD now caters for a wide range of industrial applications. CFD is interested with the efficient numerical solution of the partial differential equations that describe fluid dynamics.

Ashley [6] introduces the three main stages in a CFD study. The first is a time pre-processor which is used to input the problem geometry, generate the grid and define the flow parameters and the boundary conditions to the code. The second is a flow solver which is used to solve the governing equations of the flow subject to the conditions provided. There are four different methods used as a flow solver: (1) finite difference method, (2) finite element method, (3) finite volume method, and (4) the spectral method. The third stage is a post-processor which is used to display the data and show the results in graphical and easy to read format.

CFD simulation was carried out to compare three types of steel pipes with different internal helical fins. The simulation results are used to identify the heat transfer improvement as well as the uniformity of the distribution of heat within the pipe walls. Pipes with internal helical fins pitches of 100-, 200- and 400mm were analysed through CFD. The effect of the helical fins can only be benchmarked if compared to a pipe without helical fins and therefore results for a simple pipe are also presented in this chapter.

4.2.1 Geometry details

The total length of the pipe used for analysis was 990mm and the helical fins were created as per manufacturing drawings into 3D CAD using Autodesk Inventor. Fig4.1 shows the general dimensions of the pipe with a 100mm pitch inner helical fin. The geometries were then exported into "step" file format and imported into Hyper-mesh software which was used for meshing purposes.
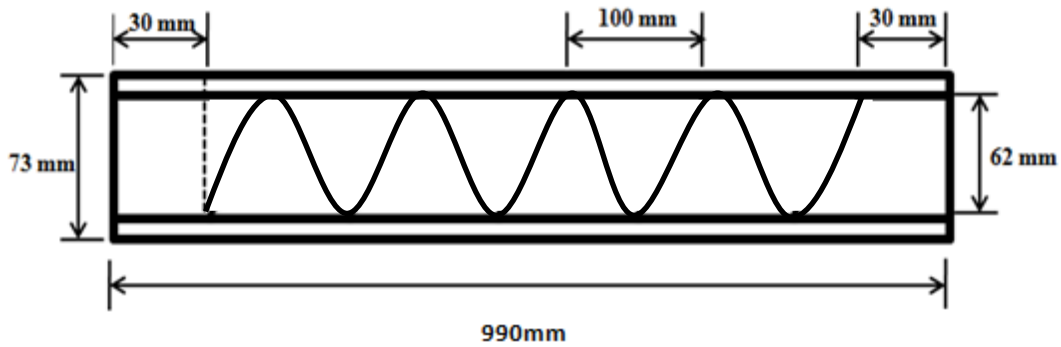
Figure 4.1 General dimensions of the pipe with inner helical fins of pitch 100mm

The outer surface of the pipe was split along the pipe axis into two main segments. One segment represented the 'hot side' while the other surface represented the 'cold side, refer see Fig4.2.
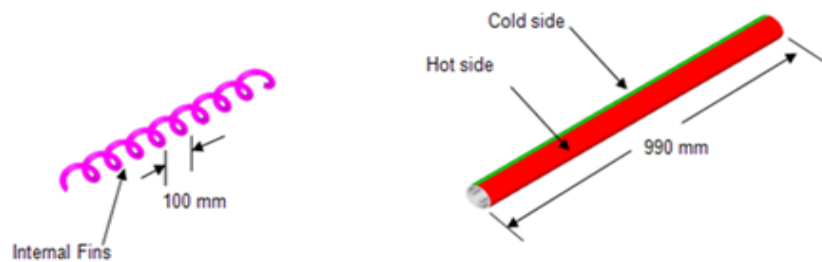
Figure 4.2 The outer surface of the pipe and the internal fins

4.2.2 Mesh details

Mesh size is an extremely important parameter for producing a valid CFD analysis. There are several parameters that need to be taken into consideration before the mesh size is determined. Computation speed and system memory are two such basic parameters. Through the information available on the internet of the CFD studies and software manual, it was clear that for a Windows NT 32 bit platform, with 2 Gigabytes of RAM (Random Access Memory), a maximum of 5 million cells was the limit. Although the system could handle higher cell numbers it became prone to system overload and eventually led to failure. Benchmark simulations further ascertained that the limitation was 5 million cells.

A general benchmark rule for CFD simulation suggests 1mm to be the minimum thickness of the cells closest to the boundary [7]. However using this criterion can lead to extremely large mesh sizes (far exceeding 5 million cell count) particularly for systems that are in the order of a few meters. Haroon Junaidi et al [7] summarized in detailed mesh sizes for convective heat transfer problems and has suggested the use of at minimum of 1 node inside the boundary layer of the convective system to be analysed. Where, the boundary layer thickness can be determined through regressions. It should be noted that moving away from the boundary, cells cannot be grown in size very rapidly as this could lead to numerical errors. A growth factor of 1.2 for the length has been suggested in the Fluent Manual [8]. A further limitation is the mesh software capability. During the meshing procedure, the possibility of generating a mesh with a high number of skewed cells increases particularly when meshing in 3D, if cells are grown in size from the boundary walls.

In light of all the above factors, a mesh size of a minimum 3mm was chosen to analyse the system. This mesh size produced around 5 million cells for the 1 meter pipe section. When the mesh was set up for analysis, for each test case, it took around 36 hours of computation time on a continuous run.

Four geometries (Pipes with internal helical fins pitches of 100-, 200-, 400mm and pipe without helical fin) were studied, i.e.

For the ease of analysis, two geometry assumptions were made:
1) The thickness of the fin was 1mm.
2) The fins were assumed to be attached to the inner surface of the pipe. When fabricating, the fins are welded over a smaller metallic pipe which slides into the main pipe.
3) The fins were represented by two walls with non-solid material between them, therefore the heat capacity of the fins was zero.
4) The fins started 30mm from the pipe inlet.

Fig4.3 shows details of one of the mesh that was used.
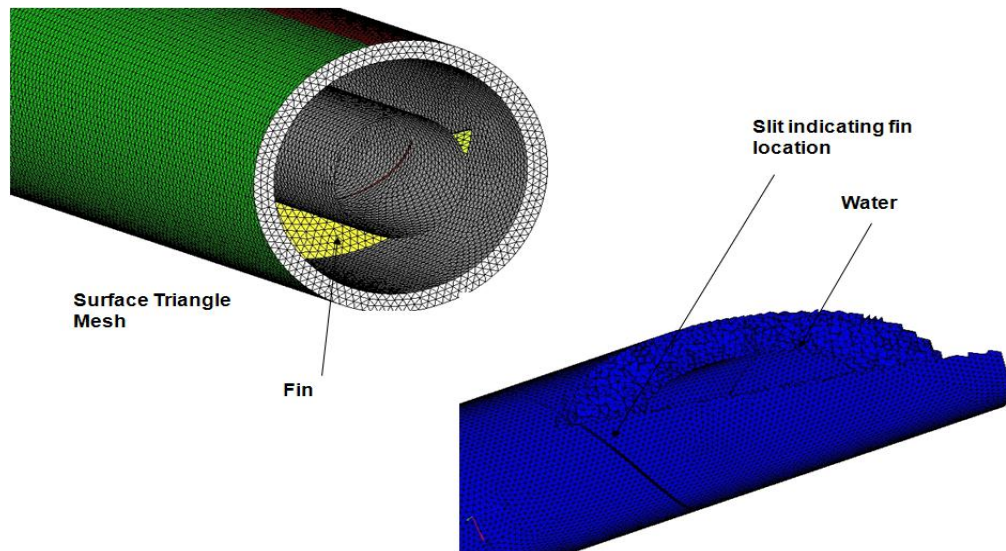
Figure 4.3 Mesh details

4.2.3 Boundary conditions and materials properties

The specification of boundary conditions is essential before starting any simulation. This specification consists of two elements: (a) the boundary conditions type, and (b) the location where it is applied. Boundaries conditions applied to the system vary with the purpose of the simulation.

Although 3mm mesh size is normally considered crude, particularly for internal flow, the length of the domain (~1m) and the available computer resources prompted two levels of analysis. As the current analysis is comparative, qualitative results allow a conclusion to be made.

The boundary conditions were as follows:

1) K- ε turbulence model was used with Turbulent intensity of 5% .
2) At the inlet, a mass flow rate of 0.8kg/s and 100 bar pressure were applied.
3) Density, viscosity and other thermal properties were assumed to be constant.
4) The number of iterations for each case was kept at a minimum of 1500. The rather large number of cells (~5 million) and iterations ensured that full convergence was achieved for each computational case.
5) An inlet temperature of 22 °C was assumed at the inlet.

Thermal properties for the materials used are shown in Table 4.1

Table 4.1 Thermal properties for Steel and Aluminium

Materials	Density kg/m^3	Specific heat J/kg.K	Thermal conductivity W/mK
Steel	8030	502.48	16.27
Aluminium	2719	871	202.4

4.3 Radiation profiles

Two different radiation profiles have been used in the analysis (Profile1 & Profile2 as shown in Fig4.4). These profiles indicate the level of solar radiation on the circumference of the pipe after concentration. Profile1 is direct usage of Cheng's profile, without alteration. Profile 2 has been calculated by using Cheng's data and finding the proportional flux for the size of the pipe used. Fig4.4 presents the solar energy flux distribution for profiles 1and 2 on the outer wall of the inner absorber tube, under concentration. Fig4.5 (a, b) indicates the heat flux for eighteen strips for Profile 2, the other have the same values mirrored about the horizontal axis. Note that the rest of the pipe was given a uniform heat flux (diffuse radiation) of 0.22 kW/m^2 and (beam and diffuse radiation) of 1.12kW/m^2 at angle 30°.
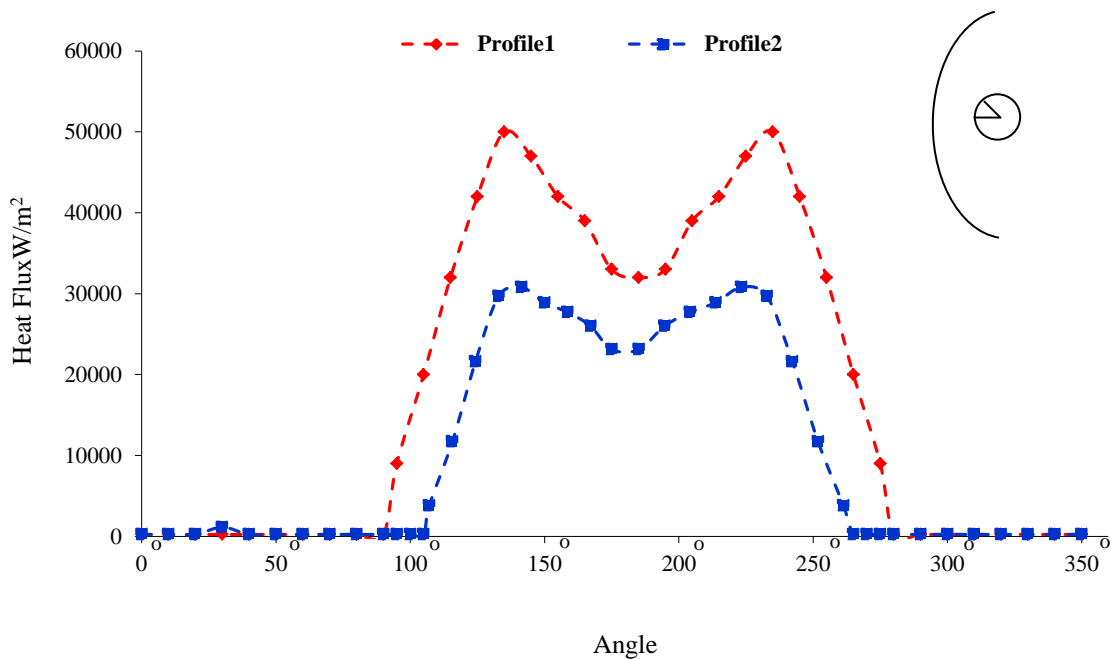
Figure 4.4 Heat flux around the absorber tube for profiles 1 and 2

<div align="center">

a   b

</div>
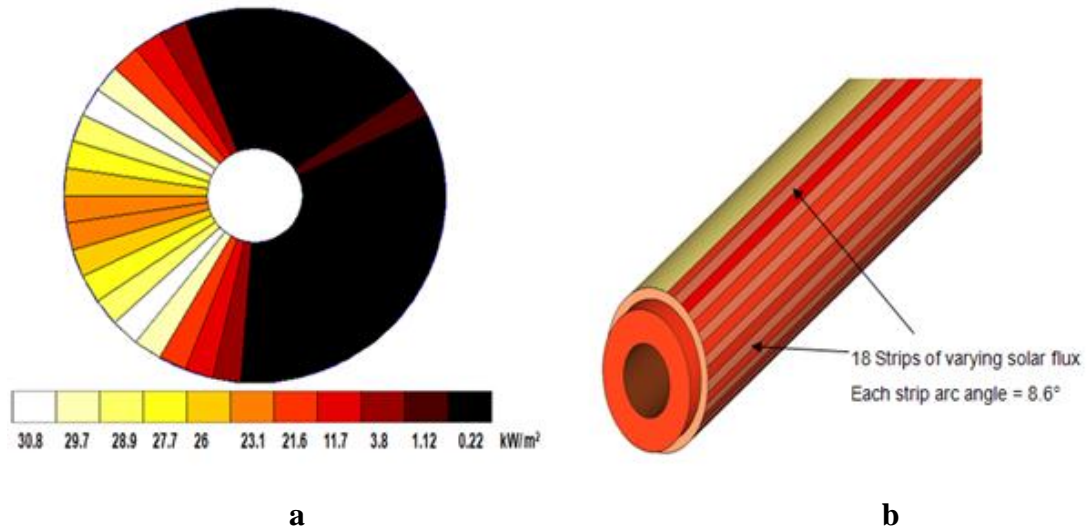
Figure 4.5 (a) Solar energy flux distribution on the outer absorber tube surface, and (b) 18 strips of varying solar flux for profile 2

4.4 Bursting pressure of Aluminium pipe

Since the operating pressure of DSG power plant is kept constant at approx. 100 bar, it is necessary to calculate the bursting pressure of the aluminium pipe. In order to determine of the aluminium pipe wall would burst under this inner pressure. The definition of the burst pressure is the pressure at which a system is expected to fail. The highest pressure borne by burst pressure is a fundamental parameter for the applications.

The quality of the material and its thickness can determine how much pressure it will withstand. Barlow's formula [9] can be used to estimate burst pressure of the aluminium pipe.

$$P = \frac{2*S*t}{D_o}$$

(4.1)

where:

P: is the maximum working pressure (psi)

S: is material strength (psi)

t :is the wall thickness (in)

D_o: is the outside diameter (in)

Once the burst pressure of the tube has been calculated, working pressure is calculated using the following formula:

$$WP = \frac{P}{SF}$$

(4.2)

Where:

SF :is the safety factor (in general 1.5 to 10)

The material yield strength in psi for pure aluminium is 24000 psi

4.5 Results and discussion

Figs 4.6, 4.7 and 4.8 show the contours of temperature distribution for a steel pipe without helical fins, a steel pipe with 100mm pitch helical fins, and an aluminium pipe also without internal helical fin for profile1. The average surface temperature for the 'cold' side was 299-, 301- and 304K and for the 'hot' side was 333-, 317- and 315K, with a maximum temperature 341-, 333- and 320K respectively for the above three cases.
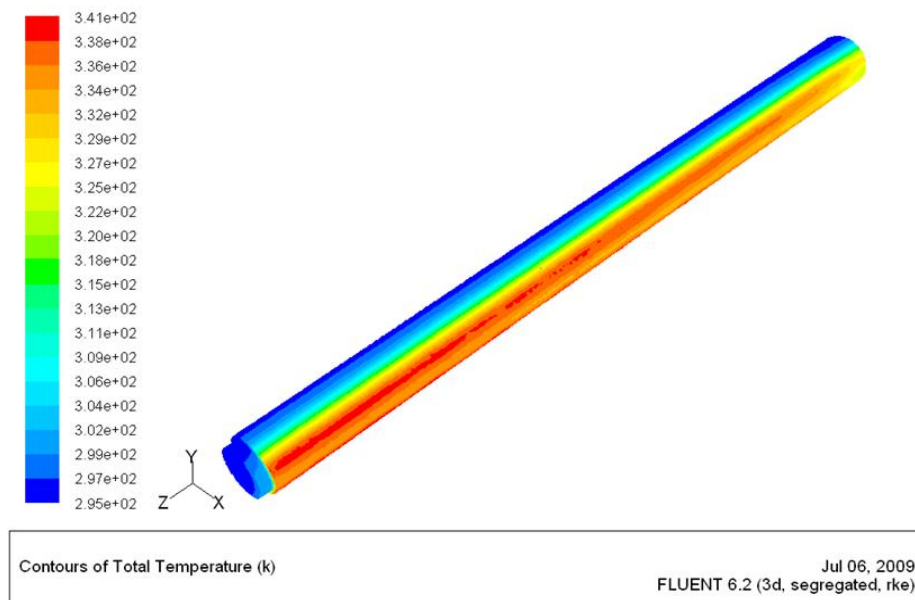
Figure 4.6 The contours of temperature (K) for a steel pipe without helical fin (profile-1)
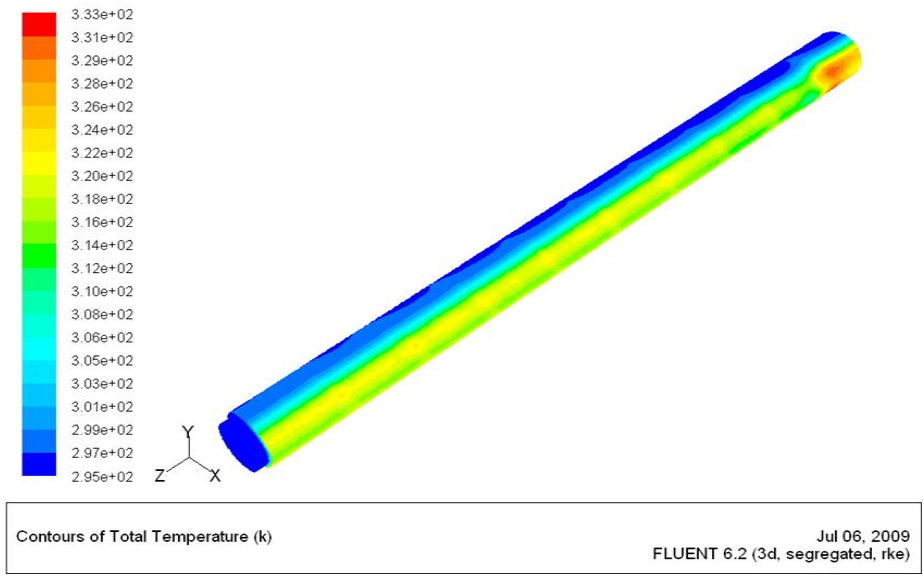
Figure 4.7 The contours of temperature (K) for a steel pipe with a 100mm pitch helical fins (Profile-1)
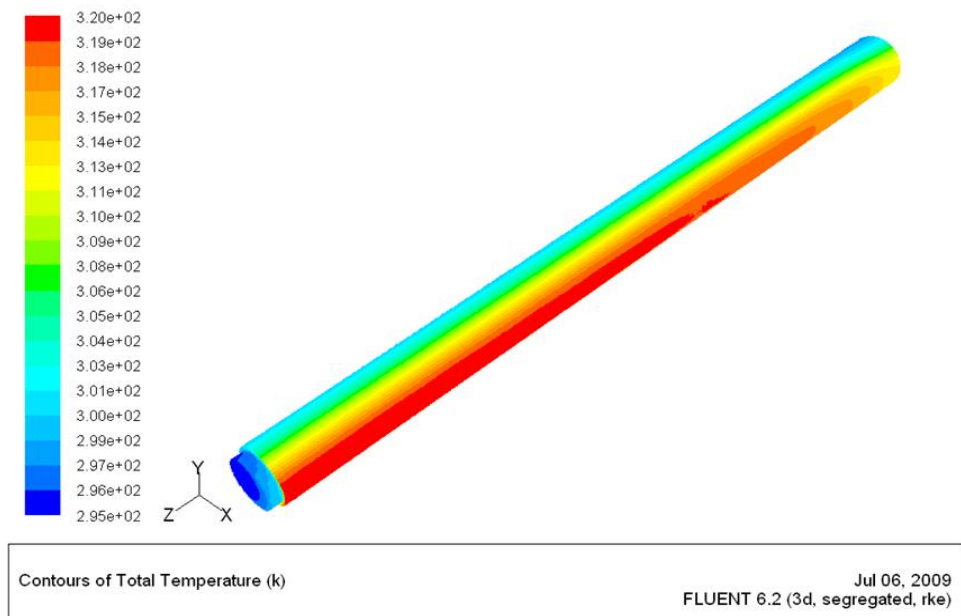
Figure 4.8 The contours of temperature (K) for Aluminium pipe without helical fins (profile-1)

The contours of temperature distribution for pipes without and with 100, 200, and 400mm helical fin pitch for profile-2 are shown in Figs4.9, 4.10, 4.11 and 4.12. The average surface temperature for 'cold' side was 296.7-, 296-, 296.5- and 297K respectively and 317-, 308-, 309.5- and 311.5K for the 'hot' side respectively. The maximum temperature was 320K for the pipe with a 100mm helical fin pitch because of stagnation of the fluid before the fin location. In the 100mm helical fin, the maximum temperature attained is much higher, however it is a localized phenomenon. Also note that for the pipes with helical fin pitches of 200- and 400mm the maximum temperature was 315- and 318K respectively, and 325K for the pipe without an internal helical fin.

It is to be noted that the average surface temperature differences between the cold and hot sides are 10.8-, 13- and 14.9K for pipes with 100-, 200- and 400mm helical fin pitch respectively, and 20.3K for the pipe without an internal helical fin.
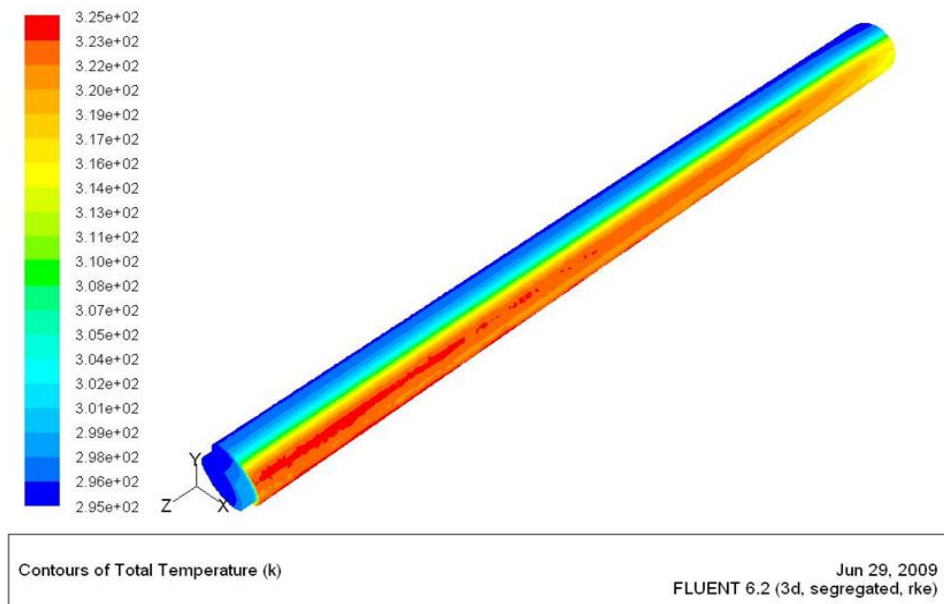
Figure 4.9 The contours of temperature (K) for a steel pipe without helical fins (profile-2)
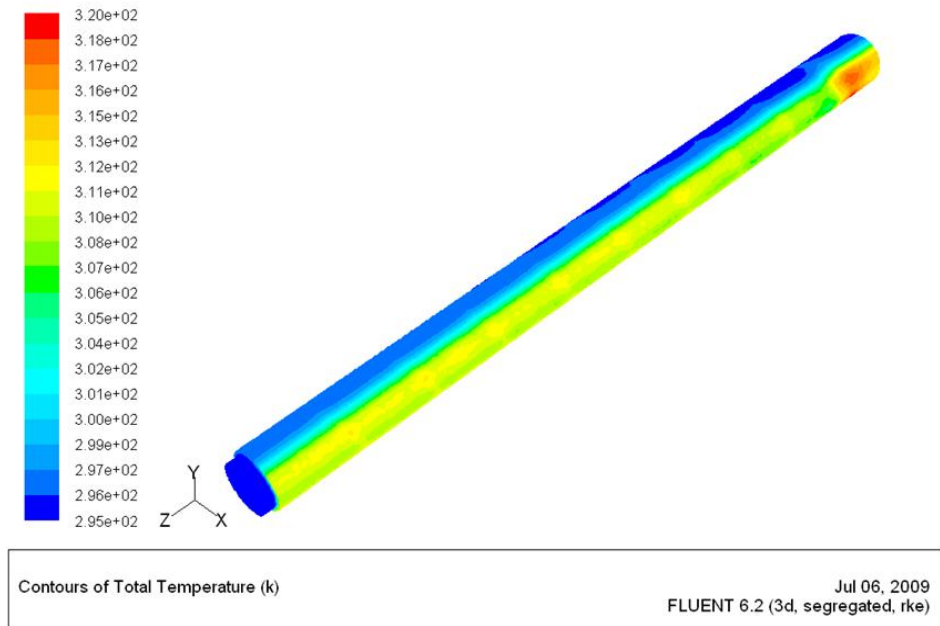
Figure 4.10 The contours of temperature (K) for a steel pipe with a 100mm pitch helical fins (profile-2)
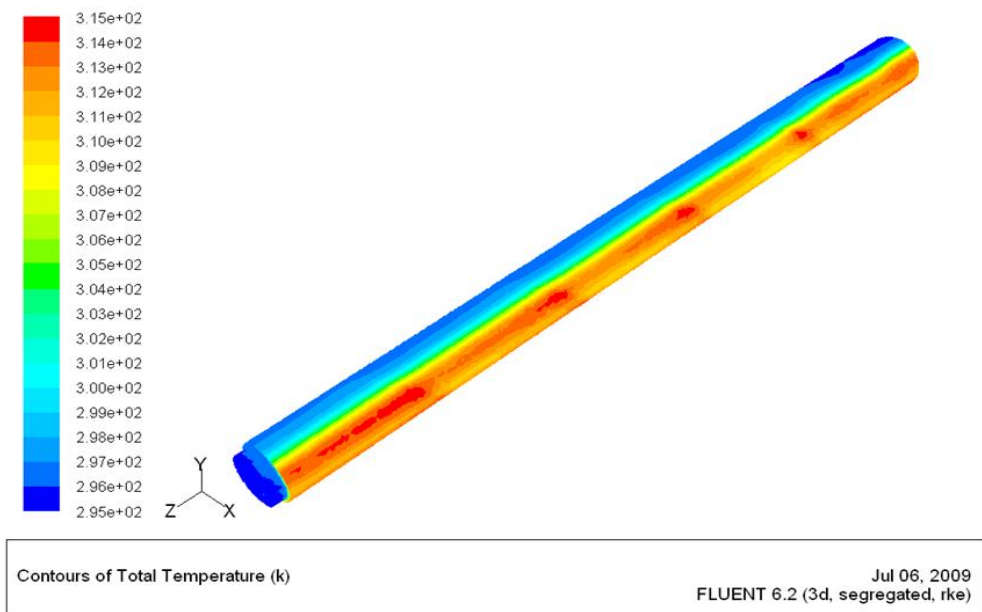
Figure 4.11 The contours of temperature (K) for a steel pipe with 200mm pitch helical fins (profile-2)
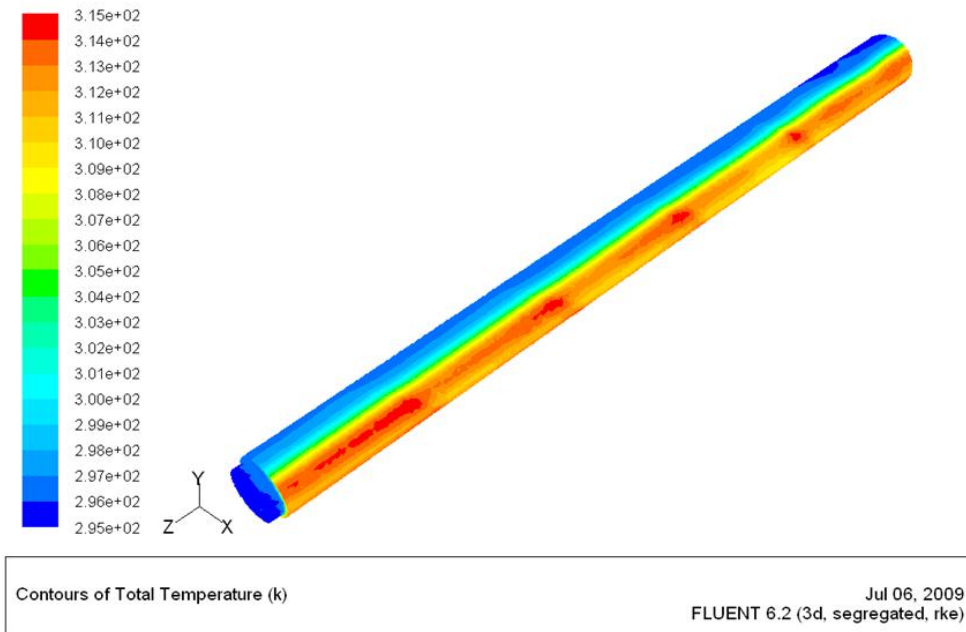
Figure 4.12 The contours of temperature (K) for a steel pipe with 400mm pitch helical fins (profile-2)

Fig 4.13. shows the temperature distribution around the outer pipe surface at a section 500mm from the inlet for all of the different pipe and helical fin configurations that have been studied. For the pipe without helical fins (profile 1), the thermal gradient between the upper and lower temperature, $\Delta T = 43.8^{\circ}\text{C}$ is higher compared with the pipes with 100mm pitch helical fins where the thermal gradient is $\Delta T = 25.8^{\circ}\text{C}$. For pipes with 100-, 200-, 400mm pitches helical fins and without helical fins (profile 2), the thermal gradient between the upper and lower temperature is 22.8- , 18- , 20.6- and 27.6°C respectively.
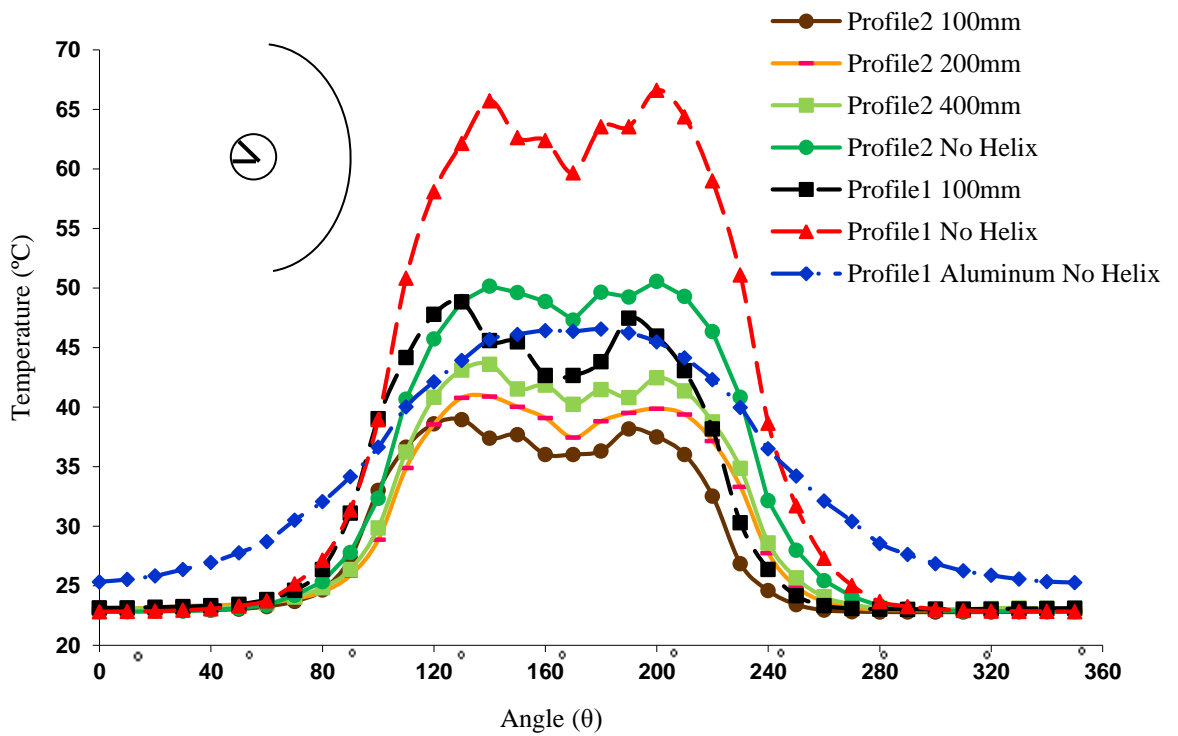
Figure 4.13 The distribution of temperature around the outer surface of pipes with and without helical fins at a section 500 mm from inlet.

For all four pipes, the temperature on the cold and hot sides was checked. The values are listed in Table 4.2 (for Profile 2).

Table 4.2 Temperature on cold and hot sides for four pipes

Pipe	Average Surface Temperature- K (Cold side)	Average Surface Temperature -K (Hot Side)	Temperature Difference	Maximum Temperature -K	Inlet velocity (m/s)
100 mm	296.24	307.7	10.76	312	0.354
200 mm	296.49	309.5	13.01	315	0.354
400 mm	296.65	311.5	14.85	318	0.354
No Helical fins	296.73	317.0	20.27	325	0.257

Also, it is to be noted that the thermal gradient between the upper and lower temperature for aluminium pipe without helical fins (profile 1) (ΔT =21.3^{o}C) is much lower when compared to the result for steel pipe without helical fins (profile1). This

is due to large difference in the thermal conductivity of the two materials under discussion.

Asymmetry indices have presently been introduced by means of the mean and standard deviation of circumferential temperature distribution. It was found that the respective mean water temperatures for the above pitches (profile2) were 301.3- , 302.3- and 303.2K compared to 307.6K for the pipe without fin and the corresponding values of standard deviation were 6.5- , 7.3- , 8.3-, and 11.6K respectively. Furthermore, the mean water temperatures for a pipe with 100mm, without helical fin and aluminium pipe without helical fin (profile 1) were 304.6- , 311.5- , and 307.6K respectively; also the corresponding values of standard deviation were 10.1- , 17.7- and 8.2K respectively.

One of the penalties of using internal helical fins though is the increased pressure drop that would occur in such systems. Presently, pressure drops occurring within finned and unfinned pipes were obtained through the CFD analysis. For each case of finned pipe a ratio of pressure drop for that case compared with the drop within an unfinned pipe was obtained and these pressure ratios are shown in Table 3. It is seen that the pressure drop across the pipe with a 100mm pitch helical fins is more than four times the pressure drop recorded in the pipe with a 400mm pitch helical fin.

Table 4.3: Pressure drop ratios for pipes with and without helical fin (pipe inner diameter = 62mm)

Helix pitch, mm	Pressure drop ratio
100	15.6
200	5.4
400	3.3

4.6 Conclusion

Solar-thermal power plants have been in use for several decades in deserts. To date, two types of fluids have been used in such ventures, i.e. synthetic aromatic fluid or direct steam generation. Fluid flow in parabolic trough systems leads to instability in the steel absorber tube, due to the highly concentrated solar flux on only one-half of the circumference of the absorber tube which results in an asymmetrical distribution

of temperature. In this chapter, a computational fluid dynamics (CFD) simulation was carried out to compare the thermal gradient within steel pipes with three alternative pitches of internal helical fins. It has been ascertained that the presence of the fins improves the thermal distribution and the 100mm pitch helical fin proved to be better than the 200 and 400mm pitch helical fin pipes. Thus, with the introduction of internal fins it was found that the circumferential temperature distribution was much more homogenous with standard deviation being halved. However, the pressure drop across the pipe with100mm pitch helical fins is more than four times the pressure drop recorded in the pipe with 400mm pitch helical fins. Furthermore, aluminium pipe showed the best results despite not having any helical fins, i.e. the absorber tube material with higher thermal conductivity appears appropriate especially in preheating and evaporating sections. This suggests that the conductivity of the material is important and has greater bearing than the presence of the fins. The heat transferred to water by the pipes with helical fins is higher than that without the fins.

References

[1].   Flores, V., Almanza,R., *Behavior of the compound wall copper–steel receiver with stratified two-phase flow regimen in transient states when solar irradiance is arriving on one side of receiver.* Solar Energy, 2004. **76**: p. 195–198.

[2].   Ecka,M.,Eickhoffa.,J. Rheinlander.,L. Valenzuela., *A pplied research concerning the direct steam generation in parabolic troughs.* Solar Energy 2003. **74**: p. 341-351.

[3].   Muneer,T.,Kubie,J.,Grassie,T.,*Heat Transfer: Aproblem Solving Approach*2003, London: Taylor and Francis.

[4].   Cheng, Z.D., Y.L.H., Xiao, J., Tao ,Y.B., Xu ,R.J., *Numerical Study of Heat Transfer Characteristics in the Solar Receiver Tube Combined With MCRT Method*, in *Proceedings of the International Solar Energy Conference 'Solar Engineering 2009'*, ASME,China

[5].   Ecka, M., Hirsch,T., *Dynamics and control of parabolic trough collector loops with direct steam generation.* Solar Energy, 2007. **81** p. 268-279.

[6].   Ashley, D. *Introduction to CFD*. Spring 2011; Available from: http://personalpages.manchester.ac.uk/staff/david.d.apsley/lectures/comphydr/introcfd.pdf#search=%22Introduction%20to%20CFD%22.

[7].   Junaidi,H.,Douglas,H.,Grassie,T.,Currie,J.,Muneer,T.,*Finitevolume computational fluid dynamics package for solving convective heat transfer cases.* International Journal of Mechanical Engineering Education, 2008. **36**: p. 92-112(21)

[8].   *FLUENT 6.3 UDF Manual*. 2006; Available from: http://www.hipecc.wichita.edu/pdfs/fludf.pdf.

[9].   *PRESSURE RATING OF HYDRAULIC TUBING*. 2001; Available from: http://4wings.com/lib/files/tubing.pdf.

CHAPTER 5

Large-Scale PV plant for Al-Kufra: Energetic, economic and environmental impact analysis

Chapter Map

5.0 Overview

5.1 Introduction

5.2 Modelling the photovoltaic IV characteristics

5.2.1 The photovoltaic equations

5.2.2 The photovoltaic IV curve

5.2.3 Estimation of PV module parameters from manufacturer's data

5.3 Mathematical method for the optimum slope for stationary PV system

5.3.1 Slope solar irradiation

5.4 Thermal performance

5.4.1 Cell temperature calculation

5.5 Selection of the PV module

5.6 The computer model

5 Large-Scale PV plant for Al-Kufra: Energetic, economic and environmental impact analysis

5.7 The proposed 50MW PV power station (stationary) for Al-Kufra Libya

5.7.1 System design

5.7.2 Requirements of the PV system components

5.7.3 Financial analysis and payback period

5.7.4 Capacity factor and solar capacity factor

5.7.5 Greenhouse gas pollution

5.7.6 Results and discusion

5.8 Evaluation of a 50MW two-axis tracking plant for Al-Kufra Libya

5.8.1 Field requirement

5.8.2 Capacity factor and solar capacity factor

5.8.3 Greenhouse gas pollution

5.8.4 Financial analysis and payback period

5.8.5 Results and discusion

5.9 Comparison of stationary and tracking systems

5.9.1 Landscape impact

5.9.2 Performance

5.10 Conclusion

5.0 Overview

As mentioned in Chapter 2, Libya has a growing demand for electricity and presently generates almost all of its electrical energy using fossil-fuelled generation plant. An opportunity exists to utilise the high solar radiation levels incident on the south of the country to meet this demand.

This chapter describes the design of a 50MW PV power plant (stationary and tracking) which has been modelled on the conditions pertaining to Al-Kufra. The general energy situation within Libya is described, along with the solar conditions at the proposed location of the power plant in Chapter 2. An HIT (hetero-junction with intrinsic thin layer technology which combines both mono crystalline and amorphous silicon in the one structure) type PV module has been selected and modelled. The effectiveness of the use of a cooling jacket on the modules has been evaluated for a stationary system. Furthermore, the comparison has been carried out between stationary and tracking (two axis) PV plant with respect to landscape impact and performance.

5.1 Introduction

Large scale use of solar energy for electricity production is currently in the demonstration phase. Lessons learnt from the pilot projects will benefit the implementation of future power plants. Presently, key examples of such pilot projects are presented in Chapter 2. These examples lead to the conclusion that the most economic implementation will be large scale, grid connected PV systems.

Since the large scale PV (LS-PV) power plant concept is relatively new, so these different technologies (stationary and tracking system) are to date competing with no clear "winners", even if most of the biggest PV plants (i.e. within the range of 40-70 MWp) have been realized as stationary systems.

The scope of this chapter is to examine and evaluate the potential of LS-PV power generation systems in the southern region of Libya at Al-Kufra for both stationary and tracking systems.

Temperature has an important effect on the power output and efficiency of photovoltaic cells. The present study shall present a simulation model for a 50MW LS-PV power plant with and without a cooling system using water as the working fluid, for a stationary system. A system without cooling for a tracking system is also modelled.

5.2 Modelling the photovoltaic IV characteristics

In sizing and designing photovoltaic power systems, it is important to model their electrical output. The electrical output of a PV module (and consequently PV arrays) is given by its current-voltage (IV) characteristic. A precise IV characteristic of a PV module is necessary to accurately estimate its performance, select appropriate components, and optimise efficiency.

This section is concerned with mathematically describing the photovoltaic current-voltage (IV) characteristic and suggesting a simple method for constructing the IV curve.

Relationships between the theoretical parameters in the PV-IV equations and measurable quantities (usually supplied by manufacturers) are provided in this section. More importantly, however, a method for translating the PV-IV characteristic from reference conditions of irradiance and module temperature (supplied by manufacturer or measured) to any general set of conditions is also provided herein.

5.2.1 The photovoltaic equations

The current produced by a PV module is calculated from,

$$I = I_{LG} - I_d - I_{sh} \tag{5.1}$$

where I_{LG} is the light-generated current , I_d is the diode current and I_{sh} is the current through the shunt resistance. Also

$$I_d = I_o(e^{\frac{V+I.R_S}{A}} - 1) \tag{5.2}$$

where I_o is the reverse saturation current, V is the voltage across the PV module, R_s is the internal series resistance and A is a curve fitting parameter.

$$I = I_{LG} - I_o(e^{\frac{V+I.R_S}{A}} - 1) - \left(\frac{V+IR_S}{R_{Sh}}\right) \tag{5.3}$$

The last term in Eq.5.3 is often neglected as R_{sh}, for most modern cells, is very large [1].

The PV-IV characteristic equation is obtained by substituting Eq. 5.2 in Eq. 5.1,

$$I = I_{LG} - I_o(e^{\frac{V+IR_S}{A}} - 1) \tag{5.4}$$

It is clear from Eq. 5.4 that in order to fully describe the PV-IV characteristic, four parameters, namely, I_{LG}, I_o, R_s and A, need to be determined. Knowing these four parameters, I values are calculated for different V values and the IV curve is then constructed.

5.2.2 The photovoltaic IV curve

A typical IV characteristic is shown in Fig 2.27. The main features of a PV-IV curve are the short circuit current (I_{sc}), the open circuit voltage (V_{oc}), the maximum power

(P_m), the current at maximum power (I_m) and the voltage at maximum power (V_m). These parameters are defined in section 2.4.2.

The curve in Fig 2.27 (section 2.4.3) is based on Eq.5.3 while some manufacturers of PV modules provide the IV curve as part of their data, the majority of manufacturers give data of I_{sc}, V_{oc}, P_m, I_m and V_m at some reference conditions of air mass (AM), irradiance (G, W/m^2) and cell temperature (T_C, ºC). Typically, Standard Test Conditions (STC) used by manufacturers refer to 1.5AM, 1000W/m^2 and 25ºC. However, some manufacturers use other reference temperatures.

If the four parameters in Eq. 5.3, i.e. A, I_{LG}, I_o, and R_s are known, values of V can be assumed, I values calculated and the IV curve plotted. However, in Eq.5.4, I is an implicit function in V. As a result, for each value of V, I must be solved iteratively. By rearranging Eq.5.4, and taking the natural log of both sides, Eq.5.5 may thus be written,

$$V = A\ln\left(\frac{I_{LG} - I + I_o}{I_o}\right) - IR_s \qquad (5.5)$$

Using Eq.5.5, values of I are assumed first and V is calculated for each of these values. The IV curve can then be plotted.

5.2.3 Estimation of PV module parameters from manufacturer's data

The values of I_{sc}, V_{oc}, V_m and I_m refer to manufacturer's data. So the resulting IV characteristic is that at reference conditions.

I_{LG} can be assumed equal to I_{sc} with no significant error.

$$I_{LG} = I_{sc} \qquad (5.6)$$

An expression for I_o can be obtained by using the point (V_{oc}, 0) on the IV curve. Letting $I = 0$ in Eq. 5.5, and using I_{sc} for I_{LG} (note that I_o is very small compared to I_{LG} - I), the following equation is thus obtained [2],

$$I_o = I_{sc}e^{-\frac{V_{OC}}{A}} \qquad (5.7)$$

The series resistance R_S can be estimated based on a method described by Kunz and Wagner [3].

$$R_s = \left(-M \frac{I_{sc}}{I_m} + \frac{V_m}{I_m} \left(1 - \frac{I_{sc}}{I_m} \right) \right) \tag{5.8}$$

Where:

$$M = \frac{V_{oc}}{I_{sc}} \left(-5.411 \frac{I_m V_m}{I_{sc} V_{oc}} + 6.450 \frac{V_m}{V_{oc}} + 3.417 \frac{I_m}{I_{sc}} - 4.422 \right) \tag{5.9}$$

The constants in Eq.5.8 are not empirical constants; they have been determined from numerical methods and are independent of material properties.

The current fitting parameter,(A), can be determined from Eq.5.9 below [4]. This equation can be derived from Eq. 5.5 by using the point (V_m, I_m) on the IV curve, making use of Eq.5.5 and then rearranging the resulting equation.

$$A = \frac{V_m - V_{oc} + I_m R_s}{\ln\left(1 - \frac{I_m}{I_{sc}} \right)} \tag{5.10}$$

The manufacturer's data can then be transferred into an IV curve.

This IV curve will be needed in order to be able to estimate the performance of a PV system by using cell temperature and that procedure is described in sections 5.4.1.1 and 5.4.1.2.

The PV IV characteristic can be determined for any irradiance and cell temperature from reference (i.e. manufacturer's data). The four parameters in Eq.5.5 need to be expressed as functions of G and T_C (which in turn is a function of ambient temperature, T_a and wind speed, v).

In the SANDSTROM model, by Buresch [5], an IV curve is generated from a reference curve by correcting every single (V,I) data point for temperature and irradiance. It can be described by the following equations:

$$V = V_{ref} + \mu_{voc}(T_C - T_{C,ref}) - R_s \Delta I \tag{5.11}$$

$$I = I_{ref} + \Delta I \tag{5.12}$$

where:

$$\Delta I = \left(\mu_{I_{SC}} \left(\frac{G}{G_{ref}} \right) (T_C - T_{C,ref}) \right) + \left(\left(\frac{(G - G_{ref})}{G_{ref}} \right) I_{sc,ref} \right) \tag{5.13}$$

V and *I* are respectively the voltage and its corresponding current on the IV curve at the desired values of *G* and T_C, the subscript "*ref* " represents measurements at reference conditions, and μ_{voc} and $\mu_{I_{sc}}$ are respectively the open-circuit voltage and short-circuit current temperature coefficients. The series resistance, R_S, is assumed constant. The equations above also assume that the voltage and current temperature coefficients are constant and equal to μ_{voc} and $\mu_{I_{sc}}$ respectively.

The SANDSTROM model for generation of IV data from reference conditions provides accurate predictions when compared to measurements.

5.3 Optimising the output of stationary and two-axis tracking PV systems

In order to estimate the long-term performance of PV systems, radiation data is required. This data is usually available on a monthly-averaged or daily basis.

Solar radiation incident on any given surface can be decomposed into two components, the direct or beam component emanating from the sun, and a diffuse component resulting from multiple reflections and scattering due to particles in the atmosphere. The diffuse component may also include reflections from the ground and local surroundings, where the surface in question is sloped rather than horizontal.

Differentiating between the two components is vital for accurate calculations in most solar energy applications; however, a number of steps may be required to arrive at realistic estimates at an appropriate level of detail for a given location depending on

the basic data available. For this study the daily global radiation on the horizontal plane was made available for Al-Kufra by the Libyan Meteorological Office. Fig 5.1 shows the computational flow for any general surface, that is, one which may have a given orientation and slope.
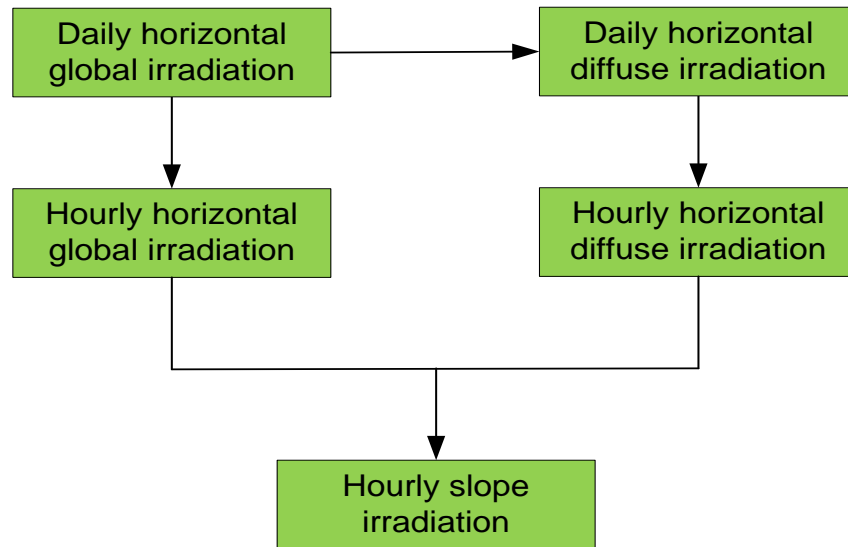
Figure 5.1 Calculation scheme for hourly slope irradiation

Furthermore, meteorological data such as hourly dry and wet bulb temperature, wind speed and relative humidity were also obtained.

5.3.1 Slope irradiation for stationary and tracking systems

The slope solar irradiation has three components, beam, diffuse and ground reflected.

$$I_S = I_{BT} + I_{DT} + I_g \tag{5.14}$$

Where I_S is slope radiation, I_{BT} the slope beam irradiance, I_{DT} the sky-diffuse irradiance and I_g the ground-reflected radiation.

According to Duffie et al [6], the optimum tilt for a fixed (non-tracking) system, would be around 24° (angle ≈ latitude) for Al-Kufra. Based on this the PV system was modelled at a tilt angle of 24° facing south.

The hourly slope beam irradiance is obtained from,

$$I_{BT} = I_B \left[\frac{\cos \theta}{\sin \phi} \right]$$

(5.15)

Where θ is solar incident angle and ϕ is solar Latitude angle.

If measured directly, I_B can be observed as the difference between the hourly horizontal global I_G and the diffuse irradiance I_D.

As previously discussed in Chapter 2, Muneer's model, [6], can be used for accurately determine tilted surface diffuse radiation by the following formula:

$$I_{DT} = I_D \cos^2(\beta/2) + \left(\frac{2b}{\pi(3+2b)} \right) \left[\sin \beta - \beta \cos \beta - \pi \sin^2 \left(\frac{\beta}{2} \right) \right]$$

(5.16)

where I_D is diffuse irradiance on horizontal plane, $\left(\frac{2b}{\pi(3+2b)} \right)$ is given by

$$\left(\frac{2b}{\pi(3+2b)} \right) = 0.04 - 0.82F - 2.0260F^2$$

(5.17)

F is the sky clarity index,

$$F = \left(\frac{I_G - I_D}{I_E} \right)$$

(5.18)

Where I_E is the horizontal extraterrestrial irradiance which can be estimated by the following formula:

$$I_E = 1367 [1 + 0.033 \cos(0.0172024 \, DN)] \sin \phi$$

(5.19)

where DN is the day number.

The ground –reflected radiation can be obtained from Eq-5.20,

$$I_g = \rho_{albedo} I_G \sin^2 \left(\frac{\beta}{2} \right)$$

(5.20)

where ρ_{albedo} is the average albedo of the ground.

Note that the surface albedo for sand is set to 0.34 (for white sand the range is from 0.34 to 0.40) [7].

For two-axis tracking system, $\gamma = 180 - \gamma_s$ and $\theta = 0$. The tilt angle of the two-tracking system was determined by

$$\text{Tilt angle} = 90 - \alpha_a \qquad (5.21)$$

5.4 Thermal performance

It is well known that the efficiency of a photovoltaic solar cell decreases with an increase in solar cell temperature, which plays a significant role in the PV cell performance and overall annual yield.

Two different methods of PV module operation are studied in this chapter: namely operation with and without a module cooling system. Mattei has proposed an accurate model for calculation of the cell temperature that is based on the energy balance[8]; that procedure is described below.

5.4.1 Cell temperature

Cell temperature T_C influences the *I-V* characteristics and therefore the electrical efficiency of the PV module. NOCT is the most common mode to determine the cell temperature and this parameter is given by the manufacturer's data for PV [8]. NOCT is defined as the cell or module temperature that is reached when the cells are mounted in their normal way at a solar radiation level of $G_T = 800 \text{W/m}^2$, a wind speed of 1m/s, an ambient temperature $T_a = 20\text{C}^\text{o}$ and no-load operation (module efficiency $\eta_C = 0$). According to Duffie et al [4], the cell temperature at any condition is found from,

$$T_c = \left(\frac{G_T \tau \alpha}{U_L} \right) \left(1 - \left(\frac{\eta_{Cell}}{\tau \alpha} \right) \right) \qquad (5.22)$$

where U_L is the overall heat transfer coefficient and $\tau \alpha$ the transmission-absorption coefficient.

The ratio $\left(\dfrac{\tau\alpha}{U_L}\right)$ can be determined from:

$$\left(\frac{\tau\alpha}{U_L}\right) = \left(\frac{T_{c,NOCT} - T_a}{G_{T,NOCT}}\right) \qquad (5.23)$$

In this chapter the energy balance has been used to compute the cell temperature with the following hypothesis.

- The radiation loss from the back-side of the PV module to ground has been neglected. (Inclusion of a basic calculation showing that there is less than 1% effect).
- Heat losses by conduction are neglected.
- The temperature on the PV surface is considered uniform.

Thermal losses from the PV module to its surroundings are an important factor, limiting the thermal performance of a photovoltaic thermal system. Such losses can be associated with all modes of heat transfer i.e., conduction, convection and radiation.

In the case of a photovoltaic thermal system, thermal losses (a) with and (b) without a cooling system can be represented by thermal network diagrams as shown in Fig5.2.
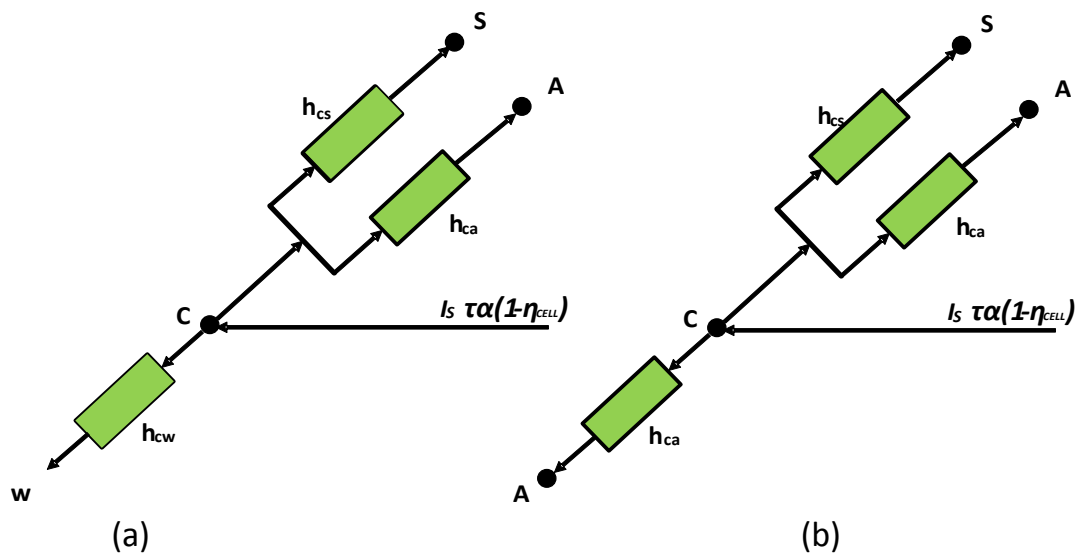
Figure 5.2 Thermal network (a) with water-cooling, and (b) without a cooling system

The analysis for the energy balance for steady state conditions is provided in the following sections.

Because it is difficult to use a cooling system in a full two-axis tracking system, section 5.8 will only discuss the full two-axis tracking system without a cooling system.

5.4.1.1 Operation without a water cooling system

The energy balance equation is given by

$$I_s \tau \alpha (1 - \eta_{cell}) = (h_{cs} * T_c - h_{cs} * T_{SKY}) + (h_{ca} * T_c - h_{ca} * T_a) \qquad (5.24)$$

where T_C is the cell temperature, T_{SKY} the sky temperature, T_a the ambient temperature, h_{cs} the heat transfer coefficient from the solar cell to the sky and h_c is the surface heat transfer coefficient for the front and back surfaces of the PV module.

- **Sky temperature**

According to EnergyPlus Engineering [9] the default calculation for the sky temperature is:

$$T_{SKY} = \left(\frac{Horizontal\_IR}{\sigma} \right)^{0.25} - T_a \qquad (5.25)$$

where $Horizontal\_IR$ is the horizontal infrared radiation intensity and T_a the ambient temperature.

Horizontal infrared radiation intensity is given by,

$$Horizontal\_IR = \varepsilon_{sky} \sigma T_a^4 \qquad (5.26)$$

where ε_{sky} is the sky emissivity and σ the Stefan-Boltzmann constant, $5.67*10^{-8}$ W/m^{2}K^4.

The ε_{sky} is given by:

$$\varepsilon_{sky} = \left(0.787 + 0.764 \ln\left(\frac{T_{dp}}{273} \right) \right) (1 + 0.0224N + 0.0035N^2 + 0.00028N^3) \qquad (5.27)$$

Where T_{dp} is the dew point temperature and N the opaque sky cover. For a clear sky, N=0

The dew point temperature may be obtained from:

$$T_{dp}= 6.091\,\alpha +0.4959\,\alpha^2 \tag{5.28}$$

where $\alpha =\ln (P_w)$ (5.29)

and where Pw is the partial pressure of water vapour which in turn is given by:

$$Pw = (P_{atm}*W_h)/(0.62198+ W_h) \tag{5.30}$$

where W_h is humidity ratio and P_{atm} is the atmospheric pressure.

- **Wind heat transfer**

Duffie and Beckman [6] suggest the use of the expression given by McAdams for flat plates exposed to outside winds,

$$h_{ca} = 5.67 + 3.8\nu \tag{5.31}$$

where h_{Ca} is the heat transfer coefficient for the flat surface and ν is the wind speed. According to Cole et al [10], $2*h_{ca}$ is the heat exchange coefficient corresponding to the total surface area of the module i.e. two times the surface area corresponding to h_{ca} because the heat is lost by the two faces of the PV module.

- **Radiative heat transfer**

The radiative heat transfer coefficient h_{cs} is determined by

$$h_{cs} = \frac{[\sigma\varepsilon_c(T_C^{\,4} - T_{SKY}^{\,4})]}{T_C - T_{SKY}} \tag{5.32}$$

Where ε_c is the emissivity of the PV module cover for long wavelength radiation.

For operation without a cooling system the initialization of the temperature T_C was first made as:

$$T_{Co} = T_a + 10$$

$$T_C = \left(\frac{I_s \tau \alpha (1 - \eta_{cell}) + (h_{cs} * T_{SKY} + 2 * h_{ca} * T_a)}{(h_{cs} + 2 * h_{ca})} \right) \qquad (5.33)$$

To set up the calculation iterative routine T_C is assumed to be 10 $^{\circ}$C above the dry-bulb temp. With the given input of dry- and wet bulb temp, the sky and dew-point temperature are obtained from Eqs 5.25 and 5.28. Then using Eqs 5.31-5.32 and 5.33, the improved value of T_C, i.e. T_{Co} is obtained. This improved value, is checked against the old value of T_C and further iterations carried out until the absolute of the difference between T_{Co} and T_C was less than 0.01.

- **Maximum power and efficiency of the PV module**

The maximum power is given by,

$$P_{max} = I_m V_m \qquad (5.34)$$

Where I and V can be calculated from Eq.s 5.11, 5.12 and 5.13.

The maximum power point efficiency η_{mp} of a module is given by:

$$\eta_{mp} = \frac{P_{max}}{A_c I_S} \qquad (5.35)$$

Where A_c is the module area.

The fill factor is a commonly used performance parameter to collectively describe the degree to which V_m matches V_{oc} and I_m matches $I_{sc.}$ Fill factor (FF) is given by,

$$FF = \frac{P_{max}}{I_{sc} V_{oc}} \qquad (5.36)$$

5.4.1.2 Operation with a water cooling system

This section covers the investigation of cooling the PV modules by the attachment of an aluminium water jacket at the back of the PV module. Fig 5.3 shows the geometry details of an experimental water-cooled jacket that was used for present investigation.
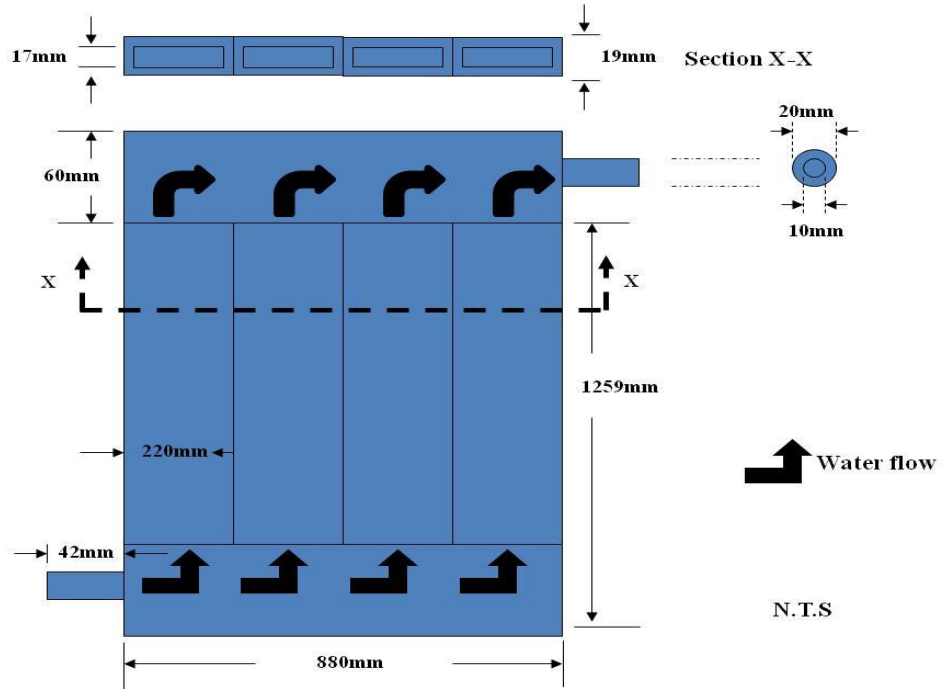
Figure 5.3 Geometry details for the cooling jacket

The energy balance equation in this case is given by,

$$I_S \tau \alpha (1 - \eta_{CELL}) = [((h_{cs} * T_C) - (h_{cs} * T_{SKY})) + ((h_{ca} * T_C) - (h_{ca} * T_a)) + ((h_{cw} * T_C) - (h_{cw} * T_w))] \quad (5.37)$$

where T_w is the water inlet temperature and h_{cw} is the heat transfer coefficient from the solar cell to the working fluid (water).

- **Convective heat transfer coefficient from the back panel of the PV module to the working fluid (cooling system)**

The convective heat transfer coefficient in enclosed spaces is calculated by the Nusselt number which is given by,

$$h_{cw} = \frac{Nuk_f}{D_e} \quad (5.38)$$

where

$$D_e = \frac{4(H * W)}{2(H + W)} \quad (5.39)$$

To evaluate whether the flow is laminar or turbulent, the Reynolds number is obtained first. Thus,

$$R_{eD} = \frac{V_f D_e}{\upsilon_f} \tag{5.40}$$

where υ_f kinematic viscosity of the fluid.

For laminar flows, from the results presented by Shah and Bhatti [11], the hydrodynamic entrance length is given by:

$$\frac{L_e}{D_e} \approx 0.0565 R_e \tag{5.41}$$

Where L_e is the hydrodynamic entrance length, R_e the Reynolds number and D_e the diameter of the tube.

For the combined entry length, a suitable correlation is of the form Sieder and Tate [12].

$$Nu = 1.86 \left(\frac{R_{eD} \, \mathrm{Pr}}{L/D} \right)^{1/3} \left(\frac{\mu}{\mu_S} \right)^{0.14} \tag{5.42}$$

$$\left(\begin{array}{l} 0.48 < \mathrm{Pr} < 16.700 \\ 0.0044 < \left(\dfrac{\mu}{\mu_s} \right)^{0.14} < 9.75 \end{array} \right)$$

The Nusselt number for laminar, fully developed, Pr $\geq$0.6 may be shown to be of the form [13].

$$Nu = 3.66 \tag{5.43}$$

For turbulent flows Bhatti and Shah [14] recommended that the hydrodynamic entrance length be computed from the formula of Zhi-qing,

$$\frac{L_e}{D_e} \approx 1.359 R_e^{\frac{1}{4}} \tag{5.44}$$

For turbulent, fully developed, the Nusselt number may be shown of the form

$$Nu = 0.023 R_e^{4/5} P_r^{0.4} \tag{5.45}$$

This equation has been confirmed experimentally for a range of conditions

$$\begin{cases} 0.7 \leq \mathbf{Pr} \leq 160 \\ R_e \geq 10{,}000 \\ \dfrac{L}{D} \geq 10 \end{cases}$$

The cell temperature for a PV module with a cooling system is given by:

$$T_C = \left(\frac{(I_S \tau \alpha (1 - \eta_{cell}) + (h_{cs} * T_{SKY} + h_{ca} * T_a) + (h_{cw} * T_w))}{(h_{cs} + h_{ca} + h_{cw})} \right) \tag{5.46}$$

Using the above mentioned equations an iterative computer program was developed using VBA.

The initialization of the temperature T_C and T_w were first made as:

$$T_{Co} = T_a + 10$$

$$T_w = T_{wb} + 5$$

where T_{wb} is the wet bulb temperature.

As mentioned in section 5.4.1.1, iterations were made until the difference between T_{Co} and T_C was less than 0.01 using the equations developed above.

- **Maximum power and efficiency operation with a water cooling system**

The maximum power for operation with a cooling system is given by:

$$P_{\max\,cooling} = IV \tag{5.47}$$

where I and V can be calculated from Eq.s 5.10, 5.11 and 5.12

The maximum power point efficiency of a module with a cooling system is given by:

$$\eta_{mpcooling} = \frac{P_{\max\,cooling}}{A_c I_S} \tag{5.48}$$

where η_{mp} is the maximum power point efficiency and A_c is the module area.

5.5 Selection of the PV module

Most commercial PV modules now available in the market have widely different characteristics. Consequently, it is important that appropriate criteria are used to

select a PV module to suit the climatic conditions in Libya. These criteria include improved efficiency at high temperature.

The HIT PV module from Sanyo, rated at 200W has been used in this study. These solar panels use hetero-junction with intrinsic thin layer technology which combines both mono crystalline and amorphous silicon in the one structure. It is composed of a textured n-type c-Si wafer sandwich between p-type/i-type (Ultra-thin amorphous silicon layer) and i-type/n-type [15].

HIT technology offers the following advantages:

1. The claimed cell efficiency is in excess of 19% with a module efficiency of 17%
2. The modules have good temperature characteristics.

The selected module specifications are summarized in Table 5.1.

Table 5.1 Specifications of the PV module [15]

Electrical specification	
Model	HIT Power 200
Rated Power (Pmax)[1]	200 W
Maximum Power Voltage (Vpm)	55.8 V
Maximum Power Current (Ipm)	3.59 A
Open Circuit Voltage (Voc)	68.7 V
Short Circuit Current (Isc)	68.7 V
Temperature Coefficient (Pmax)	-0.29% / °C
Temperature Coefficient (Voc)	-0.172 V / °C
Temperature Coefficient (Isc)	0.88 mA / °C
Cell Efficiency	19.7%
Module Efficiency	17.2%
Mechanical specification	
Module Area	$1.16m^2$
Weight	15kg
Dimensions LxWxH	1319x880x46mm
Operating conditions	
Ambient Operating Temperature	-20°C to 46°C
NOCT	46.9°C
1	STC: Cell Temp. 25^oC, AM1.5, $1000W/m^2$

5.6 The computer model

A detailed flow chart of the model is shown in Fig 5.4 and 5.5. The model of the PV module was implemented using Visual Basic for Applications (VBA), which also made use of the processing features of Microsoft Excel. The model parameters are evaluated during execution using the equations listed in sections 5.2, 5.3, and 5.4. The VBA program code can be found in print in Appendix-C for stationary system and Appendix-D for two-axis tracking system.

This program has been constructed to compute dew-point, slope radiation, sky and cell temperature, module efficiency and maximum power for operation of the PV modules for stationary PV system and slope radiation sky and dew-point, cell temperature, module efficiency and maximum power for operation of the PV modules for two-axis tracking system. Furthermore, the program calculates the current, voltage and fill factor for both stationary and two-axis tracking system.

The program is designed to compute results for ten hours each day for a period of one year. The results of this program are given in section 5.7.6 for the stationary system and section 5.8.5 for the two-axis tracking system.
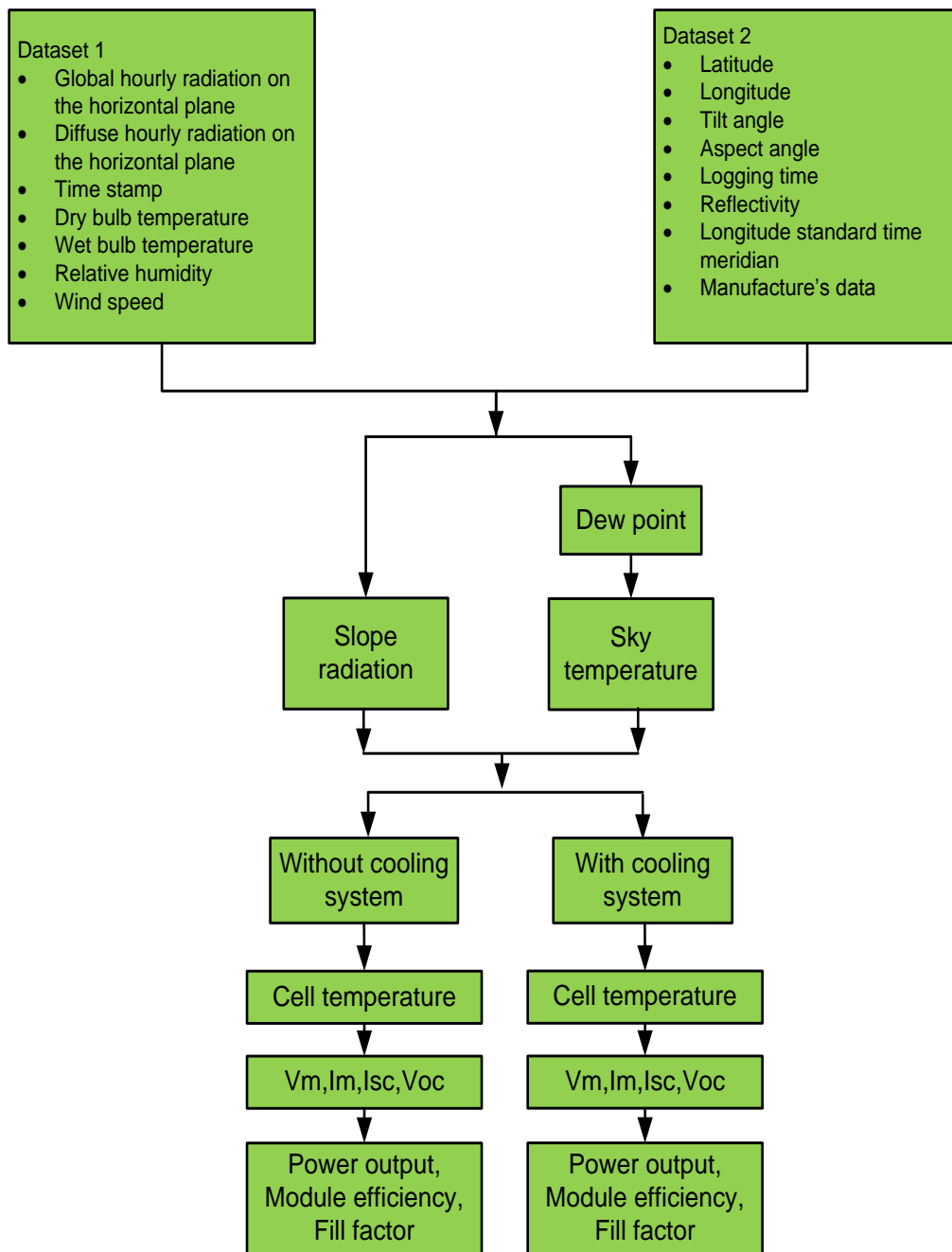
Figure 5.4 Flow chart for the computer model for stationary system with and without water cooling system
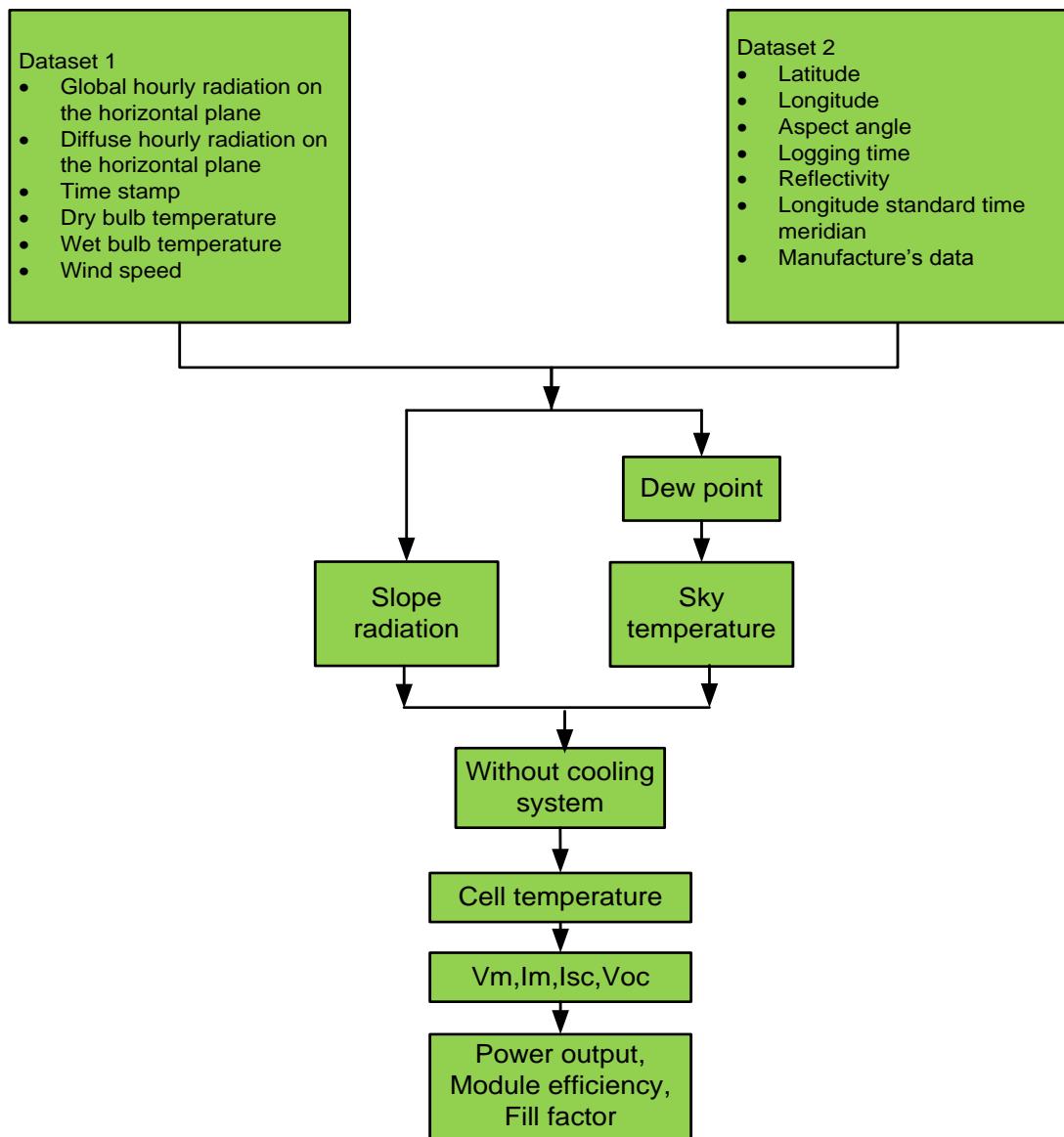
Figure 5.5 Flow chart for the computer model for two-axis tracking system without cooling system

5.7 Evaluation of a 50MW PV power station (stationary) for Al-Kufra

5.7.1 System design

The proposed 50MW photovoltaic power plant would be divided into 50 sub-stations of 1MW each and each 1MW substation would be divided into five channels each rated at 200kW. Each sub-station would feed the generated electricity to the 11kV grid through a 1000kVA transformer and each 200kW PV channel has been equipped with a grid-connected inverter to convert the DC power from the PV into

three - phase AC power for the primary of the transformer. The output from the 50MW station connects to the national grid (220kV) through a 50MVA transformer.

In this power plant each 1MW sub-station and each channel are independent of the other channels. This design has the following advantages:

1. Easier troubleshooting and maintenance.
2. Ability to install different types of PV systems.

Fig 5.6 shows a schematic diagram of the 200kW PV channels and the 1MW PV sub-station.
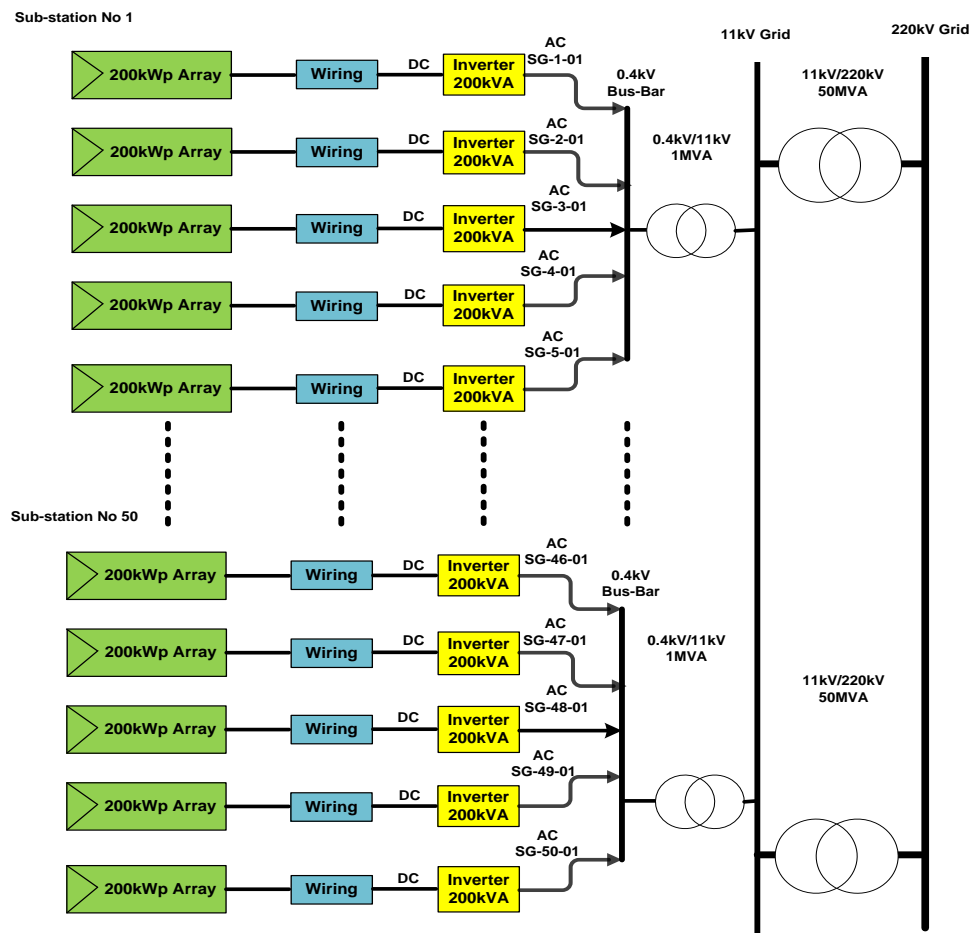
Figure 5.6 Schematic circuit diagram of the 50MW power station

5.7.2 Requirements of the PV system components

Fig 5.7 shows the configuration of the basic array which consists of 25 modules, 5 modules connected in series to form a 'string'and 5 strings in parallel. Forty basic arrays make one 200kW PV sub-station, connected to one inverter. Each 1MW substation therefore consists of 5000 modules. The specification of the proposed inverter is shown in Table 2

Table 5.2: Specifications of proposed DC/AC inverter [16]

Rated power (kVA)	200	
Maximum power (kVA)	245	
Rated input DC voltage (V)	640	
Maximum input DC voltage (V)	800	
Rated input DC current (A)	400	
AC output	Three-phase 415V±10%	
Output frequency	50Hz	
Efficiency	10%load:90%	
	50% load96%	
	100%load:96%	
Size (mm)	2000x2100x800	
Weight	1400kg	

5.7.3 Field requirements

It is important that the PV modules do not shade each other. In this study a fixed array has been used hence only the sun's apparent motion across the sky needs to be taken into consideration in order to optimize the spacing between rows of modules. Fig 5.7 (a) shows the configuration of the basic array whose dimensions are 6.59m in length and 4.4m in width.
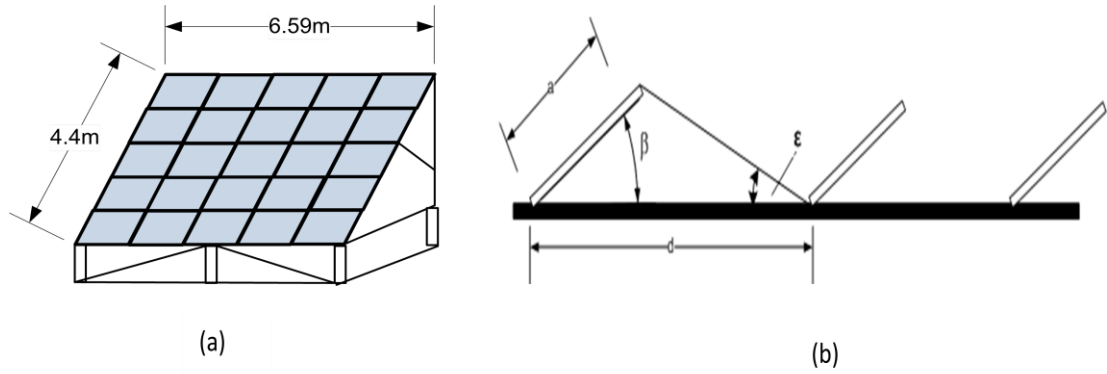
Figure 5.7 (a) Configuration of PV basic array, (b) arrangement of a large number of rows of basic array [17]

To avoid any shadowing, the distance between the PV sub-arrays is 6m which has been calculated from Eq.5.50 [17],

$$ d\!\!\Big/\!\!a = \cos\beta + \sin\beta\!\!\Big/\!\!\tan\varepsilon \tag{5.49} $$

where β is the tilt angle and ε can be estimated by the geographical latitude ϕ and the ecliptic angle $\delta = 23.5^{\circ}$

$$ \varepsilon = 90 - \delta - \phi \tag{5.50} $$

The area required for each 1MW PV sub-station is 7776m^2.

According to Kurokawa [16], a 50MW power plant requires 50,500 tonnes of steel and 70,000 tonnes of concrete and the length of cable required is 650km. In addition to 250 sets of inverters, it would need fifty 1000KVA, 0.4kV/11kV transformers and two 50MVA, 11kV/220kV transformers [16].

Based on this design, and by consideration of the need for utility buildings, the land requirements were calculated for the proposed 50MW PV power station at AlKufra at about 0.55km^2.
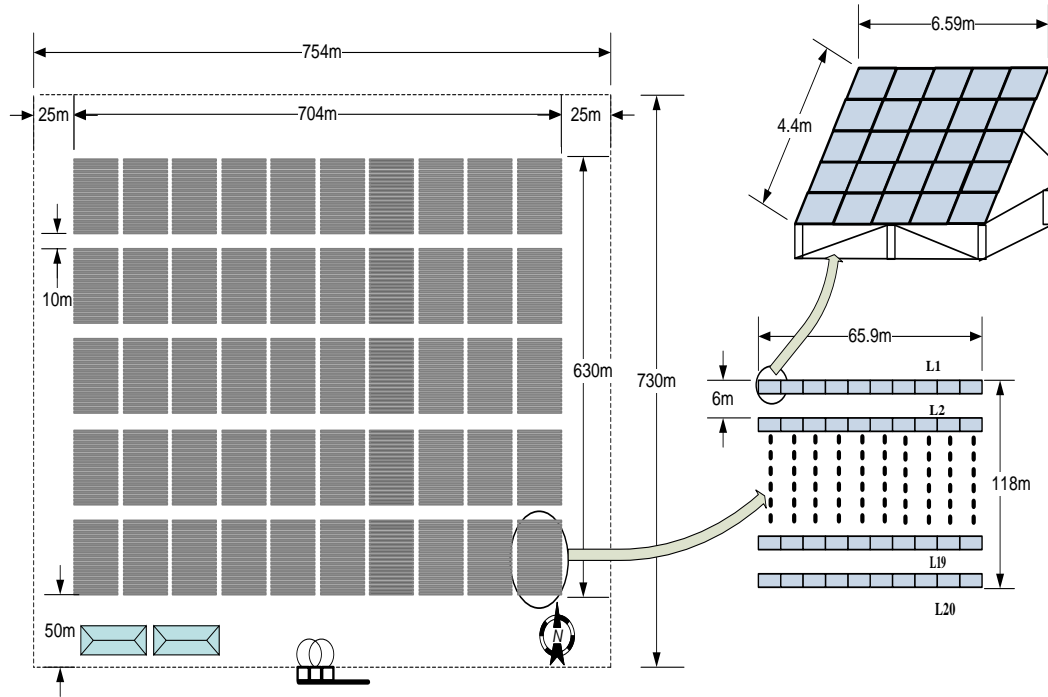
Figure 5.8 Field design for the proposed 50MW power station

5.7.4 Financial analysis and payback period

A number of economic criteria are available for evaluating solar energy systems. In order to conduct a financial analysis for this project, the total cost of the PV power plant is calculated based on the U.S. Department of Energy (DOE) report [18]. The cost per W_P of LS- PV power plant, C_w, includes the cost per W_P of: PV module cost (C_m), design cost C_d($0.08), inverters cost C_i($0.4), balance of system (BOS) development cost C_b($0.25) and installation cost C_{in}($0.4). The cost of PV modules is changing lastingly. According to Gupta [19], for the year 2010 the module cost was C_m=$1.7/ W_P. Thus, the total cost of LS-PV power plant is the product of cost per W_P and the rated power.

According to the US DOE, the cost per W_P is,

$$C_w = C_m + C_d + C_i + C_b + C_{in}$$

(5.51)

C_w =$2.8/ W_P

The total cost for 50MW PV power plant would thus be $140 million.

142

The payback time method is used here. The following steps may be used in order to estimate the present payback period:

- The solar energy on $1m^2$/year is 2300 kWh/m^2 /year
- feed-in tariff rate is assumed to be (C_{max}) \$0.45/kWh
- Cell efficiency $\eta_{cell} = 16.5\%$
- The energy output of $1m^2$ of cells is: E_y=2300*0.165=379.5kWh/m^2. The cost of $1m^2$ of PV power plant is estimated to be: C_{m2}=2.8*165=\$462/m^2, where \$2.8/ W_P is the total cost of 1 W_P
- The saving due to PV system usage is: S_{pv}=$E_y C_{max}$= 379.5*0.45=\$170.77/m^2 year.
- The payback time is: P_b=C_{m2}/S_{pv}= 462/170.77 = 2.7 years

The payback period was thus found to be 2.7 years.

Another method has been presently developed to calculate simple payback period. The simple payback time is defined as the ratio between the initial investment and the expected cash flow.

The simple payback time with:

1. Feed-in tariff \$0.45/kWh and interest rate 2%

The payback period was thus found to be 2.75 years as illustrated in Fig 5.9.
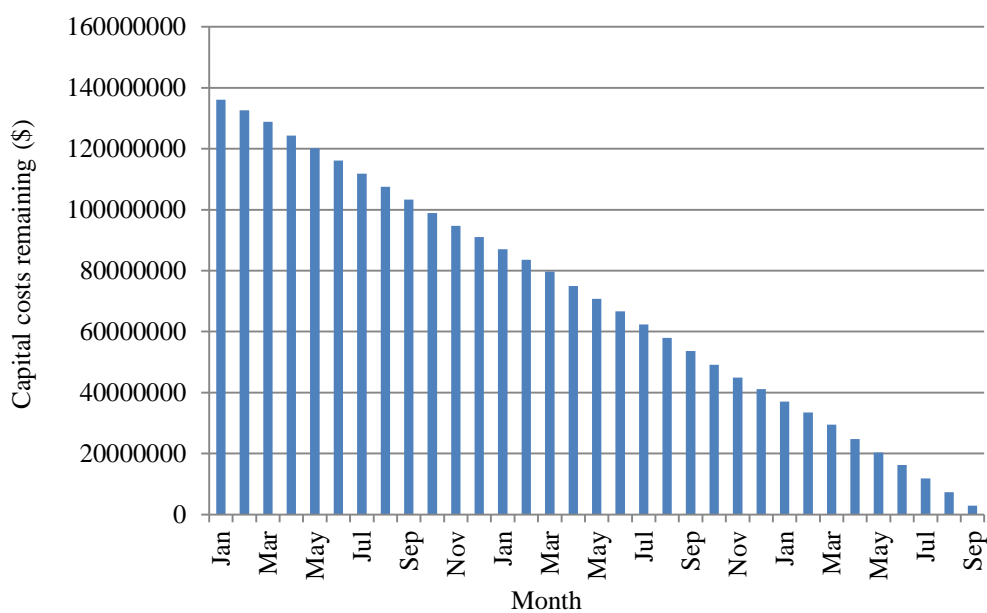
Figure 5.9 System construction payback period for stationary system

2. Feed-in tariff $0.38/kWh and interest rate 8%

The payback period was thus found to be 3.75 years as illustrated in Fig 5.10.
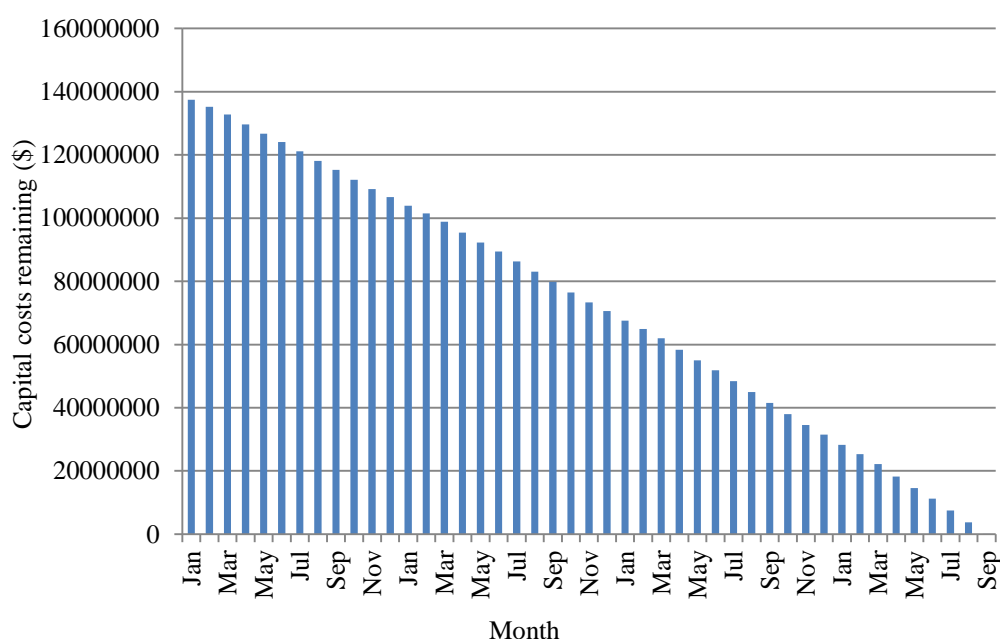
Figure 5.10 System construction payback period for stationary system

5.7.5 Capacity factor and solar capacity factor

The capacity factor, CF, is defined as the ratio of the net electrical generation for the time considered to the energy that could have been generated if the system were generating at continuous full power during the same period. The solar capacity factor SCF is defined as the ratio of the actual output of the PV power plant over a period of time, and its output if it had operated at full nameplate capacity throughout the time of the day. The capacity factor for the system was found to be 26 % and the solar capacity factor was 62.5%.

5.7.6 Greenhouse gas pollution

Electric power plants that burn fossil fuels emit several pollutants linked to the environmental problems of acid rain, urban ozone (smog), and global climate change.

As mentioned in section 2.1.4, the main emitters of CO_2 in Libya are fuel combustion in the power generation sector, the transport sector and in industry. In

total, energy-related emissions are responsible for almost all CO_2 emissions in the country.

In 2009 petroleum accounted for more than 53% of carbon emissions in Libya and natural gas was responsible for around 47% [20]. In the same year , the total generation in Libya was 29TWh, and taking into account the fact that the production of 1kWh of electricity creates 0.760kg CO_2 for oil and 0.560kg CO_2 for natural gas [21], emissions of CO_2 from the generation of electricity at oil-fired plants and natural gas-fired plants were estimated at 19.3 billion tonnes in 2009. Hence a 50MW PV system with a total energy output of 114GWh would reduce CO_2 pollution by 76,000 tonnes of CO_2 each year.

5.7.7 Results and discussion

The results obtained from the computer model for the stationary system, with and without water cooling system, for conditions at Al Kufra are shown in Figs.5.11, 5.12, 5.13 and 5.14. For comparison purposes, the hourly variation of the total energy output, average cell temperature, and average efficiency of PV module operation with, and without a cooling system are shown in Figs 5.11 and 5.12 for July and in Figs 5.13 and 5.14 for December.

These figures show that the average solar cell temperature is a maximum and the average efficiency for the PV module is a minimum as expected. Moreover, it is to be noted that the average efficiency decreases slightly with increase in solar cell temperature and vice versa. Furthermore, the average efficiency of the PV module when operating with a cooling system is 17% and 17.3% in July and December respectively, as compared to 16.2% and 16.8% in the same months when operating without a cooling system. The maximum cell temperature for operation without a cooling system in July and December has been found to be 49C^o and 37C^o respectively. On the other hand, the maximum cell temperature when operating with a cooling system only reaches 28.2C^o and 20.3C^o in July and December respectively. It is observed that the PV module operating with a cooling system gives higher total energy output (475kWh/annum) than the PV module operating without a cooling system (456 kWh/annum); this increase in total energy output is about 4.2%.
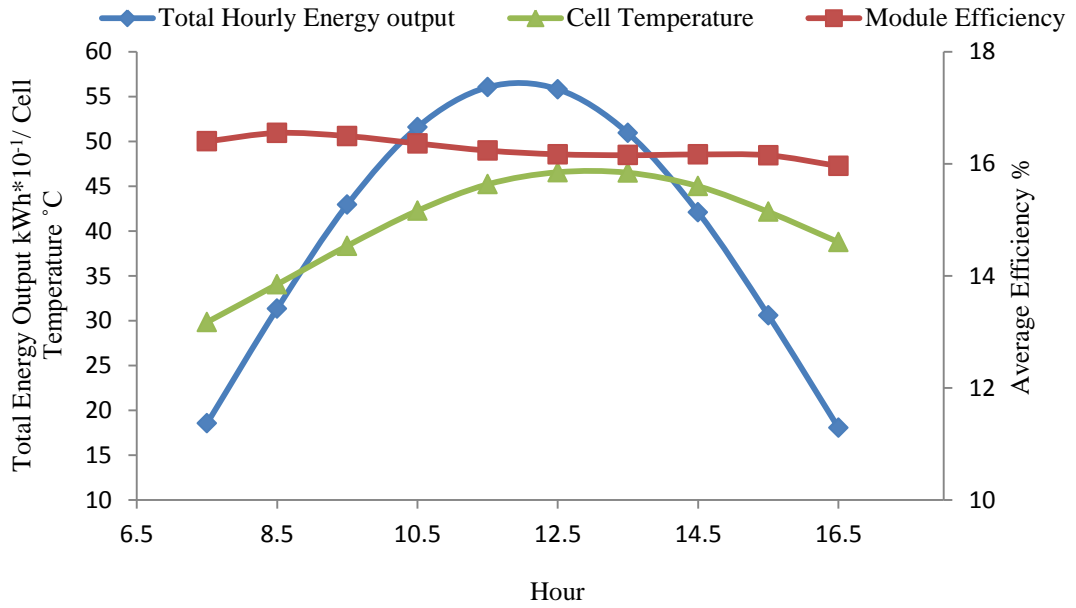
Figure 5.11 Variation in total energy output, average cell temperature and average
module efficiency without cooling system for July
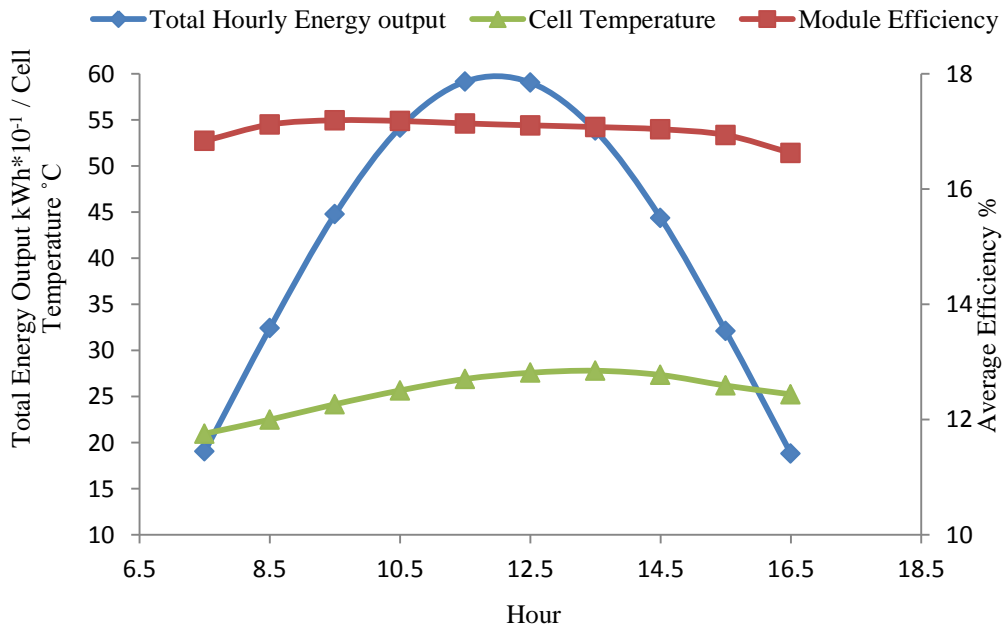
Figure 5.12 Variation in total energy output, average cell temperature and average
module efficiency with cooling system for July
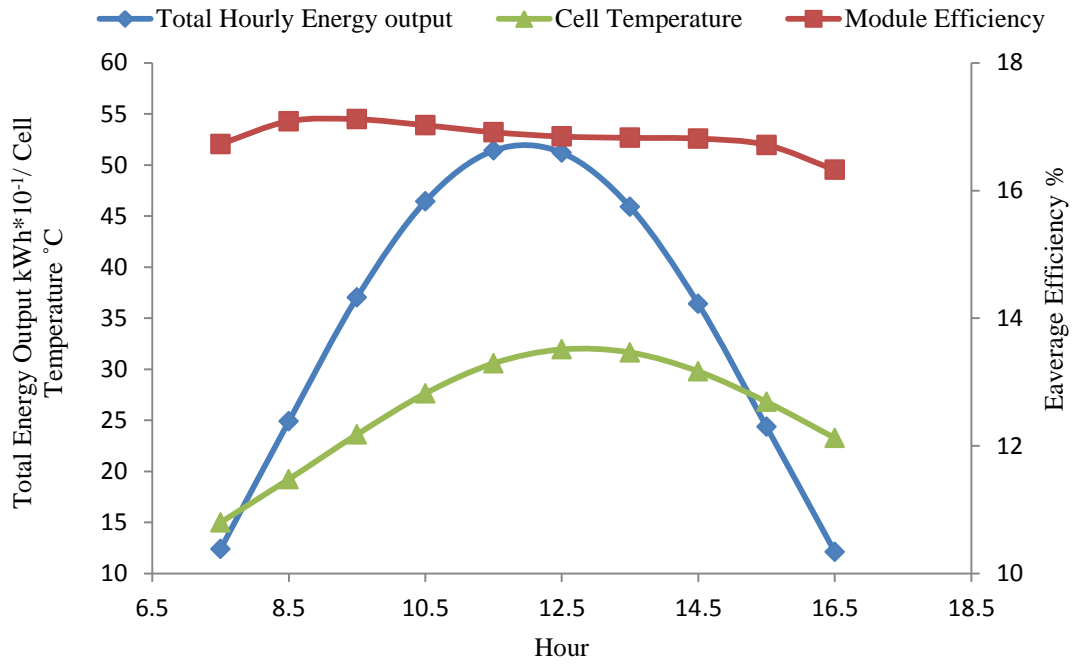
Figure 5.13 Variation in total energy output, average cell temperature and average module efficiency without cooling system for December
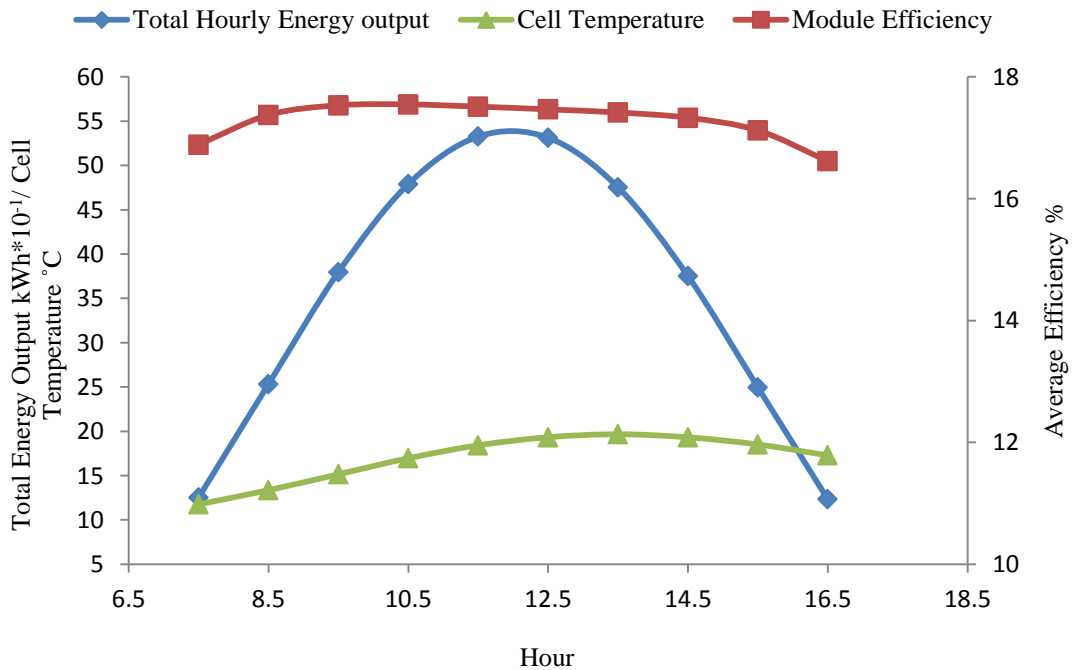
Figure 5.14 Variation in total energy output, average cell temperature and average efficiency with cooling system for December

147
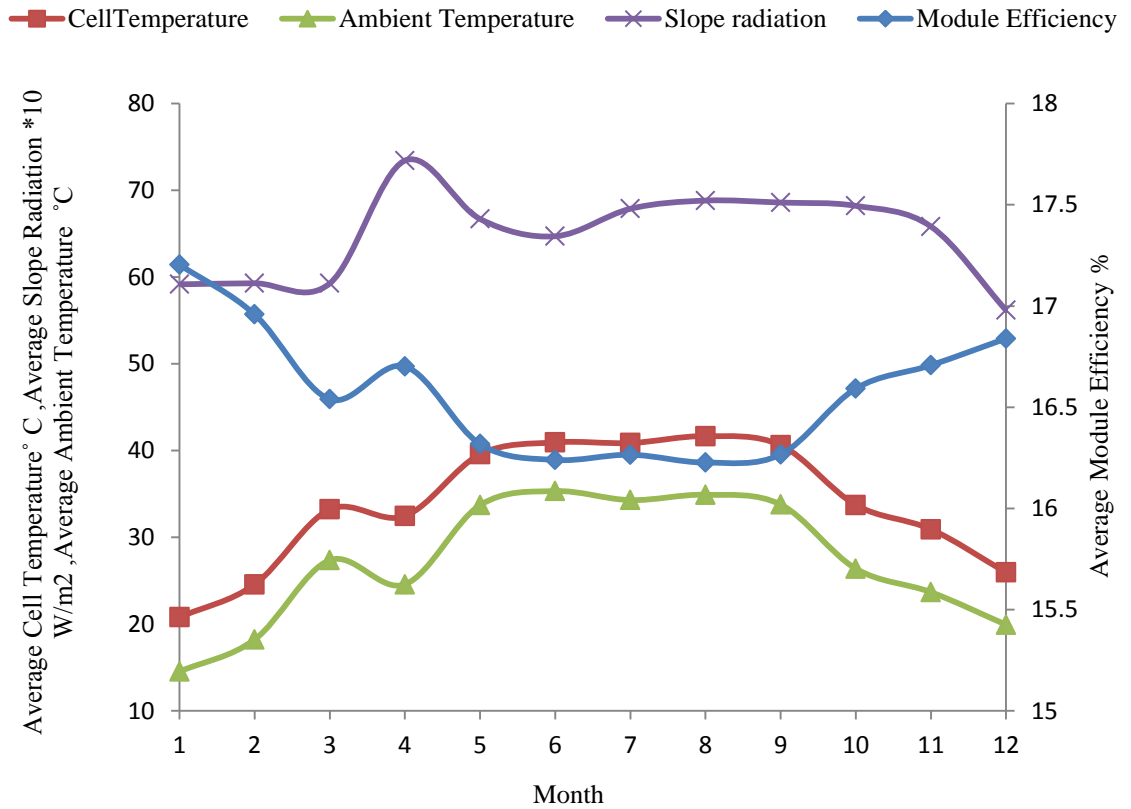
Figure 5.15 Variation of average cell temperature, ambient temperature, module efficiency and slope radiation

Fig 5.15 shows the variation of the monthly average values of slope radiation, average cell temperature, average ambient temperature and average module efficiency without cooling system throughout of the year in Al-Kufra.

The calculated average cell temperature exceeded 49°C in June and drop to 20.8^{o}C in January. Furthermore, it is seen that the cell temperature follows the ambient temperature. A strong inverse relationship between the average cell temperature and the average module efficiency can also be seen.

For operation with a cooling system, Fig 5.16 shows that the module efficiency slightly increases when the mass flow rate of the cooling water increases. A steady state condition is achieved with a mass flow rate in excess of 0.45kg /s.
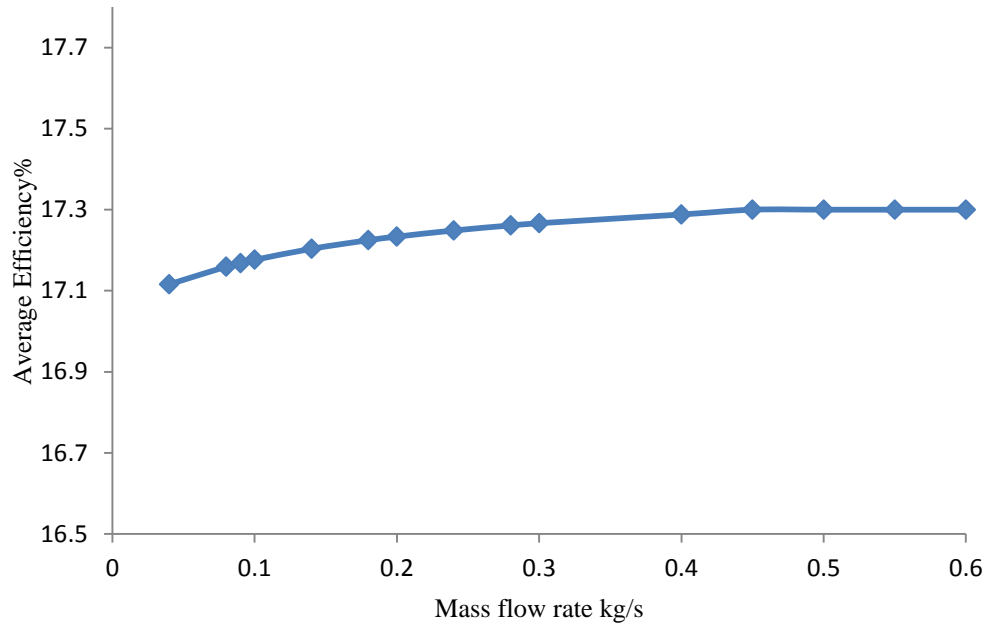
Figure 5.16 Variation of average module efficiency with mass flow rate of water cooling

A prior requirement to the design of any PV system is knowledge of the optimum orientation and surface tilt at which the peak solar energy can be collected. To analyse the optimum inclination, the annual total energy output for tilt angles between 12° and 48° oriented due south (azimuth angle=180°) were evaluated and Fig 5.17 shows those results.

The maximum total energy output is seen to accrue at a tilt angle of 24°. As the latitude of Al-Kufra is 24.28^{o}N, the results support the argument that the optimum tilt angle for total energy output should be equal to the angle equivalent to the latitude of the location.
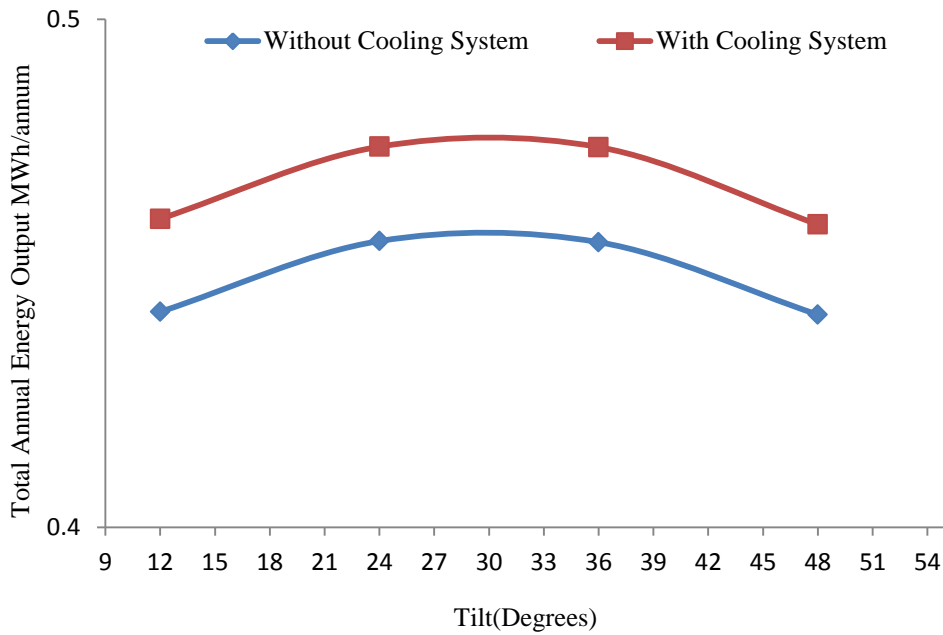
Figure 5.17 Total energy output against tilt angles for south-facing surface

It should be noted that a cooling system increases the absolute average efficiency of the PV module by 0.6%, however, the relative average efficiency increase by 3.6%.

5.8 Evaluation of a 50MW two-axis tracking plant for Al-Kufra Libya

A major attractive feature of PV technology is possibility of creating a power plant with absolutely no moving parts. This could be particularly important for LS-PV plants for which the added maintenance work associated with very large numbers of sun-tracking modules might turn out to render the project unfeasible. Nevertheless, it is important to have a quantitative measure of the potential energetic advantages of employing sun-tracking, in order that these may be weighed against the associated cost increases.

In the related literature based on the previously conducted studies in section 2.4.4.1, it was observed that the PV two-axis tracking system provided a significant increase in the amount of energy produced. The most commonly used system in sun tracking systems is controlling the motor which moves the panel by evaluating the signals received from photosensors. An example for this application is shown in Fig 5.18.
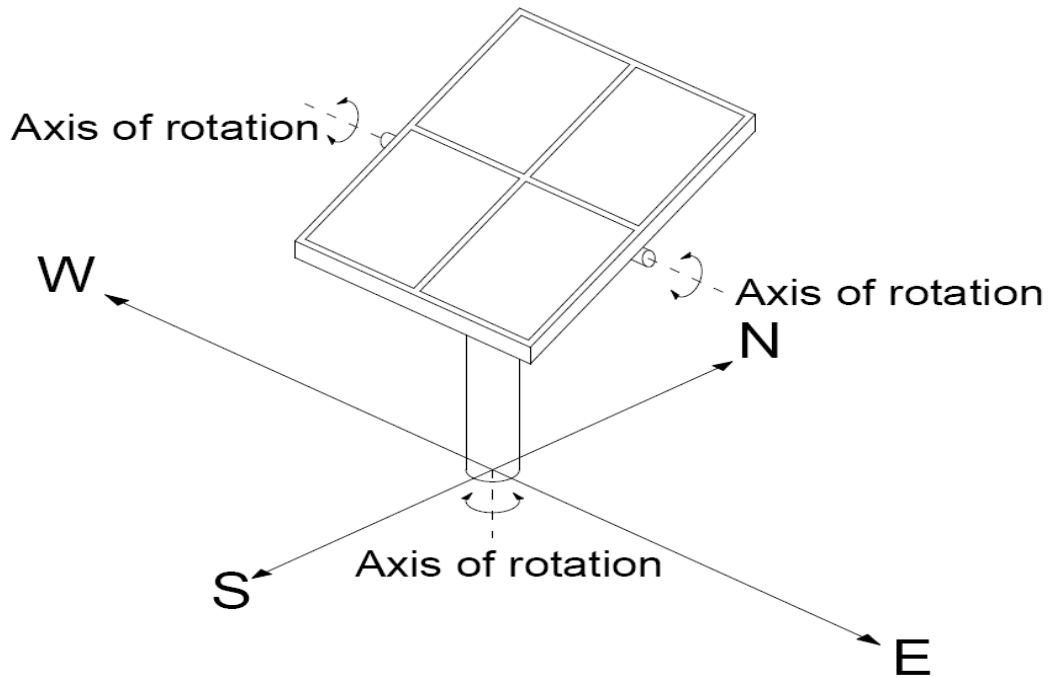
Figure 5.18 Two-axis tracking PV solar tracker

This section discusses the system which employs full two-axis tracking, ensuring that the PV modules always face directly towards the sun's position in the sky. An HIT type PV module has been selected and modelled.

The DegerTraker 6000NT module has been selected as the sun-tracker system. DegerEnergy Company designed and constructed a programmable sun-tracker. Table 5.3 shows the specification of the DegerTraker 6000NT-Dual-axis.

Table 5.3 Specification of the DegerTraker 6000NT-Dual-axis [22]

Module area up to	53m²
Rotation angle east – west	360° with adjustable limit switches
Elevation	15°-90°
Control unit	DEGERconecter
Operating voltage	80 … 265 VAC / 80 … 380 VDC
East –west drive	drive integrated in the rotating head
Elevation drive	1,100 mm stroke path
Internal power consumption:	
Control mode	1 Watt
With operating drives approx.	7 Watts
Power consumption per year. approx.	9 kWh
Mast height	4 m … 5,5 m
Load capacity	130 … 300 km/h
Weight (excluding mast)	1,000 kg
Art.no.	1600001

The proposed of solar tracking system for the 50MW photovoltaic power plant would be divided into 50 sub-stations of 1MW each and each 1MW substation would be divided into 125 solar trackers each rated at 8kW. Each substation would feed the generated electricity to the 11kV grid through a 1000kVA transformer and each 8kW PV channel has been equipped with a grid-connected inverter to convert the DC power from the PV into three - phase AC power for the primary of the 1000kVA transformer. The output from the 50MW station connects to the national grid (220kV) through a 50MVA transformer.

The system was designed to optimize performance for the annual energy output (i.e., modules facing due south) and to maximize reliability. For example, in designing the 1MW system it was determined that 125 x 8kW arrays would increase the reliability of the system. If any one array should fail, the system would still be operating at 90% capacity.

5.8.1 Field requirements

As mentioned in section 5.7.2 it is important that the PV modules do not shade each other. On the other hand, for sun tracking systems (Two-axis), the situation is more complex because the modules also move. In order to ensure that the solar trackers do not shade each other, hexagonal structures have been used in this study [23]. Fig 5.19 shows the field design for the proposed 50MW power station (Two-axis) and configuration of the PV array; each array consists of 40 PV modules.
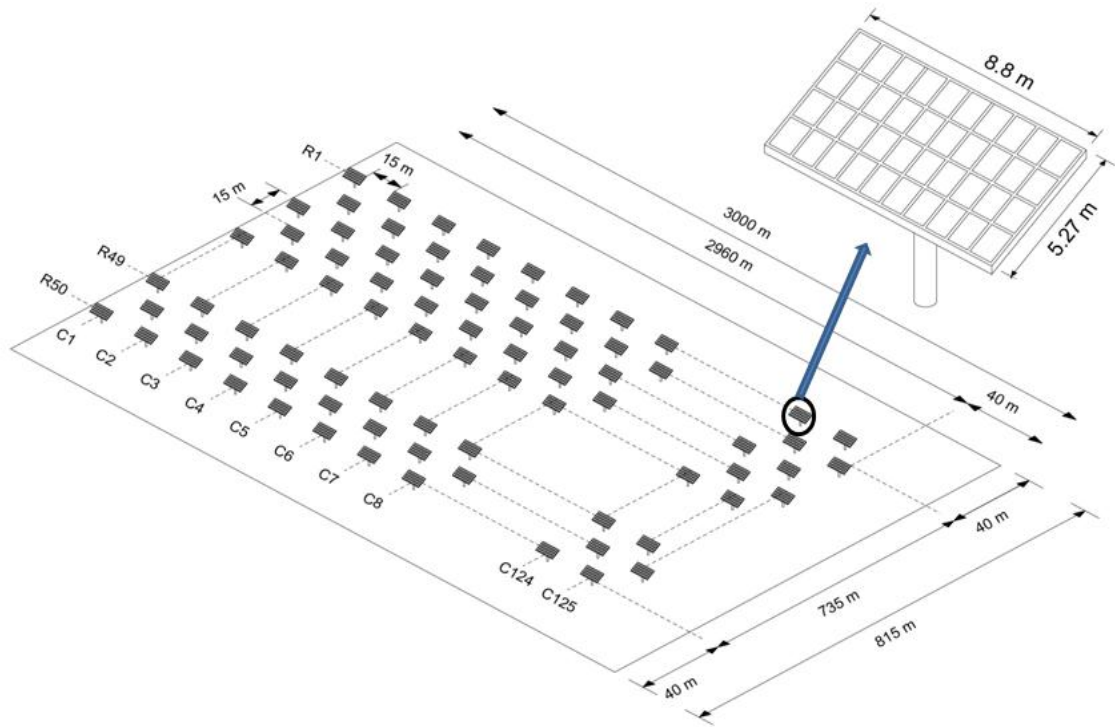
Figure 5.19 Schematic of hexagonal field layout of 50MW PV power plant (for two-axis tracking system)

The total area occupied by the solar tracking system power plant is 2.44km^2 and the total module area is 290,180 m^2.

5.8.2 Capacity factor and solar capacity factor

CF and SCF have been defined in section 5.7.4. The capacity factor for sun tracking system (two-axis) was found to be 34% and the solar capacity factor SCF was 81%.

5.8.3 Greenhouse gas pollution

A 50MW two axis tracking plant with a total energy output of 148GWh would reduce CO_2 pollution by 98,500 tonnes of each year.

5.8.4 Financial analysis and payback period

In addition to the costs presented in section 5.7.3, the cost of the system tracker is C_T=$1.79/W$_P$. For the quotation see appendix E.

According to a study by David et al [24], operation and maintenance cost (O&M) of PV solar power plant using tracking system is $C_{O\&M}$=$0.058/W

Thus, the total cost of LS-PV power plant using tracking system is the product of cost per Watt and the rated power. The cost per Watt is, C_w= $4.67/W.

The total cost for 50MW PV power plant using tracking system would thus be $234 million.

1. Feed-in tariff $0.45/kWh and interest rate 2%

The payback period was found to be 3.58 years as illustrated in Fig 5.20.
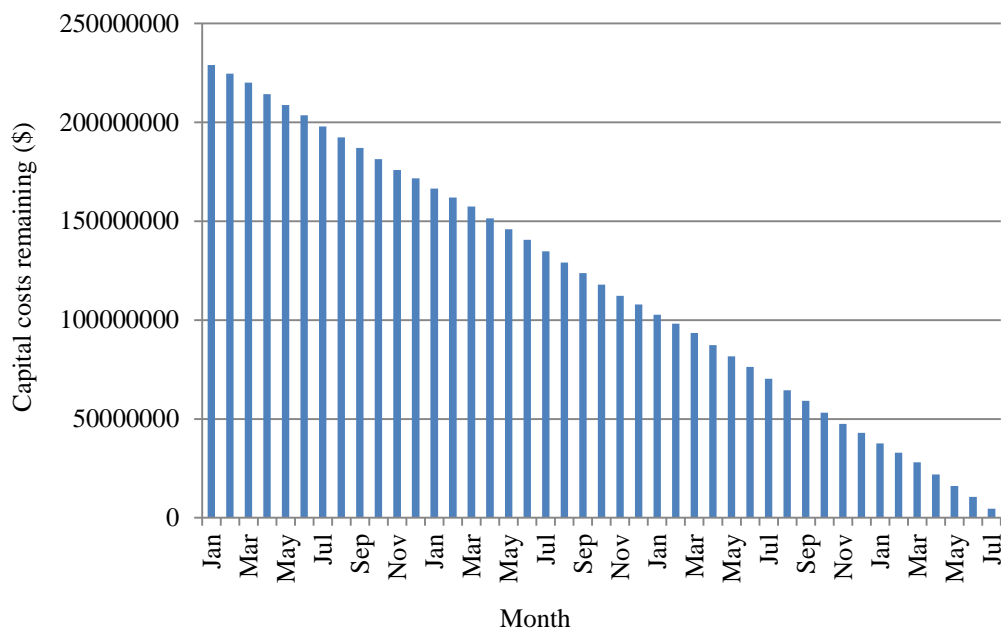
Figure 5.20 System construction payback period for tracking system

2. Feed-in tariff $0.38/kWh and interest rate 8%

The payback period was found to be 5.08 years as illustrated in Fig 5.21.
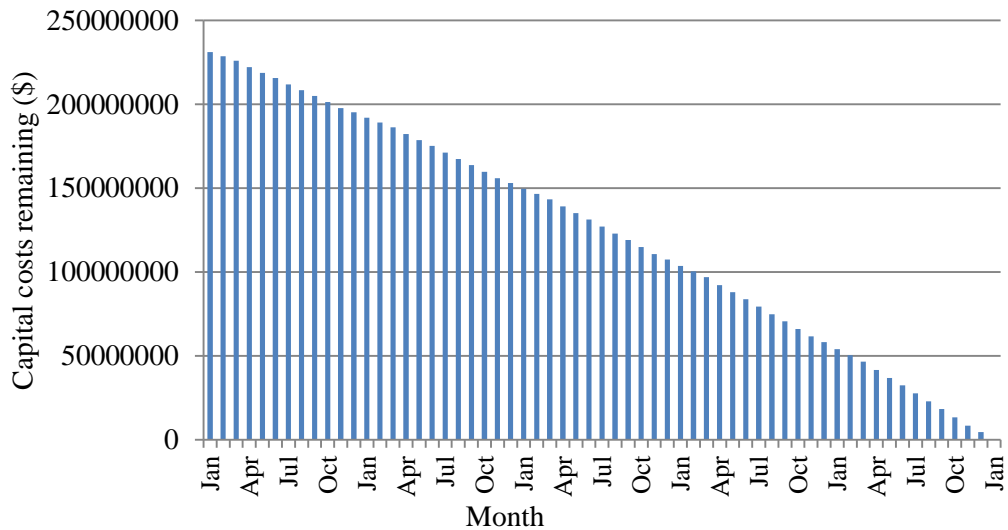
Figure 5.21 System construction payback period for tracking system

5.8.5 Results and discussion

The results obtained from the computer model for two-axis tracking system, without water cooling system for conditions at Al Kufra are shown in Figs.5.22 and 5.23. For comparison purposes, the hourly variation of the total energy output, average cell temperature, and average efficiency of PV module operation are shown in Fig 5.22 for July and in Fig 5.23 for December.
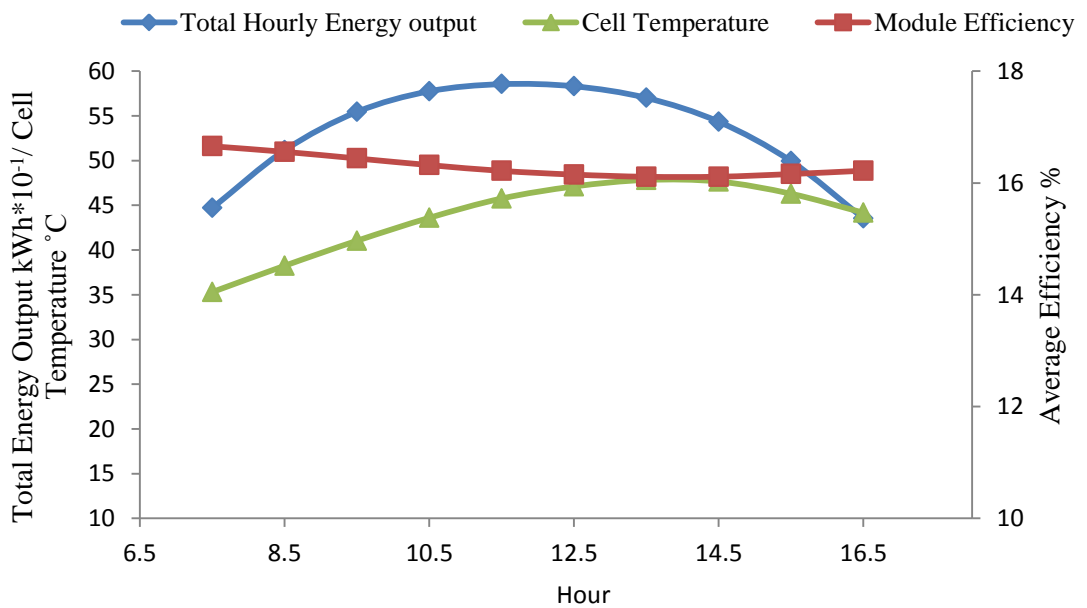
Figure 5.22 Variation in total energy output, average cell temperature and average module efficiency for July

It is observed that the total energy output in July and December has been found to be 54kWh and 41kWh respectively.
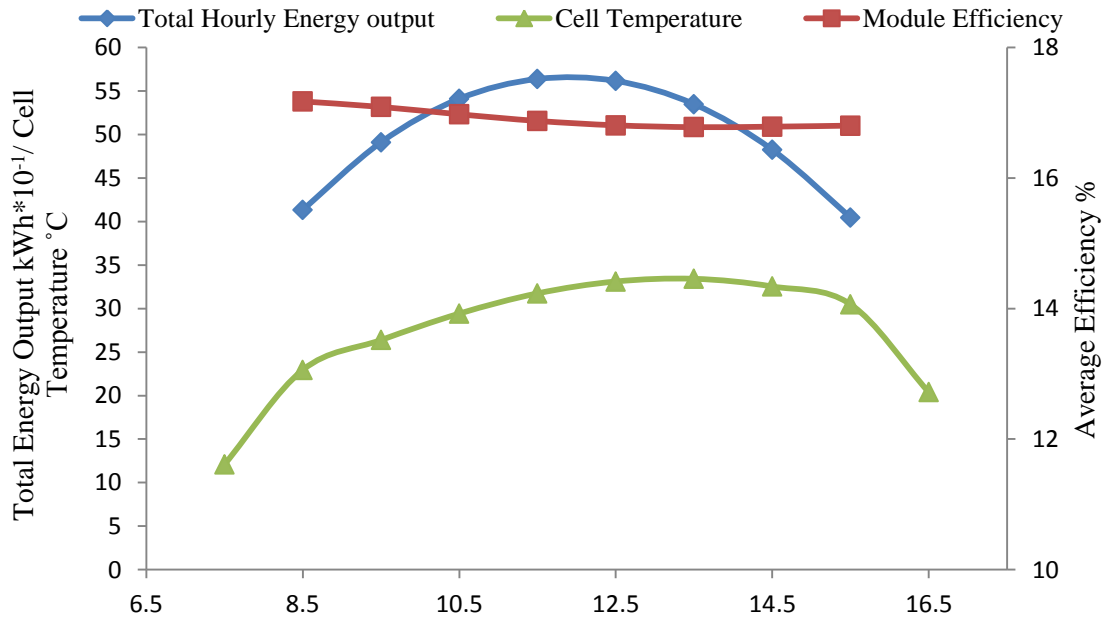
Figure 5.23: Variation in total energy output, average cell temperature and average module efficiency for December

The maximum cell temperature in June and December has been found to be 51°C and 39 $^{\circ}$C respectively. The total energy output of 50MW two-axis tracking plant is 148GWh.

5.9. Comparison of stationary and tracking systems

In the current section, the comparison between the stationary and tracking systems has been performed on the basis of the following main design principles:

- 50MW size, reasonably assumed as reference size for both technologies.
- HIT PV module technology for both stationary without water cooling and tracking systems.
- Location: southern Libya in Al-Kufra.

The main factors used for comparison have been:

- Landscape impact
- Performance

5.9.1 Landscape impact

The key factor in designing the PV plant is to gain, for any specific site, the optimal ground cover ratio (GCR) without valuable reduction of expected performance ratio. The GCR is defined as the ratio of the PV array area to the total ground area [25].The GCR for a stationary system installation localized in Libya, Al-Kufra, is 0.7, which corresponds to a tilt angle of 24°. The GCR for tracking system was found to be 0.12.

The estimated ground area needed to build a 50MW PV plant amounts to approx. $0.55km^2$ for a stationary PV field constituted by HIT PV arrays and approx. 91MW/ km^2. In case of a tracker PV field, the required ground area amounts approx.$2.4km^2$ and approx. 20.5MW/ km^2.

It can be observed, in terms of land impact, that a stationary PV field requires about quarter of the area necessary for a tracker PV system and the selection of PV modules may play an important role in determining the area required by the plant. Therefore it can be concluded that for LS-PV plant, the stationary PV field arrangement should be preferable when compared in terms of land impact.

5.9.2 Performance

The expected performance of a 50MW PV plant, located in Al-Kufra, Southern-East Libya, is shown in the table 5.4; the tracker PV system produces approximately 30% more energy per annum than a stationary PV system, with the same nominal installed power. Furthermore, the cost of a PV tracking system is greater than the cost of stationary PV system.

Table 5.4 PV power plants performance table

	Stationary PV System	Tracker PV system
Total slope radiation GWh/m^2/year	592	767
Solar field total surface m^2	290,500	290,500
Total Plant area km^2	0.55	2.4
Installed PV peak power MW	50	50
Total energy output GWh/year	114	148
Capacity factor %	26	34
Solar capacity factor %	62.5	82
Reducing CO_2 emissions, kT	76	96

Fig 5.24 shows the monthly production of energy of the stationary and tracking plant. The result was a 30% higher production of energy in the tracking plant. This increase in energy production, although significant, is not enough to compensate the other disadvantages of plants with trackers:

- Increase in cost due to trackers. Trackers are expensive, and their price is not expected to be reduced.

- Increased Operation and Maintenance cost due to trackers. While static device plants are very easy to maintain, the trackers need more maintenance work since they are a moving system.

- Risk of durability of the tracker system. It is very difficult to be sure that the tracking system will work during the whole life of the plant.

- High risk of incident related to strong winds. High speed winds can cause serious problems to the trackers that mean losses of production and cost in reparations.
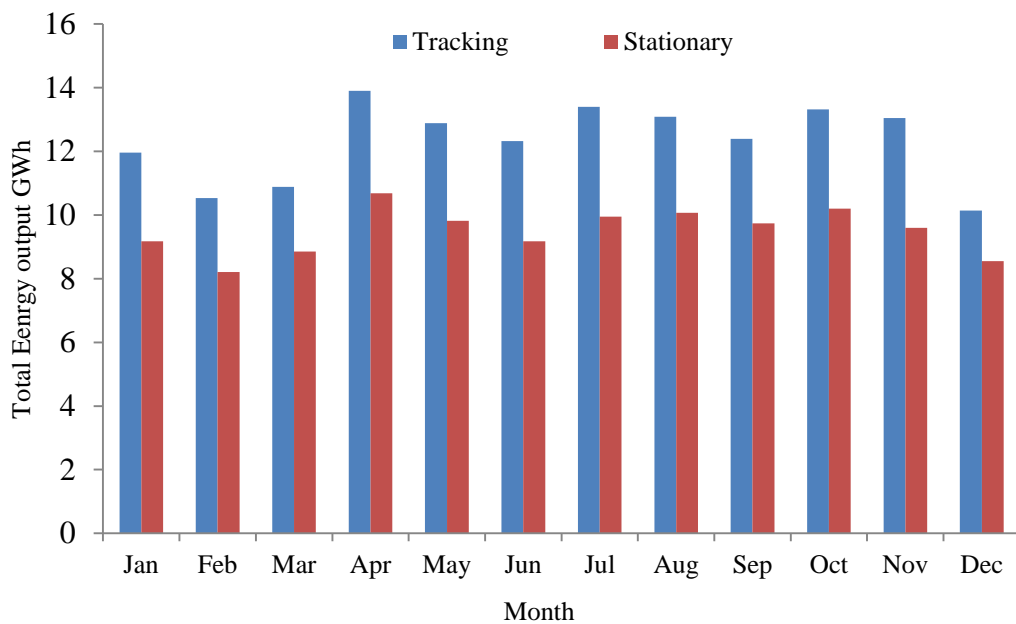
Figure 5.24 Monthly total energy output for both stationary and tracking systems

5.10 Conclusions

This chapter presented an extended analysis for installing a 50MW PV-grid connected (stationary and tracking) power plant in Al-Kufra, Libya. The HIT solar PV module from Sanyo, rated at 200W, has been used in this study due to its high efficiency.

Long-term meteorological parameters for Al-Kufra region have been collected from Renewable Energy Authority of Libya (REAOL) and the results confirm that Al-Kufra has high levels of annual solar radiation. The collected meteorological parameters were: long-term average daily global radiation, average daily sunshine hours, long-term hourly ambient temperature and average daily wind speed.

A Microsoft Excel-VBA program has been developed to compute slope radiation, dew-point, sky temperature, and then cell temperature, maximum power output and module efficiency of the system, with and without a water cooling system for stationary system and for tracking system without water cooling.

The results for energy production show that the total energy output is 114GWh/year without a water cooling system, 119GWh/year with a water cooling system for stationary system and 148GWh/year for tracking system. Also, the maximum cell temperature without a water cooling system is 49.6^{o}C on 21 June at noon for stationary system and 51°C for the tracking system. Furthermore, the minimum cell temperature is 9.4^{o}C on 21 January at 7.30 am for stationary system and 5.7^{o}C on 11 January at 7.30 am for the tracking system. These findings were consistent with the results of an experimental study conducted by Mosalam [26] . The average module efficiency with and without a cooling system for the stationary system is 17.2% and 16.6% respectively and 16.2% for the tracking system.

The values of electricity generation capacity factor (CF) and solar capacity factor (SCF) for stationary system without a water cooling system were found to be 26% and 62.5% respectively and 34% and 82% for tracking system. The payback time for the proposed LS-PV power plant was found to be 2.75 years for the stationary system and 3.58 years for the tracking system.

Therefore it can be concluded that for LS-PV plant, the stationary PV field arrangement is preferable when compared in terms of land impact and the disadvantages of plants with trackers.

Note that the modelling of the PV system indicated that cooling water introduced at a temperature of 27°C will increase the PV panel efficiency from an un-cooled cell temperature of 49.6^{o}C by an absolute value of 1.1%. This translates to a relative efficiency increase of 6.9%.

These encouraging set of results prompted the author to explore the effect of the cell temperature on the efficiency of the PV module with water cooled systems in the laboratories of Edinburgh Napier University. Further details are provided in Chapter 6.

References

[1] Rauschenbach HS. Cell Array Design Handbook. New York: Van Nostrand Reinhold Company 1980.

[2] Eckstein J, Townsend, T., Beckman, W.A., Duffie, J.A. Photovoltaic Powered Energy Systems. ASES Solar 90 Conference; 1990; Austin, TX. ; 1990.

[3] Kunz G, Wagner, A,. Internal series resistance determined of only one IV curve under illumination. 19th European Photovoltaic Solar Energy Conference; 7-11 June 2004; Paris, France; 7-11 June 2004.

[4] Duffie JA, and Beckman, W.A.,. Solar Engineering of Thermal Processes. 2nd ed. New York: Wiley Interscience 1991.

[5] Buresch M. Photovoltaic energy systems-design and installation. London: McGraw-Hill 1983.

[6] Duffie JAaWAB. Solar Energy Thermal Processes. New York: John Wiley Inc 1974.

[7] T.Muneer. Solar radaition and daylight models 2004

[8] Mattei M NG, Cristofari C, Muselli M, Poggi P. Calculation of the polycrystalline PV module temperature using a simple method of energy balance. Renewable Energy. 2006;31(4):553-67.

[9] The Reference to EnergyPlus Calculations: The University of lllinois; 2010.

[10] Sturrock RJCaNS. The convective heat exchange at the external surface of buildings   Building and Environment. 1977;12(4):207-14

[11] Bhatti MS, and R.K. Shah. Handbook of Single-Phase Convective Heat Transfer. New York: Wiley-Interscience 1987.

[12] Sieder EN, and G.E.Tate, . Ind.Eng.Chem 1936.

[13] Kays WM, and M.E. Crawford.,. Convective Heat and Mass Transfer. New York: McGraw-Hill 1980.

[14] Bhatti M, S., and R.K. SHAH,. Handbook of single-Phase Covective Heat Transfer. New York: Wiley-Inter-Science 1987.

[15] Sanyo.   [cited; Available from: http://www.sunwize.com/info_center/pdf/sanyo_HIT200W_8-08.pdf

[16] Kurokawa K, Keiichi K. Energy from the Desert.: Earthscan Publications Ltd 2003.

[17]   A.Goetz berger. V, Hoffmann. Photovoltaic Solar Energy Generation Spring Berlin 2005.

[18]   SunEdison Activates Really Big Solar PV Plant in Italy. 2010 [cited; Available from: http://www.getsolar.com/blog/sunedison-activates-really-big-solar-pv-plant-in-italy/14457/

[19]   Gupta S. How Low Will Price Fall? Photvoltaic Technology Show 2010 Europe; April 27, 2010; Stuttgart,Germany; April 27, 2010.

[20]   El-Arroudi K, Moktar,M. Demand Side Management in Libya Tripoli: General Electric Company of Libya (GECOL), Transmission System Operation and Control Department; 2009.

[21]   Berg B. The ecology of building materials: Architectural Press,Butterworth-Heinemann,Oxford 2001.

[22]   Stromsta K-E. Masdar connects 10MW solar farm to UAE's power grid. RECHARGE. 2009.

[23]   J.M. Gordon HJW. Central-station solar photovoltaic systems: Field layout, tracker, and array geometry sensitivity studies. Solar Energy. 1991;46(4):211-7.

[24]   D. Lecoufle R, Lawless, M. Hampel. . Large Scale PV Plants in North Africa and the Middle East - Are Large Scale PV Plants in the Sun-Belt Countries Overshadowed by CSP's Recent Boom? A Technical and Economical Comparison. *24th European Photovoltaic Solar Energy Conference*. Hamburg, Germany 2009:4481 - 4.

[25]   L Narvarte   EL. Tracking and Ground Cover Ratio. Prog Photovolt. 2008;16:703-14.

[26]   Mosalam S M, A., Ghettasa.A. , Fattah,Y. . Photovoltaic performance under real desert conditions near Cairo. Renewable Energy. 1995;6(5-6):533-6.

CHAPTER 6

Influence of environmental factors on PV performance

Chapter Map
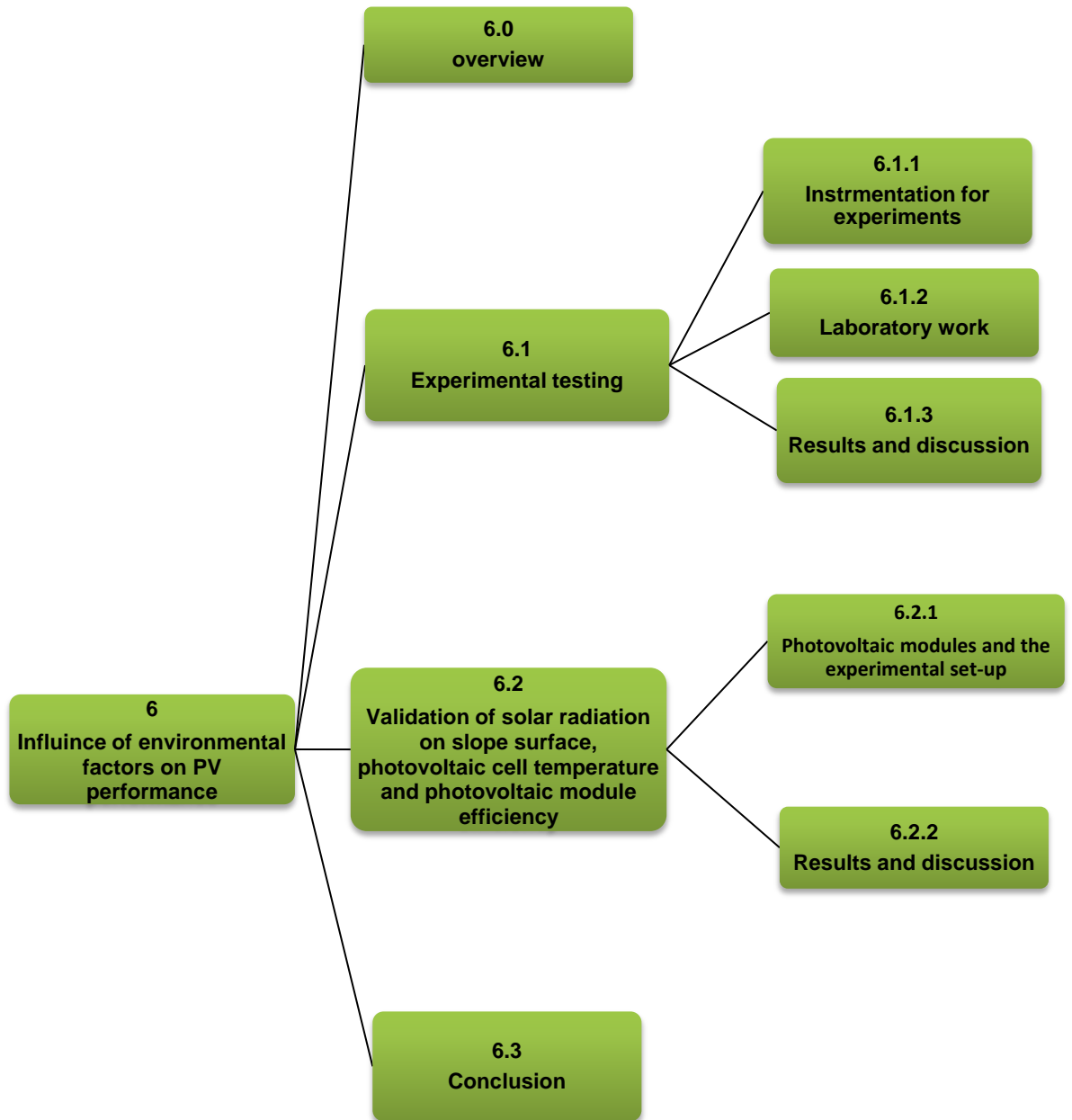
6.0 Overview

Due to certain circumstances that prevented performance of the experimental work in the actual sites of the Libyan Desert, experimental work has instead been performed in the laboratories of Edinburgh Napier University. This chapter focuses specifically on the effect of the cell temperature on the efficiency of the PV module in an attempt to improve the efficiency by using the application of a water cooling jacket (WCJ).

The first section (6.1) explains the Laboratory experimental work that was carried out on a mono crystalline type BP 222SR PV module, including the manufacturing process of the WCJ, and the measurement of the current, the voltage and the cell temperature at different water flow rates. This experimental work also included the measurement of the cell temperature at different points of irradiation (255- and 296W/m^2) by using two halogen lamps.

In section 6.2 use its mode of a database that was mounted on a PV module in the city of Iskenderun in the Southern part of Turkey. This data includes measurements of the slope and horizontal global irradiation, the voltage and current, and the cell temperature. All these measurements are recorded by Turkish team at Iskenderun. The data of horizontal global irradiation, slope irradiation, voltage, current and cell temperature were measured and used for validation purposes of mathematical model (Chapter 5 sections 5.2.1, 5.2.2, 5.2.3, 5.3.1 and 5.4.1.1) compared with the experimental work.

6.1 Experimental Testing

Experimental works are the most reliable mode of recording the PV module response because it is based on the actual performance of the PV module therefore does not exclude any physical phenomenon that might be neglected in the mathematical modelling. In light of this, the results from the experimental tests are herein used as a yardstick for benchmarking the mathematical modelling.

6.1.1 Instrumentation for Experiments

The equipment setup for the experimentation of the PV module with and without a water cooling jacket (WCJ) is described in this section.

6.1.1.1 Thermocouples (K-type)

Several types of thermocouples have been developed, each type customized to perform in different conditions or more discretely, different temperature range. K-type thermocouples are the most popular and use nickel-chromium and nickel-aluminium alloys to generate voltage. Table 6.1 illustrates the various types of thermocouples; their corresponding temperature ranges and resolution [1].

Table 6.1 Range of temperatures for different thermocouple types

Thermocouple Type	Overall Range (°C)	0.1 (°C) Resolution	0.025 (°C) Resolution
B	100-1800	1030-1800	*
E	-270-790	-240-790	-140-790
J	-210-1050	-210-1050	-120-1050
K	**-270-1370**	**-220-1370**	**-20-1150**
N	-260-1300	-210-1300	340-1260
R	-50-1760	330-1760	*
S	-50-1760	250-1760	*
T	-270-400	-230-400	-20-400

*unavailable

The relationship between the temperature and current is not linear and hence a polynomial relation is used for conversion. Grant squirrel 2020 data loggers were used for recording the temperature. The logger used the following relationship as defined by the British Standard (BS EN 60584.1),

Temperature conversion equation: $T = a_0 + a_1 x + a_2 x^2 + \ldots + a_n x^n$ (6.1)

Where the coefficients $a_0 - a_8$ are presented in table 6.2 while "x" is the current in amperes. For the common type- K thermocouple, the voltmeter must be able to resolve 4 µV to detect a 0.1°C change. The calculation of high-order polynomials is a time consuming task for a computer. Time can be saved by using a lower order polynomial for a smaller temperature range. In the software for one data acquisition system, the thermocouple characteristic curve is divided into eight sectors, and each sector is approximated by a third order polynomial.

Table 6.2 Polynomial coefficients for K- type thermocouples [1]

Polynomial Coefficients	Type K 0 °C to 1370 °C ± 0.7 °C 8th order
a_0	0.226584602
a_1	24152.10900
a_2	67233.4248
a_3	2210340.682
a_4	-860963914.9
a_5	4.83506E + 10
a_6	-1. 18452E + 12
a_7	1.38690E + 13
a_8	-6.33708E + 13

6.1.1.2 Voltage and current

In measuring the PV module output, measurements of voltage and current are taken using the two multimeters model ISO-TECH *DM66*. The voltage measurement is accurate to ±0.01V while that of the current is accurate to ±1mA. A load is simulated using a rheostat.

6.1.1.3 Flow rates

Flow rate was measured manually using a stopwatch and a graduate cylinder at three different flow rates 0.014-, 0.021- and 0.041kg/s. Each measurement was taken three times for accuracy, and the average of the readings was used in the experimental work.

6.1.1.4 Light source

As a light source, two halogen lamps each rated at 785W were used to simulate solar irradiance during the tests. The intensity of the incoming irradiance was obtained by calculating the heat flux and the irradiance.

$$Q_S = \frac{P_{lamp}}{\frac{\pi D^2}{4}} \qquad (6.2)$$

$$Q_{panel} = Q_S * \left(\frac{r}{r+d}\right)^2 \qquad (6.3)$$

Where

Q_S = Radiation flux, W/m^2

r = Radius lamp cover, m

D = Diameter lamp, m

d = Distance between lamp and PV panel, m

Q_{panel} = Radiation flux on the PV panel, W/m^2

6.1.1.5 PV module

The experiment was conducted in the Energy Laboratory in the Edinburgh Napier University. One single mono-crystalline PV module (Type BP222 SR) of rating 22W peak power was used for the experiments. Table 6.3 shows the electrical parameters for the PV module.

Table 6.3: Specifications of the PV module

Peak power (P_m)	22W
Max. Power voltage(V_m)	15.2V
Open circuit voltage(V_{oc})	19V
Max. power current(I_m)	1.45A
Short circuit current(I_{sc})	1.65A
Weight	4kg
Dimensions(LxWxD)	478x448x38.5 mm
Temperature Coefficients of V_{oc}	-0.34%/^{o}C
Temperature Coefficients of I_{sc}	+(0.036～0.04)%/ ^{o}C

6.1.2 Laboratory work

6.1.2.1 Water cooling jacket design

The WCJ is made of aluminium and was designed as 1mm thick rectangular aluminium tubes with dimensions of 364x101.5x19mm for each tube. In addition, these rectangular aluminium tubes are provided with similar two pipes for inlet and outlet with a diameter 16mm. The design of the WCJ is presented in Fig 6.1.
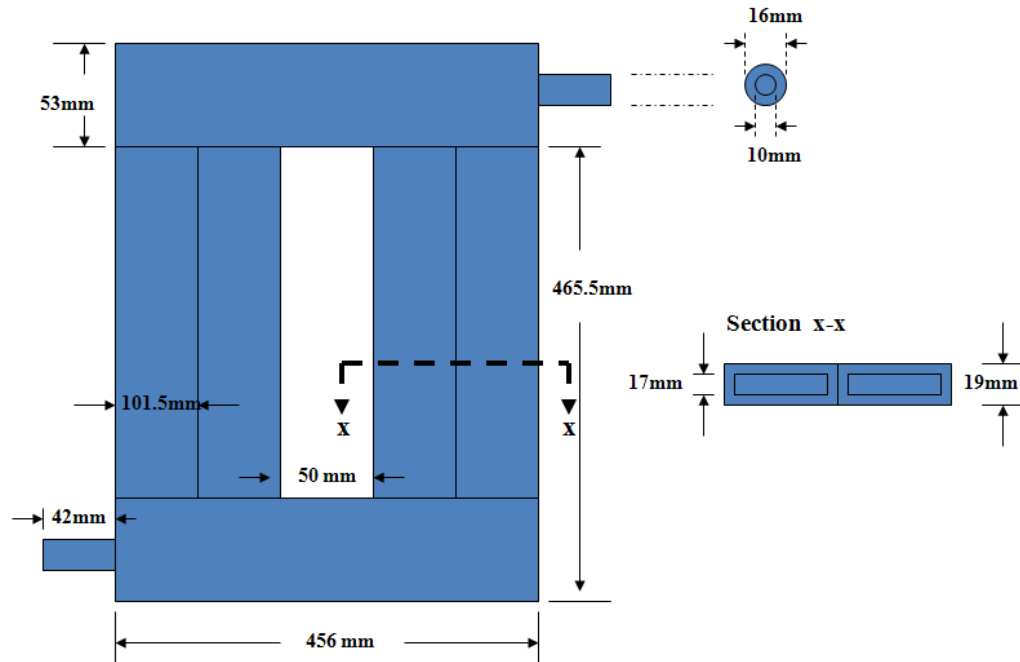
Figure 6.1 Geometry details for the WCJ

To improve heat transfer between the thermocouples, PV cell and WCJ, Dow Corning® 340 heat sink compound was used and six grooves were made on the WCJ surface. Dow Corning® 340 heat sink compound is grease like silicone fluid thickened with metal oxide filler that gives the compound its high thermal conductivity and high temperature stability. The grooves were made to avoid the clearance between PV panel and WCJ for more accurate thermocouples reading (see Fig 6.2).
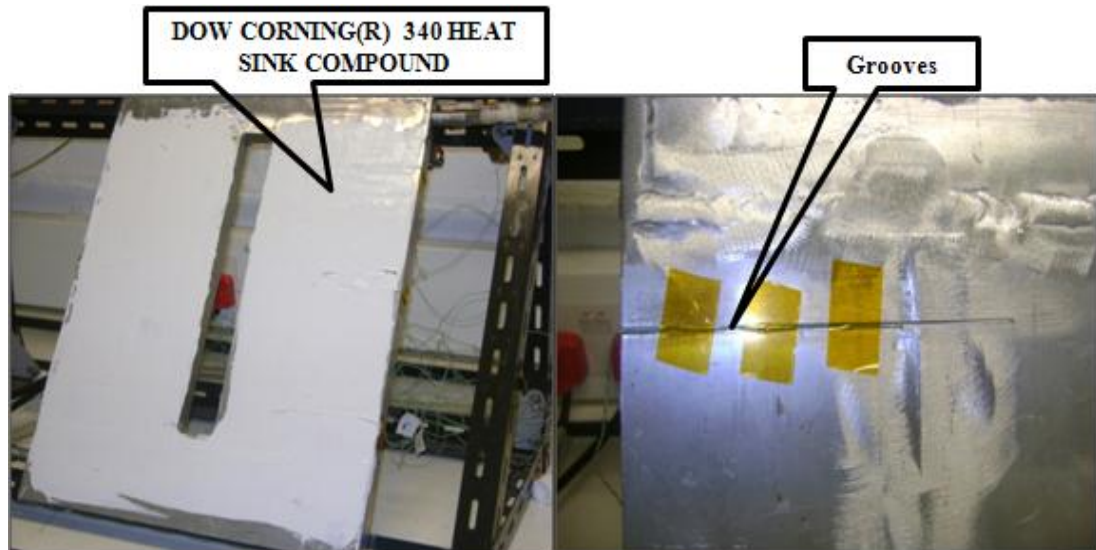
Figure 6.2 Grooves and heat sink compound on the WCJ

6.1.2.2 Test set up, measurement and data collection

- **PV module with and without WCJ**

Ten K-type thermocouples were calibrated and then were used to monitor the cell temperature, water temperature inlet and outlet and ambient profile with Grant data loggers. For PV system with WCJ, six thermocouples were installed and fixed on the back surface of PV module by thermal tapes to measure cell temperature and two thermocouples are installed to monitor inlet and outlet water temperature. Furthermore, the ambient temperature in the laboratory was monitored using another thermocouple (see Fig 6.3). The experiment was tested under three different mass flow rates (0.014- , 0.021- and 0.042 kg/s) for irradiance 255- and 296 W/m^2. Nine thermocouples were used to monitoring cell temperature and one thermocouple to measure ambient temperature for PV system without WCJ (see Fig 6.4). This experiment was tested under two different irradiance (255- and 296 W/m^2).
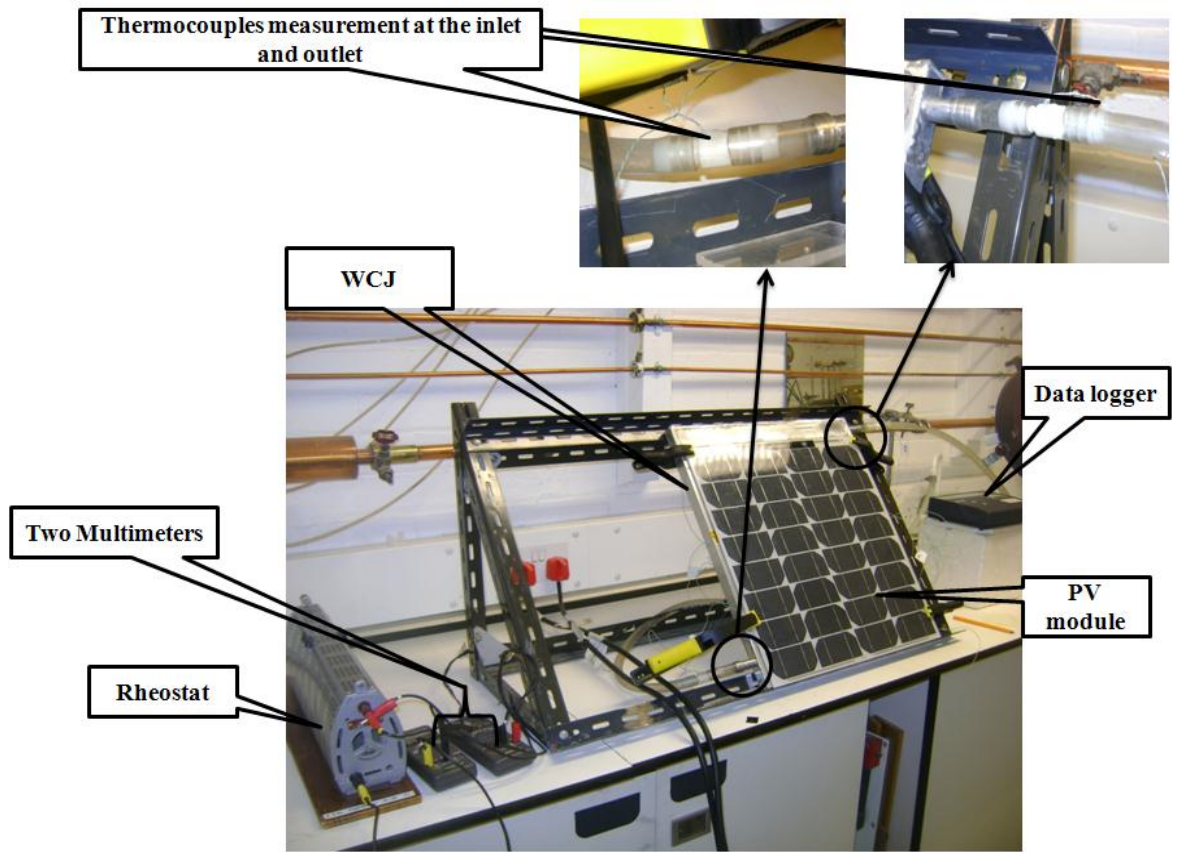
Figure 6.3 The PV system with WCJ and instrumentations
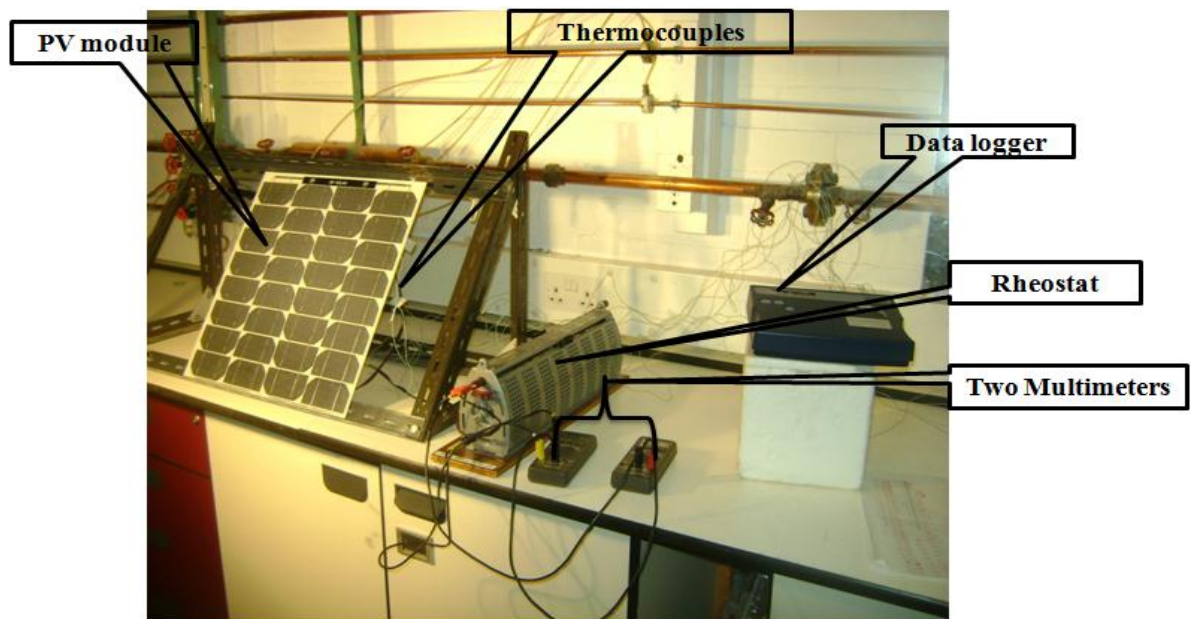
Figure 6.4 The PV system without WCJ and instrumentations

171

Tests were carried out until the system reached equilibrium. Temperatures were recorded at 1 minute intervals for a period of 30 minutes, time to reach a state of equilibrium.

I-V readings for the module were monitored by two multimeters for varying load resistances to provide detailed information about the PV module power output. Fig 6.5 illustrates the schematic diagram of the measuring system.
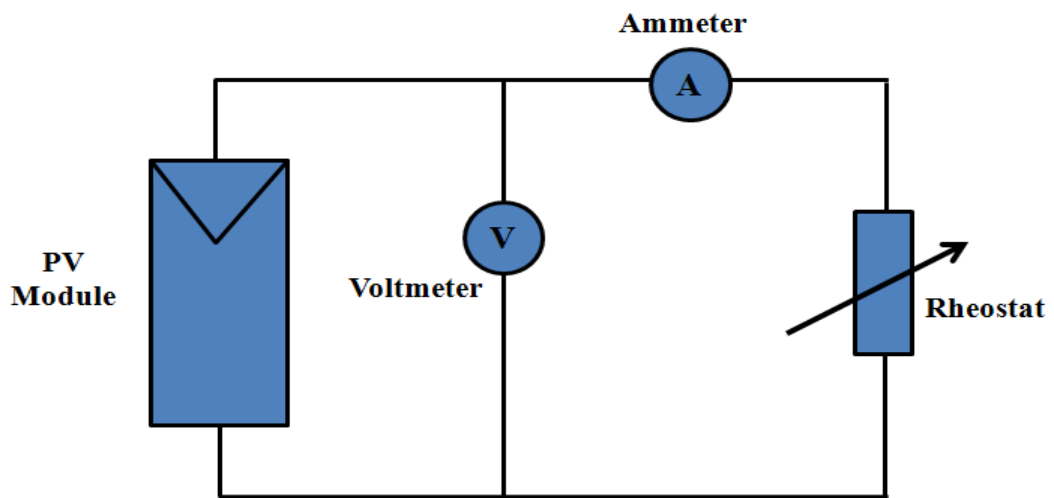
Figure 6.5 Schematic circuit diagram of PV module measurement system

Laboratory test were then carried out at three flow rates (0.014-, 0.021- and 0.042kg/s) for each irradiance (255- and 296 W/m^2) for the PV system with the WCJ. Thermocouples were placed along the length of the WCJ, T1 to T6 from bottom to top respectively and from T1 to T9 for the PV system without the WCJ. Equilibrium was experienced after a period of 30 minutes. Temperatures tended to a fixed value for any thermocouple position in the PV system with and without the WCJ. This equilibrium is the result of a heat transfer effect. The limits of error for the K-type thermocouples is reported [13] $\pm$ 2.2°C or 0.75% above 0°C (whichever is greater). As described earlier, the relation between the current produced at the junction of a thermocouple and the temperature is not linear and therefore a polynomial function to accurately define the temperature is used. This polynomial (8th order) is highly accurate and thus the uncertainty due to the polynomial-accuracy can be neglected.

In Table 6.4, the errors caused in each of readings due to instrument tolerance are given.

Table 6.4: Qualities to be measured, instruments to be used and instrumental errors

PV measurements		
Power measurement, W	PX 120 Wattmeter	0.5% of reading ±2 counts
Temperature, ^{o}C	K-type thermocouples	±0.1 ^{o}C
Voltage, V	Multimeter	±0.01 V
Current, A	Multimeter	±0.1 mA

6.1.3 Results and discussions

The performance of PV system can be depicted by the combination of efficiency expression. The main results obtained are summarized in table 6.5.

Table 6.5: Performance of the PV module with and without WCJ at irradiance 255- and 296W/m^2 under experimentation

PV system with WCJ						
Irradiance (W/m^2)	**255**			**296**		
Mass flow rate (kg/s)	**0.014**	**0.021**	**0.042**	**0.014**	**0.021**	**0.042**
Cell temperature (^{o}C)	16.9	13.5	11.9	25.5	15.5	14
Ambient temperature (C)	22	22	22	22	22	22
Inlet water temperature (^{o}C)	11.6	8.3	6.9	10	8.5	7
Outlet water temperature (^{o}C)	15.2	10.7	8.1	13.9	11	9
Current (A)	0.28	0.28	0.29	0.28	0.28	0.29
Voltage(V)	17	17.2	17.4	16.67	17.16	17.3
Power(W)	4.8	4.82	5	4.66	4.8	5
Efficiency (%)	11.2	11.3	11.8	9.4	9.7	10
PV system without WCJ						
Irradiance (W/m^2)	**255**			**296**		
Cell temperature (^{o}C)	58			61		
Ambient temperature (^{o}C)	22			22		
Current (A)	0.25			0.25		
Voltage(V)	15.2			15.17		
Power(W)	3.8			3.8		
Efficiency (%)	8.9			7.7		

Performance of electrical efficiency η_{el} is shown as below:

$$\eta_{el} = \frac{I\,V}{A_p I_s} * 100\%$$

(6.4)

Where :

I = current (A)

V = voltage (V)

A_p = Area of the PV module (m^2)

I_s = Irradiance (W/m^2)

The power output can be expressed by:

$$P = I * V$$

(6.5)

The experiment result in Figs 6.6 and 6.7 show the PV module efficiency versus the cell temperature at different mass flow rates with the WCJ for irradiance 255, and 296 W/m^2. The result shows that when mass flow rate increases, the cell temperature decreases and the PV efficiency increases.
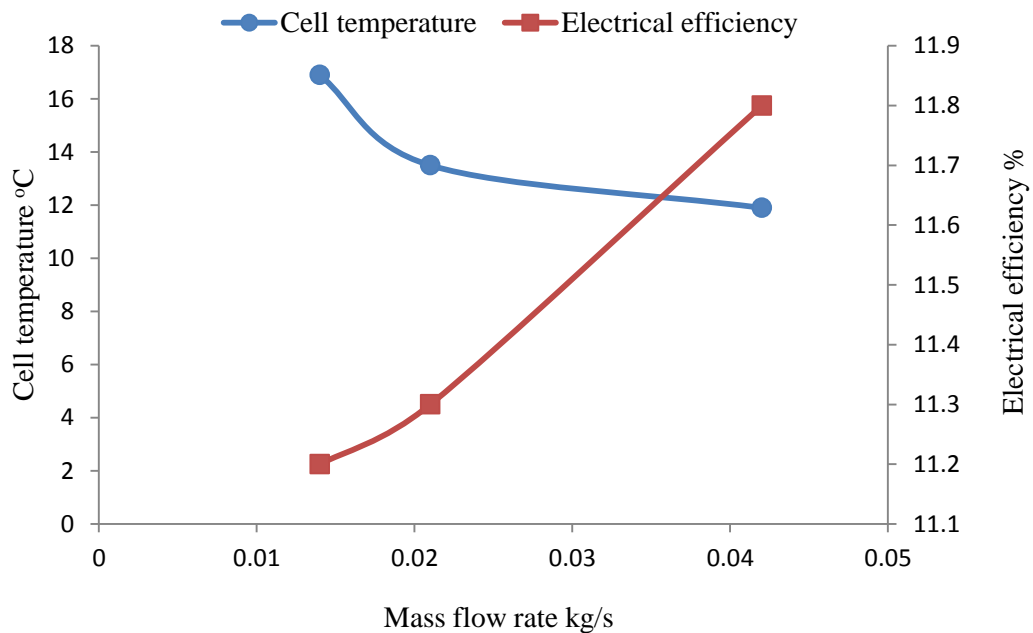
Figure 6.6 Electrical efficiency and cell temperature versus mass flow rate for 255W/m^2 with WCJ under experimentation
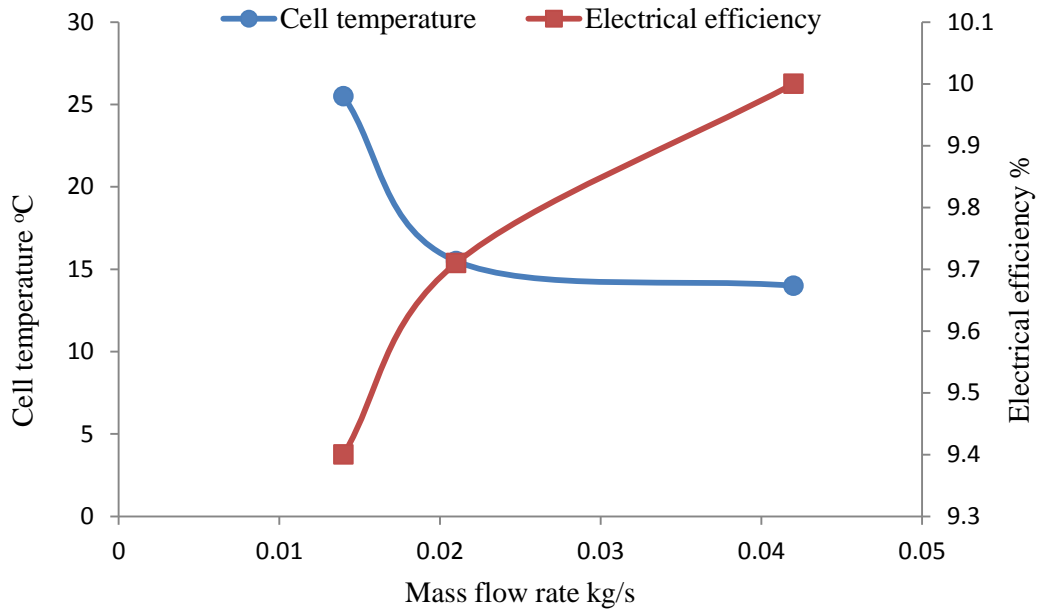
Figure 6.7 Electrical efficiency and cell temperature versus mass flow rate for 296W/m^2 with WCJ under experimentation

Figs 6.8 and 6.9 show the cell temperature and electrical efficiency for the PV system without the WCJ versus irradiance 255, and 296W/m^2. The result shows that as the cell temperature increases, the PV efficiency decreases.
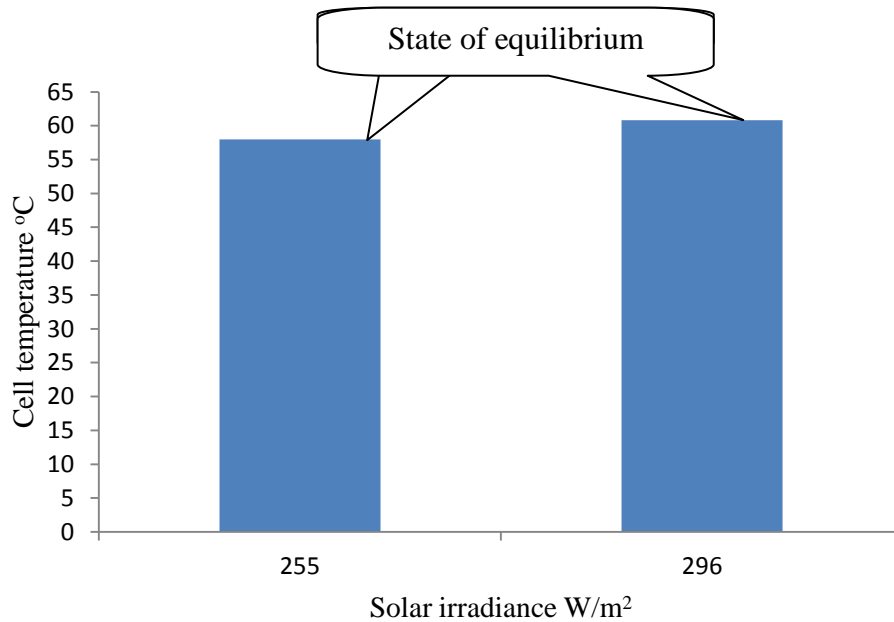
Figure 6.8 Relationship between irradiance and cell temperature under experimentation
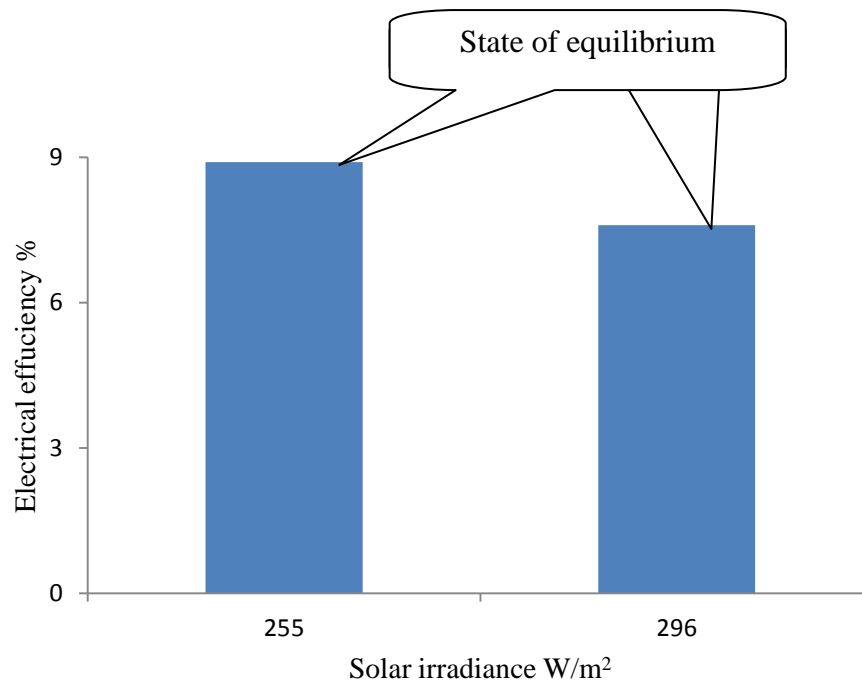
Figure 6.9 Relationship between irradiance and electrical efficiency under experimentation

Note that cooling water introduced at a temperature of 14°C managed to increase the PV panel efficiency from an un-cooled cell temperature of 61°C by an absolute value of 2.6%. This translates to a relative efficiency increase of 35%, i.e. a 2.6% efficiency increases from the 7.4% base.

6.2 Validation of solar radiation on slope surface, photovoltaic cell temperature and photovoltaic module efficiency

The objectives of the present section are the modelling and experimental verification of the conversion of solar irradiation from horizontal to sloped surface and photovoltaic cell temperature and an analysis of photovoltaic conversion efficiency. The experimental system was mounted in a city in the southern part of Turkey. All these measurements are recorded by Turkish team at Iskenderun [2].

The experimental verification of the modelling part as well as the analysis of photovoltaic conversion efficiency was carried out using the data measured from the photovoltaic system; solar irradiation on horizontal and sloped surfaces, and the cell

176

and ambient temperatures. The data were measured at 30-second intervals and were stored in data loggers and averaged further as required. The solar irradiation measured on horizontal surface were converted to sloped surface and then compared to the measured sloped surface irradiation.

6.2.1 Photovoltaic modules and the experimental set-up

The experimental system consisted of 2x120W mono-crystalline photovoltaic modules situated at the top of a building in Iskenderun (36.35^{o}N; 36.10^{o}E), on the eastern Mediterranean coast of Turkey. The modules were mounted tilted at an angle equal to the latitude of the location, facing south. Fig 6.10 shows the photovoltaic modules situated on the roof of the building.

Figure 6.10 Photovoltaic modules mounted at an angle of 36° situated on the top of a building in Iskenderun, Turkey

Technical characteristics of the photovoltaic modules are as follows: short circuit current at reference condition $I_{sc,ref}$ = 7.7 A, open circuit voltage at reference condition Voc,ref = 21 V, current at maximum power point at reference condition $I_{mp,ref}$ = 7.1 A, voltage at maximum power point at reference condition $V_{mp,ref}$ = 16.9 V, power at maximum power point at reference condition $P_{m,ref}$ = 120W. These are provided by the manufacturer for the reference conditions of 1000 W/m^{2} of irradiance level, 25 ^{o}C of cell temperature, and 1.5 air mass (AM), which is the ratio of the mass of air that the beam radiation has to traverse at any given time and

location to the mass of air that the beam radiation would traverse if the sun were directly overhead [2]. The photovoltaic modules under study are made up of 36 cells connected in series, each of 0.027 m^2, adding up to a total area of 0.974 m^2.

The layout of the experimental system is presented in Fig 6.11. in addition to the photovoltaic modules, the experimental system contains of 200Ah/12V of sealed type lead-acid battery and a DC/AC inverter of 600W/12V and 230V/50Hz, with a maximum efficiency of 98%.
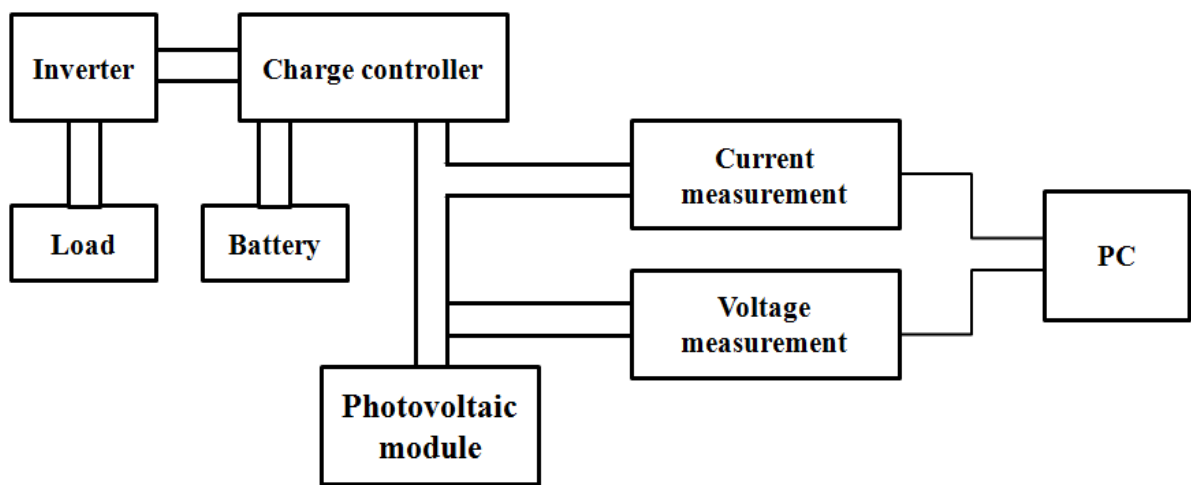
Figure 6.11 Layout of the experimental system

The load connected to the photovoltaic system is a number of light bulbs, whose power varies between 0- and 200W depending on the state of charge of the battery. The photovoltaic modules are connected to the battery and the load through an inverter and a charge controller.

As mentioned in Chapter 5 solar radiation incident on any given surface can be decomposed into two components, the direct or beam component emanating from the sun, and a diffuse component that results from multiple reflections and scattering due to particles in the atmosphere. The diffuse component may also include reflections from the ground and local surroundings, where the surface in question is sloped rather than horizontal. Differentiating between the two components is vital for accurate calculations in most solar energy applications; however, a number of steps

may be required to arrive at realistic estimates at an appropriate level of detail for a given location depending on the basic data available. Also estimation of the cell temperature was described in section 5.4.1.1.

6.2.2 Results and discussion

The solar radiation data presently converted using the above method was measured in the experimental system from January 2005 to May 2005 at 5 minutes intervals. The calculated solar radiation data are compared to that measured on a sloped surface in Fig 6.12.

One of the most important indicators of the goodness of fit of the model is the coefficient of determination (R^2), which is 0.97 in this case. The mean bias error (MBE) is -2.2 while the root mean square error (RMSE) is 60.9. The cell temperature calculated using the equations were described in 5.4 are compared to those measured in Fig 6.13 for the presently available data.
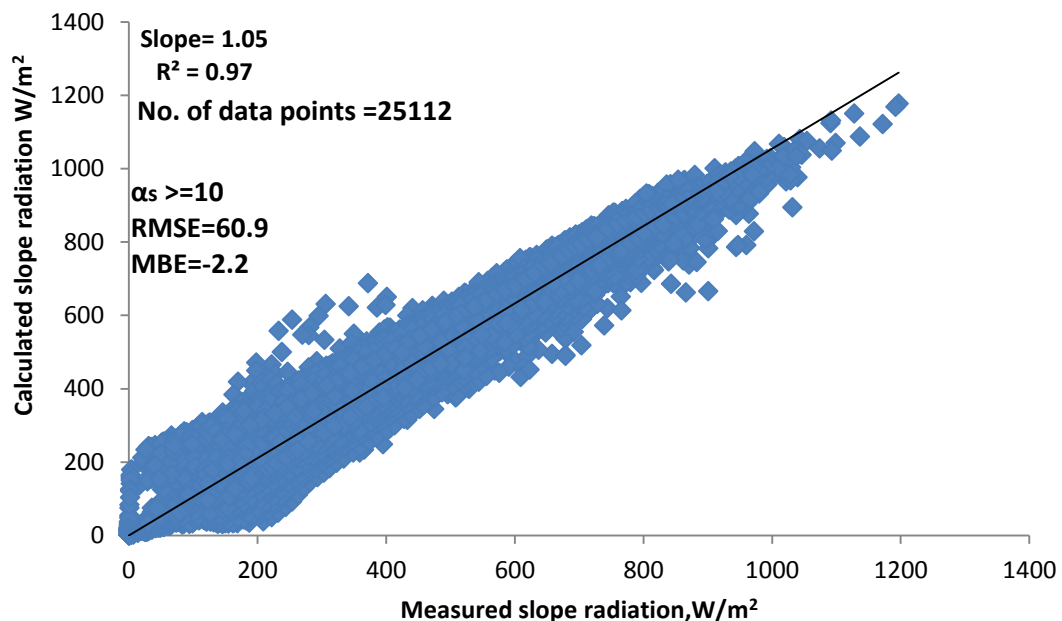
Figure 6.12 Evaluation of presently used slope radiation model
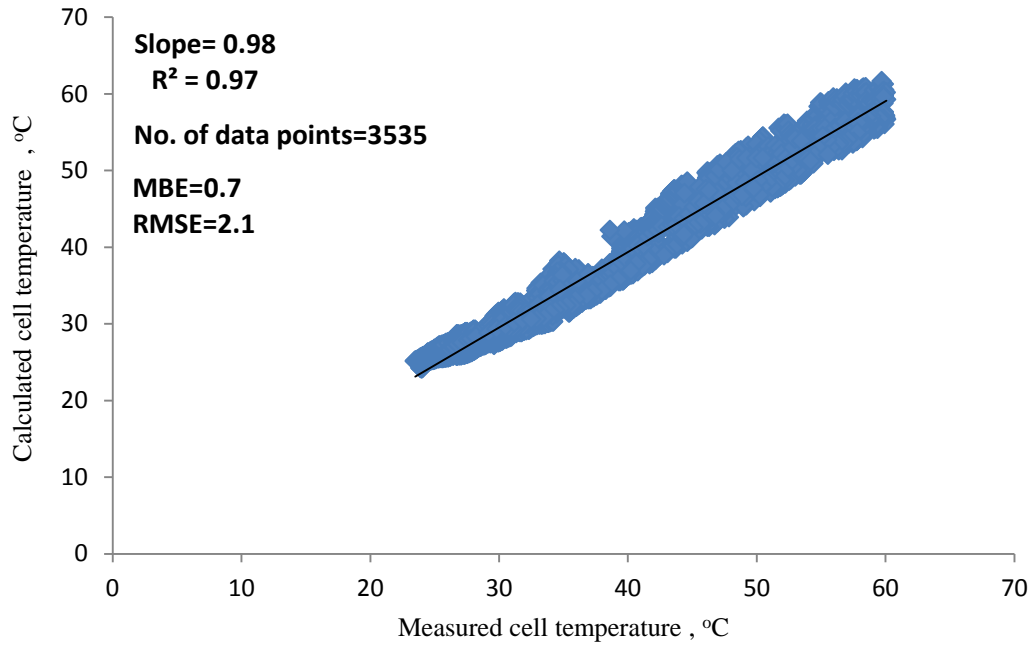
Figure 6.13 Evaluation of presently used procedure for computing cell temperature

For this correlation, R^2 is 0.97, while MBE is 0.7 and RMSE is 2.1. Note that the measured data set that was presently used was collected between 18 June and 17 July 2004. The frequency of measurement was one minute. The efficiency values calculated from the measured current and voltage values are given in Fig 6.14 in terms of frequency histograms.
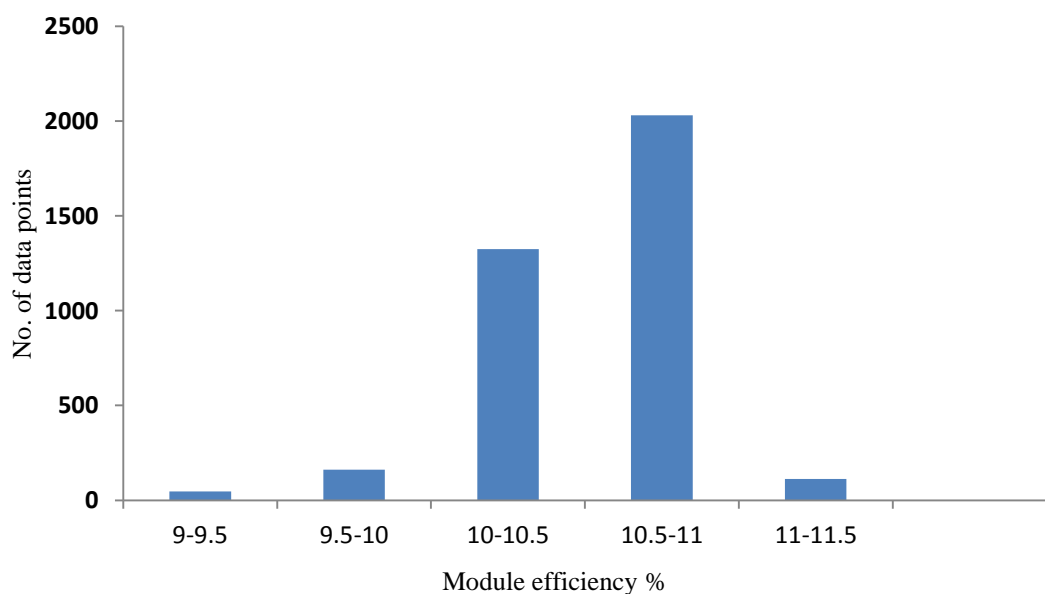
Figure 6.14 Frequency histogram for measured PV module efficiency,%

The efficiency values are an average of hourly data measured from June to July in 2004. It is obviously seen that about 90% of module efficiency values are between 10-11%.

6.3 Conclusion

In section 6.1 a testing device was specially designed to study the effect of cell temperature on the module efficiency. Two operation modes are tested: PV module without WCJ and PV module with WCJ under various mass flow rates (0.014 - , 0.021 - and 0.042kg/s) with the intensity of the incoming irradiance of 255- and 296W/m^2 by using two halogen lamps each rated at 785W.

The use of WCJ results in an observable decrease of the mean panel cell temperature and a respective increase in cell efficiency. This is true especially for the higher mass flow rate. Overall heat transfer and PV panel cooling increase with increasing the mass flow rate.

In section 6.2, based on the measurements made using an experimental PV system set in a city in the southern part of Turkey, models conversion of solar irradiation from horizontal to sloped surfaces and photovoltaic cell temperature were experimentally validated and an analysis of photovoltaic conversion efficiency was carried out. The most important conclusions drawn from the study presented above are:

1. As one of the commonly resorted methods, the conversion of solar radiation from horizontal to sloped surface can be successfully investigated using the theory developed by Muneer et al [4]. The correlation between the calculated and measured solar radiation on a sloped surface using the above model showed that the radiation values are closely predicted as indicated by the favourable value of coefficient of determination, 0.97.

2. The knowledge of cell temperature is imperative to determine the efficiency of PV modules. There are various theories developed to calculate the cell temperature from some commonly measured meteorological data. The

method used presently offers a sound theory to calculate the cell temperature based on various parameters. With the theory used, the cell temperature was predicted accurately.

3. The efficiency of a PV module and thus a PV system determines the techno-economic viability of such projects. The statistical analysis of efficiency showed that the bulk of the efficiency values fell in the interval between 10 and 11 % for this system.

References

[1].   Pico technology, *Thermocouple catalogue*. 2007.

[2].   Celik,A.,Acikgoz,N.,*Modelling and experimental verification of the operating current of mono-crystalline photovoltaic modules using four and five-parameter models.* Applied Energy, 2007. **84**(1): p. 1-15.

[3].   De Soto, W., Klein.S., Beckman,WA. , *Improvement and validation of a model for photovoltaic array performance.* Solar Energy, 2006. **80**: p. 78-88.

[4].   Muneer, T., Abodahab ,N. , *Windows in Buildings.*2000: Oxford, Elsevier.

CHAPTER 7

Conclusions and recommendations for future work

7.0 Introduction

In this chapter the overall conclusions of this thesis will be presented. Potential recommendations and future works will also be addressed.

Overall, Libya consumed 22.17 billion kWh of electricity in 2010. Libya's electricity demand is growing at a rapid rate (around 6%-8% annually) and the country will require significant additional capacity in coming years. An opportunity exists to utilise the high solar radiation levels incident on the south of the country to meet this demand.

Due to its near tropical location, Libya is blessed with plenty of daily sunshine hours and no cloud cover all year round. The measured noon clearness-index, often exceeding 0.84, is an ideal candidate for large-scale generation of solar electricity. Al-Kufra, which is a region located in Southern-East Libya has an excellent solar energy potential ranging from 2,200 to 2,600 kWh/m^2/year of direct normal irradiation. This region is also well known with its large aquifers of high-quality ground water.

Throughout the literature review, it has been clarified that the large scale concentration and photovoltaic power plants are treated separately.

7.1 The performance analysis of a DSG plant for southern Libya based on the thermodynamic and thermophysical properties of water/steam substance.

A DSG plant offers a cheaper and less risky method of generating electricity using concentrated solar energy than an HTF plant. However, it is argued that the location of a DSG plant can be critical in realising these benefits, and that the south east part of Libya is ideal in this respect. The models and calculations presented here are the result of an implementation of the 2007 revision of the IAPWS equations in a general application based on Microsoft Excel and VBA.

7.1.1 The hypothetical design discussed is shown to reduce greenhouse gas emissions by 76% compared to an equivalent gas-only plant over the ten-hour daily period of operation. The solar fraction is shown to be 76%. Land

requirement is modest at 0.7km^2, especially in a desert region where there is little competition on land. However, the design only takes into account the thermodynamic and thermophysical behaviour of the water substance circulating in the system. Indicative construction costs are provided based on formulae developed by other authors; however, further work is required to fully specify and cost the balance of plant which includes the circulatory and condensing equipment. Assuming an exchange rate of approximately 1.44499 Euro to the dollar, the total construction cost in dollars is $146,875,528 and the payback period for the plant is calculated as two years and five months.

7.1.2 It was noted that several studies have been carried out and showed that there is instability in the steel absorber tube, due to the highly concentrated solar flux on only one-half of the circumference of the absorber tube. A computational fluid dynamics (CFD) simulation was carried out to compare the thermal gradient within steel pipes with three alternative pitches of internal helical fins. It has been ascertained that the presence of the fins improves the thermal distribution and the 100mm pitch helical fin proved to be better than the 200- and 400mm pitch helical fin pipes. Thus, with the introduction of internal fins it was found that the circumferential temperature distribution was much more homogenous with standard deviation being halved. However, the pressure drop across the pipe with100mm pitch helical fins is more than four times the pressure drop recorded in the pipe with 400mm pitch helical fins. Furthermore, aluminium pipe showed the best results despite not having any helical fins, i.e. the absorber tube material with higher thermal conductivity appears appropriate especially in preheating section. This suggests that the conductivity of the material is important and has greater bearing than the presence of the fins. The heat transferred to water by the pipes with helical fins is higher than that without the fins.

7.2 Energetic, economic and environmental impact analysis for LS-PV (stationary and tracking) power plant in southern Libya

This thesis also presented an extended analysis for installing a 50MW PV-grid connected (stationary and tracking) power plant in Al-Kufra, Libya. The HIT solar

PV module from Sanyo, rated at 200W, has been used in this study due to its high efficiency.

Long-term meteorological parameters for Al-Kufra region have been collected from Renewable Energy Authority of Libya (REAOL) and the results confirm that Al-Kufra has high levels of content of annual solar radiation. The collected meteorological parameters were: long-term average daily global radiation, average daily sunshine hours, long-term hourly ambient temperature and average daily wind speed.

7.2.1 A Microsoft Excel-VBA program has been developed to compute slope radiation, dew-point, sky temperature, and then cell temperature, maximum power output and module efficiency of the system, with and without a water cooling for stationary system and for tracking system without water cooling.

The results for energy production show that the total energy output is 114GWh/year without a water cooling system , 119GWh/year with a water cooling system for stationary system and 148GWh/year for tracking system. Also, the maximum cell temperature without a water cooling system is 49.6^{o}C on 21 June at noon for stationary system and 51°C for tracking system. Furthermore, the minimum cell temperature is 9.4^{o}C on 21 January at 7.30 am for stationary system and 5.7^{o}C on 11 January at 7.30 am for tracking system. The average module efficiency with and without a cooling system for stationary system is 17.2% and 16.6% respectively and 16.2% for tracking system.

7.2.2 For stationary system, the modelling of the PV system indicated that cooling water introduced at a temperature of 27°C will increase the PV panel efficiency from an un-cooled cell temperature of 49.6^{o}C by an absolute value of 1.1%. This translates to a relative efficiency increase of 6.9%.

7.2.3 The values of electricity generation capacity factor (CF) and solar capacity factor (SCF) for stationary system were found to be 26% and 62.5%

respectively and 34% and 82% for tracking system. The payback time for the stationary PV power plant was found to be 2.75 years and 3.58 years for tracking system.

Therefore it can be concluded that for LS-PV plant, the stationary PV field arrangement is preferable when compared in terms of land impact and the disadvantages of plants with trackers.

7.3 Influence of cell temperature on PV performance

A testing device was specially designed by the author's collaborating team to study the effect of cell temperature on the module efficiency. Two operation modes are tested: PV module without WCJ (Water cooling jacket) and PV module with WCJ under various mass flow rate (0.014- , 0.021- and 0.042kg/s) with the intensity of the incoming solar radiation of 255- and 296W/m^2 by using two halogen lamps each rated at 784W.

The use of WCJ results in an observable decrease of the mean panel cell temperature and a respective increase in cell efficiency. This is true especially for the higher mass flow rate.

7.3.1 Validation of solar radiation on slope surface, photovoltaic cell temperature and photovoltaic module efficiency

Based on the measurements made on an experimental PV system and the measurements recorded by Turkish team at Iskenderun in the southern part of Turkey, the conversion of solar irradiation from horizontal to sloped surface and of a photovoltaic cell temperature model were experimentally validated and an analysis of photovoltaic conversion efficiency was carried out. The most important conclusions drawn from the analysis are:

7.3.1.1 As one of the commonly resorted method, the conversion of solar radiation from horizontal to sloped surface can be successfully made using the theory developed by Muneer. The correlation between the calculated and measured solar radiation on a sloped surface using the above model showed that the

radiation values are closely predicted indicated by the favourable value of coefficient of determination of 0.97.

7.3.1.2 The knowledge of cell temperature is imperative to determine the efficiency of PV modules. There are various theories developed to calculate the cell temperature from some commonly measured meteorological data. The method used presently offers a sound theory to calculate the cell temperature based on various parameters. With the theory used, the cell temperature was predicted very accurately.

7.3.1.3 The efficiency of a PV module and thus a PV system determines the techno-economic viability of such projects. The statistical analysis of efficiency showed that the bulk of the efficiency values fell in the interval between 10 and 11 % for this system.

7.4 Recommendations for future work

7.4.1 To ensure acceptance of solar electricity systems, it will be necessary to make people aware of advantages and potential of solar electricity generation in Libya. Such awareness creation is necessary for all levels of the local community.

7.4.2 Libyan government institutions should play a major role in decision-making and developing and implementing the right policies for smooth introduction of solar electricity on large scale.

7.4.3 Building a database of solar radiation and ambient conditions in Libya for a period of years is recommended.

7.4.4 Emphasis on the importance of solar energy resource assessment and modeling in Libya and development of accurate tools for modeling and predictions of incident solar radiation under variable local weather conditions including effect of dust storms.

7.4.5   Attention to the definition and determination of feed-in tariffs in Libya.

7.4.6   An economic assessment for the cost of exporting the electricity to the countries north of the Mediterranean from Libya.

7.4.7   Implementation of both PV systems (with and without cooling system) in real life conditions and monitoring of their performance.

7.4.8   Future CFD studies could concentrate on thermal gradients in the absorber-tube wall using boundary conditions for saturation and superheated sections. Furthermore, in order to get accurate results, the mesh size should be less that 1mm for the absorber-tube.

7.4.9   Further work is required to fully specify and cost the balance of plant which includes the circulatory and condensing equipment for large scale of DSG and PV power plants.

Appendix-A

Computed parameters for the present design study

Enthalpy of exiting water, kJ/kg

Hour	Jan	Feb	Mar	Apr	May	Jun	Jul	Aug	Sep	Oct	Nov	Dec
7.5	2219	2329	2345	2311	2318	2534	2690	2729	2495	2323	2310	2057
8.5	2260	2515	2614	2582	2597	2803	2977	3007	2746	2531	2451	2145
9.5	2309	2635	2793	2776	2808	3019	3192	3218	2917	2665	2530	2197
10.5	2238	2690	2896	2896	2946	3161	3339	3351	3025	2731	2557	2207
11.5	2196	2706	2941	2955	3015	3230	3410	3419	3073	2756	2556	2194
12.5	2196	2706	2941	2955	3015	3230	3410	3419	3073	2756	2556	2194
13.5	2238	2690	2896	2896	2946	3161	3339	3351	3025	2731	2557	2207
14.5	2309	2635	2793	2776	2808	3019	3192	3218	2917	2665	2530	2197
16.5	2260	2515	2614	2582	2597	2803	2977	3007	2746	2531	2451	2145
17.5	2219	2329	2345	2311	2318	2534	2690	2729	2495	2323	2310	2057

Gas usage MWh

Hour	Jan	Feb	Mar	Apr	May	Jun	Jul	Aug	Sep	Oct	Nov	Dec
7.5	1.1	1.0	1.0	1.0	1.0	0.8	0.6	0.6	0.8	1.0	1.0	1.2
8.5	1.0	0.8	0.7	0.7	0.7	0.5	0.4	0.4	0.6	0.8	0.9	1.1
9.5	1.0	0.7	0.6	0.6	0.5	0.4	0.2	0.2	0.4	0.7	0.8	1.1
10.5	1.0	0.6	0.5	0.5	0.4	0.2	0.1	0.1	0.3	0.6	0.8	1.1
11.5	1.1	0.6	0.4	0.4	0.4	0.2	0.0	0.0	0.3	0.6	0.8	1.1
12.5	1.1	0.6	0.4	0.4	0.4	0.2	0.0	0.0	0.3	0.6	0.8	1.1
13.5	1.1	1.0	1.0	1.0	1.0	0.8	0.6	0.6	0.8	1.0	1.0	1.2
14.5	1.0	0.6	0.5	0.5	0.4	0.2	0.1	0.1	0.3	0.6	0.8	1.1
16.5	1.0	0.8	0.7	0.7	0.7	0.5	0.4	0.4	0.6	0.8	0.9	1.1
17.5	1.0	0.7	0.6	0.6	0.5	0.4	0.2	0.2	0.4	0.7	0.8	1.1

Solar fraction

Hour	Jan	Feb	Mar	Apr	May	Jun	Jul	Aug	Sep	Oct	Nov	Dec
7.5	0.60	0.63	0.64	0.63	0.63	0.70	0.76	0.77	0.69	0.63	0.63	0.54
8.5	0.61	0.70	0.73	0.72	0.72	0.79	0.85	0.86	0.77	0.70	0.68	0.57
9.5	0.63	0.74	0.79	0.78	0.80	0.87	0.92	0.93	0.83	0.75	0.70	0.59
10.5	0.60	0.76	0.82	0.82	0.84	0.91	0.97	0.98	0.87	0.77	0.71	0.59
11.5	0.59	0.76	0.84	0.84	0.86	0.94	1.00	1.00	0.88	0.78	0.71	0.59
12.5	0.63	0.74	0.79	0.78	0.80	0.87	0.92	0.93	0.83	0.75	0.70	0.59
13.5	0.61	0.70	0.73	0.72	0.72	0.79	0.85	0.86	0.77	0.70	0.68	0.57
14.5	0.60	0.76	0.82	0.82	0.84	0.91	0.97	0.98	0.87	0.77	0.71	0.59
16.5	0.60	0.63	0.64	0.63	0.63	0.70	0.76	0.77	0.69	0.63	0.63	0.54
17.5	0.59	0.76	0.84	0.84	0.86	0.94	1.00	1.00	0.88	0.78	0.71	0.59

$$\text{Gas usage} = \frac{m(3419 - h)}{\eta_{boiler}}$$

$$\text{Solar fraction} = 1 - \left[\frac{Gasusage}{m(3419 - 104.75)}\right]$$

m: Mass flow rate, kg/s

h: Specific enthalpy, kJ/kg

η_{boiler} : Efficiency of natural gas boiler, 90%

191

Appendix-B

Visual Basic Application Code for thermodynamic and thermophysical properties

```
Sub WATER()
```

'Convection on = 1 means ON

```
convecon = 0
D0 = Sheets("WaterCPC").Cells(3, 2)
DI = Sheets("WaterCPC").Cells(4, 2)
Dci = Sheets("WaterCPC").Cells(5, 2)
Dco = Sheets("WaterCPC").Cells(6, 2)
l = Sheets("WaterCPC").Cells(7, 2)
wp = Sheets("WaterCPC").Cells(8, 2)
gcsr = Sheets("WaterCPC").Cells(10, 2)
gcea = Sheets("WaterCPC").Cells(11, 2)
atea = Sheets("WaterCPC").Cells(12, 2)
Ib = Sheets("WaterCPC").Cells(14, 2)
Ta = Sheets("WaterCPC").Cells(16, 2)
mw = Sheets("WaterCPC").Cells(18, 2)
Vwind = Sheets("WaterCPC").Cells(19, 2)
E1 = Sheets("WaterCPC").Cells(20, 2)
E2 = Sheets("WaterCPC").Cells(21, 2)
gca = 0.03
CR = (wp - D0) / (3.14159 * D0)
Tak = Ta + 273.15
Tsk = Tak - 6
Twi = Sheets("WaterCPC").Cells(15, 2).Value
Twik = Twi + 273.15
Tpk = Twik + 2
Tgk = (Tpk + Tak) / 2
hwi = Sheets("WaterCPC").Cells(15, 3)
Pw = Sheets("WaterCPC").Cells(15, 7)
mu = Sheets("WaterCPC").Cells(15, 4)
uw = mu / Pw
kw = Sheets("WaterCPC").Cells(15, 5)
prw = Sheets("WaterCPC").Cells(15, 6)
Presi = Sheets("WaterCPC").Cells(15, 9)
Apcs = 3.14159 * DI ^ 2 / 4
For lengthp = 1 To 636
Vw = mw / (Pw * Apcs)
Rew = Vw * DI / uw
f = (0.79 * Application.Ln(Rew) - 1.64) ^ (-2)
Nuw = ((f / 8) * Rew * prw) / (1.07 + (12.7 *
(f / 8) ^ 0.5 * (prw ^ 0.6666 - 1)))
hpw = (Nuw * kw) / DI
preso = Presi - 0.000001 * Pw * f * Vw * Vw
/ (2 * DI)
Presi = preso
Sheets("Input").Cells(lengthp + 1, 1).Value =
preso
Status = Sheets("Input").Cells(lengthp,
11).Value
itercount = 1
1
Tpgk = (Tpk + Tgk) / 2
Tgak = (Tgk + Tak) / 2
If (Status = "SATM") Then
GoTo 1001
End If
If (convecon >= 1) Then
Sheets("AIR PROPERTIES").Cells(6, 2) =
Tpgk
Pair = Sheets("AIR PROPERTIES").Cells(6,
3)
Cpair = Sheets("AIR PROPERTIES").Cells(6,
4)
µair = Sheets("AIR PROPERTIES").Cells(6,
5)
Uair = Sheets("AIR PROPERTIES").Cells(6,
6)
```

192

```
kair = Sheets("AIR PROPERTIES").Cells(6, 7)
sair = Sheets("AIR PROPERTIES").Cells(6, 8)
Prair = Sheets("AIR PROPERTIES").Cells(6, 9)
Tpgk1 = 1 / Tpgk
Lo = (Dci - D0) / 2
Ra = (((9.81 * Tpgk1 * (Tpk - Tgk) * Lo ^ 3) / (Uair ^ 2)) * (Prair))
If (Ra <= 0) Then
GoTo 15
End If
K1 = Application.Ln(Dci / D0)
K2 = Lo ^ 0.75 * ((1 / D0 ^ 0.6) + (1 / Dci ^ 0.6)) ^ 1.25
Raf = 0.317 * (K1 / K2) * Ra ^ 0.25
kffe = Raf * kair
hpgc = (2 * kffe) / (K1 * D0)
Else
hpgc = 0
End If
FE = (1 / E1) + ((1 - E2) / E2) * (D0 / Dco)
hpgr = 0.0000000567 * (Tpk + Tgk) * (Tpk ^ 2 + Tgk ^ 2) / FE
hpg = hpgc + hpgr
Sheets("AIR PROPERTIES").Cells(6, 14) = Tgak
Pair = Sheets("AIR PROPERTIES").Cells(6, 15)
Cpair1 = Sheets("AIR PROPERTIES").Cells(6, 16)
µair1 = Sheets("AIR PROPERTIES").Cells(6, 17)
Uair1 = Sheets("AIR PROPERTIES").Cells(6, 18)
kair1 = Sheets("AIR PROPERTIES").Cells(6, 19)
sair1 = Sheets("AIR PROPERTIES").Cells(6, 20)
Prair1 = Sheets("AIR PROPERTIES").Cells(6, 21)
Rewind = Vwind * Dco / Uair1
Nu = 0.3 + 0.62 * Rewind ^ 0.5 * Prair1 ^ 0.333 * (1 + (Rewind / 282000) ^ (5 / 8)) ^ (4 / 5) / (1 + (0.4 / Prair1) ^ (2 / 3)) ^ 0.25
hga = Nu * kair1 / Dco
hgs = 0.0000000567 * gcea * (Tgak ^ 4 - Tsk ^ 4) / (Tgak - Tsk)
Tgnew = (( CR* Ib * gca) + (hgs * Tsk) + (hga * Tak) + ((D0 / Dci) * hpg * Tpk)) / (hgs + hga + ((D0 / Dci) * hpg))
Tpnew = ((CR * Ib * gcsr * atea) + (hpw * Twik) + (hpg * Tgk)) / (hpw + hpg)
difTg = Abs(Tgnew - Tgk)
difTp = Abs(Tpnew - Tpk)
SUMDIF = Application.Max(difTg, difTp)
If (SUMDIF < 0.5) Then
GoTo 2
End If
Tgk = Tgnew
Tpk = Tpnew
Tgk = Tgnew
Tpk = Tpnew
If (itercount > 15) Then
Sheets("Error_report").Cells(itercount, 1).Value = Tgk
Sheets("Error_report").Cells(itercount, 2).Value = Tpk
End If
itercount = itercount + 1
If (itercount > 20) Then
GoTo 14
End If
GoTo 1
2
```

```vba
Qlosspg = 3.14159 * D0 * 1 * hpg * (Tpk -
Tgk)
Qlossgsa = 3.14159 * Dco * 1 * (hgs * (Tgk -
Tsk) + hga * (Tgk - Tak))
Qin = CR  * Ib * gcsr * atea
1001
hwo = hwi + 0.001 * (Qin - Qlosspg) / mw
Sheets("Input").Cells(lengthp + 1, 2).Value =
hwo
GoSub 2000
prw = Sheets("Input").Cells(lengthp + 1, 17)
kw = 0.001 * Sheets("Input").Cells(lengthp +
1, 18)
mu = 0.000001 *
Sheets("Input").Cells(lengthp + 1, 19)
Pw = Sheets("Input").Cells(lengthp + 1, 21)
uw = mu / Pw
Twik = Sheets("Input").Cells(lengthp + 1, 3)
hwi = Sheets("Input").Cells(lengthp + 1,
2).Value


Sheets("Output1").Cells(lengthp + 1, 1).Value
= Tgnew - 273.15
Sheets("Output1").Cells(lengthp + 1, 2).Value
= Tpnew - 273.15
Sheets("Output1").Cells(lengthp + 1, 3).Value
= Twik - 273.15
Sheets("Output1").Cells(lengthp + 1, 4).Value
= Qlosspg
Sheets("Output1").Cells(lengthp + 1, 5).Value
= Qlossgsa
Sheets("Output1").Cells(lengthp + 1, 6).Value
= Qin
Sheets("Output1").Cells(lengthp + 1, 7).Value
= itercount
Next lengthp
14
Sheets("Error_report").Cells(1, 1).Value =
"itercount"

Sheets("Error_report").Cells(1, 2).Value =
itercount
GoTo 21
15
Sheets("Error_report").Cells(11, 1).Value =
"Ra"
Sheets("Error_report").Cells(11, 2).Value =
Ra
21
End
2000 'Steam properties
Dim tscoef(10) As Double
Dim region, state As String
capR = 0.461526
w = lengthp + 1
P = Sheets("Input").Cells(w, 1).Value
h = Sheets("Input").Cells(w, 2).Value
hb23n = 0.000236 * P ^ 3 - 0.06244 * P ^ 2 +
8.12183 * P + 2350.762
hcr = -0.003 * P ^ 3 + 0.6337 * P ^ 2 - 42.541
* P + 2604.4
If P > 22.065 And h < hb23n And h > hcr
Then
GoTo 6
End If
pbeta = P ^ 0.25
For I = 1 To 10
tscoef(I) = Sheets("Tsatcoef").Cells(I,
1).Value
Next I
capE = pbeta ^ 2 + tscoef(3) * pbeta +
tscoef(6)
capF = tscoef(1) * pbeta ^ 2 + tscoef(4) *
pbeta + tscoef(7)
capG = tscoef(2) * pbeta ^ 2 + tscoef(5) *
pbeta + tscoef(8)
capD = 2 * capG / (-capF - (capF * capF - 4 *
capE * capG) ^ 0.5)
```

```
tsatK = 0.5 * (tscoef(10) + capD - ((tscoef(10)
+ capD) ^ 2 - 4 * (tscoef(9) + tscoef(10) *
capD)) ^ 0.5)
Sheets("Input").Cells(w, 4).Value = tsatK
Sheets("Input").Cells(w, 16).Value = tsatK -
273.15
incT = tsatK + 0.01
```

'hf

```
pipf = P / 16.53
pipfinc = (P + 0.0000001) / 16.53
tau = 1386 / tsatK
tauincT = 1386 / incT
rhs1 = 0
rhs12 = 0
rhs13 = 0
For I = 1 To 34
capI = Sheets("pTvhs").Cells(I, 6).Value
capJ = Sheets("pTvhs").Cells(I, 7).Value
smalno = Sheets("pTvhs").Cells(I, 8).Value
rhs1 = rhs1 + smalno * ((7.1 - pipf) ^ capI) *
((tau - 1.222) ^ capJ)
rhs12 = rhs12 + smalno * ((7.1 - pipf) ^ capI)
* ((tauincT - 1.222) ^ capJ)
rhs13 = rhs13 + smalno * ((7.1 - pipfinc) ^
capI) * ((tau - 1.222) ^ capJ)
Next I
gibb = capR * tsatK * rhs1
gibbincT = capR * incT * rhs12
gibbincP = capR * tsatK * rhs13
entropy = (gibb - gibbincT) / 0.01
spvolSAT = (gibbincP - gibb) / 0.0000001
enthalpy = gibb + tsatK * entropy
Sheets("Input").Cells(w, 5).Value = enthalpy
Sheets("Input").Cells(w, 6).Value = entropy
Sheets("Input").Cells(w, 7).Value = (1 /
spvolSAT) * 1000
SF = (1 / spvolSAT) * 1000
```

'hg

```
pipg = P
```

```
pipginc = P + 0.0000001
tau = 540 / tsatK
tauincT = 540 / incT
rhs1 = Log(pipg)
rhs12 = Log(pipg)
rhs13 = Log(pipginc)
For I = 1 To 9
capJ = Sheets("pTvhs").Cells(I, 1).Value
smalno = Sheets("pTvhs").Cells(I, 2).Value
rhs1 = rhs1 + smalno * (tau ^ capJ)
rhs12 = rhs12 + smalno * (tauincT ^ capJ)
rhs13 = rhs13 + smalno * (tau ^ capJ)
Next I
rhs2 = 0
rhs22 = 0
rhs23 = 0
For I = 1 To 43
capI = Sheets("pTvhs").Cells(I, 3).Value
capJ = Sheets("pTvhs").Cells(I, 4).Value
smaln1 = Sheets("pTvhs").Cells(I, 5).Value
rhs2 = rhs2 + smaln1 * (pipg ^ capI) * ((tau -
0.5) ^ capJ)
rhs22 = rhs22 + smaln1 * (pipg ^ capI) *
((tauincT - 0.5) ^ capJ)
rhs23 = rhs23 + smaln1 * (pipginc ^ capI) *
((tau - 0.5) ^ capJ)
Next I
gibb = capR * tsatK * (rhs1 + rhs2)
gibbincT = capR * incT * (rhs12 + rhs22)
gibbincP = capR * tsatK * (rhs13 + rhs23)
entropy = (gibb - gibbincT) / 0.01
spvolG = (gibbincP - gibb) / 0.0000001
enthalpy = gibb + tsatK * entropy
Sheets("Input").Cells(w, 8).Value = enthalpy
Sheets("Input").Cells(w, 9).Value = entropy
Sheets("Input").Cells(w, 10).Value = (1 /
spvolG) * 1000
SG = (1 / spvolG) * 1000
```

'Step 3

'Compressed liquid

```
hf = Sheets("Input").Cells(w, 5).Value
hg = Sheets("Input").Cells(w, 8).Value
If h < hf Then

state = "CL"
Sheets("Input").Cells(w, 11).Value = state
region = "1"
Sheets("InpuT").Cells(w, 14).Value = region
pip = P
eta = h / 2500
rhs = 0
For I = 1 To 20
capI = Sheets("phTcoef").Cells(I, 10).Value
capJ = Sheets("phTcoef").Cells(I, 11).Value
smalln = Sheets("phTcoef").Cells(I, 12).Value
rhs = rhs + smalln * (pip ^ capI) * ((eta + 1) ^
capJ)
Next I
Sheets("Input").Cells(w, 3).Value = rhs
T1 = rhs - 273.15
Sheets("Input").Cells(w, 15).Value = T1
```

'New part for entropy and density (CL)

```
pipf = P / 16.53
pipfinc = (P + 0.0000001) / 16.53
tau = 1386 / rhs
incT = rhs + 0.01
tauincT = 1386 / incT
rhs1 = 0
rhs12 = 0
rhs13 = 0
For I = 1 To 34
capI = Sheets("pTvhs").Cells(I, 6).Value
capJ = Sheets("pTvhs").Cells(I, 7).Value
smalno = Sheets("pTvhs").Cells(I, 8).Value
rhs1 = rhs1 + smalno * ((7.1 - pipf) ^ capI) *
((tau - 1.222) ^ capJ)
```

```
rhs12 = rhs12 + smalno * ((7.1 - pipf) ^ capI)
* ((tauincT - 1.222) ^ capJ)
rhs13 = rhs13 + smalno * ((7.1 - pipfinc) ^
capI) * ((tau - 1.222) ^ capJ)
Next I
gibb = capR * rhs * rhs1
gibbincT = capR * incT * rhs12
gibbincP = capR * rhs * rhs13
entropy = (gibb - gibbincT) / 0.01
spvo = (gibbincP - gibb) / 0.0000001
Sheets("Input").Cells(w, 20).Value = entropy
Sheets("Input").Cells(w, 21).Value = (1 /
spvo) * 1000
' end of new part(CL)
GoTo 5
End If
```

'Saturated mixture

```
If hf <= h And h <= hg Then
Sheets("Input").Cells(w, 3).Value = tsatK
Sheets("Input").Cells(w, 15).Value = tsatK -
273.15
state = "SATM"
Sheets("Input").Cells(w, 11).Value = state
X = (h - hf) / (hg - hf)
Sheets("Input").Cells(w, 12).Value = X
region = "4"
Sheets("Input").Cells(w, 14).Value = region
S = X * (Sheets("Input").Cells(w, 9).Value -
Sheets("Input").Cells(w, 6).Value) +
Sheets("Input").Cells(w, 6).Value
DFG = (1 / SG) - (1 / SF)
DFGH = (1 / SF)
DFGHK = (X * DFG) + DFGH
DENI = 1 / DFGHK
Sheets("Input").Cells(w, 20).Value = S
Sheets("Input").Cells(w, 21).Value = DENI
T1 = Sheets("Input").Cells(w, 15).Value
GoTo 5
```

```vba
End If


'Superheated

If h > hg Then
state = "SUPV"
Sheets("Input").Cells(w, 11).Value = state
T1 = Sheets("Input").Cells(w, 15).Value
pip = P
h2b2c = 2652.6571908428 + (Abs(pip -
4.5257578905948) / 1.2809002730136E-04) ^
0.5
Sheets("Input").Cells(w, 13).Value = h2b2c
If P <= 4 Then


'Region 2a

region = "2a"
Sheets("Input").Cells(w, 14).Value = region
pip2a = P
eta = h / 2000
rhs = 0
For I = 1 To 34
capI = Sheets("phTcoef").Cells(I, 1).Value
capJ = Sheets("phTcoef").Cells(I, 2).Value
smalln = Sheets("phTcoef").Cells(I, 3).Value
rhs = rhs + smalln * (pip2a ^ capI) * ((eta -
2.1) ^ capJ)
Next I
Sheets("Input").Cells(w, 3).Value = rhs
T1 = rhs - 273.15
Sheets("Input").Cells(w, 15).Value = T1


'New part for entropy and density
(2a)

pipg = P
pipginc = P + 0.0000001
tau = 540 / rhs
incT = rhs + 0.01
tauincT = 540 / incT
rhs1 = Log(pipg)

rhs12 = Log(pipg)
rhs13 = Log(pipginc)
For I = 1 To 9
capJ = Sheets("pTvhs").Cells(I, 1).Value
smalno = Sheets("pTvhs").Cells(I, 2).Value
rhs1 = rhs1 + smalno * (tau ^ capJ)
rhs12 = rhs12 + smalno * (tauincT ^ capJ)
rhs13 = rhs13 + smalno * (tau ^ capJ)
Next I
rhs2 = 0
rhs22 = 0
rhs23 = 0
For I = 1 To 43
capI = Sheets("pTvhs").Cells(I, 3).Value
capJ = Sheets("pTvhs").Cells(I, 4).Value
smaln1 = Sheets("pTvhs").Cells(I, 5).Value
rhs2 = rhs2 + smaln1 * (pipg ^ capI) * ((tau -
0.5) ^ capJ)
rhs22 = rhs22 + smaln1 * (pipg ^ capI) *
((tauincT - 0.5) ^ capJ)
rhs23 = rhs23 + smaln1 * (pipginc ^ capI) *
((tau - 0.5) ^ capJ)
Next I
gibb = capR * rhs * (rhs1 + rhs2)
gibbincT = capR * incT * (rhs12 + rhs22)
gibbincP = capR * rhs * (rhs13 + rhs23)
entropysup = (gibb - gibbincT) / 0.01
spvolsup = (gibbincP - gibb) / 0.0000001
Sheets("Input").Cells(w, 20).Value =
entropysup
Sheets("Input").Cells(w, 21).Value = (1 /
spvolsup) * 1000


'End of new part (2a)

GoTo 5
ElseIf P > 4 And P <= 6.5467 Then
region = "2b"
Sheets("Input").Cells(w, 14).Value = region
pip = P
```

```vba
eta = h / 2000
rhs = 0
For I = 1 To 38
capI = Sheets("phTcoef").Cells(I, 4).Value
capJ = Sheets("phTcoef").Cells(I, 5).Value
smalln = Sheets("phTcoef").Cells(I, 6).Value
rhs = rhs + smalln * ((pip - 2) ^ capI) * ((eta - 2.6) ^ capJ)
Next I
Sheets("Input").Cells(w, 3).Value = rhs
T1 = rhs - 273.15
Sheets("Input").Cells(w, 15).Value = T1
```

'New part for entropy and density (2b)

```vba
pipg = P
pipginc = P + 0.0000001
tau = 540 / rhs
incT = rhs + 0.01
tauincT = 540 / incT
rhs1 = Log(pipg)
rhs12 = Log(pipg)
rhs13 = Log(pipginc)
For I = 1 To 9
capJ = Sheets("pTvhs").Cells(I, 1).Value
smalno = Sheets("pTvhs").Cells(I, 2).Value
rhs1 = rhs1 + smalno * (tau ^ capJ)
rhs12 = rhs12 + smalno * (tauincT ^ capJ)
rhs13 = rhs13 + smalno * (tau ^ capJ)
Next I
rhs2 = 0
rhs22 = 0
rhs23 = 0
For I = 1 To 43
capI = Sheets("pTvhs").Cells(I, 3).Value
capJ = Sheets("pTvhs").Cells(I, 4).Value
smaln1 = Sheets("pTvhs").Cells(I, 5).Value
rhs2 = rhs2 + smaln1 * (pipg ^ capI) * ((tau - 0.5) ^ capJ)
```

```vba
rhs22 = rhs22 + smaln1 * (pipg ^ capI) * ((tauincT - 0.5) ^ capJ)
rhs23 = rhs23 + smaln1 * (pipginc ^ capI) * ((tau - 0.5) ^ capJ)
Next I
gibb = capR * rhs * (rhs1 + rhs2)
gibbincT = capR * incT * (rhs12 + rhs22)
gibbincP = capR * rhs * (rhs13 + rhs23)
entropysup = (gibb - gibbincT) / 0.01
spvolsup = (gibbincP - gibb) / 0.0000001
Sheets("Input").Cells(w, 20).Value = entropysup
Sheets("Input").Cells(w, 21).Value = (1 / spvolsup) * 1000
```

'End of new part (2b)

```vba
GoTo 5

ElseIf P > 6.5467 And h >= h2b2c Then
region = "2b"
Sheets("Input").Cells(w, 14).Value = region
pip = P
eta = h / 2000
rhs = 0
For I = 1 To 38
capI = Sheets("phTcoef").Cells(I, 4).Value
capJ = Sheets("phTcoef").Cells(I, 5).Value
smalln = Sheets("phTcoef").Cells(I, 6).Value
rhs = rhs + smalln * ((pip - 2) ^ capI) * ((eta - 2.6) ^ capJ)
Next I
Sheets("Input").Cells(w, 3).Value = rhs
T1 = rhs - 273.15
Sheets("Input").Cells(w, 15).Value = T1
```

'New part for entropy and density (2b)

```vba
pipg = P
pipginc = P + 0.0000001
```

198

```
tau = 540 / rhs
incT = rhs + 0.01
tauincT = 540 / incT
rhs1 = Log(pipg)
rhs12 = Log(pipg)
rhs13 = Log(pipginc)
For I = 1 To 9
capJ = Sheets("pTvhs").Cells(I, 1).Value
smalno = Sheets("pTvhs").Cells(I, 2).Value
rhs1 = rhs1 + smalno * (tau ^ capJ)
rhs12 = rhs12 + smalno * (tauincT ^ capJ)
rhs13 = rhs13 + smalno * (tau ^ capJ)
Next I
rhs2 = 0
rhs22 = 0
rhs23 = 0
For I = 1 To 43
capI = Sheets("pTvhs").Cells(I, 3).Value
capJ = Sheets("pTvhs").Cells(I, 4).Value
smaln1 = Sheets("pTvhs").Cells(I, 5).Value
rhs2 = rhs2 + smaln1 * (pipg ^ capI) * ((tau -
0.5) ^ capJ)
rhs22 = rhs22 + smaln1 * (pipg ^ capI) *
((tauincT - 0.5) ^ capJ)
rhs23 = rhs23 + smaln1 * (pipginc ^ capI) *
((tau - 0.5) ^ capJ)
Next I
gibb = capR * rhs * (rhs1 + rhs2)
gibbincT = capR * incT * (rhs12 + rhs22)
gibbincP = capR * rhs * (rhs13 + rhs23)

entropysup = (gibb - gibbincT) / 0.01
spvolsup = (gibbincP - gibb) / 0.0000001
Sheets("Input").Cells(w, 20).Value =
entropysup
Sheets("Input").Cells(w, 21).Value = (1 /
spvolsup) * 1000
```

'End of new part (2b)

```
GoTo 5
Else
region = "2C"
Sheets("Input").Cells(w, 14).Value = region
pip2c = P
eta = h / 2000
rhs = 0
For I = 1 To 23
capI = Sheets("phTcoef").Cells(I, 7).Value
capJ = Sheets("phTcoef").Cells(I, 8).Value
smalln = Sheets("phTcoef").Cells(I, 9).Value
rhs = rhs + smalln * ((pip2c + 25) ^ capI) *
((eta - 1.8) ^ capJ)
Next I
Sheets("Input").Cells(w, 3).Value = rhs
T1 = rhs - 273.15
Sheets("Input").Cells(w, 15).Value = T1
```

'New part for entropy (2c)

```
pipg = P
pipginc = P + 0.0000001
tau = 540 / rhs
incT = rhs + 0.01
tauincT = 540 / incT
rhs1 = Log(pipg)
rhs12 = Log(pipg)
rhs13 = Log(pipginc)
For I = 1 To 9
capJ = Sheets("pTvhs").Cells(I, 1).Value
smalno = Sheets("pTvhs").Cells(I, 2).Value
rhs1 = rhs1 + smalno * (tau ^ capJ)
rhs12 = rhs12 + smalno * (tauincT ^ capJ)
rhs13 = rhs13 + smalno * (tau ^ capJ)
Next I
rhs2 = 0
rhs22 = 0
rhs23 = 0
For I = 1 To 43
capI = Sheets("pTvhs").Cells(I, 3).Value
```

```vba
capJ = Sheets("pTvhs").Cells(I, 4).Value
smaln1 = Sheets("pTvhs").Cells(I, 5).Value
rhs2 = rhs2 + smaln1 * (pipg ^ capI) * ((tau -
0.5) ^ capJ)
rhs22 = rhs22 + smaln1 * (pipg ^ capI) *
((tauincT - 0.5) ^ capJ)
rhs23 = rhs23 + smaln1 * (pipginc ^ capI) *
((tau - 0.5) ^ capJ)
Next I
gibb = capR * rhs * (rhs1 + rhs2)
gibbincT = capR * incT * (rhs12 + rhs22)
gibbincP = capR * rhs * (rhs13 + rhs23)
entropysup = (gibb - gibbincT) / 0.01
spvolsup = (gibbincP - gibb) / 0.0000001
Sheets("Input").Cells(w, 20).Value =
entropysup
Sheets("Input").Cells(w, 21).Value = (1 /
spvolsup) * 1000
```

'End of new part (2c)

```vba
GoTo 5
End If
End If
6
```

'Reign 3

```vba
hboundrey = (0.201464004206875 * 10 ^ 4) +
((0.374696550136983 * 10 ^ 1) * P) + ((-
0.219921901054187 * 10 ^ -1) * P ^ 2) +
((0.87513168600995 * 10 ^ -4) * P ^ 3)
Sheets("Input").Cells(w, 13).Value =
hboundrey
If hboundrey > h Then
state = "SCR"
Sheets("Input").Cells(w, 11).Value = state
region = "3a"
Sheets("Input").Cells(w, 14).Value = region
pip2a = P / 100
eta = h / 2300
rhs = 0
```

```vba
For I = 1 To 31
capI = Sheets("CoefR3").Cells(I, 1).Value
capJ = Sheets("CoefR3").Cells(I, 2).Value
smalln = Sheets("CoefR3").Cells(I, 3).Value
rhs = rhs + smalln * ((pip2a + 0.24) ^ capI) *
((eta - 0.615) ^ capJ)
Next I
Sheets("Input").Cells(w, 3).Value = rhs * 760
Sheets("Input").Cells(w, 15).Value = (rhs *
760) - 273.15
pip3v = P / 100
eta = h / 2100
rhs = 0
For I = 1 To 32
capI = Sheets("CoefR3").Cells(I, 12).Value
capJ = Sheets("CoefR3").Cells(I, 13).Value
smalln = Sheets("CoefR3").Cells(I, 14).Value
rhs = rhs + smalln * ((pip3v + 0.128) ^ capI) *
((eta - 0.727) ^ capJ)
Next I
Sheets("Input").Cells(w, 21).Value = 1 / (rhs *
0.0028)
End If
If hboundrey <= h Then
state = "SCR"
Sheets("Input").Cells(w, 11).Value = state
region = "3b"
Sheets("Input").Cells(w, 14).Value = region
pip3b = P / 100
eta = h / 2800
rhs = 0
For I = 1 To 33
capI = Sheets("CoefR3").Cells(I, 8).Value
capJ = Sheets("CoefR3").Cells(I, 9).Value
smalln = Sheets("CoefR3").Cells(I, 10).Value
rhs = rhs + smalln * ((pip3b + 0.298) ^ capI) *
((eta - 0.72) ^ capJ)
Next I
Sheets("Input").Cells(w, 3).Value = rhs * 860
```

```
Sheets("Input").Cells(w, 15).Value = (rhs *
860) - 273.15
pip3vb = P / 100
eta = h / 2800
rhs = 0
For I = 1 To 30
capI = Sheets("CoefR3").Cells(I, 16).Value
capJ = Sheets("CoefR3").Cells(I, 17).Value
smalln = Sheets("CoefR3").Cells(I, 18).Value
rhs = rhs + smalln * ((pip3vb + 0.0661) ^
capI) * ((eta - 0.72) ^ capJ)
Next I
Sheets("Input").Cells(w, 21).Value = 1 / (rhs *
0.0088)
End If
rho = Sheets("Input").Cells(w, 21).Value
T = Sheets("Input").Cells(w, 3).Value
capR = 0.461526
incT = T + 0.0000001
tau = 647.096 / T
pipf = rho / 322
pipfinc = (rho + 0.00000001) / 322
tauincT = 647.096 / incT
rhs1 = Sheets("CoefR3").Cells(35, 4).Value *
Log(pipf)
rhs12 = Sheets("CoefR3").Cells(35, 4).Value
* Log(pipfinc)
rhs13 = Sheets("CoefR3").Cells(35, 4).Value
* Log(pipf)
For I = 36 To 74
capI = Sheets("CoefR3").Cells(I, 2).Value
capJ = Sheets("CoefR3").Cells(I, 3).Value
smalno = Sheets("CoefR3").Cells(I, 4).Value
rhs1 = rhs1 + smalno * (pipf ^ capI) * (tau ^
capJ)
rhs12 = rhs12 + smalno * (pipfinc ^ capI) *
(tau ^ capJ)
rhs13 = rhs13 + smalno * (pipf ^ capI) *
(tauincT ^ capJ)
```

```
Next I
Helm = capR * T * rhs1
HelmincT = capR * incT * rhs13
HelmincP = capR * T * rhs12
entropy = (Helm - HelmincT) / 0.0000001
Sheets("Input").Cells(w, 20).Value = entropy
T1 = T - 273.15
5
```

'Transport properties
'Prandel Number
'Compressed liquid

```
If state = "CL" Then
row_min = 145
col_min = 2
row_max = 170
col_max = 11
For ii = row_min To row_max
    If Sheets("VCP").Cells(ii, 1) = P Then
        rowequal = 1
        I2 = ii
        ii = row_max
    ElseIf Sheets("VCP").Cells(ii, 1) > P And ii
<> row_min Then
        rowgreat = 1
        I2 = ii
        ii = row_max
    End If
Next ii
    For jj = col_min To col_max
    If Sheets("VCP").Cells(142, jj) = T1 Then
        colequal = 1
        j = jj
        jj = col_max
    ElseIf Sheets("VCP").Cells(142, jj) > T1
Then
        colgreat = 1
        j = jj
        jj = col_max
```

```
        End If
    Next jj
    Z_33 = Sheets("VCP").Cells(I2, j - 1)
    prandel = Z_33
    Sheets("Input").Cells(w, 17) = prandel
    End If
```

'Superheated

```
If state = ("SUPV") Or state = ("SCR") Then
row_min = 54
col_min = 2
row_max = 79
col_max = 19
For ii = row_min To row_max
    If Sheets("VCP").Cells(ii, 1) = P Then
        rowequal = 1
        I3 = ii
        ii = row_max
    ElseIf Sheets("VCP").Cells(ii, 1) > P And ii
<> row_min Then
        rowgreat = 1
        I3 = ii
        ii = row_max
    End If
Next ii
  For jj = col_min To col_max
    If Sheets("VCP").Cells(51, jj) = T1 Then
        colequal = 1
        j = jj
        jj = col_max
    ElseIf Sheets("VCP").Cells(51, jj) > T1
Then
        colgreat = 1
        j = jj
        jj = col_max
    End If
Next jj
l = Sheets("VCP").Cells(I3, 1)
If l = P Then
Z_33 = Sheets("VCP").Cells(I3, j)
```

```
prandel = Z_33
Sheets("Input").Cells(w, 17) = prandel
ElseIf P = 0.1 Then
Z_33 = Sheets("VCP").Cells(I3, j)
prandel = Z_33
Sheets("Input").Cells(w, 17) = prandel
Else
Z_33 = Sheets("VCP").Cells(I3 - 1, j)
prandel = Z_33
Sheets("Input").Cells(w, 17) = prandel
End If
End If
```

'Saturation

```
If state = "SATM" Then
row_min1 = 1
row_max1 = 48
For ii1 = row_min1 To row_max1
    If Sheets("VCP").Cells(ii1, 1) = T1 Then
        rowequal = 1
        I1 = ii1
        ii1 = row_max1
    ElseIf Sheets("VCP").Cells(ii1, 1) > T1
And ii1 <> row_min1 Then
        rowgreat1 = 1
        I1 = ii1
        ii1 = row_max1
    End If
Next ii1
X = Sheets("INPUT").Cells(w, 12)
PRF = Sheets("VCP").Cells(I1, 6)
PRG = Sheets("VCP").Cells(I1, 7)
If X = 0 Then
PR1 = PRF
ElseIf X = 1 Then
PR1 = PRG
ElseIf T < 170 Then
PR1 = PRG
Else
PR1 = X * (PRG - PRF) + PRF
```

202

```
End If
Sheets("Input").Cells(w, 17) = PR1
End If
```

'Thermal conductivity

```
'For G = 2 To 18
'T = Sheets("Input").Cells(G, 15)
'p = Sheets("Input").Cells(G, 1)
'state = Sheets("Input").Cells(G, 11)
```

'Compressed liquid

```
If state = "CL" Then
row_min = 84
col_min = 2
row_max = 109
col_max = 11
For ii = row_min To row_max
    If Sheets("VCP").Cells(ii, 1) = P Then
        rowequal = 1
        I4 = ii
        ii = row_max
    ElseIf Sheets("VCP").Cells(ii, 1) > P And ii
<> row_min Then
        rowgreat = 1
        I4 = ii
        ii = row_max
    End If
Next ii
For jj = col_min To col_max
    If Sheets("VCP").Cells(81, jj) = T1 Then
        colequal = 1
        j = jj
        jj = col_max
    ElseIf Sheets("VCP").Cells(81, jj) > T1
Then
        colgreat = 1
        j = jj
        jj = col_max
    End If
Next jj
```

```
Z_33 = Sheets("VCP").Cells(I4, j - 1)
TC = Z_33
Sheets("Input").Cells(w, 18) = TC
End If
```

'Superheated

```
If state = ("SUPV") Or state = ("SCR") Then
row_min = 179
col_min = 2
row_max = 204
col_max = 19
For ii = row_min To row_max
    If Sheets("VCP").Cells(ii, 1) = P Then
        rowequal = 1
        I6 = ii
        ii = row_max
    ElseIf Sheets("VCP").Cells(ii, 1) > P And ii
<> row_min Then
        rowgreat = 1
        I6 = ii
        ii = row_max
    End If
Next ii
    For jj = col_min To col_max
    If Sheets("VCP").Cells(176, jj) = T1 Then
        colequal = 1
        j = jj
        jj = col_max
    ElseIf Sheets("VCP").Cells(176, jj) > T1
Then
        colgreat = 1
        j = jj
        jj = col_max
    End If
Next jj
    l = Sheets("VCP").Cells(I6, 1)
If l = P Then
    Z_33 = Sheets("VCP").Cells(I6, j)
    TC = Z_33
Sheets("Input").Cells(w, 18) = TC
```

```
ElseIf P = 0.1 Then
Z_33 = Sheets("VCP").Cells(I6, j)
TC = Z_33
Sheets("Input").Cells(w, 18) = TC
Else
Z_33 = Sheets("VCP").Cells(I6 - 1, j)
TC = Z_33
Sheets("Input").Cells(w, 18) = TC
End If
End If
```

'Saturation

```
If state = "SATM" Then
row_min1 = 1
row_max1 = 48
For ii1 = row_min1 To row_max1
   If Sheets("VCP").Cells(ii1, 1) = T1 Then
      rowequal = 1
      I7 = ii1
      ii1 = row_max1
   ElseIf Sheets("VCP").Cells(ii1, 1) > T1
And ii1 <> row_min1 Then
      rowgreat1 = 1
      I7 = ii1
      ii1 = row_max1
   End If
Next ii1


X = Sheets("INPUT").Cells(w, 12)
TCF = Sheets("VCP").Cells(I7, 4)
TCG = Sheets("VCP").Cells(I7, 5)
If X = 0 Then
TC1 = TCF
ElseIf X = 1 Then
TC = TCG
Else
TC1 = 1 / (X * (1 / (TCG) - (1 /
TCF)) + (1 /
TCF))
End If
Sheets("Input").Cells(w, 18) = TC1
```

```
End If
```

'Viscosity

```
'For M = 2 To 18
'T = Sheets("Input").Cells(M, 15)
'p = Sheets("Input").Cells(M, 1)
'state = Sheets("Input").Cells(M, 11)
```

'Compressed liquid

```
If state = "CL" Then
row_min = 114
col_min = 2
row_max = 139
col_max = 11
For ii = row_min To row_max
   If Sheets("VCP").Cells(ii, 1) = P Then
      rowequal = 1
      I8 = ii
      ii = row_max
   ElseIf Sheets("VCP").Cells(ii, 1) > P And ii
<> row_min Then
      rowgreat = 1
      I8 = ii
      ii = row_max
   End If
Next ii
   For jj = col_min To col_max
   If Sheets("VCP").Cells(111, jj) = T1 Then
      colequal = 1
      j = jj
      jj = col_max
   ElseIf Sheets("VCP").Cells(111, jj) > T1
Then
      colgreat = 1
      j = jj
      jj = col_max
   End If
Next jj
Z_33 = Sheets("VCP").Cells(I8, j - 1)
V = Z_33
Sheets("Input").Cells(w, 19) = V
```

End If

'Superheated

If state = ("SUPV") Or state = ("SCR") Then

row_min = 214

col_min = 2

row_max = 239

col_max = 19

For ii = row_min To row_max

  If Sheets("VCP").Cells(ii, 1) = P Then

    rowequal = 1

    I9 = ii

    ii = row_max

  ElseIf Sheets("VCP").Cells(ii, 1) > P And ii <> row_min Then

    rowgreat = 1

    I9 = ii

    ii = row_max

  End If

Next ii

 For jj = col_min To col_max

  If Sheets("VCP").Cells(211, jj) = T1 Then

    colequal = 1

    j = jj

    jj = col_max

  ElseIf Sheets("VCP").Cells(211, jj) > T1 Then

    colgreat = 1

    j = jj

    jj = col_max

  End If

Next jj

l = Sheets("VCP").Cells(I9, 1)

If l = P Then

Z_33 = Sheets("VCP").Cells(I9, j)

V = Z_33

Sheets("Input").Cells(w, 19) = V

ElseIf P = 0.1 Then

Z_33 = Sheets("VCP").Cells(I9, j)

prandel = Z_33

Sheets("Input").Cells(w, 19) = V

Else

Z_33 = Sheets("VCP").Cells(I9 - 1, j)

V = Z_33

Sheets("Input").Cells(w, 19) = V

End If

End If

'Saturation

If state = "SATM" Then

row_min1 = 1

row_max1 = 48

For ii1 = row_min1 To row_max1

  If Sheets("VCP").Cells(ii1, 1) = T1 Then

    rowequal = 1

    I0 = ii1

    ii1 = row_max1

  ElseIf Sheets("VCP").Cells(ii1, 1) > T1 And ii1 <> row_min1 Then

    rowgreat1 = 1

    I0 = ii1

    ii1 = row_max1

  End If

Next ii1

X = Sheets("INPUT").Cells(w, 12)

VF = Sheets("VCP").Cells(I0, 2)

VG = Sheets("VCP").Cells(I0, 3)

If X = 0 Then

V1 = VF

ElseIf X = 1 Then

V1 = VG

Else

V1 = 1 / (X * (1 / (VG) - (1 / VF)) + (1 / VF))

Sheets("Input").Cells(w, 19) = V1

End If

End If

Return

End Sub

Visual Basic Application Code for stationary PV module with and without cooling system

```
Sub HITPVFIX()
Dim a(11) As Single
Dim YLAT As Double
Dim DTOR As Double
Dim IYR As Integer
Dim IMT As Integer
Dim IDY As Integer
Dim IHR As Single
Dim Iminut As Integer
Dim NTIMES As Integer
Dim titlestring As String
Dim Voltage(1000) As String
Dim Current (1000) As String
```

'Define the file name and path

```
I1 = 0
MyPath = CurDir
IName = MyPath + "\MetData.txt"
Open IName For Input As 100
```

'Title of the text file

```
Pi = 3.14159
DTOR = 3.14159 / 180 'conversion of degree
to radian
'latitude
LAT = Sheets ("inputdata").Cells (2,
36).Value
YLAT = LAT * DTOR ' lattitude in radiant
```

'Surface Tilt

```
TLT = Sheets("inputdata").Cells(3, 36).Value
```

'Aspect angle

```
 WAZ = Sheets("inputdata").Cells(4,
36).Value
```

'Logging time

```
NTIMES = Sheets("inputdata").Cells(5,
36).Value
```

'Reflectivity

```
Rho = Sheets("inputdata").Cells(6, 36).Value
```

'Longitude standard time meridian

```
LSM = Sheets("inputdata").Cells(7, 36). Input
#100, titlestring 'End of File EOF
Do Until EOF(100)
Input #100, a(1), a(2), a(3), a(4), a(5), a(6),
a(7), a(8), a(9), a(10)

IYR = a(1) 'year
IMT = a(2)  'month
IDY = a(3)  'day
IHR = a(4)  'hour
Iminut = a(5)   'minute
GRAD = a(6) 'Global radiation
DRAD = a(7) 'diffuse radiation
dbt = a(8) 'Dry bulb temperature
xWBT = a(9) 'wet bulb temperature
vwind = a(10) 'wind speed

GoSub 101
```

'Output data

```
    I1 = I1 + 1
```

'Year

```
Sheets("Hourlyoutput").Cells(I1 + 1, 1).Value
= a(1)
```

'Month

```
Sheets("Hourlyoutput").Cells(I1 + 1, 2).Value
= a(2)
```

'Day

```
Sheets("Hourlyoutput").Cells(I1 + 1, 3).Value
= a(3)
```
'Hour
```
Sheets("Hourlyoutput").Cells(I1 + 1, 4).Value
= a(4)
```
'Minute
```
Sheets("Hourlyoutput").Cells(I1 + 1, 5).Value
= a(5)
```
'Global radiation
```
Sheets("Hourlyoutput").Cells(I1 + 1, 6).Value
= a(6)
```
'Diffuse radiation
```
Sheets("Hourlyoutput").Cells(I1 + 1, 7).Value
= a(7)
```

'Slop irradiance
```
Sheets("Hourlyoutput").Cells(I1 + 1, 8).Value
= Int(sir)
```
'Dry bulb temperature
```
Sheets("Hourlyoutput").Cells(I1 + 1, 9).Value
= a(8)
```
'Wet bulb temperature
```
Sheets("Hourlyoutput").Cells(I1 + 1,
10).Value = a(9)
```
'Wind speed
```
Sheets("Hourlyoutput").Cells(I1 + 1,
11).Value = a(10)
```

'Manufacturing Data
```
Gref = Sheets("inputdata").Cells(10,
36).Value
Tref = Sheets("inputdata").Cells(11, 36).Value
Iscref = Sheets("inputdata").Cells(12,
36).Value
Vocref = Sheets("inputdata").Cells(13,
36).Value
Pmref = Sheets("inputdata").Cells(14,
36).Value
```

```
Imref = Sheets("inputdata").Cells(15,
36).Value
Vmref = Sheets("inputdata").Cells(16,
36).Value
IscCoeff = Sheets("inputdata").Cells(17,
36).Value
VCoeff = Sheets("inputdata").Cells(18,
36).Value
HITEfficiency = Sheets("inputdata").Cells(19,
36).Value
Am = Sheets("inputdata").Cells(20, 36).Value
GoSub 1000
```
'Dew point temperature
```
Sheets("Hourlyoutput").Cells(I1 + 1, 12) =
Int(DPT)
GoSub 2000
```
'Sky temperature
```
Sheets("Hourlyoutput").Cells(I1 + 1, 13) =
Int(Tsk)
```

```
GoSub 3000
```
'Cell temperature without cooling
```
Sheets("Hourlyoutput").Cells(I1 + 1,
14).Value = Tcnewc
```

```
GoSub 4000
```
'Max power without cooling
```
Sheets("Hourlyoutput").Cells(I1 + 1,
15).Value = Pmax
```
'Efficiency without cooling
```
Sheets("Hourlyoutput").Cells(I1 + 1,
16).Value = ModuleEfficiency * 100
```
'Filling factor
```
Sheets("Hourlyoutput").Cells(I1 + 1,
17).Value = FF
Sheets("Hourlyoutput").Cells(I1 + 1,
18).Value = Voltage(mjmax)
Sheets("Hourlyoutput").Cells(I1 + 1,
19).Value = Current(mjmax)
```

```vba
Sheets("Hourlyoutput").Cells(I1 + 1,
20).Value = Voc
Sheets("Hourlyoutput").Cells(I1 + 1,
21).Value = Isc


GoSub 5000
'Cell temperature with cooling jacket
Sheets("Hourlyoutput").Cells(I1 + 1, 22) =
Tcnewc1 Tcnewc = Tcnewc1


GoSub 4000
'Max power with cooling
Sheets("Hourlyoutput").Cells(I1 + 1,
23).Value = Pmax
'Efficiency with cooling
Sheets("Hourlyoutput").Cells(I1 + 1,
24).Value = ModuleEfficiency * 100
'Filling factor
Sheets("Hourlyoutput").Cells(I1 + 1,
25).Value = FF
Sheets("Hourlyoutput").Cells(I1 + 1,
26).Value = Voltage(mjmax)
Sheets("Hourlyoutput").Cells(I1 + 1,
27).Value = Current(mjmax)
Sheets("Hourlyoutput").Cells(I1 + 1,
28).Value = Voc
Sheets("Hourlyoutput").Cells(I1 + 1,
29).Value = Isc
Loop
Close #100
End
```

'Subroutine for slope radiation computations

```vba
101
Dim IDN As Double
Dim GR As Double
Dim KT As Double
Dim ILG As Double
Dim ILD As Double
Dim SOLAZM As Double
Dim xdum2 As Double
Dim En0 As Double
Dim EOT As Double
Dim ERAD As Double
Dim dec As Double
Dim solalt As Double


'Calculate EOT (Equation of time) and
DEC (Declination)
'Local civil time
    XLCT = IHR + Iminut / 60
'Universal time
    UT = XLCT + LSM / 15
    If IMT > 2 Then
    IYR1 = IYR
    IMT1 = IMT - 3
    Else
    IYR1 = IYR - 1
    IMT1 = IMT + 9 '
    End If
    INTT1 = Int(30.6 * IMT1 + 0.5)
    INTT2 = Int(365.25 * (IYR1 - 1976))
    SMLT = ((UT / 24) + IDY + INTT1 +
INTT2  - 8707.5) / 36525
    EPSILN = 23.4393 - 0.013 * SMLT
    CAPG = 357.528 + 35999.05 * SMLT
    If CAPG > 360 Then
    G360 = CAPG - Int(CAPG / 360) * 360
    Else
    G360 = CAPG
    End If
    CAPC = 1.915 * Sin(G360 * DTOR) +
0.02 * Sin(2 * G360 * DTOR)
    CAPL = 280.46 + 36000.77 * SMLT +
CAPC
    If CAPL > 360 Then
    XL360 = CAPL - Int(CAPL / 360) * 360
    Else
```

208

```
XL360 = CAPL
End If
ALPHA = XL360 - 2.466 * Sin(2 *
XL360 * DTOR) + 0.053 * Sin(4 * XL360 *
DTOR)
GHA = 15 * UT - 180 - CAPC + XL360 -
ALPHA
If GHA > 360 Then
GHA360 = GHA - Int(GHA / 360) * 360
Else
GHA360 = GHA
End If
EOT = (XL360 - CAPC - ALPHA) / 15
dec = Atn(Tan(EPSILN * DTOR) *
Sin(ALPHA * DTOR)) / DTOR
```

'Calculate Solar Hour Angle SHA
```
If (NTIMES = 2) Then
SHA = GHA360 - (ylong)
Else
SHA = 15 * (XLCT - 12)
End If
```

'Calculate Apparent Solar Time, hour
angle horang
```
If (NTIMES = 2) Then
ast = 12 + (SHA / 15)
Else
ast = XLCT
End If
horang = 15 * DTOR * Abs(12 - ast)
```

'Calculate Solar Altitude SOLALT
```
TRM111 = Sin(YLAT) * Sin(dec * DTOR)
TRM112 = Cos(YLAT) * Cos(dec *
DTOR) * Cos(horang)
TRM11 = TRM111 + TRM112
solalt = Application.Asin(TRM11) / DTOR
```

'Calculate Day Number DN

```
DN1 = (IDY + INTT1 + INTT2)
IMT9 = 1
IYR1 = IYR - 1
IMT1 = IMT9 + 9
INTT1 = Int(30.6 * IMT1 + 0.5)
INTT2 = Int(365.25 * (IYR1 - 1976))
DN2 = (INTT1 + INTT2)
IDN = DN1 - DN2
If IDN < 300 Then
d = IDN
Else
d = IDN - 366
End If
```

'Solar Azimuth SOLAZM
```
TRM12 = -Tan(LAT * DTOR) * Tan(dec *
DTOR)
hafday = (1 / 15) *
Application.Acos(TRM12) / DTOR
srt = 12 - hafday
sst = 12 + hafday
If ((ast - 1) = Int(srt)) Then
horang = 15 * DTOR * Abs(12 - 0.5 * (ast
+ srt))
End If
If ((ast - 1) = Int(sst)) Then
horang = 15 * DTOR * Abs(12 - 0.5 * (ast -
1 + sst))
End If

xdum2 = Cos(dec * DTOR) * (Cos(LAT *
DTOR) * Tan(dec * DTOR) - Sin(LAT *
DTOR) * Cos(horang)) / Cos(DTOR * solalt)
End If
SOLAZM = (Application.Acos(xdum2))
/ DTOR
If (ast > 12) Then
SOLAZM = 360 - SOLAZM
End If
```

'Solar inclination SOLINC
```
    xdum3 = Cos(solalt * DTOR) *
Cos((SOLAZM - WAZ) * DTOR) * Sin(TLT
* DTOR) + Sin(solalt * DTOR) * Cos(TLT *
DTOR)
    SOLINC = (Application.Acos(xdum3)) /
DTOR
```

'Calculate horizontal Extraterrestrial irradiance ERAD
```
    ERAD = 1367 * (1 + 0.033 *
Cos(0.0172024 * d)) * Sin(solalt * DTOR)
    En0 = ERAD
```

'Calculate slope beam, Beam solar radiation BSRAD
```
    If (solalt > 7) Then
    If (SOLINC < 90) Then
    BSRAD = (GRAD - DRAD) *
Cos(SOLINC * DTOR) / Sin(solalt * DTOR)
    Else
    BSRAD = 0
    End If
    Else
    BSRAD = 0
    End If
```

'Sky diffuse, diffuse solar radiation DSRAD, Diffuse radiation DRAD, clear fraction CLRFRA
```
 If (solalt <= 0) Then
    DSRAD = 0
    ElseIf (solalt > 0 And solalt <= 7) Then
    CLRFRA = (GRAD - DRAD) / ERAD
    DSRAD = DRAD * (Cos(TLT * DTOR /
2) ^ 2) * (1 + CLRFRA * Sin(TLT * DTOR /
2) ^ 3) * (1 + CLRFRA * (Cos(SOLINC *
DTOR) ^ 2) * Cos(solalt * DTOR) ^ 3)
    Else
    If (SOLINC >= 90) Then
```

```
    CAPB = 0.252
    CLRFRA = 0
    Else
    CLRFRA = (GRAD - DRAD) / ERAD
```
'The user may select the following model:
```
    CAPB = 0.04 - (0.82 * CLRFRA) - (2.026
* (CLRFRA ^ 2)) '0.00333 - 0.415 *
CLRFRA - 0.6987 * CLRFRA ^ 2
'    End of model for GLOBAL
    End If
        If ((GRAD - DRAD) < 6) Then
    CAPB = 0.168
    CLRFRA = 0
    End If
        TLTFAC = (Cos(TLT * DTOR / 2) ^
2) + CAPB * (Sin(TLT * DTOR) - (TLT *
DTOR) * Cos(TLT * DTOR) - Pi * Sin(TLT
* DTOR / 2) ^ 2)
        DSFAC = TLTFAC * (1 - CLRFRA) +
CLRFRA * Cos(SOLINC * DTOR) /
Sin(solalt * DTOR)
        DSRAD = DSFAC * DRAD
    End If
```
'Clearness index KT
```
    KT = GRAD / ERAD
```
 'Global index KG
```
    KG = 136.6 - 74.541 * KT + 57.3421 * KT
^ 2
```
'Diffuse index KD
```
    KD = 130.2 - 39.828 * KT + 49.9797 * KT
^ 2
```

'Global luminance ILG (page 114 of solar radiation book)
```
    ILG = (GRAD * KG) / 1000
```
'Diffuse luminance ILD
```
    ILD = (DRAD * KD) / 1000
```
' Below 0.2, KT is considered as fully covered then Global = diffuse luminance

If KT < 0.2 Then ILG = ILD

'Ground reflect GR

GR = Rho * GRAD * Sin(0.5 * TLT * Pi / 180) ^ 2

'Slope irradiation SIr

sir = BSRAD + DSRAD + GR

Return

1000

'PSYCHROMETRIC

'PROGRAM FOR PSYCHROMETRIC PROPERTIES - GIVEN DBT, WBT AND P-ATM

PATM = 101.325

TEMP = xWBT

TEMP = TEMP + 273.15

XPSAT = PSAT(TEMP)

'CALCULATE WA

WSSTAR = 0.62198 * (XPSAT / (PATM - XPSAT))

WA = ((2501 - 2.326 * xWBT) * WSSTAR - 1.006 * (dbt - xWBT)) / (2501 + 1.86 * dbt - 4.186 * xWBT)

If (dbt < 0) Then

WA = ((2830 - 0.24 * xWBT) * WSSTAR - 1.006 * (dbt - xWBT)) / (2830 + 1.86 * dbt - 2.1 * xWBT)

End If

'CALCULATE DPT

PW = (PATM * WA) / (0.62198 + WA)

ALPHA = Log(PW)

DPT = 6.54 + 14.526 * ALPHA + 0.7389 * ALPHA ^ 2 + 0.09486 * ALPHA ^ 3 + 0.4569 * (PW ^ 0.1984)

If (DPT < 0) Then

DPT = 6.09 + 12.608 * ALPHA + 0.4959 * ALPHA ^ 2

End If

'CALCULATE RH

TEMP = dbt + 273.15

XPSATD = PSAT(TEMP)

RH = PW / XPSATD

CALCULATE SPVOL AND HENTHL

SPVOL = (8.31434 / 28.9645) * TEMP * (1 + 1.6078 * WA) / PATM

HENTHL = 1.006 * dbt + WA * (2501 + 1.86 * dbt)

Return

2000

'SKYTEMP ()

taoalpha = 0.9 * 0.85

Tco = dbt + 10

Tcko = Tco + 273.15

Tak = dbt + 273.15

DPTK = DPT + 273.15

'Sky temperature calculation

GT = I * taoalpha * (1 - HITEfficiency)

SKYemissivity = 0.787 + (0.764 * Application.Ln(DPTK / 273))

Horizontal_IR = SKYemissivity * 0.000000056697 * (Tak ^ 4)

Tsk = (Horizontal_IR / 0.0000000567) ^ 0.25

Return

3000

'Cell temperature

'WITHOUT COOLING JACKET

taoalpha = 0.9 * 0.85

GT = sir * taoalpha * (1 - HITEfficiency)

Tco = dbt + 10

Tcko = Tco + 273.15

Tak = dbt + 273.15

```
20
'Thermal
hcs = (0.0000000567 * 0.88 * ((Tcko ^ 4) -
(Tsk ^ 4))) / (Tcko - Tsk)
hca = 2 * (5.7 + 3.8 * vwind)
Pc = GT + (hcs * Tsk) + (hca * Tak)
Pb = hcs + hca
Tcnew = Pc / Pb
difTc = Abs(Tcnew - Tcko)
If (difTc < 0.01) Then
Tcnewc = Tcnew - 273.15
Else
Tcko = Tcnew
GoTo 20
End If
Return
4000
```

'Power output and Efficiency

```
G = sir
T = Tcnewc
M = (Vocref / Iscref) * (-5.411 * ((Imref *
Vmref) / (Vocref * Iscref)) + 6.45 * (Vmref /
Vocref) + 3.417 * (Imref / Iscref) - 4.422)
Rsref = (-M * Iscref / Imref) + ((Vmref /
Imref) * (1 - (Iscref / Imref)))
Rs = Rsref
Aref = ((Vmref - Vocref + (Imref * Rs)) /
(Application.Ln(1 - (Imref / Iscref))))
I0ref = (Iscref * Exp(-Vocref / Aref))
dI = (IscCoeff * (G / Gref) * (T - Tref)) + (((G
- Gref) / Gref) * Iscref)

For n = 1 To 1000
Iref = Iscref - ((n - 1) * (Iscref / 1000))
Vref = Aref * Application.Ln((Iscref - Iref +
I0ref) / I0ref) - (Iref * Rsref)
V = Vref + VCoeff * (T - Tref) - Rsref * dI
I = Iref + dI
Voltage(n) = V
Current(n) = I
```

```
Next n

Pmax = Voltage(1) * Current(1)
mjmax = 1
For nj = 2 To 1000
If (Pmax < Voltage(nj) * Current(nj)) Then
Pmax = Voltage(nj) * Current(nj)
mjmax = nj
End If
Next nj
```

'Now, looking up Isc : using interpolation

```
If Voltage(1) > 0 Then
    y9 = (Current(2) - Current(1)) / (Voltage(2)
- Voltage(1))
    Isc = Current(2) - y9 * Voltage(2)
    GoTo 1
End If
For n = 1 To 999 ' (we really do not need to go
all the way to 998 or 1000 since Isc will
' definitely be in the first few rows anyways
If Voltage(n) < 0 Then
    y1 = Voltage(n)
    y2 = Voltage(n + 1)
    y3 = Current(n)
    y4 = Current(n + 1)
    y5 = (0 - y1) / (y2 - y1)
    y6 = y5 * (y4 - y3)
    Isc = y3 + y6
End If
Next n
```

'Interpolate for Isc (the difference between
y3 and y4 is very small so you can actually
```
' take y3 or y4 as the Isc with minimal error)
1
If Current(1000) > 0 Then
    y71 = (Current(1000) - Current(999)) /
(Voltage(1000) - Voltage(999))
```

```
y81 = Current(1000) - (y71 *                    Kf = 0.606
(Voltage(1000)))                                Tw = wbt + 5
   Voc = -y81 / y71                             Tak = dbt + 273.15
   GoTo 2                                       Twk = Tw + 273.15
End If                                          vwind = a(10)
For xx = 1 To 999                               123
If Current(xx) < 0 Then                         hcs1 = (0.0000000567 * 0.88 * ((Tcko ^ 4) -
   y11 = Voltage(xx - 1)                        (Tsk ^ 4))) / (Tcko - Tsk)
   y21 = Voltage(xx)                            hca1 = 5.7 + 3.8 * vwind
   y31 = Current(xx - 1)                        Apcs = sa * sb
   y41 = Current(xx)                            Vwater = mw / (PW * Apcs)
   y51 = (0 - y31) / (y41 - y31)                De = (4 * sa * sb) / (2 * (sa + sb))
   y61 = y51 * (y21 - y11)                      Red = (Vwater * De) / um
   Voc = y11 + y61                              Le1 = De * 0.0565 * Red
   GoTo 2                                       Nu1 = 1.86 * ((Red * Pr) / (Le1 / De)) ^
End If                                          (0.33333)
Next                                            hcw1 = (Nu1 * Kf) / De
2                                               Le2 = 1.319 - Le1
FF = (Pmax / (Isc * Voc))                       Nu2 = 3.66
ModuleEfficiency = Pmax / (sir * Am)            hcw2 = (Nu2 * Kf) / De
Return                                          hcwt = (hcw1 * Le1) + (hcw2 * Le2) / (Le1 +
                                                Le2)
5000                                            Pc = GT + (hcs1 * Tsk) + (hca1 * Tak) +
'Cell temperature ()                            (hcwt * Twk)
'WITH COOLING JACKET                            Pb = hcs1 + hca1 + hcwt
                                                Tcnew1 = Pc / Pb
taoalpha = 0.9 * 0.85                           difTc1 = Abs(Tcnew1 - Tcko)
GT = sir * taoalpha * (1 - HITEfficiency)       If difTc1 < 0.01 Then
Tco = dbt + 10                                  Tcnewc1 = Tcnew1 - 273.15
Tcko = Tco + 273.15                             Else
wbt = a(9)                                      Tcko = Tcnew1
mw = 0.1                                        GoTo 123
sa = 0.88                                       End If
sb = 0.019                                      Return
um = 0.0000009781                               End
PW = 980.39                                     End Sub
Pr = 6.62
```

Appendix-D

Visual Basic Application Code for tracking PV module without cooling system

```vba
Sub HITPVtracking()
Dim a(11) As Single
Dim YLAT As Double
Dim DTOR As Double
Dim IYR As Integer
Dim IMT As Integer
Dim IDY As Integer
Dim IHR As Single
Dim Iminut As Integer
Dim NTIMES As Integer
Dim titlestring As String
Dim Voltage(1000) As String
Dim Current(1000) As String
' Define the file name and path
I1 = 0
MyPath = CurDir
IName = MyPath + "\MetData.txt"
Open IName For Input As 100
Pi = 3.14159
'Conversion of degree to radian
DTOR = 3.14159 / 180
'Latitude
LAT = Sheets("inputdata").Cells(2, 36).Value
YLAT = LAT * DTOR ' lattitude in radiant
'Aspect angle
WAZ = Sheets("inputdata").Cells(4, 36).Value
'Logging time
NTIMES = Sheets("inputdata").Cells(5, 36).Value
'Reflectivity
Rho = Sheets("inputdata").Cells(6, 36).Value

' Longitude standard time meridian
LSM = Sheets("inputdata").Cells(7, 36).Value

Input #100, titlestring 'End of File EOF
Do Until EOF(100)
Input #100, a(1), a(2), a(3), a(4), a(5), a(6), a(7), a(8), a(9), a(10)
IYR = a(1) 'year
IMT = a(2)  'month
IDY = a(3)  'day
IHR = a(4)  'hour
Iminut = a(5)   'minute
GRAD = a(6) 'Global radiation
DRAD = a(7) 'diffuse radiation
dbt = a(8) 'Dry bulb temperature
xWBT = a(9) 'wet bulb temperature
vwind = a(10) 'wind speed
GoSub 101
'Output data
    I1 = I1 + 1
'Year
Sheets("Hourlyoutput").Cells(I1 + 1, 1).Value = a(1)
'Month
Sheets("Hourlyoutput").Cells(I1 + 1, 2).Value = a(2)
'Day
Sheets("Hourlyoutput").Cells(I1 + 1, 3).Value = a(3)
'Hour
Sheets("Hourlyoutput").Cells(I1 + 1, 4).Value = a(4)
```

```vba
'Minute
Sheets("Hourlyoutput").Cells(I1 + 1, 5).Value = a(5)
 'Global radiation
Sheets("Hourlyoutput").Cells(I1 + 1, 6).Value = a(6)
'Diffuse radiation
Sheets("Hourlyoutput").Cells(I1 + 1, 7).Value = a(7)
'Slop irradiance
Sheets("Hourlyoutput").Cells(I1 + 1, 8).Value = Int(SIR)
Sheets("Hourlyoutput").Cells(I1 + 1, 29).Value = SOLAZM
Sheets("Hourlyoutput").Cells(I1 + 1, 30).Value = TLT
Sheets("Hourlyoutput").Cells(I1 + 1, 31).Value = SOLINC
Sheets("Hourlyoutput").Cells(I1 + 1, 32).Value = solalt
'Dry bulb temperature
Sheets("Hourlyoutput").Cells(I1 + 1, 9).Value = a(8)
 'Wet bulb temperature
Sheets("Hourlyoutput").Cells(I1 + 1, 10).Value = a(9)
'Wind speed
Sheets("Hourlyoutput").Cells(I1 + 1, 11).Value = a(10)
'Format for single digit output
Sheets("Hourlyoutput").Cells(I1 + 1, 11).Select
Selection.NumberFormat = "0.0"
Gref = Sheets("inputdata").Cells(10, 36).Value
Tref = Sheets("inputdata").Cells(11, 36).Value
Iscref = Sheets("inputdata").Cells(12, 36).Value
Vocref = Sheets("inputdata").Cells(13, 36).Value
Pmref = Sheets("inputdata").Cells(14, 36).Value
Imref = Sheets("inputdata").Cells(15, 36).Value
Vmref = Sheets("inputdata").Cells(16, 36).Value
IscCoeff = Sheets("inputdata").Cells(17, 36).Value
VCoeff = Sheets("inputdata").Cells(18, 36).Value
HITEfficiency = Sheets("inputdata").Cells(19, 36).Value
Am = Sheets("inputdata").Cells(20, 36).Value
GoSub 1000
Sheets("Hourlyoutput").Cells(I1 + 1, 12) = Int(DPT) 'Dew point temperature
GoSub 2000
Sheets("Hourlyoutput").Cells(I1 + 1, 13) = Int(Tsk) 'Sky temperature
GoSub 3000
Sheets("Hourlyoutput").Cells(I1 + 1, 14).Value = Tcnewc 'Cell temperature without cooling
Sheets("Hourlyoutput").Cells(I1 + 1, 14).Select
Selection.NumberFormat = "0.0"
GoSub 4000
'Max power without cooling
Sheets("Hourlyoutput").Cells(I1 + 1, 15).Value = PMAX
Sheets("Hourlyoutput").Cells(I1 + 1, 15).Select
Selection.NumberFormat = "0.0"
'Efficiency without
Sheets("Hourlyoutput").Cells(I1 + 1, 16).Value = ModuleEfficiency * 100 cooling
```

```
Sheets("Hourlyoutput").Cells(I1 + 1,
16).Select
Selection.NumberFormat = "0.0"
Sheets("Hourlyoutput").Cells(I1 + 1,
17).Value = FF
Sheets("Hourlyoutput").Cells(I1 + 1,
17).Select
Selection.NumberFormat = "0.00"
Sheets("Hourlyoutput").Cells(I1 + 1,
18).Value = Voltage(mjmax)
Sheets("Hourlyoutput").Cells(I1 + 1,
18).Select
Selection.NumberFormat = "0.0"
Sheets("Hourlyoutput").Cells(I1 + 1,
19).Value = Current(mjmax)
Sheets("Hourlyoutput").Cells(I1 + 1,
19).Select
Selection.NumberFormat = "0.0"
Sheets("Hourlyoutput").Cells(I1 + 1,
20).Value = Voc
Sheets("Hourlyoutput").Cells(I1 + 1,
20).Select
Selection.NumberFormat = "0.0"
Sheets("Hourlyoutput").Cells(I1 + 1,
21).Value = Isc
Sheets("Hourlyoutput").Cells(I1 + 1,
21).Select
Selection.NumberFormat = "0.0"
Loop
Close #100
End
```

'Subroutine for slope radiation computations

```
101
Dim IDN As Double
Dim GR As Double
Dim KT As Double
Dim ILG As Double
Dim ILD As Double
```

```
Dim xdum2 As Double
Dim En0 As Double
Dim EOT As Double
Dim ERAD As Double
Dim dec As Double
Dim diff(91) As Single
    Pi = 3.14159
    DTOR = 3.14159 / 180 'converstion of
degree to radian
```

'Calculate EOT (Equation of time) and DEC (Declination)

```
    XLCT = IHR + Iminut / 60 'local civil
time
    UT = XLCT + LSM / 15 'universal time
    If IMT > 2 Then
    IYR1 = IYR
    IMT1 = IMT - 3
    Else
    IYR1 = IYR - 1
    IMT1 = IMT + 9 '
    End If
    INTT1 = Int(30.6 * IMT1 + 0.5)
    INTT2 = Int(365.25 * (IYR1 - 1976))
    SMLT = ((UT / 24) + IDY + INTT1 +
INTT2 -8707.5) / 36525
    EPSILN = 23.4393 - 0.013 * SMLT
    CAPG = 357.528 + 35999.05 * SMLT
    If CAPG > 360 Then
    G360 = CAPG - Int(CAPG / 360) * 360
    Else
    G360 = CAPG
    End If
    CAPC = 1.915 * Sin(G360 * DTOR) +
0.02 * Sin(2 * G360 * DTOR)
    CAPL = 280.46 + 36000.77 * SMLT +
CAPC
    If CAPL > 360 Then
    XL360 = CAPL - Int(CAPL / 360) * 360
    Else
```

216

```
XL360 = CAPL
End If
ALPHA = XL360 - 2.466 * Sin(2 *
XL360 * DTOR) + 0.053 * Sin(4 * XL360 *
DTOR)
GHA = 15 * UT - 180 - CAPC + XL360 -
ALPHA
If GHA > 360 Then
GHA360 = GHA - Int(GHA / 360) * 360
Else
GHA360 = GHA
End If
EOT = (XL360 - CAPC - ALPHA) / 15
dec = Atn(Tan(EPSILN * DTOR) *
Sin(ALPHA * DTOR)) / DTOR
```

'Calculate Solar Hour Angle SHA

```
If (NTIMES = 2) Then
SHA = GHA360 - (ylong)
Else
SHA = 15 * (XLCT - 12)
End If
```

'Calculate Apparent Solar Time,
hour angle horang

```
If (NTIMES = 2) Then
ast = 12 + (SHA / 15)
Else
ast = XLCT
End If
horang = 15 * DTOR * Abs(12 - ast)
```

'Calculate Solar Altitude
SOLALT

```
TRM111 = Sin(YLAT) * Sin(dec * DTOR)
TRM112 = Cos(YLAT) * Cos(dec *
DTOR) * Cos(horang)
TRM11 = TRM111 + TRM112
solalt = Application.Asin(TRM11) / DTOR
```

'Calculate Day Number DN

```
DN1 = (IDY + INTT1 + INTT2)
```

```
IMT9 = 1
IYR1 = IYR - 1
IMT1 = IMT9 + 9
INTT1 = Int(30.6 * IMT1 + 0.5)
INTT2 = Int(365.25 * (IYR1 - 1976))
DN2 = (INTT1 + INTT2)
IDN = DN1 - DN2
If IDN < 300 Then
d = IDN
Else
d = IDN - 366
End If
```

'Solar Azimuth SOLAZM

```
TRM12 = -Tan(LAT * DTOR) * Tan(dec *
DTOR)
hafday = (1 / 15) *
Application.Acos(TRM12) / DTOR
srt = 12 - hafday
sst = 12 + hafday
If ((ast - 1) = Int(srt)) Then
horang = 15 * DTOR * Abs(12 - 0.5 * (ast
+ srt))
End If
If ((ast - 1) = Int(sst)) Then
horang = 15 * DTOR * Abs(12 - 0.5 * (ast -
1 + sst))
End If
xdum2 = Cos(dec * DTOR) * (Cos(LAT
* DTOR) * Tan(dec * DTOR) - Sin(LAT *
DTOR) * Cos(horang)) / Cos(DTOR * solalt)
If (xdum2 <= -1) Then
xdum2 = -0.99999999
End If
SOLAZM = (Application.Acos(xdum2))
/ DTOR
If (ast > 12) Then
SOLAZM = 360 - SOLAZM
End If
```

'Solar inclination SOLINC

TLT = 90 - solalt

WAZ = SOLAZM

xdum3 = Cos(solalt * DTOR) * Cos((SOLAZM - WAZ) * DTOR) * Sin(TLT * DTOR) + Sin(solalt * DTOR) * Cos(TLT * DTOR)

SOLINC = (Application.Acos(xdum3)) / DTOR

'Calculate horizontal Extraterrestrial irradiance ERAD

ERAD = 1367 * (1 + 0.033 * Cos(0.0172024 * d)) * Sin(solalt * DTOR)

En0 = ERAD

'Calculate slope beam, Beam solar radiation BSRAD

If (solalt > 10) Then

If (SOLINC < 90) Then

BSRAD = (GRAD - DRAD) * (Cos(SOLINC * DTOR) / Sin(solalt * DTOR))

Else

BSRAD = 0

End If

'Sky diffuse, diffuse solar radiation DSRAD, Diffuse radiation DRAD, clear fraction CLRFRA

If (solalt <= 0) Then

DSRAD = 0

ElseIf (solalt > 0 And solalt <= 7) Then

CLRFRA = (GRAD - DRAD) / ERAD

DSRAD = DRAD * (Cos(TLT * DTOR / 2) ^ 2) * (1 + CLRFRA * Sin(TLT * DTOR / 2) ^ 3) * (1 + CLRFRA * (Cos(SOLINC * DTOR) ^ 2) * Cos(solalt * DTOR) ^ 3)

Else

If (SOLINC >= 90) Then

CAPB = 0.252

CLRFRA = 0

Else

'Model for the Globe

CLRFRA = (GRAD - DRAD) / ERAD

CAPB = ((0.04) - (0.82 * CLRFRA) - ((2.026) * CLRFRA ^ 2))

'End of model for the Globe

End If

If ((GRAD - DRAD) < 6) Then

CAPB = 0.168

CLRFRA = 0

End If

TLTFAC = (Cos(TLT * DTOR / 2) ^ 2) + CAPB * (Sin(TLT * DTOR) - (TLT * DTOR) * Cos(TLT * DTOR) - Pi * Sin(TLT * DTOR / 2) ^ 2)

DSFAC = TLTFAC * (1 - CLRFRA) + CLRFRA * Cos(SOLINC * DTOR) / Sin(solalt * DTOR)

DSRAD = DSFAC * DRAD

End If

'Clearness index KT

KT = GRAD / ERAD

'Global index KG

KG = 136.6 - 74.541 * KT + 57.3421 * KT ^ 2

'Diffuse index KD

KD = 130.2 - 39.828 * KT + 49.9797 * KT ^ 2

'Global luminance ILG (page 114 of solar radiation book)

ILG = (GRAD * KG) / 1000

'Diffuse luminance ILD

ILD = (DRAD * KD) / 1000

'Below 0.2, KT is considered as fully covered then Global = diffuse luminance

If KT < 0.2 Then ILG = ILD

'Ground reflect GR

GR = Rho * GRAD * Sin(0.5 * TLT * Pi / 180) ^ 2

'Slope irradiation SIr

SIR = BSRAD + DSRAD + GR

'If (IYR = 1989) And (IMT = 10) Then

'If IDY = 7 And IHR = 16 Then

'Stop

'End If

'End If

Else

SIR = 0

End If

If SIR = 0 Then

'Max power without cooling

PMAX = 0

'Efficiency without cooling

FF = 0

Voltage(mjmax) = 0

Current(mjmax) = 0

Voc = 0

Isc = 0

ModuleEfficiency = 0

TLT = 0

Else

End If

Return

1000

'PROGRAM FOR PSYCHROMETRIC PROPERTIES - GIVEN DBT, WBT AND P-ATM

PATM = 101.325

TEMP = xWBT

TEMP = TEMP + 273.15

XPSAT = PSAT(TEMP)

'CALCULATE WA

WSSTAR = 0.62198 * (XPSAT / (PATM - XPSAT))

WA = ((2501 - 2.326 * xWBT) * WSSTAR - 1.006 * (dbt - xWBT)) / (2501 + 1.86 * dbt - 4.186 * xWBT)

If (dbt < 0) Then

WA = ((2830 - 0.24 * xWBT) * WSSTAR - 1.006 * (dbt - xWBT)) / (2830 + 1.86 * dbt - 2.1 * xWBT)

End If

'CALCULATE DPT

PW = (PATM * WA) / (0.62198 + WA)

ALPHA = Log(PW)

DPT = 6.54 + 14.526 * ALPHA + 0.7389 * ALPHA ^ 2 + 0.09486 * ALPHA ^ 3 + 0.4569 * (PW ^ 0.1984)

If (DPT < 0) Then

DPT = 6.09 + 12.608 * ALPHA + 0.4959 * ALPHA ^ 2

End If

'CALCULATE RH

TEMP = dbt + 273.15

XPSATD = PSAT(TEMP)

RH = PW / XPSATD

'CALCULATE SPVOL AND HENTHL

SPVOL = (8.31434 / 28.9645) * TEMP * (1 + 1.6078 * WA) / PATM

HENTHL = 1.006 * dbt + WA * (2501 + 1.86 * dbt)

Return

2000

'SKYTEMP()

taoalpha = 0.9 * 0.85

Tco = dbt + 10

Tcko = Tco + 273.15

Tak = dbt + 273.15

DPTK = DPT + 273.15

'Sky temperature calculation

GT = I * taoalpha * (1 - HITEfficiency)

SKYemissivity = 0.787 + (0.764 *

Application.Ln(DPTK / 273))

Horizontal_IR = SKYemissivity *

0.000000056697 * (Tak ^ 4)

Tsk = (Horizontal_IR / 0.0000000567) ^ 0.25

Return

3000

'TCELL1 ()

'WITHOUT COOLING JACKET

taoalpha = 0.9 * 0.85

GT = SIR * taoalpha * (1 - HITEfficiency)

Tco = dbt + 10

Tcko = Tco + 273.15

Tak = dbt + 273.15

20

'Thermal

hcs = (0.0000000567 * 0.88 * ((Tcko ^ 4) -

(Tsk ^ 4))) / (Tcko - Tsk)

hca = 2 * (5.7 + 3.8 * vwind)

Pc = GT + (hcs * Tsk) + (hca * Tak)

Pb = hcs + hca

Tcnew = Pc / Pb

difTc = Abs(Tcnew - Tcko)

If (difTc < 0.01) Then

Tcnewc = Tcnew - 273.15

Else

'HITEfficiency = ModuleEfficiency

Tcko = Tcnew

GoTo 20

End If

Return

4000

'POWEREFFICIENCY1()

If SIR = 0 Then

PMAX = 0 'Max power without cooling

FF = 0 'Efficiency without cooling

Voltage(mjmax) = 0

Current(mjmax) = 0

Voc = 0

Isc = 0

ModuleEfficiency = 0

TLT = 0

GoTo 123456

Else

End If

G = SIR

T = Tcnewc

M = (Vocref / Iscref) * (-5.411 * ((Imref *

Vmref) / (Vocref * Iscref)) + 6.45 * (Vmref /

Vocref) + 3.417 * (Imref / Iscref) - 4.422)

Rsref = (-M * Iscref / Imref) + ((Vmref /

Imref) * (1 - (Iscref / Imref)))

Rs = Rsref

Aref = ((Vmref - Vocref + (Imref * Rs)) /

(Application.Ln(1 - (Imref / Iscref))))

I0ref = (Iscref * Exp(-Vocref / Aref))

dI = (IscCoeff * (G / Gref) * (T - Tref)) + (((G

- Gref) / Gref) * Iscref)

For n = 1 To 1000

Iref = Iscref - ((n - 1) * (Iscref / 1000))

Vref = Aref * Application.Ln((Iscref - Iref +

I0ref) / I0ref) - (Iref * Rsref)

V = Vref + VCoeff * (T - Tref) - Rsref * dI

I = Iref + dI

Voltage(n) = V

Current(n) = I

Next n

PMAX = Voltage(1) * Current(1)

mjmax = 1

For nj = 2 To 1000

If (PMAX < Voltage(nj) * Current(nj)) Then

PMAX = Voltage(nj) * Current(nj)

mjmax = nj

End If

Next nj

'Now, looking up Isc from column 2 in Sheet 2: using interpolation

```
If Voltage(1) > 0 Then
    y9 = (Current(2) - Current(1)) / (Voltage(2) - Voltage(1))
    Isc = Current(2) - y9 * Voltage(2)
    GoTo 1
End If
For n = 1 To 999 ' (we really do not need to go all the way to 998 or 1000 since Isc will
' definitely be in the first few rows anyways
If Voltage(n) < 0 Then
    y1 = Voltage(n)
    y2 = Voltage(n + 1)
    y3 = Current(n)
    y4 = Current(n + 1)
    y5 = (0 - y1) / (y2 - y1)
    y6 = y5 * (y4 - y3)
    Isc = y3 + y6
End If
Next n
' Interpolate for Isc (the difference between y3 and y4 is very small so you can actually
' take y3 or y4 as the Isc with minimal error)
1
If Current(1000) > 0 Then
    y71 = (Current(1000) - Current(999)) / (Voltage(1000) - Voltage(999))
    y81 = Current(1000) - (y71 * (Voltage(1000)))
    Voc = -y81 / y71
    GoTo 2
End If
For xx = 1 To 999
If Current(xx) < 0 Then
    y11 = Voltage(xx - 1)
    y21 = Voltage(xx)
    y31 = Current(xx - 1)
    y41 = Current(xx)
    y51 = (0 - y31) / (y41 - y31)
    y61 = y51 * (y21 - y11)
    Voc = y11 + y61
    GoTo 2
End If
Next
2
FF = (PMAX / (Isc * Voc))
ModuleEfficiency = PMAX / (SIR * Am)
123456
Return
End
End Sub
```

Function PSAT(TEMP)

$$PSAT = Exp((-5800.2206 / TEMP) - 5.516256 - (0.048640239 * TEMP) + 0.000041764768 * TEMP \wedge 2 - 0.000000014452093 * TEMP \wedge 3 + 6.5459673 * Log(TEMP))$$

End Function

Appendix- E

Quotation for the supply of 6250 DegerTraker 6000NT

BeBa *Energy UK* Ltd
Natural Power from the Sun

DEGERENERGIE
SOLAR TRACKING SYSTEMS

Date:	28/06/2011
Customer:	Morgan Sindall
System Size:	50 MW, 6250 Trackers
Job Reference:	

KIT PRICING TOOL

				Quantity	Sub Total
DEG-160001	DEGERtraker 6000NT	Active tracking system for up to 53 m² module surface.	£6,813.39	6250	£42,583,705.36
DEG-1990001	Central Control Box (CCB) II	Windguard function, manual control and connection possibility for snow sensor.	£375.00	32	£12,000.00
DEG-5100032	Sunlight Sensor	For improved security returns trackers to horizontal position in absence of sunlight.	£118.30	32	£3,785.71
DEG-1600006	Mast	Total length 4.0m (Tube 3.4m + Rotating Head 0.6m)	£655.36	6250	£4,095,982.14

Total	£46,695,473.21
Vat	£9,339,094.64
Total	£56,034,567.86

Andrew Boulton, BEng. (Hons), MSc.
Technical & Sales Support
Beba Energy UK Limited

BeBa

E Mail : **andrew.boulton@beba-energy.co.uk**
Tele : **01442 220 100**
Website: www.beba-energy.co.uk

Tue 28/06/2011

List of Publications

Journals:

[1]   Gago EJ, Etxebarria S, Tham Y, Aldali Y, Muneer T. Inter-relationship between mean-daily irradiation and temperature, and decomposition models for hourly irradiation and temperature. International Journal of Low-Carbon Technologies. 2011 March 1, 2011;6(1):22-37.

[2]   Aldali Y, Henderson D, Muneer T. A 50 MW very large-scale photovoltaic power plant for Al-Kufra, Libya: energetic, economic and environmental impact analysis. International Journal of Low-Carbon Technologies. 2011 December 1, 2011;6(4):277-93.

[3]   Aldali Y, Muneer T, Henderson D. Solar absorber tube analysis: thermal simulation using CFD. International Journal of Low-Carbon Technologies. 2011 December 4, 2011.

[4]   Aldali Y, Davison B, Muneer T, Henderson D. Modeling the behavior of a 50MW DSG plant for southern Libya based on the thermodynamic and thermophysical properties of water substance. Journal of American Society of Mechanical Engineering(ASME). 2012. (Accepted).

[5]   Aldali Y, Celik A, Muneer T. Modelling and experimental verification of solar radiation on a sloped surface, photovoltaic cell temperature, and photovoltaic efficiency. Journal of American Society of Civil Engineering. 2012 (ASCE).(Accepted)

Conferences:

[1]   Aldali Y, Henderson, D., Muneer, T. . Prospects for large-scale solar thermal electricity generation from the Libyan desert: technical feasibility. Proceedings of ES2009 ASME 3rd International Conference on Energy Sustainability 2009; San Francisco, California, USA; 2009.